

**Disrupting Androgen Receptor Transactivation Domains to Identify Lead Compounds
with Potential to be Optimized and Developed into Prostate Cancer Therapeutics**

by

Ashley Taylor Fancher

Bachelor of Science in Biochemistry, Binghamton University, 2013

Submitted to the Graduate Faculty of
The School of Pharmacy in partial fulfillment
of the requirements for the degree of
Doctor of Philosophy

University of Pittsburgh

2019

UNIVERSITY OF PITTSBURGH
SCHOOL OF PHARMACY

This dissertation was presented

by

Ashley Taylor Fancher

It was defended on

April 25, 2019

and approved by

Barry Gold, PhD, Professor, Pharmaceutical Sciences

Zhou Wang, PhD, Professor of Urology, Pathology and Pharmacology, UPMC Chair in

Urological Research

Wen Xie, MD, PhD, Professor, Chair of Pharmaceutical Sciences

Paul A. Johnston, PhD, Associate Professor, Pharmaceutical Sciences

Copyright © by Ashley Taylor Fancher

2019

Disrupting Androgen Receptor Transactivation Domains to Identify Lead Compounds with Potential to be Optimized and Developed into Prostate Cancer Therapeutics

Ashley Taylor Fancher, PhD

University of Pittsburgh, 2019

Prostate cancer (PCa) is the leading cause of cancer in men in the USA, with more than 160,000 new cases each year. PCa patients receiving standard of care androgen deprivation therapy (ADT) eventually acquire what's known as castration resistant prostate cancer (CRPC), and 20% of all PCa cases progress to this metastatic and incurable form of the disease. PCa is the second leading cause of cancer-related death in American men. Current FDA approved drugs for CRPC only provide a 2-5-month survival benefit due to the emergence of resistance to these therapies. Resistance involves continued androgen receptor (AR) signaling despite castrate serum levels of androgens. CRPC cells express elevated levels of both full-length AR (AR-FL), and constitutively active AR splice variants which lack the ligand binding domain (LBD) and display altered AR coactivator interactions, both of which contribute to persistent AR signaling. Overexpression of steroid-receptor coactivators are implicated in the progression of CRPC and amplify AR-mediated transcription by binding to either the activation function 2 (AF-2) surface formed by the AR-LBD, or the activation function 1 (AF-1) surface located in the amino-terminal domain of the receptor. Coactivator binding interactions enhance the recruitment of the basal transcriptional machinery and activate the transcription of AR target genes. Our lab has designed a screening paradigm to identify compounds with novel mechanisms of action to prevent or delay resistance. The screening paradigm uses a primary high content screening assay (HCS) designed to identify compounds that inhibit or disrupt protein-protein interactions (PPI's) between AR and one of its coactivators, transcriptional intermediary factor 2 (TIF2), together with panels of counter screens and

characterization assays to prioritize hit compounds that inhibit or disrupt AF-2 and/or AF-1 transactivation. The ideal hit compound would prevent the transcription of both AR-FL and AR-V7 thereby providing a dual approach to preventing CRPC progression.

Table of Contents

| | |
|---|-----------|
| 1.0 Prostate Cancer (PCa) Overview | 1 |
| 1.1 PCa: An Introduction..... | 1 |
| 1.1.1 Statistics and Epidemiology | 1 |
| 1.1.2 PCa Diagnosis | 2 |
| 1.1.3 Stages of PCa | 5 |
| 1.1.4 Current therapeutics approved to treat PCa..... | 7 |
| 1.1.5 Outcomes for approved drugs for Castration Resistant Prostate Cancer (CRPC) therapy | 10 |
| 1.2 Mechanisms of Resistance to Current Therapeutics and Progression into Castration Resistant Prostate Cancer (CRPC)..... | 13 |
| 1.3 AR and its Role in Prostate Cancer | 18 |
| 1.3.1 Functional Domains of the AR..... | 18 |
| 1.3.2 Transactivation Surfaces of the AR | 20 |
| 1.3.3 AR Coactivators | 21 |
| 1.3.4 AR Target Gene Activation..... | 24 |
| 1.4 Objectives and Hypothesis..... | 25 |
| 2.0 Identification of Hit Compounds Targeting the AR AF-2 Interaction Surface | 29 |
| 2.1 Introduction | 29 |
| 2.2 AR-TIF2 Biosensor High Content Screen..... | 31 |
| 2.2.1 Description of the AR-TIF2 Biosensor..... | 31 |
| 2.2.2 Identifying cytotoxic compounds and auto-fluorescent outliers..... | 34 |

| | |
|--|-----------|
| 2.3 Description of Counter Screening Assays to Run hits from the AR-TIF2 Biosensor | 35 |
| | |
| 2.3.1 P53-hDM2 PPIB Counter Screening Assay | 35 |
| 2.3.2 AR Nuclear Localization Counter Screen | 35 |
| 2.3.3 Dex-Induced GR Translocation Counter Screen | 36 |
| 2.4 AR-TIF2 PPIB Assay Protocol | 36 |
| 2.5 Compound Libraries Screened in Primary and Counter Screens | 37 |
| 2.6 Results | 39 |
| 2.6.1 LOPAC Set Performance in the AR-TIF2 HCS and Counter Screen Assays | 39 |
| | |
| 2.6.2 143,000 Compound Performance in the AR-TIF2 PPIB and Counter Screen Assays | 42 |
| 2.6.2.1 HTS performance and QC statistics of AR-TIF2 PPIB | 42 |
| 2.6.2.2 AR-TIF2 PPIB Primary HCS and Active Confirmation | 43 |
| 2.6.2.3 Testing Paradigm to identify and eliminate compound artifacts | 43 |
| 2.6.2.4 IC₅₀ Determinations – Potency & Efficacy | 46 |
| 2.7 Conclusion | 47 |
| 3.0 Targeting the AR AF-2 Protein-Protein Interactions with Coactivators | 58 |
| 3.1 Introduction: Development of a Panel of Assays to Identify Compounds Targeting the AR AF-2 Transactivation Domain/Coactivator Binding Surface | 58 |
| 3.2 How Did Test Compounds Perform in the Primary AR-TIF2 PPIB Assay? | 60 |
| 3.3 Assays Developed to Characterize AR-TIF2 PPIB Inhibitor/Disruptor Hits that Target the AR AF-2 Transactivation Domain/Coactivator Binding Surface | 62 |

| | |
|--|-----------|
| 3.3.1 Mammalian 2-Hybrid (M2H) Assay..... | 62 |
| 3.3.1.1 Assay Principle..... | 62 |
| 3.3.1.2 Materials and Methods..... | 63 |
| 3.3.1.3 Assay Development and Optimization..... | 66 |
| 3.3.1.4 Inhibition of the AR-TIF2 Biosensor assay to Measure DHT-induced AR-LBD Interactions with the TIF2 by Test Compounds..... | 68 |
| 3.3.2 PSA6.1-Luc Reporter-Based Assay Developed in PC3-GFP-AR-FL Cells . | 69 |
| 3.3.2.1 Assay Principle..... | 69 |
| 3.3.2.2 Materials and Methods..... | 70 |
| 3.3.2.3 Assay Development and Optimization..... | 71 |
| 3.3.2.4 Test set performance in PSA6.1 Reporter Assay | 73 |
| 3.3.3 AR-LBD H³-DHT RadioligandBinding Assay | 75 |
| 3.3.3.1 Assay Principle..... | 75 |
| 3.3.3.2 Materials and Methods..... | 76 |
| 3.3.3.3 Assay Development and Optimization..... | 78 |
| 3.3.3.4 Test set performance in H³-DHT radioligandbinding assay..... | 79 |
| 3.3.1 ALPHAScreen AR-LBD::TIF2-LXXLL-Peptide Binding Assay..... | 79 |
| 3.3.1.1 Assay Principle..... | 79 |
| 3.3.1.2 Materials and Methods..... | 81 |
| 3.3.1.3 Assay Development and Optimization..... | 81 |
| 3.3.1.4 Test Set Performance in ALPHAScreen Assay..... | 83 |
| 3.3.2 Growth Inhibition Assays..... | 84 |
| 3.3.2.1 Assay Principle..... | 84 |

| | | |
|---------|--|-----|
| 3.3.2.2 | Materials/Reagents | 84 |
| 3.3.2.3 | Test Set Performance in Growth Inhibition Assays | 85 |
| 3.3.3 | Conclusions | 85 |
| 4.0 | Targeting the Transactivation potential of the AR amino-terminal domain | 121 |
| 4.1 | Introduction: Development of a Panel of Assays to Interrogate the Ability of Compounds to Block the Transactivation Potential of the AR-NTD | 121 |
| 4.2 | Assays Developed to Characterize AR-TIF2 PPIB Inhibitor/Disruptor Hits that Block the AR AF-1 Transactivation Domain..... | 123 |
| 4.2.1 | AR-NTD (1-503) Transactivation Assay | 123 |
| 4.2.1.1 | Assay Principle..... | 123 |
| 4.2.1.2 | Materials and Methods..... | 124 |
| 4.2.1.3 | Assay Development and Optimization..... | 126 |
| 4.2.1.4 | Test set performance in pGal4-AR-NTD based Transactivation assays | 129 |
| 4.2.2 | PSA6.1-Luc and UBE2C-Luc Reporter based assays developed in PC3-GFP- AR-V7 Cells..... | 131 |
| 4.2.2.1 | Assay Principle..... | 131 |
| 4.2.2.2 | Materials and Methods..... | 132 |
| 4.2.2.3 | Assay Development and Optimization..... | 134 |
| 4.2.2.4 | Test set performance in PSA6.1-Luc and UBE2C-Luc reporter assays | 136 |
| 4.2.3 | Conclusions | 138 |

| | |
|--|------------|
| 5.0 Compound Performance in Assays Developed to Prioritize Hits from the AR-TIF2 | |
| PPIB | 160 |
| 5.1 Introduction | 160 |
| 5.2 Initial Hit Triage..... | 161 |
| 5.2.1 LOPAC Set | 161 |
| 5.2.2 10K Library | 164 |
| 5.2.3 50K Library | 165 |
| 5.2.4 83K Library | 166 |
| 5.3 Prioritized Hit Characterization | 167 |
| 5.3.1 Implementation of Assays Developed for Characterizing hits from the AR-TIF2 PPIB | 169 |
| 5.3.1.1 PSA6.1-Luc Reporter Assay in PC3-AR-FL-GFP Cells | 169 |
| 5.3.1.2 AR-LBD H³-DHT Radioligand Binding Assay | 170 |
| 5.3.1.3 TIF2 Box III LXXLL peptide binding ALPHAScreen Assay | 171 |
| 5.3.1.4 Growth Inhibition Assays | 171 |
| 5.3.1.5 Transactivation Assay using pGal4-AR-NTD..... | 172 |
| 5.3.1.6 PSA6.1-Luc & UBE2C-Luc Reporter Based Assay Development in PC3-AR-V7-GFP Cells..... | 172 |
| 5.3.2 Conclusion: Which Compounds are Prioritized and Why?..... | 173 |
| 6.0 Perspectives, Limitations and Future Directions..... | 189 |
| 6.1 Perspectives | 189 |
| 6.2 Limitations | 200 |
| 6.3 Future Directions..... | 201 |

Bibliography 214

List of Tables

| | |
|---|------------|
| Table 1. Testing paradigm to identify and eliminate compound artifacts from the AR-TIF2 PPIB | 54 |
| Table 2. IC₅₀ results of the test set run in the AR-TIF2 Biosensor..... | 90 |
| Table 3. PCR primer sequence for amplification and cloning of full-length TIF2 into pVP16 vector | 92 |
| Table 4. Primers for sequence confirmation of pVP16-TIF2 | 93 |
| Table 5. IC₅₀ results of test set run in mammalian 2-hybrid assay | 100 |
| Table 6. IC₅₀ results of test set run in the PSA6.1-Luc reporter based assay..... | 107 |
| Table 7. IC₅₀ results of test set run in H³-DHT radio ligand binding assay | 113 |
| Table 8. TIF2-box-III (738-756) peptide sequence used in ALPHAScreen assay..... | 115 |
| Table 9. IC₅₀ results of test set run in AR AF-2::LXXLL-TIF2 peptide binding ALPHAScreen assay..... | 118 |
| Table 10. IC₅₀ results of test set run in growth inhibition assays | 120 |
| Table 11. PCR primer sequence for amplification and cloning of AR-NTD (1-558) into pGal4 vector | 141 |
| Table 12. PCR primer sequence for amplification and cloning of AR-V7 (AR3) into pGal4 vector | 142 |
| Table 13. IC₅₀ results of test set run in pGal4-AR-NTD based transactivation assays | 150 |
| Table 14. IC₅₀ results of test set run in PSA6.1-Luc reporter based | 157 |
| Table 15. IC₅₀ results of test set run in UBE2C-Luc reporter based assay | 159 |
| Table 16. Selection process used to prioritize hits from the AR-TIF2 HCS campaign | 176 |

| | |
|--|------------|
| Table 17. IC₅₀ results of selected AR-TIF2 PPI inhibitor/disruptor hit analogs tested in initial hit triage assays | 178 |
| Table 18. IC₅₀ results of selected AR-TIF2 PPI inhibitor/disruptor hit analogs tested in mammalian 2-hybrid assays..... | 179 |
| Table 19. IC₅₀ results of selected AR-TIF2 PPI inhibitor/disruptor hit analogs screened in PCa cell line growth inhibition assays..... | 180 |
| Table 20. IC₅₀ results of prioritized AR-TIF2 PPI inhibitor/disruptor hit analogs in AF-2 transactivation domain hit characterization assays that employ the AR-LBD..... | 184 |
| Table 21. IC₅₀ results of prioritized AR-TIF2 PPI inhibitor/disruptor hit analogs in AF-1 transactivation domain hit characterization assays developed with the AR-NTD. | 188 |

List of Figures

| | |
|--|-----------|
| Figure 1. Androgen receptor signal transduction pathway | 28 |
| Figure 2. AR-RFP Recombinant Adenovirus..... | 48 |
| Figure 3. TIF2-GFP Recombinant Adenovirus..... | 49 |
| Figure 4. AR-RFP and TIF2-GFP Co-infected in U-2 OS Cells..... | 50 |
| Figure 5. AR-TIF2 PPIB Assay Principle..... | 51 |
| Figure 6. Image Segmentation Derived TIF2-GFP Positive Nucleolar Masks in the FITC and Texas Red Channels..... | 52 |
| Figure 7. DHT Concentration Response of AR-RFP in the AR-TIF2 PPIB..... | 53 |
| Figure 8. Concentration-dependent confirmation of LOPAC active that inhibit the DHT- induced formation of AR-TIF2 PPIs or disrupt preexisting AR-TIF2 PPI complexes | 55 |
| Figure 9. Non-Nuclear Receptor AR-TIF2 PPIB Actives | 56 |
| Figure 10. AR-TIF2 PPIB Actives: Nuclear Hormone Receptor Ligands | 57 |
| Figure 11. Chemical structures of the test set for the hits characterization assays | 88 |
| Figure 12. Inhibition of the AR-TIF2 Biosensor assay to measure DHT-induced AR-LBD interactions with TIF2 by test compounds | 89 |
| Figure 13. Mammalian 2-Hybrid assay principle | 91 |
| Figure 14. Western blot confirmation of pVP16-coactivator constructs..... | 94 |
| Figure 15. Determining which cell background enables the most robust mammalian 2-hybrid assay | 95 |
| Figure 16. Mammalian 2-Hybrid assay development and optimization..... | 96 |

| | |
|--|------------|
| Figure 17. Concentration Responses of the mammalian 2-hybrid assays to measure DHT-induced AR-LBD interactions with the A) TIF2 or B) SRC1 Coactivators | 97 |
| Figure 18. Mammalian 2-hybrid assay development and optimization: DMSO tolerance for HEK 293 cells transfected with pGal4-AR-LBD/pVP16-TIF2 and pGal4-AR-LBD/pVP16-SRC1 | 98 |
| Figure 19. Inhibition of the mammalian 2-hybrid assays to measure DHT-induced AR-LBD interactions with TIF2 or SRC1 coactivators by test compounds | 99 |
| Figure 20. PSA6.1-luciferase reporter assay principle | 101 |
| Figure 21. Endogenous expression of TIF2 and AR in 5 PCa cell lines | 102 |
| Figure 22. IXM images of PC3 cells stably transfected with pEGFP-C1-AR in the presence or absence of DHT | 103 |
| Figure 23. Nuclear Translocation of AR-FL-GFP in PC3 cells exposed to increasing concentrations of DHT | 104 |
| Figure 24. Concentration responses of the PSA6.1-Luc reporter assay to measure DHT-induced transcriptional activity of AR-FL-GFP in PC3 cells | 105 |
| Figure 25. Test set performance in PSA6.1-Luc reporter assay | 106 |
| Figure 26. Radio ligand binding assay principle | 108 |
| Figure 27. pET28a-His₆-AR-LBD construct | 109 |
| Figure 28. pET28a-His₆-AR-LBD | 110 |
| Figure 29. H³-DHT radio ligand binding assay development | 111 |
| Figure 30. Test set performance in H³-DHT radio ligand binding assay | 112 |
| Figure 31. AR AF-2::LXXLL-TIF2 peptide binding ALPHAScreen assay principle | 114 |
| Figure 32. AR AF-2::LXXLL-TIF2 peptide binding ALPHAScreen assay development . | 116 |

| | |
|--|------------|
| Figure 33. Test set performance in AR AF-2::LXXLL-TIF2 peptide binding ALPHA Screen assay | 117 |
| Figure 34. Test set performance in growth inhibition assays | 119 |
| Figure 35. Mammalian 2-hybrid assay. pGal4-AR-NTD transactivation assay principle. | 140 |
| Figure 36. Western blot confirmation of pGal4-AR-NTD constructs..... | 143 |
| Figure 37. Determining which cell background enables the most robust mammalian 2-hybrid assays..... | 144 |
| Figure 38. Mammalian 2-Hybrid assay development and optimization: cross-titration of pGal4-AR-NTD (1-558) with A) pVP16-TIF2 or B) pVP16-SRC1 | 145 |
| Figure 39. Mammalian 2-hybrid assay development and optimization: cross-titration of pGal4-AR3 (AR-V7) with A) pVP16-TIF2 or B) pVP16-SRC1 | 146 |
| Figure 40. Determining which pGal4-AR-NTD plasmid construct enables the most robust mammalian 2-hybrid assays..... | 147 |
| Figure 41. Determining if each of the pGal4-AR-NTD plasmid constructs requires pVP16-coactivator to produce 5xGal4-TATA-Luc reporter based assay signal | 148 |
| Figure 42. Test set performance in pGal4-AR-NTD based transactivation assays | 149 |
| Figure 43. UBE2C-Luc reporter assay principle | 151 |
| Figure 44. IXM images of PC3 cells stably transfected with pEGFP-C1-AR-V7 in the presence or absence of DHT..... | 152 |
| Figure 45. Optimizing transfection conditions: Determining the optimal amounts of DNA plasmid reporter construct and FuGENEHD:DNA ratio to use in the PSA6.1-Luc reporter assay | 153 |

| | |
|---|------------|
| Figure 46. Optimizing transfection conditions: Determining the optimal amounts of DNA plasmid reporter construct and FuGENEHD:DNA ratio used in the UBE2C-Luc reporter assay | 154 |
| Figure 47. Demonstrating PSA6.1-Luc and UBE2C-Luc reporter response in different cell lines: PC3, PC3-AR-FL-GFP, and PC3-AR-V7-GFP | 155 |
| Figure 48. Test set performance in PSA6.1-Luc reporter assay | 156 |
| Figure 49. Test set performance in UBE2C-Luc reporter assay | 158 |
| Figure 50. AR-TIF2 PPI inhibitor/disruptor hit analogs selected for testing in characterization assays..... | 177 |
| Figure 51. Performance of prioritized AR-TIF2 PPI inhibitor/disruptor hits in the AR-FL directed PSA6.1 reporter assay performed in PC3-AR-FL-GFP cells | 181 |
| Figure 52. Performance of prioritized AR-TIF2 PPI inhibitor/disruptor hits in the H³-DHT radio ligand and TIF2 Box III LXXLL peptide ALPHAScreen binding assays | 182 |
| Figure 53. Performance of prioritized AR-TIF2 PPI inhibitor/disruptor hit analogs in the pGal4-AR-NTD transactivation assay | 185 |
| Figure 54. Inhibition of the PSA6.1-Luc reporter assay to measure AR-V7's transcriptional activity in the presence of AR-TIF2 PPI inhibitor/disruptor hit compound analogs | 186 |
| Figure 55. Inhibition of the UBE2C-Luc reporter assay to measure AR-V7's transcriptional activity in the presence of AR-TIF2 PPI inhibitor/disruptor hit compound analogs | 187 |
| Figure 56. AR-TIF2 PPI inhibitor/disruptor hit characterization and prioritization bioactivity profiles..... | 204 |

| | |
|--|------------|
| Figure 57. AR-TIF2 PPI inhibitor/disruptor hit compound profiles | 205 |
| Figure 58. 9864798 & 55803564 analogs | 206 |
| Figure 59. 14977726 & 36998335 analogs | 207 |
| Figure 60. 62209680 analogs | 208 |
| Figure 61. AR-TIF2 PPI parent hits & structurally related analog hit characterization profiles..... | 209 |
| Figure 62. AR AF-2 transactivation domain assay profiles | 210 |
| Figure 63. AR AF-1 transactivation domain assay profiles | 211 |
| Figure 64. Bioassay activity profile of a representative AR-TIF2 PPI hit from cluster 1.. | 212 |
| Figure 65. Bioassay activity profile of a representative AR-TIF2 PPI hit from cluster 2.. | 213 |

1.0 Prostate Cancer (PCa) Overview

1.1 PCa: An Introduction

1.1.1 Statistics and Epidemiology

Prostate Cancer (PCa) is the 2nd leading type of cancer in men in the U.S., behind skin cancer, with nearly 200,000 new incidences diagnosed and 30,000 deaths reported annually [1], [2]. The 5-year survival rate of men with localized or regional PCa is nearly 100% [3]. However, as soon as this disease becomes metastatic, the 5-year relative survival rate drops to nearly 29% [4]. Metastatic PCa is an aggressive type of cancer that responds poorly to current standard of care therapeutics. PCa that no longer responds to current hormonal therapies is termed Castration Resistant Prostate Cancer (CRPC). 20% of PCa patients develop CRPC within 5 years of PCa diagnosis. The prognosis for CRPC is terminal, and the mean survival of patients with metastatic CRPC is only 9-13 months [5].

PCa is a disease of age, with around 6 out of 10 diagnoses detected in patients older than 65. Patients that are younger than 50 tend to be at lower risk for diagnosis of this disease [6]. However, there are certain risk factors that can increase the likelihood of developing PCa in younger men. For example, certain countries and ethnicities have an increased tendency to be diagnosed with and die from this disease than others. Western countries including those in Europe, and North America have a notably higher incidence rate than those in the East. There is a

particularly low incidence rate observed in Asia [7]. One possible explanation for the difference in PCa incidence is based on the differences in diet observed between western and eastern countries, notably, the increased consumption of foods high in saturated fats, dairy, and meat in the west [8]. This hypothesis is supported by the finding that, men from Asia who have immigrated to either Europe or North America and have adopted a western diet, develop an increased risk of PCa incidence [9]. Along the same lines, obesity, although it hasn't been consistently proven as a risk factor for developing PCa, has been associated with a shorter overall survival. Specifically, men with a BMI of $>35 \text{ kg/m}^2$, have a 34% higher rate of prostate cancer death compared to men who have a more normal weight [10]. In terms of ethnicity, African American men have an elevated rate of diagnosis, with more than double the incidence than Caucasian Americans [7], [11]. Similarly, heredity can play a role in developing PCa, as men with a direct relative, such as a brother or father, with a PCa diagnosis are at a 2-3 fold increase in likelihood of also being diagnosed with this disease than those who do not have a direct relative diagnosed with PCa [12]. Despite this fact, 90-95% of all prostate cancers do not have an association with heredity [13].

1.1.2 PCa Diagnosis

Screening for PCa: Physical Examination and Diagnostic Biomarkers

A PCa diagnosis is typically based on the results of a physical examination of the prostate and/or a blood test for serum prostate specific antigen (PSA) levels. If either test suggests the possibility of PCa, the physician will usually request that a biopsy be taken. The results of the physical prostate exam and serum PSA levels combined with the histological grading of prostate tissue obtained by biopsy allow a physician to both confirm the PCa diagnosis, and stage the extent of cancer development [14].

The physical examination is a method of palpating the prostate gland for evidence of tumor formation. Unfortunately, this type of examination is not very sensitive, as early stage PCa may not result in a palpable tumor. The PSA blood test measures the serum levels of a protein called prostate specific antigen (PSA) [14]. PSA belongs to a group of serine proteases called kallikreins and PSA levels are elevated in the bloodstream of patients with an enlarged prostate due to inflammation, or due to the presence of a tumor [15]. Normal PSA levels can differ from patient to patient, but many doctors consider patients with PSA levels of ≤ 4 ng/mL to have a decreased risk of having prostate cancer. This type of test is quite sensitive, however, it is not always specific for cancer. For example, PSA levels can be elevated in men with benign prostatic hyperplasia (BPH), urinary tract infection, or non-cancer related inflammation [16]. Similarly, 65-75% of men with PSA levels between 4-10 ng/mL, have negative biopsy results [17], [18]. Furthermore, based on recommendations set-forth by the U.S. Preventive Services Task Force, testing for PSA is only recommended in men aged 55-69, and this decision is made on a patient to patient basis based on potential risk factors of incidence, such as ethnicity and family history [19]. These tests therefore can be informative, but must be confirmed by the results from a tissue pathology report to make a more accurate diagnosis.

Histological grading

Prostate cancer can be classified clinically, as being localized or metastatic, or pathologically, which involves the observation of prostate tissue samples taken from a patient. The prostate is comprised of glands surrounded by the stroma. The gland is composed of acini which consists of epithelial cells which line a central lumen [20]. Prostate epithelium is comprised of luminal columnar epithelial cells, and of basal cells that lie adjacent to these. It has

been shown that nearly all cells identified as adenocarcinoma, are of luminal origin, with very few infiltrating basal cells [21]. Prostate adenocarcinoma can be staged using a scoring system, termed as a “Gleason score” or based on the TNM staging system which was developed as a tool to stage tumor spread through the extent of the tumor (T), the extent of spread to the lymph nodes (N), and the presence of metastasis (M). Both use histopathology as a means for staging a primary tumor. A Gleason score enables a pathologist to assign a score to the prostatic tissue as an indicator of cancer grade. The Gleason score ranks a biopsy sample with two numbers based on patterns observed from retrieved cells. The first number includes the assignment of a Gleason grade to the most predominant cell pattern seen in the tissue sample, and the second number indicates the second most predominant cell pattern seen in the tissue sample. Each score ranges between 1 and 5, where one is the most differentiated and least likely to be cancerous, and 5 is the least differentiated and most likely to be cancerous [22]. The two values represent an overall score which can inform decision making when determining treatment options. Patients with a Gleason score of 6 or lower, are seen to have better outcomes than those with high Gleason scores such as those that are 8 or above. The outcomes of patients with a Gleason score of 7 tend to be variable, and treatment may or may not be recommended given this score [23]. Of the TNM staging system, the T stage includes information regarding the primary tumor itself, where T1 indicates results directly obtained from the pathology report. T1 prostatic carcinomas can be deemed as T1a, T1b or T1c. T1a and T1b represent pathological grading based on specimens that were isolated using transurethral resection of the prostate (TURP). T1a represents tissue with less than 5% area of cancerous tissue. T1b represents tissue with more than 5% area of cancerous tissue. T1c is represented by pathological grading based on specimens that were isolated using a needle biopsy. The physicians request for a needle biopsy is usually as a result of high levels of

serum PSA [24]. Results obtained from a histopathology report combined with results of clinical staging allow the physician to make a more informed prognosis of the disease.

1.1.3 Stages of PCa

There are 4 major stages of PCa. Stage I includes the presence of a localized tumor that is typically present in one lobe of the prostate and cannot be detected upon physical examination. Stage II involves the growth of the initial tumor, and tumor formation in other lobes of the prostate. This stage may be accompanied by inflammation of the prostate. Stage III is generally accompanied by a breach in the outer membrane of the prostate by the tumor. It also includes the narrowing of seminal vesicles and the ureter which may be symptomatic. Stage IV includes lymph node involvement, eventually becoming metastatic.

Stages of prostate cancer can be determined using the two different types of classification systems that have been previously described in the last section: the TNM system, and Gleason Scoring [25]. The Gleason scoring system described above uses histopathology to determine disease stage, whereas the TNM system is used to determine the extent of disease progression and the spread of cancer based on both histopathology and other methods. These methods include physical examination of the prostate itself and staging the extent of metastasis via certain imaging techniques such as computed tomography (CT), magnetic resonance imaging (MRI), and positron emission tomography (PET). T2 is defined by a tumor that is evidenced by palpation or visible by imaging techniques. T2 can be subcategorized based on its presence in lobes of the prostate. T3 is based on the tumors ability to locally extend past the basement membrane of the prostate gland. Stage T4 is represented by a prostate tumor that has invaded adjacent structures/tissues. The N stage involves information regarding spread of the cancer to regional lymph nodes. N0 demarcates

no regional metastasis, N1-3 represent metastases in regional lymph nodes. M is then representative of a distant metastasis. Where M0 represents no distant metastasis, and M1 represents distant metastasis [24], [25]. Results from the physical examination, PSA blood test, TNM staging, and Gleason score can all aid in determining the proper type of therapy for the prostate cancer patient to be administered.

Primary, localized tumors: Molecular Hallmarks

In the earliest events of prostate carcinogenesis, the loss of Nkx3.1 occurs as a result of the loss of specific regions of chromosome 8p. Nkx3.1 is a homeobox containing gene, involved with prostate development and function, and acts as a prostate specific tumor suppressor gene [26]. This is a frequent occurrence, in as many as 80% of prostate tumors [26]. The fusion of TMPRSS2, which is an androgen-regulated gene, with ERG, which is part of the family of ETS transcription factor genes, has been shown to be an early molecular hallmark of the development of prostate cancer itself. It has even been reported in 30-70% of patients who have undergone a surgical procedure as a means of PCa treatment [27], [28]. Other drivers include an increase in expression of oncogene, MYC, as well as loss of either tumor suppressors PTEN, or p53, both of which are associated with poor prognosis [29].

Castration Resistant, metastatic tumors: Molecular Hallmarks

Castration resistant prostate cancer is characterized by disease progression – consecutive rises in PSA levels and/or an increase in soft tissue or bone lesions - despite treatment with androgen deprivation therapies (ADT's) [30]. ADT's target the proper functioning of the AR by blocking the production of androgens that bind to and activate it, or by antagonizing ligand binding

to the AR. Since the progression of PCa relies on the function of the AR signaling axis, targeting elements along this pathway is a strategic approach to the treatment of prostate cancer. The types of ADT's used in the treatment of localized prostate cancer and locally advanced disease include luteinizing hormone-releasing hormone (LHRH) or gonadotropin releasing hormone (GnRH) agonists or antagonists such as Leuprolide, Goserelin, Triptorelin, and Histrelin. These types of compounds act by targeting the hypothalamic pituitary gonadal (HPG) axis, which represents three endocrine glands that act in concert. The hypothalamus, residing in the brain, secretes GnRH, which travels to the pituitary where it binds to receptors of secretory cells which then produce LH which travels through the blood stream to the leydig cells of the testis, directing them to produce androgen. GnRH agonists cause a negative feedback loop which downregulates GnRH receptors in the anterior pituitary gland resulting in a decrease in LH release, and a subsequent decrease in testosterone release from the leydig cells [31, 32].

Disease progression occurs due to mechanisms of resistance that arise in the CRPC cell against standard of care ADT's. This resistance involves molecular events surrounding aberrant androgen receptor (AR) function in the prostate cancer cell. The dysregulation of coregulators, specifically the overexpression of coactivators, AR mutations, AR overexpression and the emergence of constitutively active AR splice variants, such as AR-V7 are other ways in which continued AR signaling, and therapeutic resistance occurs [33]. These mechanisms of resistance will be described in further detail later in the chapter.

1.1.4 Current therapeutics approved to treat PCa

Localized therapeutic treatment options

The therapies that are offered to patients who have localized PCa include the following: active surveillance, prostatectomy, radiotherapy, cryosurgery, high intensity focused ultrasound and focal therapy. Surgery can include a partial or radical prostatectomy, which involves the removal of part or all of the prostate gland depending on severity of the cancer, using either retropubic or perineal methods. Radiation can also be used as a means to eradicate a more localized tumor, the two main types being external beam or brachytherapy, which is a type of seed therapy, using internal beams of radiation [34]. Androgen deprivation therapies can be used to complement the removal of a tumor by surgery or radiation [34]. These different methods are employed based on the severity of the localized disease. PCa is considered to be low risk if a patient has PSA blood serum levels of less than 10 ng/mL, tumor staging of T1-T2a based on DRE and pathology report, and a Gleason score of less than 6. PCa is considered to be of intermediate risk if the patient has a PSA level of either less than 10 ng/mL, or 10-20 ng/mL, combined with a Gleason score of 7, and tumor staging between T1-T2. Finally, patients with high risk disease have a PSA of greater than or equal to 20 ng/mL, a Gleason score of 8 or above, and tumor stage of T1-T2. Based on the 2017 guidelines approved by the American urological association, for a low risk prostate cancer, active surveillance is the recommendation [34]. For intermediate-risk localized disease, clinicians are suggested to recommend radical prostatectomy or radiotherapy plus androgen deprivation therapy (ADT) as the standard of care treatment option [34]. Similarly, for a high-risk localized disease, clinicians are encouraged to recommend radical prostatectomy or radiotherapy plus ADT as a standard treatment option. Both intermediate risk, and high risk localized PCa staging with CT or MRI and a bone scan is suggested. Similarly, for a high risk localized disease, clinicians should stage the extent of tumor spread using CT or MRI and bone scan [34]. Treatment options such as focal therapy or high intensity focused ultrasound are not standard of care options, but

despite not being recommended, they may still be used as a treatment option. ADT's may be used concurrently in patients undergoing radiotherapy, in order to shrink the tumor and prevent possible metastasis.

For patients with non-metastatic castration resistant prostate cancer, apalutamide or enzalutamide can be used concurrently with androgen deprivation therapies [35].

Metastatic therapeutic treatment options

The 2019 National Comprehensive Cancer Network (NCCN) guidelines provide recommendations for treating advanced prostate cancer that has failed local therapy. These therapeutic options include LHRH agonists, or antagonists, or complete androgen blockade, using LHRH agonist or antagonist with an oral antiandrogen [36]. This type of treatment reduces the levels of androgen in the blood stream. A decrease in circulating androgens decreases the AR's signaling potential in PCa cells. This reduction in androgen levels can be achieved through either surgical or chemical means. Surgery involves an orchiectomy, or removal of the testis, while chemical castration involves the use of LHRH agonists or GnRH agonists [31, 32]. Although these agonists have been shown to be just as effective as surgical castration, they can lead to an initial “flare-up” of the disease, due to the initial increase in androgen production observed [37]. This flare up presents clinically with an increase in serum PSA levels observed, but also symptomatically [37]. Therefore, antiandrogens, which block the action of androgens at the receptor present in different tissues, by targeting the androgen receptor directly at the LBD, can mitigate disease flare. Antiandrogens commonly used include bicalutamide, flutamide, or nilutamide [37].

The guidelines set forth by the American Urological Association suggest treating metastatic CRPC based on the extent of disease progression [34]. For example, for patients who

are asymptomatic or minimally symptomatic, either abiraterone plus prednisone, or enzalutamide should be offered [34]. Abiraterone Acetate is a type of ADT which targets the production of adrenal androgens. This compound is a pregnenolone analog inhibitor of CYP17A1. Abiraterone specifically inhibits the 17alpha-hydroxylase enzyme function of this cytochrome P450. This ultimately prevents the synthesis pathway of cholesterol into testosterone [38], [39]. Enzalutamide is an AR antagonist that prevents the AR signaling pathway by inhibiting nuclear translocation of the receptor, and blocks coactivator recruitment of the AR [40]. Alternatively, docetaxel, if not used in prior treatment, or sipuleucel-T can be used to treat patients. For patients who are symptomatic, abiraterone plus prednisone, or enzalutamide can be used. Similarly, docetaxel can be used. For patients who have mCRPC symptoms related to bone metastasis, such as bone pain, and loss of integrity in bone structure that is prone to fracture, therapies such as radium-223 can be used in patients who have received prior docetaxel. Patients who have poor bone health can be offered preventative treatment (supplemental calcium, vitamin D) for fractures or other skeletal related events. Also, clinicians can use zoledronic acid or denosumab as a preventative treatment for fracture or other skeletal related events for patients who experience bone metastases [41].

1.1.5 Outcomes for approved drugs for Castration Resistant Prostate Cancer (CRPC) therapy

Progression free survival, overall survival

LHRH agonists and antagonists are used when the cancer has spread too far to be cured by surgery or radiation. It is also used if cancer remains or comes back after treatment with surgery or radiation therapy [37]. First generation antiandrogens such as flutamide, nilutamide, or bicalutamide may be added to the treatment if LHRH agonists or antagonists are no longer working

on their own, or used as a first line hormone therapy in conjunction with LHRH agonists [37]. Physicians use LHRH agonists and antiandrogens in conjunction with one another to achieve what is known as combined androgen blockade or CAB, as a means to prevent AR signaling in the cell both directly and indirectly [37]. Unfortunately, despite efforts in treatment with both LHRH agonists and antiandrogens, cancer continues to progress. For example, many different studies were conducted to determine the efficacy of CAB compared with castration alone. It was found by one group, Crawford et al, that patients either undergoing CAB with LHRH plus flutamide, and LHRH plus placebo, that PFS was prolonged in the flutamide group compared to the control arm by 2.6 months, from 13.7 months to 16.5 months [42]. Conversely, another group, Eisenberger et al compared CAB using flutamide and an LHRH agonists compared to placebo and found that there were no significant differences in PFS [43]. In either case, patients succumbed to death, which is consistent with cancer progression and relapse due castration resistance.

The two most recently approved CRPC therapeutic agents are Enzalutamide and Abiraterone, which antagonize AR and inhibit androgen synthesis, respectively. They have a similar, yet more potent mechanism of action than their ADT predecessors. Unfortunately, the survival benefit conferred by Enzalutamide and Abiraterone in CRPC patients is only a few months, and these drugs fail to prevent the emergence of resistance [38, 44].

According to the PREVAIL clinical trial, a multinational study to test the effects of enzalutamide compared to placebo, it has been shown that outcomes in terms of overall survival of patients who were treated with enzalutamide plus LHRH therapy was 35.3 months, vs. patients who were treated with placebo with LHRH therapy was 31.3 months, with an overall advantage of 4 months OS of patients taking Enzalutamide compared to placebo control [44].

In a randomized phase 3 study funded by Janssen Research & Development, it was shown that in patients who were receiving abiraterone acetate plus prednisone vs. those who were taking placebo plus prednisone, the overall survival in the abiraterone acetate arm was longer on average than those taking placebo plus prednisone, 34.7 months vs. 30.3 months, respectively, with an overall increase in survival of 4.4 months [38].

Toxicities &/or dose limiting adverse events

Adverse events from ADT's such as LHRH and GnRH agonists, used in the treatment of localized prostate cancer include osteoporosis, loss of muscle and muscle weakness, weight gain, hot flashes, sweats, gynecomastia and decreased libido. Disease flare-up, also associated with these compounds can lead to ureteral obstruction, urinary retention, spinal cord compression, or even death. Also, men who have cancer that has spread to the bones might experience bone pain associated with flare-up. Similarly, a burst in tumor growth could result because of flare up which could lead to pain, or other skeletal or spinal cord related injury [37].

Adverse events associated with antiandrogens are similar to those seen with surgical and chemical castration but are less severe than those associated with LHRH and GnRH agonists. However, when used in conjunction with LHRH agonists, diarrhea, nausea, liver problems, and fatigue often result [42]. The side effects of taking Enzalutamide and apalutamide include diarrhea, fatigue, and hot flashes. These drugs have also seen to have effects such as dizziness, and in very rare cases, seizures [42]. The side effects of taking Abiraterone include pain in the joints or muscles, high blood pressure, hot flashes, nausea, and diarrhea [45]. Given these side effects, it would be beneficial for the patient's quality of life if a therapeutic with lower adverse effects could be developed.

1.2 Mechanisms of Resistance to Current Therapeutics and Progression into Castration Resistant Prostate Cancer (CRPC)

The majority of PCa patients progress to CRPC despite receiving the current standard of care therapeutics because of a variety of mechanisms of resistance. ADT is seen to be effective initially, but ultimately patients progress into a castrate resistant state. This progression is due to persistent androgen receptor signaling in the cell despite achieving castrate levels of androgen [46]. The AR's normal biological role involves mediating the growth and function of the prostate gland, however its aberrant signaling can lead to the development of CRPC [47]. AR dependent mechanisms of resistance are due to AR over-expression, continued intra-tumoral androgen synthesis, and promiscuous AR activation by non-androgenic ligands [48], [49], [50]. These mechanisms occur to compensate for low cellular DHT levels.

The overexpression of the AR is one such mechanism of resistance. AR protein expression is significantly elevated in more advanced stages of PCa, due to either increases in gene copy number or by increased transcription of the AR gene. This AR overexpression has been reported to occur in 30-80% of PCa cases [51]. Also, around 81% of mCRPC carried AR enhancer region amplifications which allowed of the overexpression of AR. This is seen to occur after the exposure of patients to ADT's [52].

Alternative androgen synthesis is another mechanism of resistance. Despite surgical or chemical methods of castration, androgen synthesis can still occur via alternative synthesis pathways. These pathways allow for androgen production both intratumorally, and by the adrenal glands. Increase in androgen synthesis combined with elevated AR expression leads to increased DHT::receptor binding, receptor activation, and reduces patient responses to ADT [53].

AR mutations in the ligand-binding domain also lead to ineffective responses to ADT. The mutations are generally somatic and allow the AR to become activated by non-androgen based steroid hormones, such as progestins, estrogens, and even antiandrogens [54]. These mutations are less frequently seen in early stages of the disease and only seem to represent 10% of the population in CRPC [54], meaning that there must be other forms of resistance in play that have yet to be targeted by drugs.

The dysregulation of co-regulators, specifically the overexpression of coactivators represents another way in which continued AR signaling, and therapeutic resistance occurs [55-59]. It has been hypothesized that the overexpression of AR coactivators can cause progression of PCa into CRPC, no longer responsive to current ADT [60]. Coactivators possess different functionality and can aid in the transcription process by recruiting proteins that unwind DNA from the histones at the site of transcription, or through their recruitment of general transcriptional factors (GTF's). Some coactivators seen to be overexpressed in CRPC include the family of p160 coactivators, SRC1, TIF2, and RAC3, as well as Vav3, FKBP51, p300/CBP, MED1, FHL2, and others [56-59, 61-63]. These coactivators act as adaptor proteins, allowing for the interaction between AR, and the basal transcriptional machinery. Some coactivators also have intrinsic HAT (histone acetyltransferase) activity which allows for unwinding of the DNA from the histones for gene transcription to occur. Corepressors include proteins such as SMRT, and NCoR. These act to control chromatin structure with their endogenous histone deacetyltransferase (HDAC) activity [64]. The p160 coactivators act as bridging proteins that recruit proteins with histone acetylating function to the DNA bound AR [59].

Another form of resistance can be attributed to alternative splicing of full-length AR mRNA, leading to the production of truncated receptors [65-69]. Patients that express alternative splice

variants like AR-V7 which have lost the ligand-binding domain in the C-terminus of the receptor, will not respond to the current antiandrogens [67, 68]. AR-V7 has been shown to be constitutively active and drives the expression of cell cycle genes, and some canonical androgen responsive genes, including the PCa biomarker PSA, in reporter assays and expression microarray analyses [67, 68, 70]. Since the overexpression of coactivators and emergence of AR splice variants remain un-broached by current CRPC therapeutics, the targeting of these resistance mechanisms might represent an untapped therapeutic strategy.

AR Splice Variants

Identification of

Splice variants were first identified by two different groups. Dehm et al utilized 3' rapid amplification of cDNA ends (RACE) in which they identified constitutively active proteins that only contained exons 1, 2 and/or 3, and cryptic exons derived from introns 2 and 3 of the full length AR (AR-FL) [65, 68]. Similarly, Hu et al describe the design of primers and *in silico* sequencing methods to identify 7 different splice variants, AR-V1 to AR-V7 [67]. To date, there are 18 identified AR splice variants [69]. Some of these are constitutively active, meaning that even in the absence of ligand, these variants are transcriptionally active. Some are conditionally active, which means that different cell contexts, produce different extents of transcriptional activity [69]. AR-V7 and ARv567es are LBD lacking versions of the full-length AR. These are constitutively active and are the most clinically relevant splice variants seen to emerge in CRPC patients, due to an upregulation of AR splice variant expression after ADT therapy [71-74].

Structure and Function

Whereas wild type FL-AR (wtAR) consists of 8 canonical exons, the AR-V7 splice variant contains exons 1-3, and a 3' untranslated region (3' UTR), which translates to a protein containing

a variable region, uncharacteristic of the full-length receptor [65-68]. Functionally, AR-V7 is considered constitutively active because many ARE containing luciferase-based reporter constructs become activated by the transfection of AR-V7 without the addition of androgens to stimulate reporter response. This demonstrates that these splice variants lacking a LBD have constitutive activity, and do not require androgen based stimulation [67, 68, 70]. AR-V7 has been shown to regulate the transcription of both genes that are canonically targeted by the AR-FL in androgen dependent (AD) forms of PCa, such as PSA, and those non-canonical genes associated with androgen independent (AI) forms of PCa, such as ubiquitin conjugating enzyme E2C (UBE2C) [70, 75, 76]. Proteins are tagged with ubiquitin as a means of signaling them for proteasomal degradation [77]. Ubiquitination involves ubiquitin-activating enzymes, ubiquitin conjugating enzymes, and ubiquitin-protein ligases. The UBE2C gene specifically codes for a member of the E2 ubiquitin-conjugating enzyme. This protein allows for the destruction of mitotic cyclins, which is a necessary process for cells to leave mitosis and enter into cytokinesis. Overall, the function of UBE2C leads to cell cycle progression, therefore implicating it in cancer progression [70, 75, 76]. CRPC, an AI form of PCa is characterized by a shift from the transcription of genes involved in metabolism and biosynthesis to genes involved in cell cycle regulation. For example, an increase in transcription of UBE2C, involved in the degradation of mitotic cyclins, is observed in patients with CRPC. Specifically, the overexpression of AR-V7 is associated with an increase in transcription of UBE2C [70, 75, 76]. Therefore, targeting AR-V7 may be able to target the aggressive phenotype of CRPC by decreasing the transcription of these target genes associated with cellular proliferation.

Clinical Implications

The emergence of the AR-V7 splice variant has been shown to be clinically relevant in patients with CRPC and is one of the mechanisms by which resistance develops to current anti-androgen therapies. AR-V7 emerges through a process of mRNA splicing, [65-68] resulting in the truncation of the ligand-binding domain (LBD) from the full length AR. This renders current therapeutic compounds whose action depends on targeting this domain, ineffective. AR-V7 expression levels, determined via immunohistochemistry, have been shown to be elevated in more advanced and hormone resistant states of the disease after therapy with ADT's compared to more hormone naïve PCa's [78]. Similarly, expression of AR-V7 is elevated 20-fold in xenografts from patients that have received ADT, when compared to samples taken from hormone naïve PCa patients [71]. Four different studies have shown that AR-V7 has been detected in circulating tumor cells CTC's of PCa patients, where between 38-55% CRPC patients were determined as being AR-V7 positive [71-74]. Not only is AR-V7 expression increased in CRPC patients, but it has been shown that this increase is directly related to treatment with ADT's. For example, the percentage of patients expressing AR-V7 increases dramatically after treatment with the most recently approved ADT therapies, abiraterone and enzalutamide. One study has shown that after exposure to abiraterone and enzalutamide, the percent of patients expressing the AR-V7 splice variant increases from 12% to 67% [71]. Notably, patients who express AR-V7 in PCa have worse clinical outcomes compared to those patients who are AR-V7 negative in terms of biochemical recurrence (PSA-progression free survival), clinical, and or radiographic progression free survival, and overall survival [71-74]. This shows that expression of the AR-V7 splice variant is a major factor contributing to the development of resistance in CRPC, and agents that inhibit AR-V7 activity might be of therapeutic value.

AR-V Interactions with Coactivators

SRC1, and TIF2 are histone acetyltransferases and when they form protein-protein interactions with the AR, they recruit secondary co-activators that possess chromatin remodeling activity that allows for recruitment of the transcriptional machinery to promoters of AR target genes [58, 59]. These co-activators interact with the AF1 region found in the N-terminal domain of the AR [79-82]. This allows for these coactivators to bind to and interact with AR splice variants such as AR-V7. It was discovered by Claessens et al that TAU5 was the required interacting surface in the AR-NTD and is a prerequisite for p160 recruitment [79, 81, 82]. When TAU5 was deleted from the AR-NTD this prevented co-activation by SRC1 [79, 81, 82].

1.3 AR and its Role in Prostate Cancer

1.3.1 Functional Domains of the AR

The androgen receptor is a 110 kDa type I nuclear receptor located on chromosome Xq11-12, consisting of 2.7 kb gene which codes for a 919 amino acid protein. The AR is made up of 8 exons that are involved in the protein coding sequence of four functional domains [83] [84]. These are exon 1 which codes of the amino-terminal domain (NTD), exons 2 and 3 which encode the DNA binding domain (DBD), part of exon 4 which codes for the Hinge Region, and exons 4-8 which encode the COOH-terminal domain (CTD), containing the Ligand Binding Domain (LBD) [84]. The structure of both the AR-LBD in the CTD, and the DBD have been elucidated via crystal structure.

Amino-Terminal Domain

The AR-NTD is intrinsically disordered and is not structured in solution. Therefore, no crystal structure has been identified for this domain. The AR-NTD houses one of the transcriptional activation domains of the AR, activation function 1 (AF-1) [85].

DNA-binding Domain

The DBD of the AR is one of the most highly conserved regions between the different members of the steroid hormone nuclear receptor family. The AR's DBD consists of two zinc fingers which allows for homodimerization and binding to the DNA along androgen responsive elements (ARE's). The ARE's are characterized by a particular binding sequence, typically characterized by, 5'AGGTCANNNTGACCT3', and this binding allows for the receptor to regulate transcription of particular AR-target genes [86].

Hinge Region

The DBD is linked to the LBD via the hinge region. The hinge region contains the nuclear localization sequence (NLS) which allows for nuclear localization of the AR [86].

Ligand-Binding Domain

The LBD also contains a NLS, and DHT binding allows for the exposure of the nuclear localization sequences, and nuclear import of the AR. A nuclear export signal (NES), responsible for export of the AR from the nucleus to the cytoplasm in the absence of DHT is located between the DBD and hinge region [83, 86]. The AR-LBD also houses one of the transcriptional activation functions of the AR, activation function 2 (AF-2), which is implicated in transcriptional activity of the AR [84, 86]. Classical AR signaling in the cell (Figure 1 on pg. 28), involves androgens, such as dihydrotestosterone (DHT). In the absence of androgen, the AR is sequestered in the cytoplasm, bound to heat shock protein, Hsp90. Testosterone is converted to the more potent androgen, dihydrotestosterone by 5 α -reductase. DHT binding of the AR causes a conformational change of

the receptor, and leads to the dissociation of Hsp90. When bound by DHT, N/C interactions mediated by the FQNLF sequence in the AR NTD binding to the ligand-induced AF-2 surface in AR LBD occurs, and the NLS is exposed, allowing for the receptor to transverse the nuclear membrane and enter into the nucleus of the cell. There the AR dimerizes, binds ARE's along the genome, binds coactivators that recruit the general transcriptional machinery and leads to the transcription of AR target genes [84, 86-88]. PSA, as mentioned previously, is a serine protease synthesized by both benign and malignant prostate epithelial cells and used as a measure of PCa progression. PSA is a canonical target gene of the AR, and standard marker of AR's transcriptional activity in the cell. Serum PSA levels reflect AR signaling in the PCa cell as both are seen to increase in more advanced forms of the disease [89].

1.3.2 Transactivation Surfaces of the AR

The AR has two major transactivation surfaces that serve as binding surfaces involved in the interaction of co-regulatory proteins [79-82, 84, 85].

Activation Function 1 (AF-1) – Amino Terminal Domain

Activation function 1 (AF-1) is the binding surface present in the N-terminal domain of the receptor. Although this surface is intrinsically disordered, specific regions within this range have been mapped according to their transactivation abilities [85]. This mapping was done by deletion analysis. The sub-regions within the AF-1 are termed TAU1 and TAU5. TAU1 is mapped to amino acid residues 101-370, and TAU5 is mapped to amino acid residues 360-485 [79, 81, 82, 85]. The minimum region that is necessary to produce the full AR-NTD based transcriptional activity is located between residues 142-485, which contains regions of TAU1, and all of TAU5, with TAU5 characterized as being necessary for p160 coactivator recruitment [79, 81, 82]. It's been shown

that the AF-1 region of the AR is ligand-independent, as the AR-NTD is able to be transcriptionally active even in the absence of androgen. The AR-NTD is able to activate reporter genes even when the ligand-binding domain is truncated and is able to achieve reporter activity to the same degree as the full-length receptor, and in the presence of ligand. Therefore, the AR AF-1 regions is deemed as the ligand-independent activation function [79-82].

Activation Function 2 (AF-2) - Carboxy-terminal Domain

Activation function 2 (AF-2) is the binding surface present in the C-terminal domain of the receptor [90]. Upon DHT binding to the AR-LBD, helix 12 completes the AF-2 binding surface [90]. This surface allows for AR's interaction with coactivators and corepressors that affect the transcriptional activity of the AR. The AR AF-2 surface can also interact intramolecularly with motifs such as ²³FQNLF²⁷, and ⁴³³WHTLF⁴³⁷, present in the AR-NTD. The AR-NTD competes with coregulators with similar interacting motifs such as those with LXXLL and/or FXXLF motifs, in its binding to AR AF-2. This intramolecular interaction stabilizes ligand binding to AR and prevents the AR from nuclear export and degradation [90-93].

1.3.3 AR Coactivators

Coactivator Expression in CRPC

Elevated expression levels of several AR coactivators have been associated with CRPC [94], [95], [96], [97], [98]. This is because AR coactivators have the ability to activate AR's transcriptional activity even under castrate conditions, or conditions of exceedingly low levels of androgens [98]. One family of coactivators implicated in PCa progression includes that of the ARA family. The ARA coactivators have been shown to regulate transcriptional activity of the AR;

albeit, they are not AR-specific. ARA55 is one example of those belonging to this family of coactivators that contributes to tumor progression by regulation of Wnt signaling [62]. ARA55 is a transforming growth factor-beta inducible coactivator, and is also crucial for facilitating stromal epithelial interactions in benign and malignant prostate [62]. ARA54 is also a coactivator which mediates growth and differentiation through interaction with the AR [63]. The beta isoform an AR coactivator ARA70 has been shown to be up-regulated in PCa. ARA70 has multiple functions in prostate cancer; however, it is established that this coactivator also regulates activity of other steroid receptors [99].

Vav3 is another such coactivator that enhances both WT AR, and AR splice variant, AR-V7. Vav3 is a Rho GTPase guanine nucleotide exchange factor. It's been shown that expression of vav3 becomes elevated during the progression to castration therapy resistance. Furthermore, the overexpression of vav3 in LNCaP cells abolished requirement for androgens in cell growth [61]. Next, there is Tip60, which is another coregulatory that is upregulated by androgen ablation in PCa cell lines. It's also involved with AR-mediated proliferation of cells in the absence of androgens [100]. The next group of coactivators includes the transcriptional integrators CBP/p300. These are coactivators who modulate a large number of transcription factors through chromatin remodeling. Both CBP and p300 expression is increased during androgen ablation [101]. Finally, FHL2, is an androgen regulated coactivator that is important in regulation of proliferation, in particular in castration resistant PCa [102]. FHL2 is important for activation of both AR-FL and AR-V7 splice variant. It's shown that a higher nuclear expression of FHL2 predicts risk of prostate cancer recurrence [102].

The p160 family of coregulators comprise another such group of coactivators that are implicated in CRPC and are shown to interact with AR-splice variants, such as AR-V7 [79, 80]. P160's consist

of SRC1, SRC2, and SRC3, which all show sequence homology and possess histone acetyltransferase activity [59]. This family of proteins ultimately enhance AR-induced transcription by allowing for complex formation between AR and promoter regions of AR target genes [59]. Cumulative evidence suggests that elevated TIF2 expression might be especially relevant to CRPC; TIF2 stabilizes AR-ligand binding, enhances receptor stability, facilitates AR N/C interactions, and promotes both the recruitment of chromatin remodeling coactivators and assembly of the transcriptional machinery on the promoters of AR target genes [103], [104]. Furthermore, there is a significant correlation between tumor TIF2 expression and PCa aggressiveness [49], [105]. Also, in comparison to benign prostatic hyperplasia tissue or androgen-dependent PCa, TIF2 levels are significantly elevated in relapsed PCa after ADT [96]. Finally, over-expression of TIF2 enhanced AR responses to androgens and non-AR ligands, whereas TIF2 knockdown reduced AR target gene expression and inhibited the growth of androgen-dependent and androgen-independent PCa cells [96], [49]. Similarly, SRC1 is found to be expressed in more advanced forms of prostate cancer compared to levels found in localized PCa or normal prostate tissue, and expression of SRC1 in clinically localized samples were associated with a more aggressive disease [106]. It has also been shown that silencing SRC1 reduced growth in AR-dependent cell lines, LNCaP, and C4-2, as well as decreased androgen receptor target gene activation [106]. SRC1 is shown to increase both ligand-dependent, and ligand-independent transactivation of the AR to the same degree.

Coactivator Interaction with AR

Coactivators bind to either of two activation functions in the AR, AF-2 or AF-1.

Coactivator interaction with AF-2 binding surface

AF-2, located in the C-terminal domain of the receptor, binds coactivators with an LXXLL containing motif [90-93]. AF-2 is the more canonical binding surface that is also present in other steroid hormone receptors (SHR's). For most NR's, this is the most important binding surface for transcriptional activation [90-93].

Coactivator interaction with AF-1 binding surface

AF-1 resides in the N-terminal domain of the receptor, and tends to bind coactivators with non-canonical motifs. Since the AF-2 region has been truncated in AR splice variants like AR-V7, coactivators must bind to the AF-1 region. It has been shown that for the AR, the AF-1 transactivation domain located in the AR-NTD, is also an important coactivator binding surface, leading to transcriptional activation [79-82]. Some coactivators that have been shown to interact with the AR-NTD at the AF-1 surface are p160's SRC1, and TIF2. The AR AF-1 domain contains Tau-1 and Tau-5 regions. Tau-1 and Tau-5 regions are both required for AR transcriptional activity [79-82]. Tau-5 is characterized by a WHTLF motif, which represents a binding motif for p160 coactivators [67, 79, 80].

1.3.4 AR Target Gene Activation

AR-FL is most commonly involved in activating a set of genes responsible for prostate cell proliferation, communication, biosynthesis and differentiation. As well as steroid synthesis, and ultimately cancer progression. There are different transcriptional profiles associated with androgen dependent (AD) and androgen independent (AI) PCa. Some of the most common genes targeted in AD PCa include PSA/KLK3 and KLK2, serine proteases, NKX3.1, an androgen-regulated gene, and prostatic tumor suppressor gene [26], TMPRSS2, a gene that is seen to fuse with ETS genes which acts as a driver of PCa [27], FKBP5, involved in protein folding and transport and

trafficking, and TMEPA1 [107], [108]. Those transcriptional profiles associated with AI PCa, or CRPC include E2F, STAT, and MYC. In CRPC tissue, it's been shown that there is a higher AR binding enrichment at the promoters of target genes compared to binding sites in untreated PCa tissue. These genes are involved in cell proliferation, and regulation of progression through cell cycle [109].

1.4 Objectives and Hypothesis

Existing FDA approved PCa drugs target the AR-LBD, either in a direct or indirect manner. Currently, there are no compounds that block or disrupt the AF-2 or AF-1 regions of the receptor. The AF-2 region of AR is important because it engages in coactivator interactions and leads to androgen dependent transcriptional activity. The AF-1 region is important because it's the region of the AR involved in androgen independent transcription. Furthermore, the AF-1 domain is the only transactivation region present in LBD lacking AR splice variants whose emergence coincides with the development of CRPC after ADT therapy. Therefore, a compound able to target either or both transactivation regions would represent an untapped therapeutic strategy that might avoid the development of resistance observed with current ADT's.

Our lab has developed an AR-TIF2 biosensor HCS assay that can identify compounds that can prevent or disrupt interactions between the DHT-induced AF-2 region of AR and its coactivator, TIF2. We then developed a panel of AR AF-2 based assays to further determine the mechanism of action of these compounds identified in an HCS campaign of 143,000 compounds screened in the AR-TIF2 biosensor assay. The AF-2 assays include an AR-LBD H³-DHT Radioligand Binding assay, AR-LBD::TIF2-LXXLL peptide binding assay, a PSA6.1 luciferase

reporter assay, and TIF2 and SRC1 Mammalian 2-hybrid assays. In addition, we conducted PCa growth inhibition assays in AR positive and AR null cell lines.

We also wanted to address the emergence of AR splice variants, since they represent a mechanism of disease progression, resistance and persistent AR activity in CRPC cells after ADT treatment. To do this we developed a series of assays to identify compounds that inhibit or disrupt the AF-1 surface of the androgen receptor. These assays include a pGal4-AR-NTD transactivation assay, and two reporter assays driven by AR-V7, the PSA6.1-Luc and UBE2C-Luc reporter assays. The AF-1 assays can be used to determine if the hits identified in the primary HCS are also capable of modulating AR-NTD transactivation.

A compound that could target both the AF-2 and AF-1 transactivation regions to prevent the transcription of both AR-FL and AR-V7 would be the ideal type of drug candidate, providing a dual approach to the treatment of PCa and the emergence of CRPC.

Hypothesis We believe that small molecule inhibitors with the ability to block or disrupt androgen receptor interactions with the TIF2 p160 coactivator will provide effective therapies against more advanced forms of PCa by decreasing AR transcriptional activity. Compounds that inhibit or disrupt both the AF-2 and AF-1 transactivation domains of AR would have therapeutic potential for both the androgen dependent and independent forms of PCa.

Objectives

- (Chapter 3) Develop a suite of AF-2 directed assays to help characterize small molecule inhibitors/disruptors of AR-TIF2 PPIs identified in the primary AR-TIF2 biosensor HCS campaign
 - 1) AR-LBD H³-DHT RadioligandBinding Assay
 - 2) AR AF-2:: TIF2-LXXLL peptide binding ALPHAScreen Assay
 - 3) Mammalian 2-Hybrid Assay developed with both TIF2 and SRC1

- 4) PSA6.1-Luc Reporter-Based Assay in PC3-GFP-AR-FL cells
 - 5) Growth Inhibition assays developed in 5 different cell lines
- Test compounds that are known AR-modulators through the suite of AF-2 characterization assays

- (Chapter 4) Develop a suite of AF-1 directed assays to determine whether AR-TIF2 PPI prioritized hits can also block or disrupt AR-NTD's transcriptional activity in cells
 - 1) pGal4-AR-NTD Transactivation Assay
 - 2) PSA6.1-Luc Reporter Assay in PC3-GFP-AR-V7 cells
 - 3) UBE2C-Luc Reporter Assay in PC3-GFP-AR-V7 cells
- Test compounds that are known AR-modulators through the suite of AF-1 characterization assays

- (Chapter 5) Characterize Selected Hits Identified in 143,000 compound Primary AR-TIF2 PPIB HCS campaign in the suite of AF-2 and AF-1 profiling assays

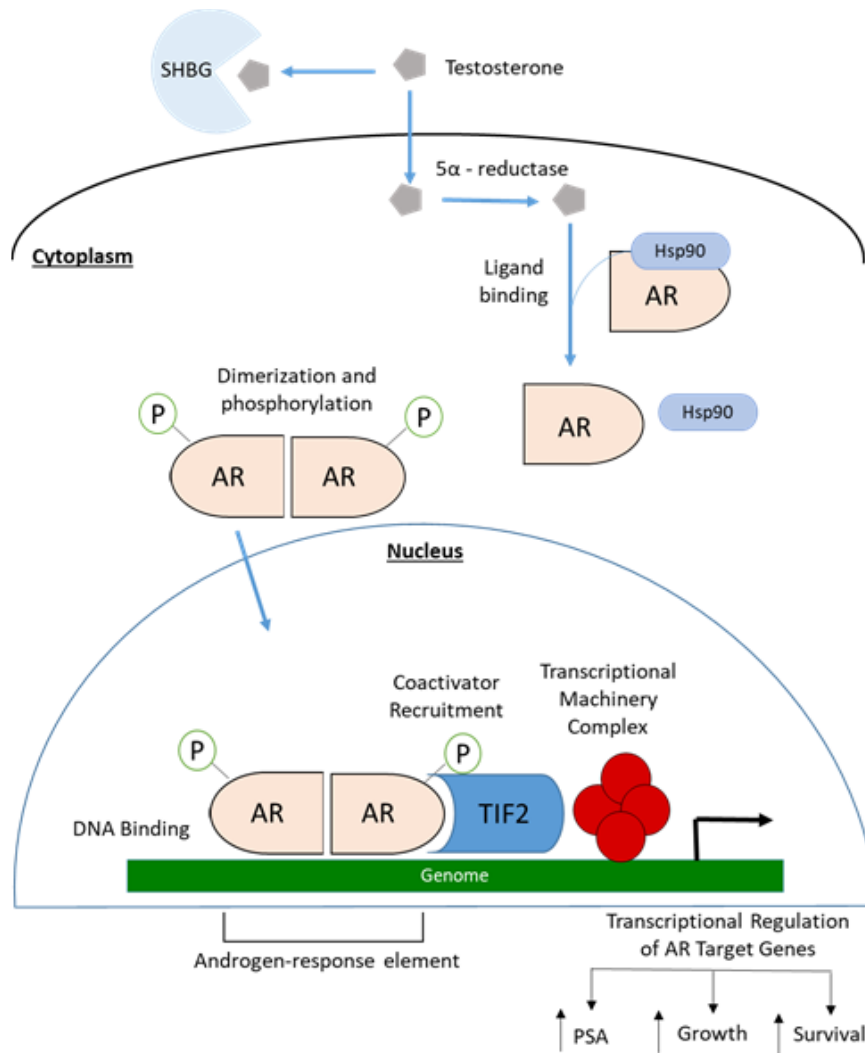


Figure 1. Androgen receptor signal transduction pathway

DHT binding to the AR induces dissociation from HSPs and receptor phosphorylation. Next, the AR dimerizes and can bind to androgen-response elements in the promoter regions of target genes. Coactivator recruitment by the AR complex allows for its interaction with the general transcriptional apparatus (GTA). Subsequent activation of target genes leads to biological responses including growth, survival and the production of PSA, a biomarker of disease progression.

2.0 Identification of Hit Compounds Targeting the AR AF-2 Interaction Surface

2.1 Introduction

Prostate cancer's progression into CRPC is due to continued androgen receptor (AR) transcriptional activity in cells [110]. The primary therapy for PCa is androgen deprivation therapy (ADT) which targets AR functions by blocking the production of androgen ligands or by antagonizing AR binding. Although ADT drugs are effective initially, ultimately patient's progress to a castrate resistant state [48, 111]. This progression is due to continued AR signaling after ADT, due to AR amplification, intra-tumoral androgen synthesis, AR mutations that lead to receptor promiscuity, the emergence of AR splice variants, and androgen-independent AR activation [48, 66, 111]. Furthermore, most cases of CRPC are accompanied by overexpression of AR coactivators, which lead to poor patient outcomes by increasing AR-transcriptional activity [103, 112] of target genes associated with cellular biosynthesis, survival, and proliferation, leading to disease progression [113]. Therefore, therapeutics that block AR-transcriptional activity represent an alternate strategy for slowing the progression of CRPC [46, 114]. One way to inhibit AR's transcriptional activity would be to block the recruitment of the transcriptional machinery to target gene AREs by preventing or disrupting the interactions between AR and its co-activators [56, 94-97, 115]. Elevated expression levels have been observed in relapsed PCa for several AR coregulators, including TIF2, SRC1, RAC3, p300, CBP, Tip60, MAGE-11, and ARA 70 [49, 56, 94-98]. AR-transcriptional intermediary factor 2 (TIF2/SRC-2/NCoA-2/GRIP1) protein-protein interactions (PPIs) are promising targets for CRPC because TIF2 overexpression occurs in more advanced stages of PCa compared to benign prostate tissue, and increased TIF2 levels correlate

with biochemical recurrence, and a rise in prostate specific antigen (PSA) levels in PCa patients. Similarly, knockdown of TIF2 by siRNA reduced AR target gene expression and slowed the proliferation of androgen-dependent and androgen independent PCa cells [96]. The AR interacts with TIF2 through the hydrophobic activation function 2 (AF2) region formed by helix 12 of the androgen receptor ligand binding domain (AR-LBD) when dihydrotestosterone (DHT) is bound [79, 116]. TIF2 modulates AR-transcriptional activity and its overexpression has been shown to result in cellular resistance to AR antagonists such as bicalutamide [117]. Therefore, our lab has developed a high-content screening (HCS) assay to identify small molecules that inhibit the formation of agonist-induced AR-TIF2 PPIs or disrupt preexisting AR-TIF2 complexes [118, 119]. A detailed description of the development, optimization, and validation of the AR-TIF2 PPIB HCS assay together with suitable counter screens has been described in our previous publications [119-126].

In this chapter I will describe how we identified the hit compounds that were to be run in the characterization assays that I developed (discussed in chapters 3 and 4). I will briefly describe the implementation of the AR-TIF2 PPIB assay to screen the Library of Pharmacologically Active Compounds (LOPAC) and to screen three larger compound libraries totaling 143,000 compounds. I will also provide descriptions of the counter screens that were used to triage the actives from the primary HCS to generate a hit list, made up of concentration dependent compounds that were active in the primary screen and inactive in the counter screens. The confirmed hit compounds along with commercially available structurally related analogs progressed into the characterization assays that were developed to target either the AF-2 or AF-1 transactivation domains of AR (described in detail in chapters 3 and 4).

2.2 AR-TIF2 Biosensor High Content Screen

2.2.1 Description of the AR-TIF2 Biosensor

The AR-TIF2 PPIB HCS assay utilizes two adenovirus constructs to express AR-LBD residues 662–919 in one biosensor component, and TIF2 residues 725–840 in the other biosensor component. AR-LBD was cloned into an adenovirus expression biosensor construct which drives its expression as a chimeric fusion protein with red fluorescent protein (RFP) that contains both a nuclear localization sequence (NLS) and a nuclear export sequence (NES), which are part of the chimera and not specific to AR (Figure 2, on pg. 48). In cells infected with the AR-RFP biosensor alone, AR-RFP expression is localized predominantly to the cytoplasm. However, after exposure to AR agonists such as DHT, the subcellular localization of the AR-RFP shifts to a predominantly nuclear distribution (Figure 2). The TIF2 insert contains the receptor interacting domain box III LXXLL motif that mediates binding to ligand-bound AR-LBD. The TIF2 residues are expressed as a chimeric fusion protein with green fluorescent protein (GFP) and high-affinity nuclear localization (NLS) and nucleolar localization (NoLS) sequences derived from HIV Rev, which tethers the TIF2-GFP biosensor in the nucleolus of the cell (Figure 3, on pg. 49) [127]. In cells infected with the TIF2-GFP biosensor alone, TIF2-GFP expression is restricted to the nucleolus within the nucleus. The nucleolar localization of the TIF2-GFP biosensor remains constant and does not change when exposed to AR agonists, antagonists or test compounds (Figure 3). In cells that are co-infected with both AR-RFP and TIF2 biosensors, TIF2-GFP expression is localized only in the nucleoli and AR-RFP expression is predominantly cytoplasmic – as is shown by images of the cells, red present in the cytoplasm, and blue Hoechst-stained nuclei containing bright green TIF2-GFP puncta (Figures 4 & 5, on pgs. 50 & 51). After exposure of cells co-infected with both

biosensors to DHT, the AR-RFP biosensor traffics from the cytoplasm into the nucleus where the PPI's between the AR and TIF2 components of the fusion proteins causes them to co-localize within the nucleoli, as indicated in the images by the bright yellow AR-TIF2 puncta present in the nucleoli (Figures 4 & 5) [127].

To quantify AR-TIF2 PPIs, digital images of the cells were acquired on an IXM imager, and then analyzed with a translocation enhanced TE image analysis module as described in previous publications [118, 119, 121-123]. The TIF2-GFP biosensor component acquired in the FITC channel was used to create a translocation mask of the nucleoli within Hoechst-stained nuclei. The TIF2-GFP remains localized to bright fluorescent puncta anchored within the nucleolus, and objects in Ch2 that had TIF2-GFP fluorescent intensities above background with appropriate morphologic characteristics (width, length, and area) were classified by the image segmentation as nucleoli and used to create a TIF2 mask and count the number of TIF2-GFP-positive nucleoli (Figure 6, on pg. 52). Objects that met these criteria were used to create masks of the nucleoli within the Hoechst-stained nuclei of each cell. AR-RFP images from the Texas Red channel were segmented into an “Inner” nucleolus region with a mask set using the edge of the detected TIF2-GFP-positive nucleoli in the FITC channel (Figure 6). The TE image analysis module outputs quantitative data such as the average fluorescence intensities of the TIF2-GFP-stained objects in the FITC channel; the selected object or nucleoli count in the FITC channel; and the integrated and average fluorescent intensities of the AR-RFP signal in the TIF2-positive nucleolus (inner) region. The mean average inner fluorescent intensity (MAIFI) of AR-RFP within the TIF2-GFP-positive nucleolus output of the TE image analysis module was used to quantify AR-TIF2 PPIs.

The sub-cellular distribution phenotype of the AR-RFP “prey” biosensor is influenced by two major factors, whether the cells have been exposed to AR agonists, demonstrated by the nuclear

translocation of AR-RFP in the presence of increasing concentrations of DHT (Figure 7, on pg. 53), and the presence of the TIF2-GFP “bait” protein in the nucleolus. In the AR-TIF2 PPIB LOPAC pilot screen and the 143K HCS campaign the assay was conducted in two formats (Figure 4). In the first format U-2 OS cells co-infected with the AR-TIF2 biosensors were exposed to compound 3h before treatment with 25 nM DHT for 90 min. This allowed us to determine if compounds inhibited DHT-induced AR-TIF2 PPI formation. In the second format U-2 OS cells co-infected with the AR-TIF2 biosensors were exposed to 25 nM of DHT for 90 min before treatment with compounds for 3h. This allowed us to determine if compounds disrupted preexisting AR-TIF2 PPI complexes (Figures 4 & 5).

We also developed the AR-TIF2 biosensor assay in PC3's, a PCa cell background that could capture disease relevant expression levels of AR coactivators and corepressors. It's been shown that small molecules can elicit tissue selective effects, because the cells of distinct tissues express different levels and cohorts of coregulatory proteins [115, 128-130]. Reconfiguring the AR-TIF2 PPI biosensor (PPIB) assay in the PC3 PCa cell line therefore allowed us to determine whether AR modulators and hits from an AR-TIF2 PPIB screen conducted in U-2 OS cells would behave differently in the PCa cell background. We did not observe any significant differences in the compound responses between the assays performed in osteosarcoma and PCa cells. However, compared with the AR-TIF2 PPIB assay performed in U-2 OS cells [131], PC3 cells required 10-fold more rAV for infection, the maximum co-infection rate achieved was only ~50%, and we needed to seed 2.4-fold more PC3 cells per well in the 384-well assay plates. From a purely logistical standpoint therefore, the AR-TIF2 PPIB assay performed in U-2 OS cells would be more amenable to screening, because both the virus and cell culture demands are lower [118].

After determining whether compounds run in the AR-TIF2 biosensor were active or inactive, we needed a way to remove outliers that included compounds that were cytotoxic or fluorescent, or those that acted in the AR-TIF2 biosensor in a non-specific, or non-selective manner. To flag and eliminate such compounds, the following methods and counter screens were applied.

2.2.2 Identifying cytotoxic compounds and auto-fluorescent outliers

In order to identify cytotoxic and auto-fluorescent outlier compounds, a z-score plate-based statistical scoring method was applied to flag compounds that behaved as outliers, compared to the other substances tested on the plate. These outlier analyses were performed on an $n = 320$ compounds, as no controls were used in these analyses. These analyses were run based on certain HCS multiparameter measurements by the image analysis module, $Z - \text{score} = (X_i - \overline{X})/\sigma$, where X_i is the raw measurement on the i th compound, and \overline{X} and σ are the mean, and standard deviation of all the sample measurements on a plate. The number of compartments that represents the number of TIF2-GFP-positive nucleoli identified in the FITC channel was used to flag compounds that were cytotoxic. Compounds with z-scores < -3 were flagged as cytotoxic. We also calculated z-scores for the average and integrated fluorescence intensity parameters from the DAPI, FITC, and Texas Red channels, and compounds with z-scores > 3 in one or more of the intensity parameters in any channel were flagged as fluorescent outliers.

2.3 Description of Counter Screening Assays to Run hits from the AR-TIF2 Biosensor

2.3.1 P53-hDM2 PPIB Counter Screening Assay

The p53-hDM2 PPIB HCS assay was used as a counter screen to determine if compounds identified in the AR-TIF2 PPIB interfered with the assay format or were non-specific PPI disruptors. The p53-hDM2 PPIB counter screen uses the same adenovirus chimeric biosensor co-infection assay format and PPI detection strategy in U-2 OS cells as the AR-TIF2 assay, except that the protein-interacting partner components of the chimeric GFP and RFP fusion protein biosensors contain the interacting domains from p53 and hDM2, respectively [121-123]. The p53-hDM2 PPIB assay therefore serves as both an assay format interference and PPI selectivity counter screen [118].

2.3.2 AR Nuclear Localization Counter Screen

The AR-GFP nuclear localization assay was used as a counter screen to identify compounds that reduced expression levels of AR, and/or shifted the predominant nuclear localization of AR into the cytoplasm [124]. If compounds were reducing nuclear expression levels of AR, or shifting localization of AR to the cytoplasm in the AR-GFP nuclear localization counter screen, they could also be reducing AR-RFP biosensor expression levels, or promoting AR-RFP nuclear exit, and therefore inhibiting the AR-TIF2 PPI's in the AR-TIF2 HCS assay in an indirect manner. Therefore, any compounds identified in this assay would be deprioritized.

2.3.3 Dex-Induced GR Translocation Counter Screen

The dexamethasone induced GR-GFP nuclear translocation assay was used as a counter screen to identify compounds that potentially inhibited shared elements of nuclear receptor trafficking to the nucleus [125]. This assay was also used to determine if compounds were able to target other nuclear receptors and were therefore non-selective for the androgen receptor. Confirmed actives in the AR-TIF2 PPIB assay that also inhibit GR nuclear translocation either lack AR specificity or selectivity, or they may inhibit a shared trafficking component of the AR and GR signaling pathways.

2.4 AR-TIF2 PPIB Assay Protocol

In the AR-TIF2 PPIB HCS assay protocol, rAV expression constructs bearing the individual TIF2-GFP (TagGFP; Evrogen, Inc., Moscow, Russia) and AR-RFP (Tag RFP; Evrogen, Inc.) PPI partners were utilized to infect U-2 OS cells according to the manufacturer's (Cyprotech US, Watertown, MA) instructions. Typically, 1×10^6 U-2 OS cells were co-infected with the TIF2-GFP and AR-RFP adenovirus expression constructs by incubating cells with the manufacturer's recommended volume of virus (usually 5 uL/ 10^6 U-2 OS cells) in 1.0 mL of culture medium for 1 h at 37C, 5% CO₂, and 95% humidity with periodic shaking (every 10 min) to maintain cells in suspension. Co-infected cells were then diluted to 6.25×10^4 cells/mL in culture media, and 40 uL (2,500 cells) was seeded in each well of a 384-well collagen-coated barcoded microplate (#781956; Greiner Bio-One) using a Matrix pipettor (ThermoFisher), and plates were incubated overnight at 37C, 5% CO₂, and 95% humidity. Pre-diluted compounds or DMSO (5 uL) were

added to appropriate wells using the Janus MDT automated liquid handling platform (Perkin Elmer), for a final screening concentration of 50 μ M and 0.2% DMSO. Compound-treated assay plates were incubated at 37C, 5% CO₂, and 95% humidity for 3h min, pre- or post- 90 min treatment with DHT. DHT (5 uL) was added to maximum plate control wells and compound-treated wells, and 5 uL of media was added to minimum plate control wells using a Matrix pipettor (ThermoFisher), for a final DHT concentration of 25 nM. After treatment with compound and DHT, assay plates were fixed by the addition of 50 μ L of pre-warmed (37°C) 7.4% formaldehyde and 2 mg/mL Hoechst 33342 in PBS using a Matrix pipettor (ThermoFisher) and incubated at room temperature for 30 min. Liquid was then aspirated and plates were then washed twice with 85 uL PBS using a Matrix pipettor (ThermoFisher) and sealed with adhesive aluminum plate seals, with the last 85 uL wash of PBS in place. Fluorescent images were then acquired on an IXU automated HCS platform (Molecular Devices LLC), and images were analyzed with the TE image analysis module of the MetaXpress software (Molecular Devices LLC) as described in our previous publications [118, 127, 131].

2.5 Compound Libraries Screened in Primary and Counter Screens

Four compound libraries were screened in the AR-TIF2 PPIB HCS including: A Library of Pharmaceutically Active Compounds (LOPAC) set (Sigma Aldrich) [118, 131], a 10K non-peptide peptido-mimetic library (ChemDiv), a 50K diversity library (ChemBridge), and a 83K library selected for cancer drug screening (NCI) [127].

The LOPAC set is comprised of 1,280 pharmaceutically active compounds that show biological activity towards some of the most common targets in drug discovery. The LOPAC set is frequently used to validate new drug discovery assays such as the AR-TIF2 PPIB HCS assay.

The 10K non-peptide peptido-mimetic library (ChemDiv) was specifically designed with PPI targets in mind. This is a diversity subset of the ChemDiv 142K PPI library that includes mimetics of α -helices and β - and γ - turns based on many combinatorial templates modified with both flexible and rigid substituents. The geometry of the designed fragments was compared computationally with the dihedral angles reported for 'natural' β - and γ - turn motifs to select for the best match.

The 50K diversity library (ChemBridge) was selected from the ChemBridge 410K core library. It was designed to provide the widest coverage of pharmacophore space within 50K compounds while still maintaining structural diversity. Compounds were filtered for enhanced physiochemical properties while allowing exploration of available chemical space, and the rule of five was applied to each of the compounds.

The 83K library selected for cancer drug screening (NCI) was specifically assembled for anti-cancer drug screening and contains a 12K legacy set selected from the NIH MLSMR collection and two diversity subsets that contain 15 privileged scaffolds.

Compounds from each of these libraries were run in the AR-TIF2 biosensor at one concentration in singlicate to determine activity. If they were able to produce inhibition of $\geq 45\%$ for the 10K library or $\geq 40\%$ for the other two libraries, and were not cytotoxic or fluorescent, they were cherry picked, and confirmed in the AR-TIF2 PPIB at one concentration in triplicate and run in three developed counter screening assays. Confirmed actives that passed this testing paradigm

were progressed into concentration response assays to determine their relative potencies and efficacies at inhibiting/disrupting AR-TIF2 PPIs.

2.6 Results

2.6.1 LOPAC Set Performance in the AR-TIF2 HCS and Counter Screen Assays

To confirm that the optimized AR-TIF2 PPIB assay would perform well in the presence of compounds, we screened the 1,280-member LOPAC at 20 μ M to identify compounds that could either inhibit the DHT-induced formation of AR-TIF2 PPIs or disrupt preexisting AR-TIF2 complexes. Although the majority of compounds exhibited AR-TIF2 PPI responses that coincided with those of the Max controls, indicating that they were inactive, 24 compounds achieved $\geq 50\%$ inhibition of DHT-induced AR-TIF2 PPI formation (g, on pg. 54) compared with only three compounds that disrupted preexisting AR-TIF2 complexes by $\geq 50\%$. An additional 13 compounds disrupted preformed AR-TIF2 complexes by $\geq 30\%$ (Table 1). To qualify compounds flagged as actives in either format, we used parameters output by the image analysis algorithm to identify and eliminate compounds that were acutely cytotoxic (z -score cell counts < -4) or that were average of integrated fluorescent intensity outliers (z -scores < -4 or > 4) in the Hoechst (Ch1), GFP (Ch2), and RFP (Ch3) channels. Any active compounds that were not eliminated were cherry picked the compounds flagged as inhibitors of AR-TIF2 formation ($> 50\%$) or disruptors of preexisting AR-TIF2 complexes ($> 30\%$) into a 384-well hit confirmation daughter plate and rescreened them at 20 μ M in triplicate wells in both assay formats. A total of 17 compounds were confirmed to reproducibly inhibit the DHT-induced formation of AR-TIF2 PPIs by $\geq 50\%$ at 20 μ M. Eleven of

the inhibitors are known modulators of steroid family nuclear hormone receptors (NRs): nilutamide and cyproterone acetate are antiandrogens; mifepristone, 17 α -hydroxy-4-pregnene-3,20-dione, and allopregnan-3- α -ol-20-one are progesterone receptor (PR) modulators; spironolactone and cortexolone are mineralocorticoid receptor (MR) modulators; 2-hydroxyestradiol 2-methyl ether and estrone are estrogen receptor (ER) modulators; guggulsterone is a farnesoid X receptor (FXR) antagonist; and budesonide is a glucocorticoid receptor (GR) modulator (Figure 9, on pg. 56). The remaining six inhibitors are not NR ligands (Figure 8, on pg. 55): 1-chloro-3-tosylamido-4-phenyl-2-butanone (TPCK), Bay 11-7085, N-Carbobenzyloxy-L-phenylalanyl chloromethyl ketone (ZPCK), parthenolide, 4-phenyl-3-fluoroxane carbo-nitrile, and (\pm) Bay K 8644. Although none of the qualified actives achieved $\geq 50\%$ disruption of preexisting AR-TIF2 complexes, nine compounds were confirmed to reproducibly disrupt preformed AR-TIF2 PPIs by between 32% and 42% at 20 μ M. Five compounds inhibited DHT-induced formation of AR-TIF2 PPIs by $\geq 50\%$ and also disrupted preformed AR-TIF2 PPIs by $\geq 34\%$ at 20 μ M.

To determine the potencies of actives confirmed in triplicate, in the two AR-TIF2 PPIB assay formats, we purchased dry powder samples for 15 compounds and conducted three independent 10-point concentration–response experiments starting at a maximum of 50 μ M (Figure 8, on pg. 55). Exposure of U-2 OS cells to the indicated concentrations of the 15 compounds for 3 h before treatment with 20 nM DHT inhibited AR-RFP translocation into TIF2-GFP-positive nucleoli in a concentration-dependent manner with IC_{50} s ranging from 12 nM to 3 μ M. The five non-NR ligand AR-TIF2 PPI inhibitors exhibited high-quality curve fits with IC_{50} s in the 0.5–1.0 μ M range. Five of the NR ligand AR-TIF2 PPI inhibitors also produced high-quality curve fits with IC_{50} s in the 0.7–3.0 μ M range: 17 α -hydroxy-4-pregnene-3,20-dione,

nilutamide, cortexolone, 2-hydroxyestradiol 2-methyl ether, and estrone (Figures 8 & 10 on pg. 57). However, the activity of the other five NR ligand AR-TIF2 PPI inhibitors was not $\leq 50 \mu\text{M}$ in the concentration range tested, and their corresponding IC_{50}s were extrapolated from incomplete curve fits: mifepristone, guggulsterone, spironolactone, budesonide, and cyproterone. The corresponding AR-RFP distribution phenotypes for some of these NR ligand AR-TIF2 PPI inhibitors were also less definitive. Guggulsterone displayed a predominant cytoplasm AR-RFP distribution phenotype, whereas both spironolactone and budesonide produced a diffuse AR-RFP nuclear distribution phenotype. However, the other NR ligand AR-TIF2 PPI inhibitors exhibited a mixed and diffuse AR-RFP distribution phenotype in both the cytoplasm and nuclear compartments. Exposure of U-2 OS cells to the indicated concentrations of compounds for 3 h after a 30 min pretreatment with 20 nM DHT disrupted the preexisting AR-TIF2 complexes in a concentration-dependent manner. Although none of the compounds achieved $>90\%$ disruption of the preformed AR-TIF2 complexes and their corresponding IC_{50}s were typically ≥ 10 -fold less potent than for the inhibition of DHT-induced AR-TIF2 PPIs, these data indicate that the AR-TIF2 biosensor is reversible. All 10 disruptors of preexisting AR-TIF2 complexes produced a mixed and diffuse AR-RFP distribution phenotype in both the cytoplasm and nuclear compartments.

When we ran the compounds in the developed counter screens none of the 15 AR-TIF2 PPI LOPAC hits were active in the p53-hDM2 PPIB assay, indicating that they are unlikely to interfere with either the biosensor assay format or to be non-selective PPI inhibitors. To evaluate the NR selectivity of the AR-TIF2 PPI LOPAC hits, we tested their activity in a dexamethasone (Dex)-induced glucocorticoid receptor (GR) nuclear translocation assay [132, 133]. Since none of the 10 steroid NR ligands inhibited Dex-induced GR nuclear translocation [132, 133] these AR-TIF2 PPI hits appear to be selective for AR over GR. In contrast, the five non-steroid hits all

inhibited the agonist-induced trafficking of GR to the nucleus. Finally, when run in the AR nuclear localization counter screen, the AR-TIF2 PPIB hits from the LOPAC set either enhanced AR-GFP nuclear localization or were inactive, suggesting that some hits were partial AR agonists and therefore would not be expected to inhibit or disrupt AR-TIF2 PPIs [118].

We were able to use the LOPAC set as a pilot screen to confirm that the AR-TIF2 PPIB performed well in HTS and to prove that our testing paradigm would effectively identify and eliminate false positives or interference compounds.

Therefore, we then screened 143,000 compounds, from three larger compound libraries previously described in the AR-TIF2 PPI biosensor [127]. These compound libraries were specifically chosen to increase the structural diversity of compounds run in the AR-TIF2 PPI HCS to increase the probability of success. Compound performance in the AR-TIF2 PPIB assay, and hit confirmation is described below.

2.6.2 143,000 Compound Performance in the AR-TIF2 PPIB and Counter Screen Assays

2.6.2.1 HTS performance and QC statistics of AR-TIF2 PPIB

We successfully implemented the AR-TIF2 PPIB assay in an HCS campaign of 143,000 compounds from three distinct compound libraries. The AR-TIF2 PPIB assay performed robustly and reproducibly throughout the primary HCS campaign which enabled us to identify compounds that inhibited DHT-induced AR-TIF2 PPI formation and disrupted preexisting AR-TIF2 PPIs. Our assay QC statistics were based on the maximum plate control wells (n=32), and minimum plate control wells (n=32), on each assay plate. Maximum plate control wells were in columns 1 and 2 and were exposed to 25 nM DHT and 0.25% DMSO, and minimum plate control wells (n=32) were in columns 23 and 24, and were treated with 0.25% DMSO. In the format to find inhibitors

of AR-TIF2 PPI formation, the mean Z' -factor coefficient was 0.71 ± 0.08 ($n = 451$) and the mean S:B ratio was 7.8 ± 1.1 ($n = 451$). Similarly, in the format to find disruptors of preexisting AR-TIF2 PPI complexes, the mean Z' -factor coefficient was 0.78 ± 0.07 ($n = 451$) and the mean S:B ratio was 19.5 ± 3.3 ($n = 451$). None of the assay plates in either assay format met our failed plate criteria of having both a Z' -factor coefficient ≤ 0.25 and an S:B ratio ≤ 3 .

2.6.2.2 AR-TIF2 PPIB Primary HCS and Active Confirmation

Compounds were screened at concentrations of 10 $\mu\text{g/mL}$, 25 μM , and 20 μM for the 10K ChemDiv PPI, 50K ChemBridge diversity, and 83K NCI CBC libraries, respectively. The % inhibition threshold for active compounds was set at $\geq 45\%$ for the 10K ChemDiv library, and $\geq 40\%$ for the other two libraries. In the primary HCS to find inhibitors of DHT-induced AR-TIF2 PPI formation, the median % inhibition was 11.5%, and 97.5%, or 139969 compounds were below our active thresholds and were considered inactive (Table 1). In the primary screen to identify disruptors of preexisting AR-TIF2 PPI complexes, the median % inhibition was 7.6%, and 99.3%, or 142560 of all compounds were below our active thresholds and were considered inactive (Table 1).

Actives were triaged to identify and eliminate for cytotoxic and fluorescent outliers and then cherry picked and confirmed in the testing paradigm described above.

2.6.2.3 Testing Paradigm to identify and eliminate compound artifacts

Cytotoxic and auto-fluorescent outlier compounds

After applying the cytotoxic and fluorescent compound outlier analysis to the AR-TIF2 multiparameter HCS data, we flagged 1224, and 454 compounds for elimination from the AR-TIF2 inhibitor and disruptor screens, respectively (Table 1). All three of the compound libraries exhibited similar cytotoxic and fluorescent outlier rates, and essentially similar qualified active rates in the AR-TIF2 disruptor screen. In the AR-TIF2 inhibitor format, however, the qualified active rate for the three libraries was higher than in the disruptor format and differed among the libraries. A total of 1,930 qualified active compounds were cherry picked and confirmed in triplicate wells at the original screening concentrations in both assay formats. Confirmed actives were then run in a series of counter screens.

p53-hDM2 PPIB Counter Screening Assay

None of the confirmed AR-TIF2 PPI inhibitors or disruptors from the current HCS campaign was active in a p53-hDM2 PPIB counter screen that utilizes the same PPI assay format and biosensor design but different interacting partners. Since these compounds were not able to alter the hDM2-RFP subcellular distribution phenotype in this assay, this indicates that they are unlikely to be either nonselective PPI inhibitors or to interfere with the biosensor assay format.

AR Nuclear Localization Counter Screen

Compounds that could reduce AR-RFP biosensor expression levels or restrict its localization to the cytoplasm would be expected to inhibit the AR-TIF2 PPIB assay. Similarly, compounds that inhibit AR-RFP trafficking and nuclear entry, or that promote its nuclear export, might also be

expected to inhibit the AR-TIF2 PPIB assay. Previously, it has been shown that known AR antagonists such as flutamide and bicalutamide, and the HSP 90 inhibitor 17-AAG, inhibit the AR-TIF2 PPIB assay and produce a predominantly cytoplasmic AR-RFP distribution phenotype [118, 119, 131]. AR antagonists block DHT binding to the AR-RFP biosensor, and HSP 90 inhibitors prevent the molecular chaperone-mediated maturation of the AR-RFP biosensor into a conformational state capable of high-affinity ligand binding. AR antagonists and HSP 90 inhibitors block DHT-induced translocation of the AR-RFP biosensor into the nucleus, thereby preventing the PPIs with the TIF2-GFP biosensor anchored in the nucleolus that results in the accumulation and colocalization of AR-RFP in TIF2-GFP positive nucleoli [118, 119, 131]. Any compounds with a similar mechanism of action of those previously described could be acting in an indirect manner in the AR-TIF2 biosensor. Twenty-nine of the confirmed AR-TIF2 PPI inhibitors/disruptors also reduced AR-GFP nuclear localization by >50%, suggesting that they might be indirectly inhibiting the AR-TIF2 PPIB assay rather than directly blocking/disrupting PPIs.

Dex-Induced GR Translocation Counter Screen

Next, compounds were run in the Dex-induced GR translocation counter screen. Both AR and GR are members of the steroid receptor subfamily of [120, 125] Like AR, the folding of *de novo* synthesized GR and its maturation to a conformational state capable of high-affinity hormone binding occurs in the cytoplasm and involves contributions from molecular chaperones and cochaperones [120, 125]. Ligand binding induces GR trafficking from the cytoplasm to the nucleus, entry through the nuclear pore complex, binding to specific glucocorticoid response element DNA sequences in the promoter/enhancer regions of target genes, and modulation of gene transcription levels [120, 125]. The Dex-induced GR-GFP nuclear translocation assay provides a

steroid NR selectivity counter screen that also shares components of the AR signaling pathway. Components shared by the AR and GR signaling pathways include the HSP 90 and HSP 70 chaperones that maintain both NRs in high-affinity structural conformations for ligand binding, ligand-bound AR and GR that are both cargos of dynein-mediated retrograde trafficking along microtubules to the nucleus, and the importin- α/β adaptor system that mediates entry through the nuclear pore complex for both NRs [120, 125, 134-136]. Eight confirmed AR-TIF2 PPIB actives that also inhibited GR-GFP nuclear translocation by >50% were deprioritized.

2.6.2.4 IC₅₀ Determinations – Potency & Efficacy

After cytotoxic and fluorescent outliers, and non-specific/non-selective compounds were removed, confirmed active compounds were selected for testing in 10-point, two-fold serial dilution AR-TIF2 PPI inhibitor and disruptor IC₅₀ determinations starting at a maximum concentration of 40 μ M. A total of 178 of the qualified confirmed actives inhibited DHT-induced AR-TIF2 PPI formation in a concentration dependent manner with IC₅₀s < 40 μ M, and 170 also disrupted preexisting AR-TIF2 PPI complexes in a concentration dependent manner (Table 1). The IC₅₀s are in the range that one would reasonably anticipate for PPI inhibitors and disruptors from a high-throughput screen. In the disruption of preexisting AR-TIF2 PPI format, the IC₅₀ data typically exhibited response curves with maximal inhibition levels around 80%, and r^2 values in the 0.7 to 0.9 range.

2.7 Conclusion

The overall hit rate for the 143,000- compound AR-TIF2 PPIB HCS campaign was 0.12% in both assay formats. Compounds active in the primary AR-TIF2 HCS were eliminated if they were cytotoxic or fluorescent, didn't confirm in triplicate, or were active in any of the counter screens. Confirmed actives that produced calculable IC_{50} s in the AR-TIF2 biosensor might be acting as direct disruptors of AR-TIF2 PPI's. To further prioritize and characterize these hits we developed a suite of assays to identify compounds that can disrupt interactions between the AF-2 coactivator binding surface of the AR and p160 coactivators such as TIF2 (SRC2) or SRC1 or disrupt the AF-1 transactivation domain. The hit characterization assays include the following: 1) AR::TIF2 and AR::SRC1 mammalian 2-hybrid (M2H) assays, 2) PSA6.1-LUC and UBE2C-LUC reporter based transcriptional activation assays in PC3 cells stably expressing either GFP-tagged full length AR (AR-FL), or GFP-tagged AR-V7, 3) a pGal4-AR-NTD transactivation assay developed in HEK 293 cells, a 4) H^3 -DHT radioligand binding assay, 5) an ALPHAScreen AR-LBD::LXXLL-peptide binding assay, and 6) tumor growth inhibition assays developed in five different PCa cell lines.

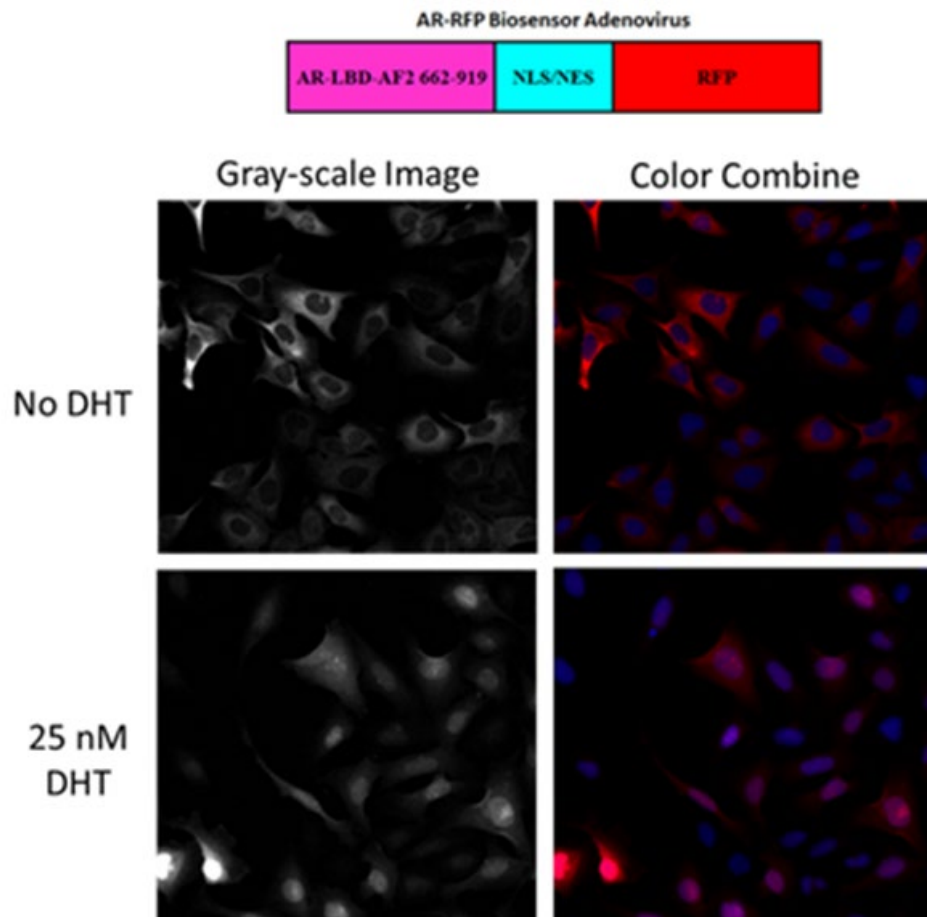


Figure 2. AR-RFP Recombinant Adenovirus

Grayscale and color combine images of U-2 OS cells infected with the AR-RFP recombinant adenovirus, cultured overnight and treated with or without DHT for 90 min and then fixed and stained with Hoechst, were acquired on the IXM platform in the fluorescent channels: Ch1 Hoechst, *blue*; and Ch3 AR-RFP, *red*.

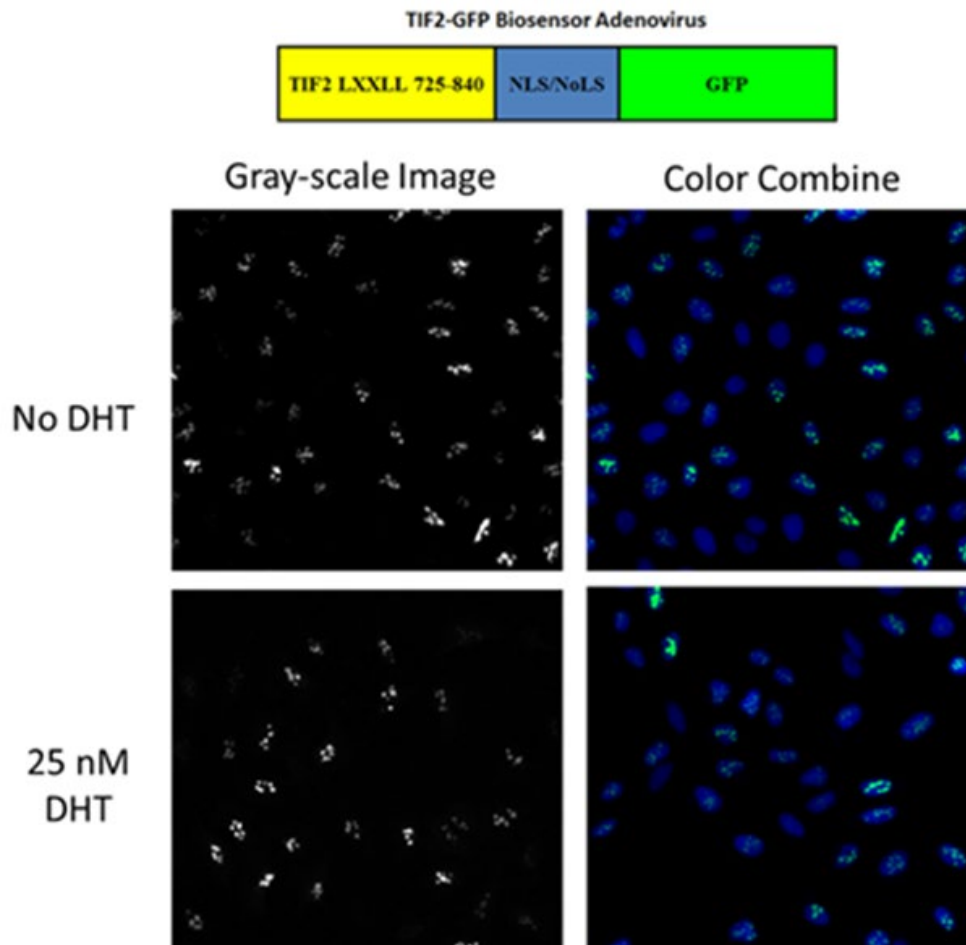


Figure 3. TIF2-GFP Recombinant Adenovirus

Grayscale and color combine images of U-2 OS cells infected with the TIF2-GFP recombinant adenovirus, cultured overnight and treated with or without DHT for 90 min and then fixed and stained with Hoechst, were acquired on the IXM platform in the fluorescent channels: Ch1 Hoechst, *blue*; and Ch2 TIF2-GFP, *green*.

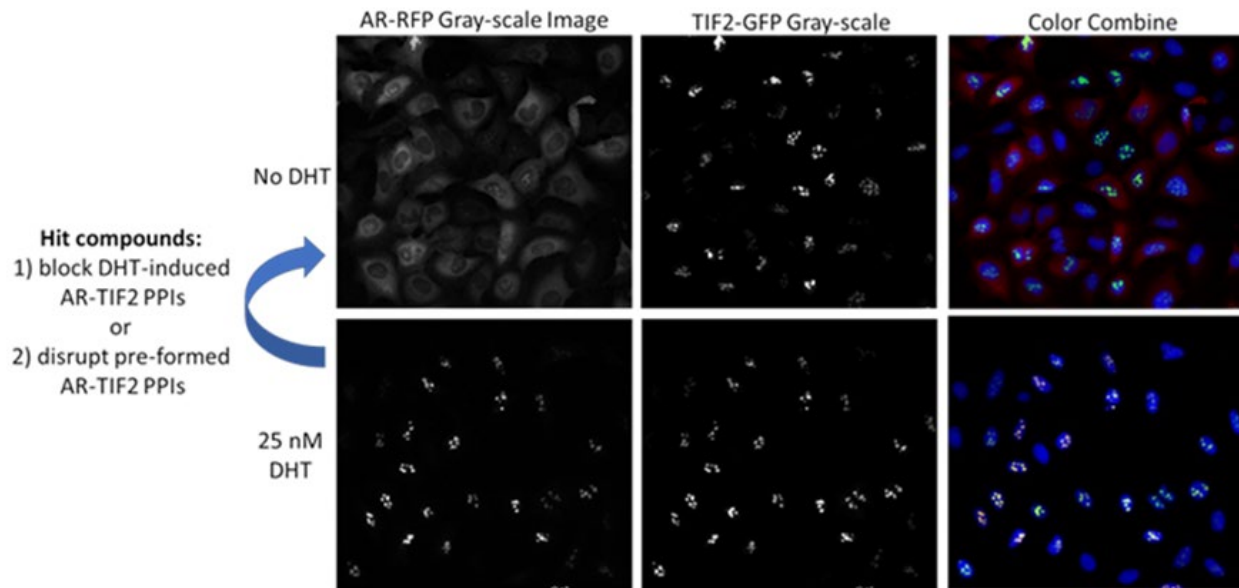


Figure 4. AR-RFP and TIF2-GFP Co-infected in U-2 OS Cells

Grayscale and color combine images of U-2 OS cells co-infected with both the TIF2-GFP and AR-RFP recombinant adenovirus, cultured overnight and treated with or without DHT for 90 min and then fixed and stained with Hoechst, were acquired on the IXM platform in the fluorescent channels: Ch1 Hoechst, *blue*; Ch2 TIF2-GFP, *green*; and Ch3 AR-RFP, *red*. This assay was run in two different formats. In the first format U-2 OS cells co-infected with the AR-TIF2 biosensors were exposed to compound 3 h before treatment with 25 nM DHT for 90 min. This allowed us to determine if compounds acted by (1) blocking DHT induced formation of PPI's. In the second format U-2 OS cells co-infected with the AR-TIF2 biosensors were exposed to 25 nM of DHT for 90 min before treatment with compounds for 3h. This allowed us to determine if compounds were acting by (2) disrupting pre-formed AR-TIF2 PPI's.

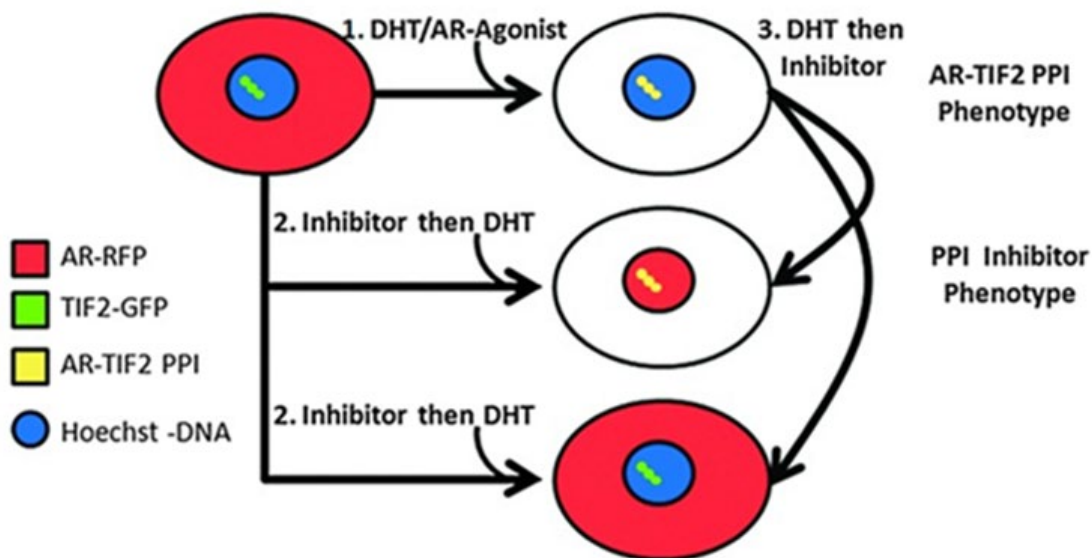


Figure 5. AR-TIF2 PPIB Assay Principle

Cartoon schematic representation of the AR-TIF2 PPIB assay formats and predicted phenotypes. In untreated cells, AR-RFP expression is localized predominantly in the cytoplasm and TIF2-GFP is restricted to nucleoli within the nucleus. Upon exposure to an AR agonist such as DHT, the AR-RFP biosensor translocated to the nucleus where it forms bright fluorescent puncta colocalized with the TIF2-GFP partner in the nucleolus. The AR-TIF2 PPIB assay therefore recapitulates the ligand-induced translocation of AR from the cytoplasm to the nucleus, and colocalization of the AR-RFP with the TIF2-GFP in the nucleolus reflects the protein-protein interactions between AR and the TIF2 coactivator. The AR-TIF2 PPIB assay can therefore be screened in three formats: (1) to screen for any compounds that act as AR agonists, or compounds that induce the formation of AR-TIF2 PPI's; (2) to screen for compounds that block DHT induced formation of PPI's, such as AR-antagonists, Hsp 90 inhibitors, or compounds that block trafficking to the nucleus, and (3) to identify compounds capable of disrupting preexisting AR-TIF2 complexes.

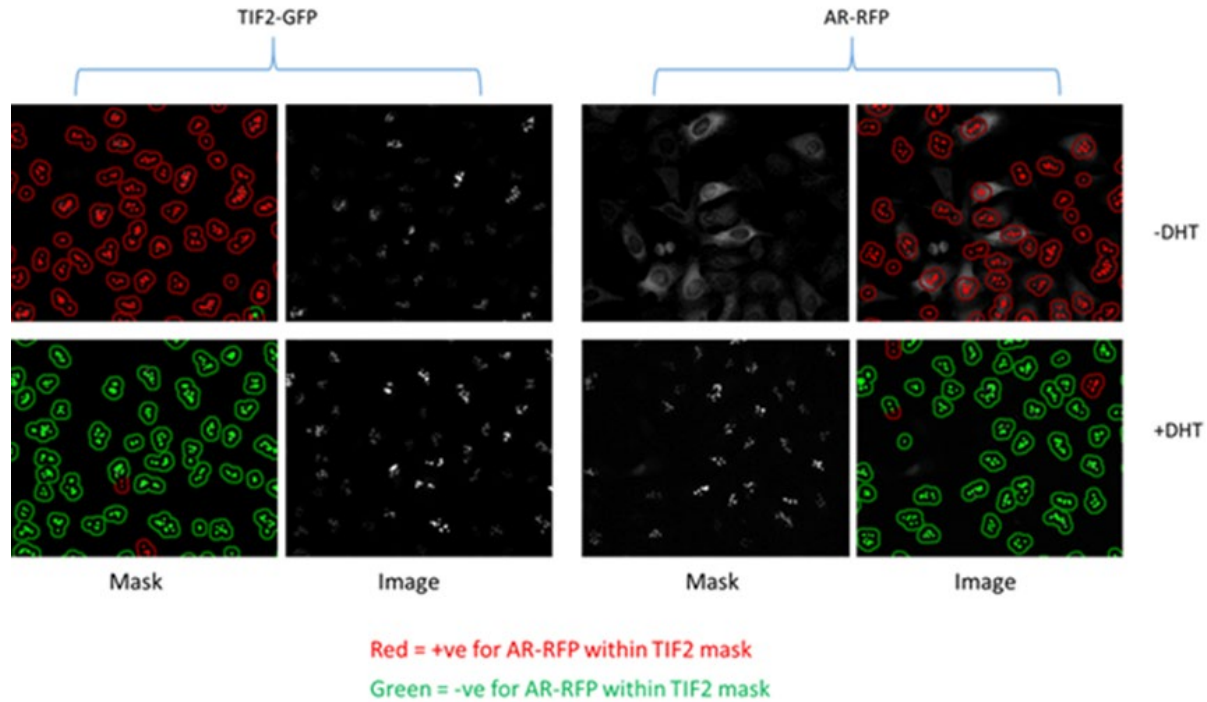


Figure 6. Image Segmentation Derived TIF2-GFP Positive Nucleolar Masks in the FITC and Texas Red Channels

Image segmentation derived TIF2-GFP-positive nucleolar masks in the FITC and Texas Red channels. Grayscale images of TIF2-GFP (Ch2 TIF2-GFP, *green*) and AR-RFP (Ch3 AR-RFP, *red*) from U-2 OS cells co-infected with both the TIF2-GFP and AR-RFP adenoviruses, cultured overnight and then treated with or without DHT for 90 min. The TE image analysis module utilized the TIF2-GFP biosensor compartment in Ch2 to create a mask of the nucleoli based on fluorescent intensity and size. TIF2-GFP-positive nucleoli were then used to create translocation masks within the nucleus of cells. AR-RFP images from Ch3 were segmented into a nucleolus region using the mask derived from the detected TIF2-GFP-positive nucleoli in Ch2. The red or green color of the nucleolus masks indicate whether both TIF2-GFP and AR-RFP signals within the nucleoli were below (red) or above (green) a certain fluorescent threshold.

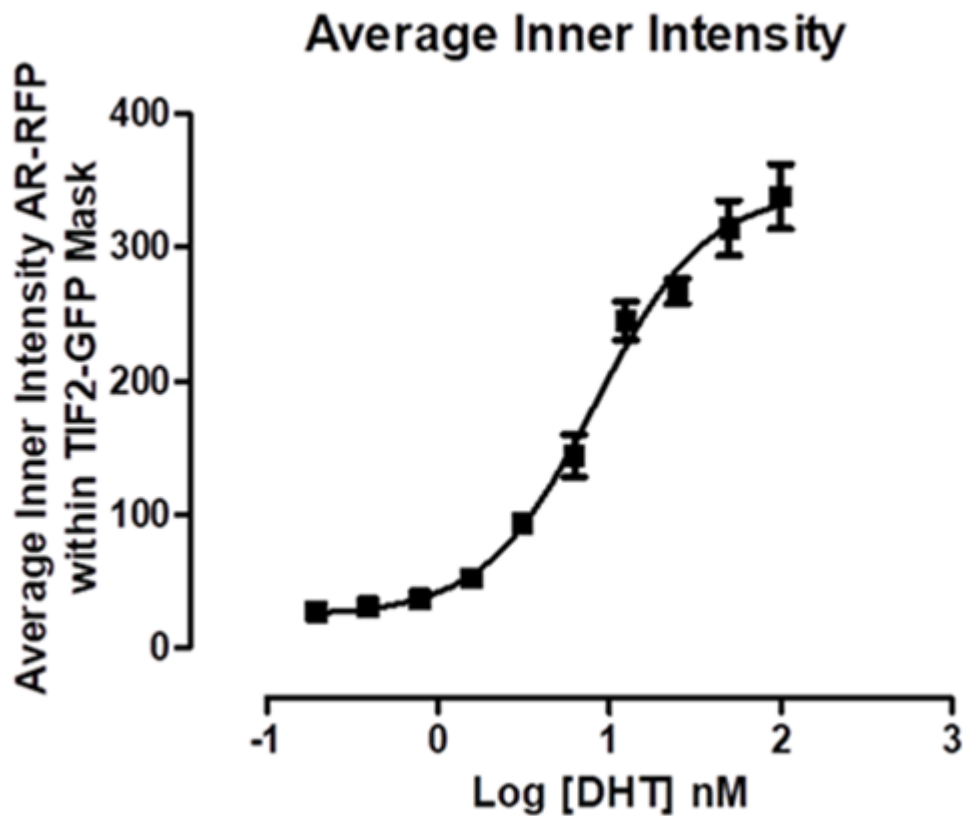


Figure 7. DHT Concentration Response of AR-RFP in the AR-TIF2 PPIB

U-2 OS cells were co-infected with the AR-RFP and TIF2-GFP rAV biosensors, 2,500 cells were seeded into the wells of 384-well assay plates, cultured overnight at 37°C, 5% CO₂, and 95% humidity, and then treated with the indicated concentrations of DHT for 30 min. Cells were then fixed and stained with Hoechst, images in three fluorescent channels were acquired on the IXU automated imaging platform, and the DHT-induced AR-TIF2 PPIs were quantified using the TE image analysis module as described previously. The mean – SD (n = 3) average inner intensity of AR-RFP within the TIF2-GFP-positive nucleoli at concentrations ranging between 0.001 and 100 nM DHT are presented. Representative experimental data from five independent experiments are shown.

Table 1. Testing paradigm to identify and eliminate compound artifacts from the AR-TIF2 PPIB

| | Inhibition of DHT-induced AR-TIF2 PPI formation¹ | Disruption of Existing AR-TIF2 PPI Complexes² |
|--|--|---|
| | Compound then DHT | DHT then Compound |
| LOPAC Screen | | |
| Active ^{3,4} | 24 ³ | 16 ⁴ |
| Inactive | 1256 | 1264 |
| Eliminated ⁶ | 16 | 16 |
| Active in Counter Screens ⁷ | 5 | 5 |
| Confirmed in Triplicate | 17 | 9 |
| Exhibited Calculable IC ₅₀ | 15 | 15 |
| 10K, 50K, 83K Screen | | |
| Active ⁵ | 3566 | 975 |
| Inactive | 139969 | 142560 |
| Eliminated ⁶ | 1224 | 454 |
| Active in Counter Screens ⁷ | 37 | 37 |
| Confirmed in Triplicate | 443 | 49 |
| Exhibited Calculable IC ₅₀ | 178 | 170 |

1. To determine if compounds could block DHT-induced AR-TIF2 PPI formation, assay plates were pre-exposed to compounds for 3 h prior to treatment with 25 nM DHT for 90 minutes.
2. To identify compounds that could disrupt pre-existing AR-TIF2 PPI complexes, assay plates were pre-exposed to 25 nM DHT for 90 minutes prior to compound transfer and an additional 3 h incubation.
3. Compounds that met the activity threshold % inhibition criterion of $\geq 50\%$ Inhibition of DHT-induced AR-TIF2 PPI formation
4. Compounds that met the activity threshold % inhibition criterion of $\geq 30\%$ of Disruption of preexisting AR-TIF2 complexes.
5. Compounds that met the activity threshold % inhibition criterion of $\geq 40\%$ or $\geq 45\%$ Inhibition of DHT-induced AR-TIF2 PPI formation, or disruption of preexisting AR-TIF2 complexes.
6. A z-score plate-based statistical scoring method was used to flag compounds that behaved as outliers compared to the other substances (n=320, no controls) tested on an assay plate. The number of compartments which represents the number of TIF2-GFP positive nucleoli identified in the FITC channel was used to flag compounds with z-scores < -3 as cytotoxic. Compounds with z-scores > 3 in one or more of the average or integrated fluorescent intensity parameters in any channel were flagged as fluorescent outliers.
7. Compounds that were active in p53-hdM2 PPIB, AR-Nuclear Localization, or Dex-Induced GR Translocation Counter Screens.

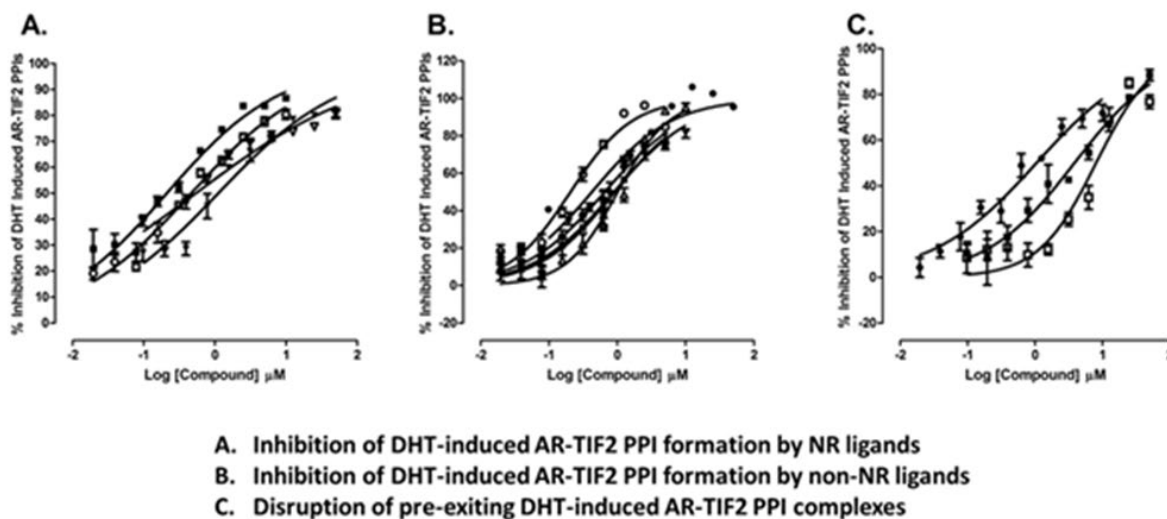
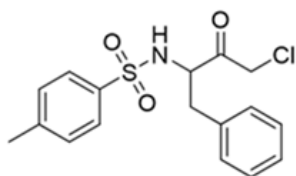
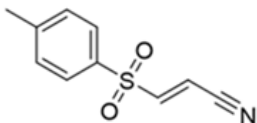


Figure 8. Concentration-dependent confirmation of LOPAC active that inhibit the DHT-induced formation of AR-TIF2 PPIs or disrupt preexisting AR-TIF2 PPI complexes

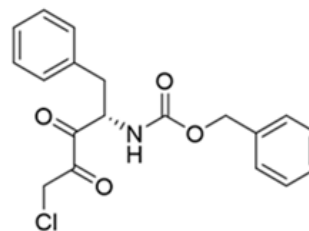
(A) Concentration-dependent inhibition of DHT-induced AR-TIF2 PPI formation by NR ligands. The mean – SD (n = 3) percent inhibition of DHT-induced AR-TIF2 PPIs in cells exposed to the indicated concentrations 17-alpha-hydroxyprogesterone (17-a-H-PG) (○), nilutamide (■), 2-methoxyestradiol (2-MOED) (▼), or estrone (▽) are presented. Representative experimental data from one of the three independent experiments are shown. (B) Concentration-dependent inhibition of DHT-induced AR-TIF2 PPI formation by non-NR ligands. The mean – SD (n = 3) percent inhibition of DHT-induced AR-TIF2 PPIs in cells exposed to 4- phenyl-3-furoxancarbonitrile (4-P-3-FOCN) (●), Bay 11-7085 (■), parthenolide (D), 1-chloro-3-tosylamino-4-phenyl-2-butanone (TPCK) (▼), or N-Carbobenzyloxy-L-phenylalanyl chloromethyl ketone (ZPCK) (○) are presented. Representative experimental data from one of the three independent experiments are shown. (C) Concentration-dependent confirmation of disruptor actives identified in the AR-TIF2 PPIB LOPAC screens. The mean – SD (n = 3) percent disruption of preformed AR-TIF2 PPI complexes in cells exposed to the indicated concentrations of mifepristone (●), 4-phenyl-3-fluroxane carbo-nitrile (4-P-3-FOCN) (□), and guggulesterone (■) are presented. Representative experimental data from one of the three independent experiments are shown.



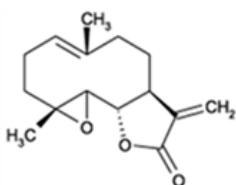
1-chloro-3-tosylamido-4-phenyl-2-butanone (TPCK)
C then D = 0.764 μ M
D then C = Not Tested



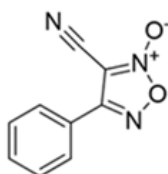
Bay-11-7085
C then D = 0.922 μ M
D then C = Not Tested



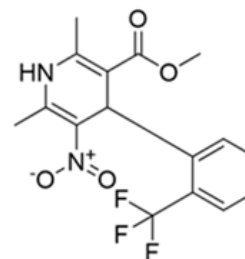
N-Carbobenzyloxy-L-phenylalanyl chloromethyl ketone (ZPCK)
C then D = 0.559 μ M
D then C = Not Tested



Parthenolide
C then D = 1.170 μ M
D then C = Not Tested



4-phenyl-3-furoxan carbo-nitrile
C then D = 0.598 μ M
D then C = 12.093 μ M



(±)-Bay K 8644
C then D = 0.922 μ M
D then C = Not Tested

Figure 9. Non-Nuclear Receptor AR-TIF2 PPIB Actives

Library of Pharmacologically Active Compounds (LOPAC) run in a 10-point concentration manner in the AR-TIF2 biosensor assay. Chemical structures, names, and calculable IC_{50} values of Non-Nuclear Receptor AR-TIF2 PPIB actives from the LOPAC set that inhibited (C then D) or disrupted (D then C) dihydrotestosterone (DHT)-induced androgen receptor (AR)-TIF2 protein-protein interaction (PPI) complexes.

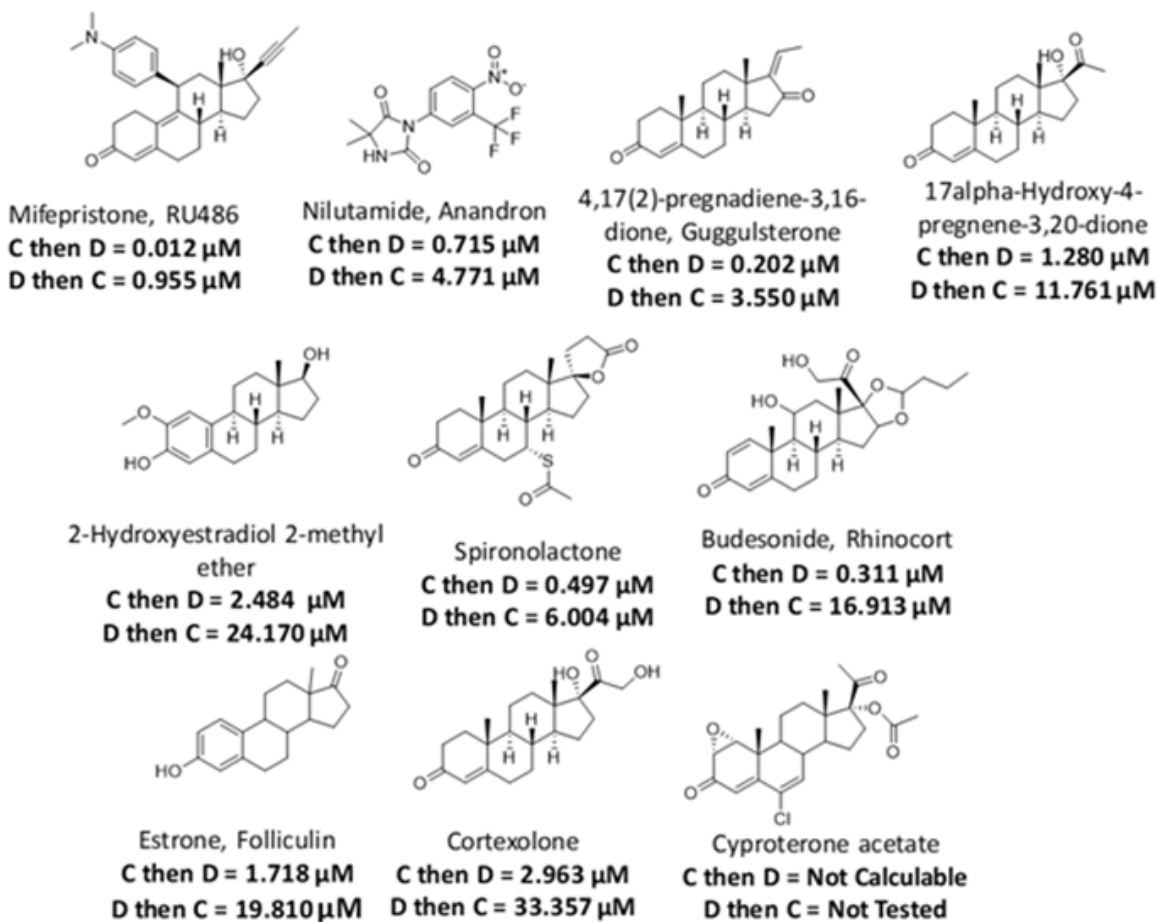


Figure 10. AR-TIF2 PPIB Actives: Nuclear Hormone Receptor Ligands

Library of Pharmacologically Active Compounds (LOPAC) run in a 10-point concentration manner in the AR-TIF2 biosensor assay. Chemical structures, names, and calculable IC_{50} values of nuclear receptor ligands from the LOPAC set that inhibited (C then D) or disrupted (D then C) dihydrotestosterone (DHT)-induced androgen receptor (AR)-TIF2 protein-protein interaction (PPI) complexes.

3.0 Targeting the AR AF-2 Protein-Protein Interactions with Coactivators

3.1 Introduction: Development of a Panel of Assays to Identify Compounds Targeting the AR AF-2 Transactivation Domain/Coactivator Binding Surface

Prostate cancer progression is largely dependent on AR's transcriptional activity in PCa cells which is reliant on AR's interaction with coactivators such as TIF2 [110]. TIF2's involvement in PCa disease progression has been well documented, and over-expression of this coactivator in recurrent forms of PCa, results in cellular resistance to the standard of care ADT's [96, 112, 117]. AR's regulation of gene transcription occurs via ligand-induced AR nuclear translocation, DNA binding to specific androgen response elements (ARE's) in target gene promoter and/or enhancer regions, and recruitment of coactivators [137]. Some coactivators bind to AR at the AF-2 hydrophobic activation surface that is formed by helix 12 of the AR-LBD after DHT binding [79, 116, 138]. These coactivators enable histone remodeling, additional coactivator recruitment, and subsequent assembly of the transcriptional machinery [137]. AR target genes associated with cellular biosynthesis, survival, and proliferation lead to PCa disease progression [113]. Although increased expression of several other AR coactivators have also been associated with PCa disease severity, blocking AR mediated transcription by disrupting the interactions between AR and TIF2 represents an attractive therapeutic strategy for slowing the progression of CRPC.

We have developed a suite of five assays to be used for the characterization of hit compounds that can disrupt interactions between the AF-2 surface of AR and the p160 coactivators TIF2 (SRC2) or SRC1. The assays were developed to characterize hit compounds identified in a screen of 143,000 compounds conducted in an AR-TIF2 PPI biosensor HCS assay (described in

chapter 2). The AR-TIF2 PPIB assay was used to identify compounds that inhibited the DHT-induced formation of AR-TIF2 PPIs or that disrupted pre-existing AR-TIF2 PPIs. The hit characterization assays include the following: 1) AR::TIF2 and AR::SRC1 mammalian 2-hybrid (M2H) assays, which represent the gold-standard assays for detecting co-regulator recruitment to nuclear receptors in cells [139-142]. In M2H assays, DHT binding enhances the interactions between the AR-LBD and either TIF2 or SRC1, which is detected by enhanced reporter gene activity. Compounds that decrease reporter gene activity may be blocking AR AF-2 interactions with TIF2 or SRC1 coactivators. 2) We developed a PSA6.1-LUC reporter based transcriptional activation assay in PC3 cells stably expressing GFP-tagged full length AR (AR-FL). This assay measures the transcriptional activity of AR at AREs in the promoter region of the PCa biomarker gene Prostate Specific Antigen (PSA). Any compound that can disrupt PPI's between AR and its coactivator should reduce AR's ability to transcribe genes, such as PSA in cells. The third assay we developed was a 3) H³-DHT radioligand binding assay. The radioligand binding assay measures a compound's ability to displace H³-DHT from binding to the AR-LBD. Since one potential mechanism of blocking the formation of DHT-induced AR-TIF2 PPI's would be to antagonize DHT binding to the AR-LBD, we needed an assay to identify compounds that were acting in this manner. The fourth assay we developed was an 4) ALPHAScreen AR-LBD::LXXLL-peptide binding assay. This assay was designed to measure the direct interactions between the NR box III LXXLL motif of the TIF2 coactivator with the AR AF-2 binding groove. Compounds that effectively inhibit TIF2-LXXLL peptide binding to AR AF-2 would be expected to block AR-TIF2 PPIs. Finally, we developed tumor growth inhibition assays in five different PCa cell lines, two that are AR negative and three that are AR positive. We would anticipate that AR-TIF2 PPI inhibitors/disruptors would be more effective at inhibiting the growth of PCa cell

lines that express AR than those that do not express AR. We then ran these assays using a test set of 7 compounds comprised of FDA approved therapeutics and investigational drugs for the treatment of PCa (Figure 11, on pg. 88) to see if they would perform the way we expected them to. The development and optimization of these assays together with the results for these seven test compounds are described in this chapter.

3.2 How Did Test Compounds Perform in the Primary AR-TIF2 PPIB Assay?

To begin with, we screened our set of test compounds in the AR-TIF2 HCS biosensor to determine how these compounds with different mechanisms of action would perform. Flutamide, bicalutamide, and enzalutamide are AR-antagonists that are prescribed as components of an androgen deprivation therapy (ADT) strategy [143-145]. Similarly, the Cyp17a1 inhibitor abiraterone acetate which prevents androgen synthesis is also used as a component of ADT [146]. Compounds #10 and EPI-001 target the amino-terminus of AR rather than the ligand binding site [124, 147-149], and 17-AAG is an inhibitor of the Hsp90 chaperone involved in the folding, maturation and maintenance of AR in a high affinity ligand binding conformation [150] (Figure 11). The assay was conducted in two distinct assay formats. In the first format, U-2 OS cells co-infected with the AR-RFP and TIF2-GFP biosensors were exposed to compounds for 3h before treatment with 25 nM DHT for 90 min. This allowed us to determine whether compounds could prevent DHT induced AR-TIF2 PPI formation. In the second format, U-2 OS cells co-infected with both biosensors were exposed to 25 nM of DHT for 90 min before treatment with the indicated concentrations of compounds for 3h. This allowed us to determine whether the compounds could disrupt pre-existing DHT-induced AR-TIF2 PPI's. As expected, exposure to the indicated

concentrations of the AR antagonists flutamide, bicalutamide, and enzalutamide for 3h prior to treatment with DHT inhibited AR-TIF2 PPI formation in a concentration dependent manner (Figures 12B-D, on pg. 89 and Table 2, on pg. 90). Flutamide, bicalutamide, and enzalutamide, exhibited IC_{50} s of 8.77 ± 1.59 , 2.49 ± 0.20 , and $1.44 \pm 0.16 \mu\text{M}$, respectively (Table 2). DHT binding facilitates both AR's entry into the nucleus, and the formation of the AF-2 coactivator binding surface of the AR. Through their ability to block DHT binding to the AR-LBD, AR antagonists therefore inhibit the DHT-induced PPIs of the AR-TIF2 biosensors. Interestingly, flutamide, bicalutamide, and enzalutamide also disrupted pre-existing AR-TIF2 PPI complexes with IC_{50} s of 20.6 ± 4.46 , 4.01 ± 1.37 , and $2.71 \pm 0.27 \mu\text{M}$, respectively (Table 2). Similarly, the Hsp90 inhibitor 17-AAG produced IC_{50} s in the AR-TIF2 biosensor assays, with an IC_{50} of $0.39 \pm 0.01 \mu\text{M}$ in the AR-TIF2 PPI formation format, and an IC_{50} of $0.20 \pm 0.01 \mu\text{M}$ in the disruption of pre-existing AR-TIF2 PPIs format (Figure 12G and Table 2). Since the Hsp90 chaperone protein maintains AR in a high-affinity conformation for ligand binding, inhibition of this function can also prevent ligand-induced AR nuclear translocation and AF-2 surface formation. In contrast, compound #10, EPI-001, and abiraterone acetate failed to produce a response in the AR-TIF2 HCS assay in either format at $\leq 50 \mu\text{M}$ (Figure 12E-F, H and Table. 2). Since compound #10 and EPI-001 both target the amino-terminal domain of AR, they would not be expected to interfere with the interactions between the AR-RFP and TIF2-GFP biosensors because the AR-RFP biosensor contains amino acids 622-919 of the AR-LBD derived from the carboxy-terminus of AR. Abiraterone acetate is a Cyp17a1 inhibitor and since it does not directly interact with the AR-LBD it would not be expected to exhibit activity in the AR-TIF2 biosensor assay. None of the test compounds had a significant impact on the total number of U-2 OS cells (Hoechst stained nuclei)

detected in the DAPI channel images, suggesting that at 3h of exposure they were not acutely cytotoxic at the concentrations tested.

3.3 Assays Developed to Characterize AR-TIF2 PPIB Inhibitor/Disruptor Hits that Target the AR AF-2 Transactivation Domain/Coactivator Binding Surface

3.3.1 Mammalian 2-Hybrid (M2H) Assay

3.3.1.1 Assay Principle

The mammalian 2-hybrid (M2H) assay is the gold standard for measuring the interactions between a nuclear receptor and co-regulator proteins to modulate transcriptional activity [139-142]. A gene coding for the nuclear receptor of interest, is cloned into a Gal4 vector containing the DNA-binding domain of the galactose expression Gal4 protein derived from yeast (Figure 13, on pg. 91). The respective co-regulator binding partner, either a coactivator or a corepressor, is cloned into a VP16 vector which contains the activation domain of the herpes simplex virus transcription factor. The M2H assay involves the transfection and expression of three main components including the Gal4-fused nuclear receptor protein, the VP16-fused coactivator or corepressor protein, and the 5xGal4-TATA-Luc luciferase reporter [151, 152]. Ligand binding to the nuclear receptor-Gal4 fusion protein acts to direct DNA-binding to the 5xGal4-TATA-Luc reporter plasmid, while ligand-induced binding interactions with the co-regulator-VP16 fusion protein recruits the transcriptional machinery of the cell, leading to overall transcription of the luciferase reporter gene, whose levels can be quantified as luciferase light output after addition of ATP substrate. This transcriptional activity of the reporter is a measure of the nuclear receptor::co-regulator protein interactions in the

cell [151, 152] (Figure 13). Co-activators enhance reporter activity while corepressors reduce reporter responses [153, 154].

We have developed M2H assays to interrogate the ability of hit compounds identified in the AR-TIF2 PPI HCS campaign to inhibit the PPI's between the AF-2 surface formed by DHT ligand binding to the AR-LBD and two of its coactivators, either transcriptional intermediary factor 2 (TIF2/SRC2) or SRC1. The M2H assays were developed using either full-length TIF2 or SRC1 protein, cloned into the VP16 transcriptional activation domain. SRC1 is another member of the steroid nuclear receptor p160 coactivator family and is a homologue of TIF2 [58, 59]. By developing the M2H assay with both TIF2 and SRC1, we will be able to determine if our hit AR-TIF2 PPI inhibitors and disruptors exhibit selectivity for TIF2 relative to SRC1. During assay development and optimization, the DNA concentrations of the 3 plasmid constructs were cross-titrated to select the optimal amounts of coactivator-VP16, AR-LBD-Gal4 and 5xGal4-TATA-Luc reporter DNA for the assays, which were then used to prioritize the hits identified from the 143K AR-TIF2 PPIB screen. The AR-LBD::TIF2 M2H assay allowed us to confirm that hits identified in the AR-TIF2 PPIB campaign inhibited the direct interactions between the DHT-induced AF-2 binding surface of the AR-LBD and TIF2, and whether they exhibited selectivity towards the related SRC1 p160 coactivator family member.

3.3.1.2 Materials and Methods

Plasmid DNAs. The 5xGAL4-TATA-luciferase reporter plasmid was a gift from Dr. Richard Maurer from the Oregon Health and Science University [155], and constructs pGAL4-hAR-658-919 (AR-LBD amino acids 658-919 expressed as a fusion protein with Gal4-DBD) [156], pVP16-SRC1 (full-length SRC1 expressed as a fusion with VP16 activation domain) [157] and pVP16-Empty vector were kindly provided to us by Dr. Elizabeth Wilson, from UNC Chapel

Hill. pVP16-TIF2 was generated by ligating TIF2, PCR amplified from pCR-BluntII-TOPO-NCOA2 (TIF2) cDNA (purchased from Dharmacon), into the empty pVP16 vector.

Cloning of TIF2 into a mammalian 2-hybrid pVP16 vector. The full-length TIF2 insert was amplified by polymerase chain reaction (PCR) from the pCR-BluntII-TOPO-NCOA2 (TIF2) cDNA using Phusion High-Fidelity DNA Polymerase (NEB). The primers for PCR were designed for the addition of EcoRI and BamHI cloning sites at the 5' and 3' flanking regions, respectively (ThermoFisher Scientific) (Table 3, on pg. 92). After PCR and the purification step, the insert was digested with EcoRI and BamHI. The VP16 vector was also double digested with EcoRI and BamHI enzymes. After overnight ligation, using T4 DNA ligase (New England Biolabs) at 16°C the insert was cloned into the pVP16 vector. Following the ligation, a small amount of the ligation mixture was transformed into DH5 α competent cells and plated on ampicillin containing LB agar to select bacteria containing the pVP16-TIF2 plasmid DNA. Following overnight incubation at 37°C, colonies were selected and expanded in ampicillin containing LB media. Next, DNA was isolated from cells expanded from an individual clone, and clones were analyzed via restriction analysis. Clones with bands at the correct molecular size were sent for sequencing. Sequencing analysis confirmed the correct cloned TIF2 construct, and plasmid DNA was isolated from DH5 α cells (Table 4, on pg. 93).

SDS-PAGE and Western Blot Confirmation of VP16-Coactivator Constructs. Coactivator containing pVP16 vectors were then confirmed through western blot analysis. pVP16-TIF2 and pVP16-SRC1 were transfected into HEK 293 cells and allowed to express for 48 hrs. Forty-eight hours post transfection, cells were lysed, and the BCA reagent was used to determine protein concentrations of transfected cell lysates. An SDS-PAGE gel was then run to separate 25 μ g of protein of each transfected cell lysate per well and compared to non-transfected HEK 293 cells.

Protein was then transferred to a nitrocellulose membrane and probed with either α -TIF2 or α -SRC1 antibodies (Figure 14, on pg. 94). HEK 293 cells endogenously express coactivators TIF2 and SRC1, which is evident in non-transfected HEK 293 lysates. A second immuno-positive band was detected in lanes loaded with protein from pVP16-TIF2 and pVP16-SRC1 transfected HEK 293 cells, consistent with a higher molecular weight due to the fusion with VP16 (Figure 14).

Mammalian-2-Hybrid Assay. HEK 293 cells were co-transfected with 5 ng of pGal4-AR-LBD, 10 ng of either pVP16-TIF2 or pVP16-SRC1, and 20 ng of the 5xGal4-TATA-Luc reporter. Cells were transiently bulk co-transfected with the three plasmids using the Fugene6 transfection reagent. Prior to the transfection of cells each of the pGAL4-hAR-658-919, 5xGAL4-TATA-luciferase reporter, and either pVP16-TIF2 or pVP16-SRC1 plasmid DNAs were individually incubated with Fugene6 at a 3:1 ratio for 25 min at room temperature (RT). Each Fugene6:plasmid DNA mixture was then added to HEK 293 cells that were suspended in DMEM (Cellgro10013CV) with 2 mM L-glutamine (Invitrogen) that was supplemented with 10% fetal bovine serum, and 5,000 cells in a volume of 40 μ L were seeded into the wells of 384-well assay plates and cultured overnight at 37°C, 5% CO₂, and 95% humidity. After 24 h control wells were exposed to \pm 25 nM DHT and the assay plate was returned to the incubator for an additional 24 h before BrightGlo® reagent was added to the plate and the relative luminescence units (RLUs) were captured on a SpectraMax M5e microtiter plate reader. Test compounds were run in the M2H assay in a 10-point 2-fold dilution series spanning a concentration range between 0.0977 to 50 μ M. 24 h post cell seeding into assay plates, 5 μ L of the serially diluted test compounds was transferred to the wells using a Janus MDT automated liquid handling platform outfitted with a 384-well transfer head before 5 μ L of 0.25 μ M DHT (25 nM final) was transferred into each well, and the assay plates were returned to the incubator for an additional 24 h.

3.3.1.3 Assay Development and Optimization

Determining the optimal cell background for the AR-LBD Mammalian 2-Hybrid TIF2 and SRC1 Coactivator assays. We began by conducting the mammalian 2-hybrid assay in 3 different cell lines (Figure 15, on pg. 95). We selected PC3 cells because they provided an AR-null PCa cell line background, and we selected HeLa cells and HEK 293 cells because they have frequently been used in mammalian 2-hybrid assays [88, 92, 157-159]. In cells co-transfected with 5 ng of pGal4-AR-LBD, 10 ng of pVP16-TIF2, and 20 ng of the 5xGal4-TATA-Luc reporter construct only cells that were treated with DHT exhibited a luciferase response substantially greater than untreated background levels. Surprisingly PC3 cells produced very little response with or without DHT treatment, and the DHT-induced response in HeLa cells was ~60-fold lower than in HEK 293 cells. Based on our experience with other transient transfection assays, we attribute the much higher responses observed in HEK 293 cells to their much higher transfection efficiencies. We therefore selected the HEK 293 cell background to conduct our remaining mammalian 2-hybrid assays (Figure 15).

Determining the optimal amounts of DNA plasmid constructs to use in the M2H Assays. To determine the optimal amount of pGal4-AR-LBD, pVP16-TIF2, or pVP16-SRC1 plasmid DNA to use in the M2H assays conducted in HEK 293 cells we performed cross-titration transient transfection experiments with increasing amounts of the AR and coactivator plasmid DNAs (Figure 16, on pg. 96). The amount of 5xGal4-TATA-Luc reporter construct in the assays was kept constant at 20 ng, which had been previously been determined to be optimal in transient transfection experiments conducted in our lab. The cross-titration experiments were performed in 384-well, white opaque plates. pGal4-AR-LBD plasmid DNA was added to cells at increasing amounts (0, 2.5, 5, 10 ng/well) and cross-titrated with increasing amounts (0, 5, and 10 ng/well)

of pVP16-TIF2 or pVP16-SRC1 plasmid DNA. Only cells that were treated with DHT exhibited a luciferase response substantially greater than untreated background levels (Figure 16). In both the TIF2 and SRC1 M2H assays, the DHT-induced luciferase response increased in a linear fashion as the amount of pGal4-AR-LBD transfected into the HEK 293 cells was increased. Similarly, the DHT-induced M2H luciferase response increased in a roughly linear fashion as the amounts of the pVP16-coactivator constructs transfected into the HEK 293 cells was increased. The magnitude of the TIF2 M2H response was ~ 30-fold higher than the signal in the SRC1 M2H assay (Figure 16A versus 16B). The final amounts of plasmid DNAs selected for the optimized the M2H assays were 5 ng for pGal-AR-LBD, and 10 ng each of the pVP16-Coactivator constructs (Figure 16).

Determining the optimal DHT concentration for the M2H assays. A DHT-concentration response was performed to determine the optimal concentration of DHT to use in subsequent M2H experiments. HEK 293 cells were co-transfected with the 5xGal4-TATA-Luc reporter construct and the pGal4-AR-LBD plasmid with either the pVP16-TIF2 or pVP16-SRC1 coactivator constructs and exposed to the indicated concentrations of DHT. DHT exhibited EC_{50s} of 0.619 nM and 2.23 nM for the TIF2 and SRC1 M2H formats respectively (Figure 17, on pg. 97). We therefore selected 25 nM of DHT as a suitable agonist concentration for activating both M2H assay formats as it was the second lowest concentration that gave us the highest signal when we ran DHT-concentration curves.

Determining the DMSO tolerance for the M2H assays. A DMSO-concentration response was performed to determine the optimal concentration of DMSO to use in subsequent M2H experiments (Figure 18, on pg. 98). DMSO exhibited IC_{50s} of 1.97% and 1.16% for the TIF2 and SRC1 M2H formats respectively. Therefore, we were able to determine that 0.5% DMSO would not interfere either TIF2 or SRC1 M2H assay formats (Figure 18).

3.3.1.4 Inhibition of the AR-TIF2 Biosensor assay to Measure DHT-induced AR-LBD Interactions with the TIF2 by Test Compounds

All seven compounds in the test set inhibited DHT-induced AR-LBD interactions with the TIF2 and SRC1 coactivators in a concentration dependent manner (Figure 19, on pg. 99). In TIF2 M2H assays, the anti-androgens flutamide, bicalutamide, and enzalutamide exhibited IC_{50} s of 3.01 ± 0.75 , 2.01 ± 0.99 , and 2.36 ± 1.44 μ M respectively, and the Hsp 90 inhibitor 17-AAG produced an IC_{50} of 0.33 ± 0.02 μ M (Figure 19B-D, H and Table 5, on pg. 100). In SRC1 M2H assays flutamide, bicalutamide, and enzalutamide exhibited IC_{50} s of 2.53 ± 0.66 , 1.49 ± 0.69 , and 1.37 ± 0.91 μ M respectively, and 17-AAG produced an IC_{50} of 0.45 ± 0.08 μ M (Figure 19B-D, H and Table 15). Compound #10, EPI-001, and Abiraterone acetate also exhibited concentration-dependent inhibition in both the TIF2 and SRC1 M2H assay formats, however, they also displayed substantial concentration-dependent cytotoxicity in HEK 293 cells that complicates the interpretation of the data (Figure 19E, F, G and Table 5). Overall, there was no apparent selectivity for any of the validation compounds for their ability to disrupt DHT-induced AR-LBD interactions with either TIF2 or SRC1. The antiandrogens were likely active in both formats of the M2H assay because they block DHT binding to the AR-LBD, thereby inhibiting PPI's from forming with either of the p160 coactivators. Similarly, the Hsp 90 inhibitor 17-AAG blocks the folding and stabilization of the AR-LBD into a high affinity ligand binding conformation, thereby inhibiting DHT from inducing PPI's formation with the p160 coactivators. Compound #10, EPI-001, and abiraterone acetate all exhibited IC_{50} s in both p160 M2H assay formats, however, viability assays run simultaneously with the M2H assay suggest that compound-mediated cytotoxicity may be the primary mechanism for decreasing the M2H reporter signal.

3.3.2 PSA6.1-Luc Reporter-Based Assay Developed in PC3-GFP-AR-FL Cells

3.3.2.1 Assay Principle

The PSA6.1-Luc reporter-based assay measures DHT-induced transcriptional activity of the AR, in PCa cells. The PSA-6.1 LUC plasmid luciferase reporter activity is controlled by a fragment of the PSA promoter that contains three androgen response elements (AREs), fused to a luciferase reporter gene (Figure 20, on pg. 101). When AR is transcriptionally active, it leads to the transcription of luciferase, and in the presence of the CellTiterGlo reagent, luciferase will convert the ATP substrate into light output, a quantifiable measurement of transcription. Any compound that can disrupt AR's interaction with coactivator, TIF2, should prevent the further recruitment of the transcriptional machinery of the cell. Therefore, an AR AF-2-TIF2 inhibitor/disruptor should decrease the transcriptional activity of full-length AR (AR-FL) target genes, such as PSA. During assay development and optimization, we obtained and generated reagents that were necessary for conducting our reporter assay. We developed a PC3 cell line, stably transfected with AR-FL-GFP. We transiently transfected this cell line with our reporter construct, and we determined which DHT concentrations were optimal for AR's subcellular localization in the nucleus, and those that were optimal for AR's transcriptional activity. The appropriate conditions were then chosen to be used when prioritizing hits identified from the 143K AR-TIF2 PPIB screen. The PSA6.1-Luc reporter assay allowed us to interrogate the ability of hit compounds to modulate AR's transcriptional activity in PC3 cells. Any compound that could decrease reporter activity was further prioritized along our screening paradigm.

3.3.2.2 Materials and Methods

We developed the PSA6.1-LUC reporter-based assay in a PC3 cell line stably transfected with pEGFP-C1-AR-FL. PC3 cells are an AR-null PCa cell background into which we could stably transfect either pEGFP-C1-AR-FL or pEGFP-C1-AR-V7 (splice variant) constructs in order to compare AR-FL and AR-NTD related transcriptional events. The development of reporter assays using PC3 cells stably transfected with the pEGFP-C1-AR-V7 construct is described in chapter 4. The pPSA-6.1 LUC luciferase reporter plasmid was kindly provided by Dr. Zhou Wang in the Urology department of the University of Pittsburgh Cancer Institute. We developed the PC3 cell line stably transfected with full-length AR, using the pEGFP-C1-AR construct that was kindly gifted to us from Dr. Michael Mancini, Baylor College of Medicine. The PC3 cell line was purchased from the American Type Culture Collection.

Developing the PC3 Cell Line Stably Transfected with pEGFP-C1-AR-FL. In order to generate a stable cell line, we transfected PC3 cells with the pEGFP-C1-AR-FL plasmid and then sorted these cells based on the presence of GFP. On day 1, PC3 cells were plated at a seeding density of 1.0×10^6 cells in a 100 mm TC dish. On day 2, at 70% confluency, PC3 cells were transfected with 19 μg of pEGFP-C1-AR-FL, at a 3:1 Ratio of FuGENE6: plasmid DNA. Transfection conditions were based on those that were previously optimized in our lab that generated the highest transfection efficiency in PC3 cells. 48 h post transfection, the cells were initially sorted with the help of Dr. Hongmei Shen, University of Pittsburgh School of Medicine. They were then placed under selection with 600 $\mu\text{g}/\text{mL}$ of G418. Prior to transfection, we ran kill curves in PC3 cells by exposing cells to increasing concentrations of antibiotic (G418) and determining the amount that was necessary to kill all of the cells over a 7-day period of time. 600 $\mu\text{g}/\text{mL}$ of G418 was chosen for selection and maintenance of the antibiotic resistance plasmid

DNA in PC3 cells. Two weeks after the first sort, the cells were harvested, counted, and sorted a second time. Again, they were placed under selection with 600 µg/mL of G418. A third and final sort was performed 2 weeks after the second. Cells were sorted into two groups: those that expressed high levels of pEGFP-C1-AR-FL, and those that expressed low levels of pEGFP-C1-AR-FL. The population of cells expressing lower levels of pEGFP-C1-AR-FL performed better in both the DHT-induced AR-FL-EGFP nuclear translocation, and PSA6.1-reporter assays (data not shown), and therefore we selected this population for use in subsequent experiments.

PSA6.1-LUC Reporter Assay. Fugene HD and PSA-6.1 LUC were combined at a 3:1 (µL:µg) ratio, respectively, in Opti-MEM and incubated for 25 min at room temperature (RT) before being combined with AR-FL-EGFP-PC3 cells that were suspended in RPMI 1640 media containing 1% L-glutamine, and 10% fetal bovine serum. Transfected cells were then seeded into white opaque 384-well assay plates (#781080; Greiner Bio-one) at a seeding density of 3,000 cells per well in a volume of 40 uL and incubated at 5% CO₂, 37C, and 95% humidity for 24 h. Each well received 20 ng of PSA-6.1 LUC plasmid DNA. After 24 h, 5 uL of serially diluted compounds was transferred to the wells by using a Janus MDT automated liquid handling platform outfitted with a 384- well transfer head; then, 5 uL of 0.25 µM DHT (25 nM final in well) in SFM was transferred to each well; and the assay plates were returned to the incubator for an additional 24 h before 25 µL of BrightGlo luciferase reagent (Promega) was added to the wells and the relative light units (RLUs) were captured on a SpectraMax M5e plate reader (Molecular Devices LLC).

3.3.2.3 Assay Development and Optimization

Determining which cell background to develop reporter assays in. To determine which PCa cell line to use for developing a stably transfected AR-FL EGFP line, we characterized the endogenous expression levels of coactivator TIF2, and the AR in the 5 PCa cell lines: PC3, DU-

145, 22Rv1, and C4-2 (Figure 21, on pg. 102). Cells were cultured in a 100 mm tissue culture dish, and once they were 60-70% confluent, they were washed by adding cold PBS to the culture dish which was placed on ice. PBS was then aspirated and a second wash was performed. Next, 800 μ L of chilled RIPA buffer with protease inhibitors was added to the plate as a lysis buffer. Cells were removed from the surface of the plate using a cell scraper. Cells were transferred to a microcentrifuge tube and sonicated on ice 3x; 5s each at 20% amplitude. Next, cells were incubated on ice for 30 min. Finally, cells were centrifuged for 25 minutes at 14,000 rpm at 4°C. Supernatant was transferred to a fresh tube and BCA reagent was used to determine protein concentrations of each lysate. Then an SDS-PAGE was performed and 20 μ g of protein was added to each lane of the gel from each cell lysate. After the gel was run for protein separation, it was transferred to a nitrocellulose membrane. The membrane was then probed with TIF2 (Bethyl Labs #A300-356A), and AR (Cell Signaling #5153), rabbit antibodies at a 1:1000 dilution for 1 hr at RT. Next the membrane was washed 3x with Tris buffered saline and 0.01% Tween20 (TBS-T) and secondary goat anti-rabbit IgG (Santa Cruz #2004), was added to the membrane at a 1:2000 dilution for 1 hr at RT. Next, the membrane was probed with a GAPDH antibody (Pierce #MA1-16757), added at a 1:1000 dilution, for 1 hr at RT. The membrane was washed 3x with Tris buffered saline and 0.01% Tween20 (TBS-T) and secondary goat anti-mouse antibody, at a dilution of 1:10,000, for 1 hr at RT (Figure 21). We chose PC3 cells as our cell background because it is an AR-null cell line, and it expresses the TIF2 coactivator.

DHT concentration response in AR-FL-EGFP Nuclear Translocation assay. The DHT concentration response was conducted in the pEGFP-C1-AR-FL-PC3 cell line (Figure 23, on pg. 104). To quantify DHT-induced nuclear translocation of AR-FL-EGFP in PC3 cells, cells were plated, and treated with increasing concentrations of DHT for 24 hrs, before being fixed, and

imaged on an IXM automated HCS platform (Molecular Devices LLC). Images were then analyzed with the TE image analysis module of the MetaXpress software (Molecular Devices LLC). Exposure of cells to increasing amounts of DHT, increased the inner/outer intensity ratio in the cells, which is a measure of the mean average fluorescence intensity of AR-FL-GFP in the nucleus, divided by the mean average fluorescence intensity of AR-FL-GFP in the cytoplasm. Exposure of the PC3-AR-FL-EGFP cells to increasing amounts of DHT, resulted in a concentration-dependent increase in inner/outer intensity ratio with an EC₅₀ of 1.23 +/- 0.131 nM (Figure 23). Representative images of subcellular localization of AR-FL-GFP in PC3 cells in the absence or presence of DHT are shown in Figure 22, on pg. 103.

DHT concentration response in PSA6.1-LUC reporter assay. The DHT concentration response was conducted in pEGFP-C1-AR-FL containing PC3 cells transiently transfected with the PSA6.1-LUC reporter construct (Figure 24, on pg. 105). Cells were transfected with the following conditions, 20 ng of PSA6.1-LUC reporter construct combined with FugeneHD at a 3:1 ratio, which had been previously determined in transient transfection assays run in our lab. Cells were treated with increasing amounts of DHT for 24 hrs, which increased reporter response in a concentration dependent manner, and produced an EC₅₀ of 0.280 +/- 0.034 nM (Figure 24). We therefore selected 25 nM of DHT as a suitable agonist concentration for conducting the PSA6.1-LUC reporter based assay.

3.3.2.4 Test set performance in PSA6.1 Reporter Assay

In PC3-AR-FL-GFP cells transfected with the PSA-6.1-LUC reporter, the anti-androgens flutamide, bicalutamide, and enzalutamide inhibited DHT-induced reporter activity in a concentration dependent manner, exhibiting IC₅₀s of 17.4 ± 3.91, 21.9 ± 4.80, and 19.5 ± 3.45 μM, respectively (Figure 25B-D, on pg. 106 and Table 6, on pg. 107). This was expected, since these

compounds are FDA-approved compounds for the treatment of PCa, and act by antagonizing DHT binding to the AR-LBD, thereby preventing AR activation of transcription. The Hsp 90 inhibitor, 17-AAG, also decreased AR-FL's transcriptional activity in cells in a concentration dependent manner, producing an IC_{50} of $1.72 \pm 0.48 \mu\text{M}$ (Figure 25H and Table 6). This is likely due to this compound's ability to block the folding and stabilization of the AR in a high affinity ligand binding conformation, thereby inhibiting DHT binding, and therefore diminishing AR's transcriptional activity in the cell. Surprisingly, investigational drugs, compound #10, and EPI-001, which target the AR-NTD, did not inhibit AR's transcriptional activity in PC3-AR-FL-GFP cells at $\leq 50 \mu\text{M}$ (Figure 25E, F and Table 6). Finally, abiraterone acetate also didn't inhibit reporter activity at $\leq 50 \mu\text{M}$ (Figure 25G and Table 6). Abiraterone inhibits Cyp17a1's ability to synthesize androgen, and since this assay is supplemented with 25 nM DHT, this compound does not affect AR's ability to function in the cell. To control for the potential cytotoxicity of these compounds, growth inhibition assays were run for each compound, simultaneously, to determine whether a decrease in reporter based activity was due to a decrease in AR transcriptional activity or due to compound induced cell death. Under the conditions described above, validation compounds exhibited no apparent cytotoxicity in the PC3 cell line stably expressing pEGFP-AR-FL, indicating that any decrease in reporter signal was actually due to a compound's ability to block DHT-induced AR transcriptional activity (Figure 25 and Table 6).

3.3.3 AR-LBD H³-DHT Radioligand Binding Assay

3.3.3.1 Assay Principle

The competitive radioligand binding assay employs radiolabeled H³-DHT, a known ligand and agonist of AR. This assay specifically measures the displacement of H³-DHT from AR-LBD in the presence of increasing concentrations of each test compound. AR-LBD was cloned into a pET28a expression vector that bears a 6x histidine tag, and was further expressed and purified for use in the radioligand binding assay. Histidine tagged AR-LBD was added to the wells of 96-well copper coated plates (Pierce) overnight, where histidine chelates the Cu²⁺ coating of the plate's surface. The next day, any unbound protein is washed away. Next, compound and 10 nM of the radiolabel, H³-DHT, is added to each well of the plate. If a compound can antagonize AR, it will compete with H³-DHT for binding. If a compound is not an AR-antagonist then H³-DHT will bind AR, unencumbered. After 1 hr of incubation, any unbound radiolabel and compound are washed away. If the compound was an antagonist, it will compete with and displace H³-DHT from binding AR, and result in low quantifiable β -emissions (counts per minute, CPMs) in the well. If the compound was not an antagonist, it will not have displaced H³-DHT from binding to AR, and there will be high CPMs in the well (Figure 26, on pg. 108). The H³-DHT radioligand binding assay was incorporated into our screening paradigm to identify and deprioritize hits from the HCS AR-TIF2 biosensor assay that inhibited/disrupted AR-TIF2 PPIs through antagonism of the AR at its ligand binding domain (AR-LBD). Any compound with the ability to displace H³-DHT from binding to the AR-LBD was able to antagonize the receptor, and represented an undesirable compound profile. Any compound that did not antagonize the AR-LBD could be a direct PPI inhibitor/disruptor.

3.3.3.2 Materials and Methods

The pET28a expression vector containing a 6x Histidine-tagged AR-ligand binding domain (LBD) residues 622-919 (pET28a-His₆-AR-LBD) was kindly provided by Dr. Fletterick and Dr. Nguyen of UCSF (Figure 27, on pg. 109). We purchased radioligand, H³-Dihydrotestosterone (H³-DHT) from Perkin Elmer. Copper coated high capacity plates (96-well), were purchased from Pierce. We expressed and purified His₆-AR-LBD for use in our assay development and validation experiments.

Transformation and Expression of 6xHis-AR-LBD (622-919). OneShot BL21 (DE3) competent *E. coli* cells (Life Technology; C6060-10) were transformed with the pET28a-His₆-AR-LBD plasmid and streaked on kanamycin containing LB agar plates to select colonies for preparing bacterial glycerol stocks. The pET28a-His₆-AR-LBD plasmid was isolated from transformed bacteria and sequenced to confirm the identity of the plasmid DNA. Bacteria transformed with pET28a-His₆-AR-LBD were used to inoculate cultures that were incubated overnight at 37°C and then used to inoculate an expansion culture that was incubated at 37°C until it reached an OD of 0.1 and was then supplemented with 50 μM DHT. Cultures were switched to 18°C and incubated until they reached an O.D. of 1.0–1.2, and then, His₆-AR-LBD expression [118, 160] was induced by incubation with 200 μM IPTG for an additional 18–20 h at 16°C. Cells were pelleted by centrifugation for 20 min at 5,000 g at 4°C and stored frozen at –80°C.

Purification Strategy for 6xHis-AR-LBD (622-919). Frozen cell pellets were thawed on ice, and they were suspended in “buffer A”: 50 mM HEPES pH of 7.65, 300 mM Li₂SO₄, 250 μM TCEP, 10% glycerol, and 50 μM DHT containing protease inhibitors and lysozyme (0.1 mg/mL). After 20–30 min of lysozyme treatment, cells were lysed by twelve, 30 s 30% amplitude bursts of a probe

sonicator (Fisher Scientific Model 505 Sonic Dismembrator), and they were then centrifuged at 20,000 g for 30 min at 4°C; the supernatant was added to Ni²⁺-conjugated resin beads that had been pre-washed and equilibrated with “buffer A.” The resin was washed twice with approximately eight bed volumes of buffer A, then once with four bed volumes of buffer A supplemented with 2 mM ATP and 10 mM MgCl₂, and finally once again with four bed volumes of “buffer A.” The resin was then washed once with approximately four bed volumes of 20 mM imidazole in “buffer A,” and the His₆-AR-LBD was eluted in four fractions of two bed volumes of 300 mM imidazole in “buffer A.” The protein concentrations in each elution fraction were determined in the BCA protein assay; the protein constituents were separated on 12% SDS-PAGE gels and transferred to nitrocellulose membranes; and western blots were probed with anti-AR and anti-His antibodies obtained from Santa Cruz Biotechnology (Figure 28, on pg. 110). The His₆-AR-LBD containing fractions were pooled and then dialyzed in buffer containing 50 mM HEPES pH 7.65, 150 mM Li₂SO₄, 5% glycerol, 0.2 mM TCEP, and 20 μM DHT. The concentration of pooled, dialyzed protein concentration was determined in the BCA protein assay, and aliquots were stored at -80°C [118, 160].

H³-DHT Radioligand Binding Assay. The His₆-AR-LBD H³-DHT competition binding assay was carried out in 96-well Cu²⁺-coated plates (ThermoFisher) that were incubated overnight at 4°C with 5 μg per well His₆-AR-LBD in 100 μL of PBS. Unbound His₆-AR-LBD was aspirated; the plate was washed 3 × with 100 μL of 0.05% Tween 20 in PBS and then blocked with 100 μL of 1 mg/mL bovine serum albumin (BSA) in PBS for 1 h. After three more washes with 100 μL of PBS and 0.05% Tween 20, 40 μL of PBS were added to the wells, via a Matrix pipettor (ThermoFisher). Next 5 μL of compound was transferred to the wells also using the Matrix pipettor (ThermoFisher), followed by 5 μL of 100 nM H³-DHT. Compounds were tested in the assay

ranged from 0.0977 to 50 μM , at a 1:2 dilution for 10-assay points, in the presence of 10 nM H^3 -DHT. After a 1 h co-incubation, compound and H^3 -DHT were aspirated and washed $3 \times$ with 0.05% Tween 20 in PBS; 100 μL of micro-scintillation cocktail buffer was added to each well; plates were sealed with adhesive plastic covers; and the counts per minute (CPMs) were captured in a TopCount NXT microtiter plate reader (Perkin Elmer).

3.3.3.3 Assay Development and Optimization

Determining the optimal amounts of His₆-AR-LBD (622-919) protein to use in the Radioligand Binding Assay. To determine the optimal amount of protein to use in the radioligand binding assay, we performed a protein titration with increasing amounts of His₆-AR-LBD (Figure 29A, on pg. 111). Increasing amounts of His₆-AR-LBD (0-15 $\mu\text{g}/\text{well}$) were added to wells of 96-well Cu^{2+} -coated plates, incubated overnight at 4°C, after which, unbound His₆-AR-LBD was aspirated. After blocking the plate with bovine serum albumin (BSA) and a series of washes, 10 nM H^3 -DHT was added to the wells. The protein amount selected for use in the H^3 -DHT binding assay was 5 μg AR-LBD/well (Figure 29A).

Determining the optimal amounts of H^3 -DHT to use in the radio-ligand binding assay. A H^3 -DHT saturation binding assay was performed to measure total and non-specific binding of H^3 -DHT to AR-LBD (622-919) protein (Figure 29B). Increasing concentrations (0-40 nM) of H^3 -DHT were incubated in Cu^{2+} -coated plates coated with 5 $\mu\text{g}/\text{well}$ His₆-AR-LBD. Signal (CPMs) increased with increasing concentrations of H^3 -DHT, until 5 nM, where it looked like the signal began to plateau. The maximal binding capacity (B_{max}) was determined to be 3837, and dissociation constant (K_d) was 3.23 nM. 10 nM of H^3 -DHT was selected for use in the radioligand binding assay (Figure 29B). This concentration was used for all subsequent radioligand binding experiments.

Competition Binding Assay. We then conducted competitive displacement binding experiments with unlabeled DHT, to confirm that this assay could identify drugs that can compete with and antagonize H³-DHT binding to the AR-LBD (Figure 29C). The displacement binding assay was run using a fixed amount of AR-LBD (5 ug/well) protein, and 10 nM of H³-DHT. Increasing concentrations of unlabeled DHT were added to the assay ranging from 0 μM to 10 μM, in a 10-point 1:2 dilution series. The assay signal (CPMs) decreased in a concentration dependent manner and exhibited an IC₅₀ for displacement binding of 0.058 μM (Figure 29C).

3.3.3.4 Test set performance in H³-DHT radioligandbinding assay

When the AR-antagonists, flutamide, bicalutamide, and enzalutamide were run in the competitive radioligandbinding assay, all three of them were able to displace H³-DHT from binding to His₆-AR-LBD, as expected, exhibiting IC₅₀ values of 48.6 ± 19.5, 5.53 ± 3.27, and 50.2 ± 14.4 μM, respectively (Figure 30B-D, on pg. 112 and Table 7, on pg. 113). Neither compound #10, nor EPI-001 displaced H³-DHT binding to His₆-AR-LBD at ≤ 50 μM (Figure 30E-H and Table 7). Since these compounds target the amino-terminal domain of the receptor, they would not be expected to compete with H³-DHT binding to the AR-LBD. Similarly, neither 17-AAG nor abiraterone acetate displaced H³-DHT binding to His₆-AR-LBD, likely because these compounds also do not bind the AR ligand binding pocket.

3.3.1 ALPHAScreen AR-LBD::TIF2-LXXLL-Peptide Binding Assay

3.3.1.1 Assay Principle

The ALPHAScreen AR-LBD::LXXLL-peptide binding assay is a biochemical assay that measures the interaction of the AR AF-2 surface formed by His₆-AR-LBD, and a peptide containing the

LXXLL motif located in box III of the TIF2 coactivator's nuclear interaction domain (NID) (Figure 31, on pg. 114). A literature search indicated that LXXLL motifs from box III of the NID were most important for TIF2's interaction with the AR AF-2 surface, and it was therefore selected for use in the development of the ALPHAScreen assay [91, 93, 161, 162]. The ALPHAScreen is a homogenous mix and read assay that uses coated acceptor and donor beads to bind tagged proteins. In our assay, histidine-tagged AR-LBD protein chelates to Ni²⁺ coated acceptor beads, and the TIF2 Box III LXXLL motif peptide conjugated to biotin binds to streptavidin donor beads. Binding between the two interacting partners leads to close proximity between the donor and acceptor beads. Upon laser excitation of the donor bead, a singlet oxygen species is released and reacts with thioxene derivatives found within the acceptor bead, located within a distance of 200 nm relative to the donor bead, which creates energy that when transferred to fluorophores within the bead, can be quantified via light emission at a wavelength of 520-620 nm [163] (Figure 31). This assay is performed by incubating Ni²⁺ coated acceptor beads with AR-LBD and 10 μM of DHT prior to mixing them with compound plus streptavidin bound TIF2 peptide donor beads. The pre-incubation of the acceptor beads allows for the DHT-induced formation of the AF-2 coactivator binding surface. Development and optimization of the ALPHAScreen included cross-titrating both the His₆-AR-LBD protein and biotinylated-TIF2-box-III peptide to select the optimal amounts to use in the assay. The ALPHAScreen AR-LBD::TIF2-LXXLL-peptide binding assay was validated in competitive displacement binding experiments with increasing amounts of unlabeled TIF2-III-LXXLL peptide, and used to prioritize the hits identified in the 143K AR-TIF2 PPIB screen. The ALPHAScreen assay allowed us to determine whether AR-TIF2 PPI inhibitor or disruptor hits were capable of blocking the direct binding interactions between the LXXLL motifs of the TIF2 NR box III peptide and His₆-AR-LBD.

3.3.1.2 Materials and Methods

The pET28a-AR-LBD (622-919) construct was a gift from Dr. Fletterick and Dr. Nguyen of UCSF, and its expression and purification were described earlier in this chapter. Both biotinylated-TIF2-box-III (738-756), and Non-biotinylated TIF2-box-III (738-756) were synthesized by the Peptide & Peptoid Synthesis Facility, at the University of Pittsburgh Health Sciences Core Research Facilities (Table 8, on pg. 115). The ALPHAScreen Kit, which consisted of streptavidin donor beads and nickel chelate (Ni-NTA) acceptor beads, was purchased from Perkin Elmer.

ALPHAScreen Assay. Validation compounds were run in this assay at a 0.0977 to 50 μM concentration range, at a 1:2 dilution, to generate a 10-point response curve. The assay validation was carried out in 384-well, white opaque plates. 150 nM of biotinylated TIF2-box III was incubated with streptavidin donor beads for 30 min at room temperature, in the dark. 18 μL of the streptavidin immobilized biotinylated TIF2 peptide mixture was added to the plate. A fixed amount of His₆-AR-LBD (400ng/well), was incubated with 10 μM DHT, and Ni²⁺ chelate acceptor beads for 30 min at room temperature in the dark. 27 μL of this mixture was added to the plate. 32 wells of 0.5% DMSO controls were used as a maximum control, and 32 wells of 500x excess unlabeled TIF2-box-III (75 μM) were used as a minimum control. The bead-protein mixtures were then combined and incubated for 1 h at room temperature, in the dark, and after, read on an Envision plate reader (Perkin Elmer).

3.3.1.3 Assay Development and Optimization

Determining the optimal amounts of His₆-AR-LBD (622-919) protein to use in the ALPHAScreen assay. To determine the amount of protein to use in the ALPHAScreen assay, we performed a protein titration with His₆-AR-LBD (Figure 32A, on pg. 116). The amount of biotin-TIF2-LXXLL-peptide in the assay was fixed at 100 nM. Increasing amounts of His₆-AR-LBD (0-

2 µg/well) were incubated with DHT, and Ni²⁺ coated acceptor beads for 30 min, before being mixed with streptavidin bound TIF2 donor beads in the plate. The ALPHASignal (CPMs) increased with increasing amounts of His₆-AR-LBD, up until 1 µg of protein/well was reached, after which the signal did not increase further (Figure 32A). The final amount of His₆-AR-LBD protein selected for the optimized ALPHAScreen assay was 400 ng/well, as this was the lowest protein amount that we could use that produced the highest signal.

Determining the optimal amounts of Biotinylated-TIF2-box-III (738-756) Peptide to use in the ALPHAScreen assay. Biotinylated-TIF2-box-III titration experiments were performed to select for the optimal concentration of peptide to use in the ALPHAScreen assay (Figure 32B). Increasing concentrations of biotinylated TIF2-box III (0-200 nM) were incubated with streptavidin donor beads for 30 min before being mixed with DHT bound His_{6x}-AR-LBD (0.4 µg/well) chelated by Ni²⁺ acceptor beads. The ALPHASignal (CPMs) increased with increasing concentrations of TIF2-LXXLL-peptide, up to around 100 nM, after which it appeared to plateau. The apparent K_d for TIF2 peptide binding to His₆-AR-LBD was 151.3 nM, and the B_{max} was projected at 42880 (Figure 32B). The final concentration of TIF2 peptide selected for the optimized ALPHAScreen assay was 150 nM.

Conducting Competition/Displacement Binding Assays using Non-biotinylated TIF2-box-III (738-756). We then conducted competitive displacement binding experiments with unlabeled TIF2-III-LXXLL to confirm that this assay would identify AR AF-2::TIF2-LXXLL inhibitors (Figure 32C). Using the optimized ALPHAScreen assay conditions of biotinylated-TIF2-box III (150 nM/well) streptavidin donor beads plus His₆-AR-LBD (400 ng/well) Ni²⁺ chelate acceptor beads in the presence of DHT, the addition of non-biotinylated TIF2-LXXLL-peptide decreased

the ALPHASignal (CPMs) in a concentration dependent manner and exhibited an IC₅₀ for displacement binding of 2.76 nM (Figure 32C).

3.3.1.4 Test Set Performance in ALPHAScreen Assay

Only the Hsp90 inhibitor 17-AAG, and to a small extent the anti-androgen flutamide, inhibited the AR AF-2 interaction with TIF2 Box III LXXLL motif peptide (Figure 33B-H, on pg. 117 and Table 9, on pg. 118). Pre-incubating Ni²⁺ coated acceptor beads with AR-LBD and DHT prior to mixing with compound plus streptavidin bound TIF2-LXXLL peptide, allows the AF-2 coactivator binding surface to form. Anti-androgens bind the ligand binding pocket of the AR, which is composed of polar amino acids that are able to establish hydrogen bonds with the polar substituents of these compounds [164], however they should have no effect on direct AF-2::coactivator interactions. Neither Compound #10 nor EPI-001 inhibited AR AF-2 interactions with TIF2, which is justifiable as both compounds target the amino-terminus of the AR (Figure 33E-F, and Table 9). Abiraterone Acetate, a compound that inhibits the enzyme Cyp17a1, was also inactive in the ALPHAScreen, which makes sense, because this compound doesn't directly interact with the AR-LBD. Surprisingly, the Hsp 90 Inhibitor, 17-AAG exhibited an IC₅₀ value of 29.8 ± 9.78 μM in this assay (Figure 33G and Table 9). 17-AAG is a compound that inhibits the ATPase activity of the chaperone protein Hsp90. Since, His₆-AR-LBD is a protein expressed and purified from *E. coli* cells, it's possible that 17-AAG may disrupt AR's interaction with bacterial chaperone proteins, which may prevent the AF-2 coactivator binding surface from folding correctly and binding the TIF2-LXXLL-peptide.

3.3.2 Growth Inhibition Assays

3.3.2.1 Assay Principle

We would anticipate that AR-TIF2 PPI inhibitors/disruptors would be more effective at inhibiting the growth of PCa cell lines that express AR compared with those that do not express AR. To test this hypothesis, we implemented CTG growth inhibition assays in five PCa cell lines: the LNCaP, C4-2, and 22Rv1 PCa cell lines express AR, while the PC3 and DU-145 cell lines are AR null. The development of CTG based growth inhibition assays has been described in one our previous publications [118].

3.3.2.2 Materials/Reagents

Growth Inhibition Assay. The PCa cell line growth inhibition assays were developed and optimized using methods that were previously applied in other tumor cell lines [118]. On day 1, each PCa cell line was harvested, counted, and seeded into 384-well assay plates: PC3, DU-145, LNCaP, C4-2, and 22Rv1 cells were seeded at 1,000 cells per well in 45 μ L of tissue culture media into uncoated, white, clear-bottom 384-well assay plates (VWR Cat. No. 82050-076) by using a Matrix electronic multichannel pipette (ThermoFisher) and cultured overnight at 37°C, 5% CO₂, and 95% humidity. On day 2, 5 μ L of compounds diluted in SFM was transferred into the test wells of the 384-well assay plates on the Janus MDT automated liquid handler equipped with a 384-well transfer head and the compound-treated assay plates were cultured for an additional 72 h in an incubator at 37°C, 5% CO₂, and 95% humidity. Control wells received DMSO alone. On day 5, 25 μ L of the CTG detection reagent was dispensed into the wells of the assay plates by using a

Matrix electronic multichannel pipette, and the luminescence signal was captured on the SpectraMax M5e microtiter plate reader platform.

3.3.2.3 Test Set Performance in Growth Inhibition Assays

We anticipated that the AR-antagonists might selectively inhibit the growth AR-positive PCa cell lines. However, flutamide was equipotent against all 5 cell lines with IC₅₀s in the 10-20 μ M range, bicalutamide only inhibited PCa cell growth at concentrations greater >100 μ M, and enzalutamide only inhibited growth at concentrations greater than 200 μ M (Figure 34B-D, on pg. 119 and Table 10, on pg. 120). Strangely enough, compound #10 and EPI-001, did appear to preferentially inhibit growth of cell lines that were AR-positive over cell lines that were AR-negative. Compound #10 exhibited IC₅₀s of 17.6 ± 7.8 , 14.5 ± 0.58 , and 19.4 ± 4.63 μ M, for LNCaP, C4-2, and 22Rv1's, respectively, and IC₅₀s of 40.8 ± 0.60 and >50 for PC3 and DU-145's, respectively. EPI-001 exhibited IC₅₀s of 33.0 ± 5.97 , 38.6 ± 3.25 , and 41.2 ± 1.30 , for LNCaP, C4-2, and 22Rv1's, respectively, and IC₅₀s of >50 for both PC3 and DU-145's (Figure 34 and Table 10). This may be due to the fact that AR-null, androgen-independent cells, PC3's, and DU-145's are more resistant to cell death than AR-containing, androgen-dependent lines, LNCaP, C4-2, and 22Rv1's [165]. 17-AAG, and Abiraterone acetate inhibited the growth of all PCa cell lines, but not in an AR-selective manner (Figure 34G, H and Table 10).

3.3.3 Conclusions

We have successfully developed and tested 5 different characterization assays that will allow us to prioritize hit compounds that inhibit the formation of or disrupt pre-existing PPI's between the AR AF-2 surface and TIF2. The M2H assays provide an orthogonal assay that will allow us to

confirm that the AR-TIF2 PPIB hits block AR-coactivator interactions and to evaluate the selectivity for TIF2 versus the related SRC1 p160 family member. The PSA6.1 reporter assay in PC3 cells stably expressing AR-FL will allow us to confirm that our AR-TIF2 PPI inhibitor/disruptor hits block AR mediated transcriptional activity. The His₆-AR-LBD H³-DHT ligand binding assay will help us to distinguish between compounds that are PPI inhibitors and those that are AR antagonists. The AR-LBD-TIF2-LXXLL-peptide binding assay will enable us to determine whether AR-TIF2 PPI hits are blocking the direct binding interactions between the LXXLL motifs of the TIF2 NR box III peptide and AF-2 surface of the AR-LBD. Since we anticipate that AR-TIF2 PPI inhibitors/disruptors would be more effective at inhibiting the growth of PCa cell lines that express AR compared to those that do not, our PCa growth inhibition assays will allow us to identify and prioritize such compounds. We are looking for hit compounds with the following bioactivity profile: active in the primary AR-TIF2 biosensor assay, can disrupt AR-TIF2 PPIs in the mammalian 2-hybrid and AR-LBD-TIF2-LXXLL peptide binding assays, inhibit AR transcriptional activation, do not antagonize AR ligand binding, and selectively inhibit the growth of AR-positive cell lines. Hit compounds that fit this profile will be prioritized for lead optimization and further development as a therapeutic candidate for CRPC.

Of the 7 test compounds run in our characterization assays, only 4 of them were able to inhibit AR-TIF2 PPI's in the biosensor. These were AR-antagonists flutamide, bicalutamide, and enzalutamide, and Hsp90 inhibitor, 17-AAG. Although all 4 compounds were able to inhibit both TIF2/SRC1 recruitment to the AR-LBD in M2H assays, and DHT-induced PSA6.1-Luc reporter activity in PC3-AR-FL-GFP cells, all 3 antagonists were active in the H³-DHT radioligandbinding assays, as expected. Furthermore, none of the AR-antagonists were able to inhibit PPI's in the ALPHAScreen assay at <50 μ M, and none of them were able to selectively inhibit AR-positive

cell lines. As they don't fit the bioactivity profile of an AR-TIF2 PPI inhibitor, we wouldn't prioritize them. 17-AAG on the other hand did fit the bioactivity profile we were looking for. However, based on this compound's mechanism of action, we know that this compound may be acting to inhibit AR's function in these assays by preventing Hsp90's ability to maintain AR in a high-affinity conformation for ligand binding, thereby prevent ligand-induced AR nuclear translocation and AF-2 surface formation. Therefore we would not prioritize any of them for lead optimization and development.

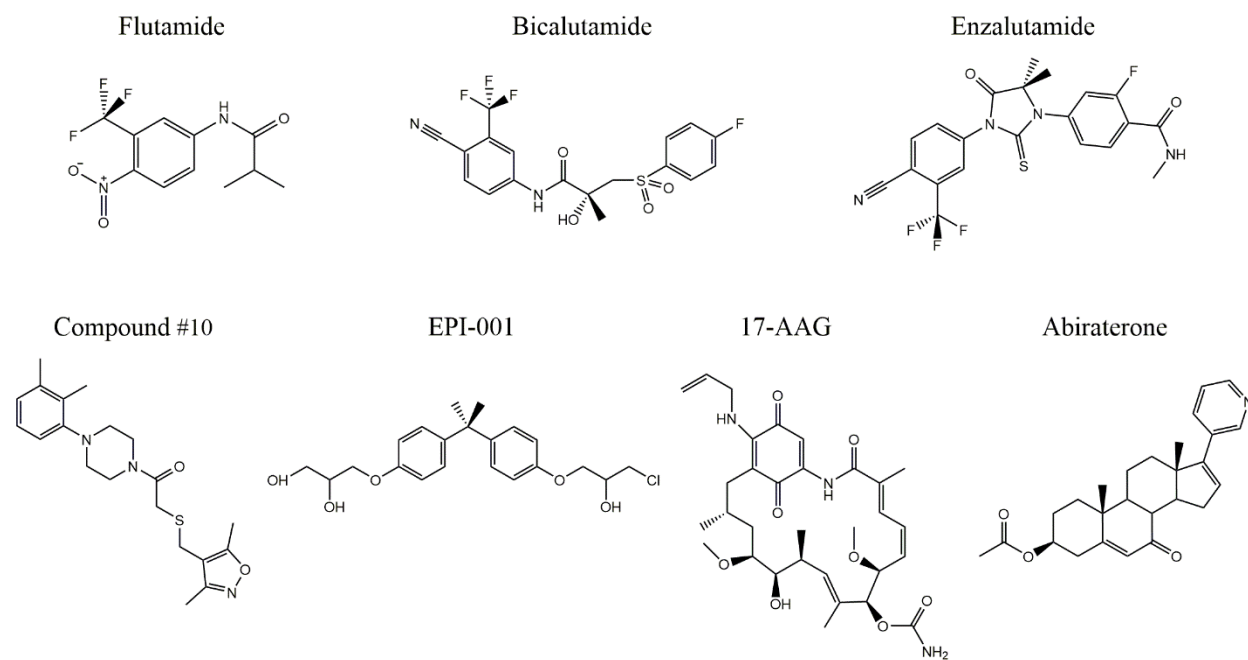


Figure 11. Chemical structures of the test set for the hits characterization assays

Presented here are the chemical structures of compounds in the test set that we used to run in our hit characterization assays. These compounds include FDA approved therapeutics and experimental drugs for the treatment of PCa. Flutamide, bicalutamide, and enzalutamide are AR-antagonists that are prescribed as components of an androgen deprivation therapy (ADT) strategy. Similarly, the Cyp17a1 inhibitor abiraterone acetate that prevents androgen synthesis is also used as a component of ADT. Compounds #10 and EPI-001 target the amino-terminus of AR rather than the ligand binding site, and 17-AAG is an inhibitor of the Hsp90 chaperone involved in the folding, maturation and maintenance of AR in a high affinity ligand binding conformation.

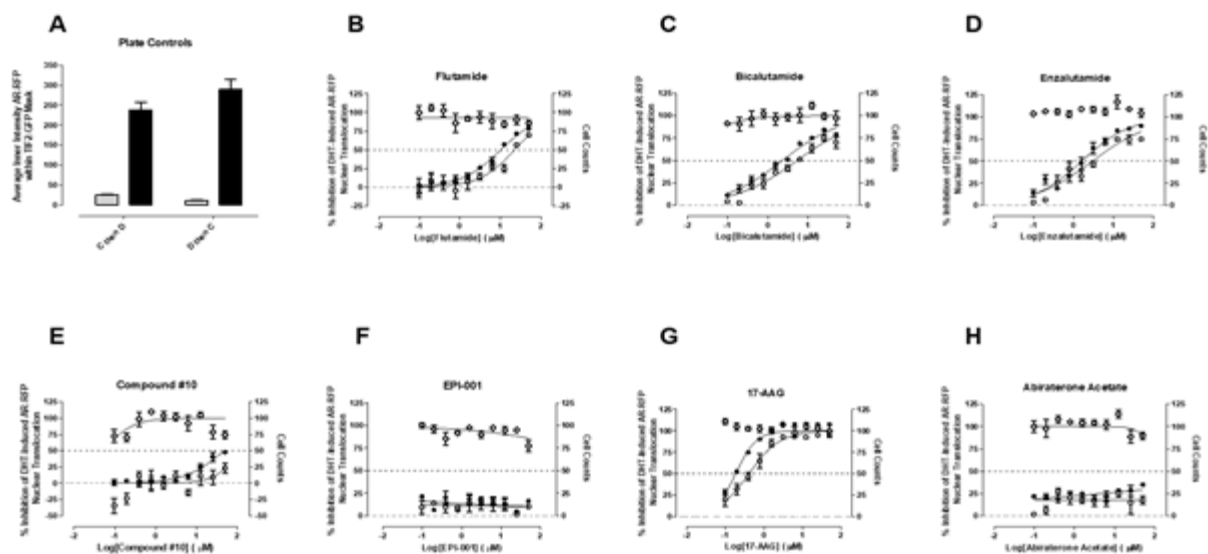


Figure 12. Inhibition of the AR-TIF2 Biosensor assay to measure DHT-induced AR-LBD interactions with TIF2 by test compounds

U2-OS cells were co-infected with AR-RFP and TIF2-GFP rAV biosensors, and 3,000 cells were seeded into the wells of 384-well assay plates, and cultured overnight at 37°C, 5% CO₂, and 95% humidity. After 24 h test compound and DHT were added to cells in two different formats. In format 1 (C then D), AR-TIF2 co-infected U2-OS cells were exposed to 3 hr of compound before treatment with 25 nM DHT for 90 min. In format 2 (D then C), AR-TIF2 co-infected U-2 OS cells were exposed to 25 nM of DHT for 90 min before treatment with the indicated concentrations of compounds for 3 hr. The AR-TIF2 data for compound treated wells were normalized to maximum (25 nM DHT + 0.5% DMSO, n=32) and minimum (0.5% DMSO, n=32) plate controls, and the % inhibition was plotted as the mean +/- SD (n = 3) values from triplicate wells for each compound concentration plotted on the left Y-axis. The corresponding cell viability data for compound treated wells were normalized to 25 nM DHT + 0.5% DMSO control wells (n=32), and the % cell viability (◇) was plotted as the mean +/- SD (n = 3). **A**) Representative plate control data for C then D (○) and D then C (●) AR-TIF2 biosensor formats are plotted on the left and right Y axis respectively. The concentration dependent normalized % inhibition of the C then D and D then C biosensor formats (left Y-axis) and cell viability data (right Y-axis) for **B**) Flutamide, **C**) Bicalutamide, **D**) Enzalutamide, **E**) Compound #10, **F**) EPI-001, **G**) 17-AAG, and **H**) Abiraterone acetate are presented. Representative experimental data from one of two independent experiments are shown.

Table 2. IC₅₀ results of the test set run in the AR-TIF2 Biosensor

| Assay | AR-TIF2 Biosensor | | | |
|---------------------|----------------------------|------|----------------------------|------|
| | C then D | | D then C | |
| | Mean IC ₅₀ (μM) | sdm | Mean IC ₅₀ (μM) | sdm |
| Flutamide | 8.77 | 1.59 | 20.6 | 4.46 |
| Bicalutamide | 2.49 | 0.20 | 4.01 | 1.37 |
| Enzalutamide | 1.44 | 0.16 | 2.71 | 0.27 |
| Compound #10 | >50 | N/A | >50 | N/A |
| EPI-001 | >50 | N/A | >50 | N/A |
| 17-AAG | 0.20 | 0.02 | 0.39 | 0.01 |
| Abiraterone Acetate | >50 | N/A | >50 | N/A |

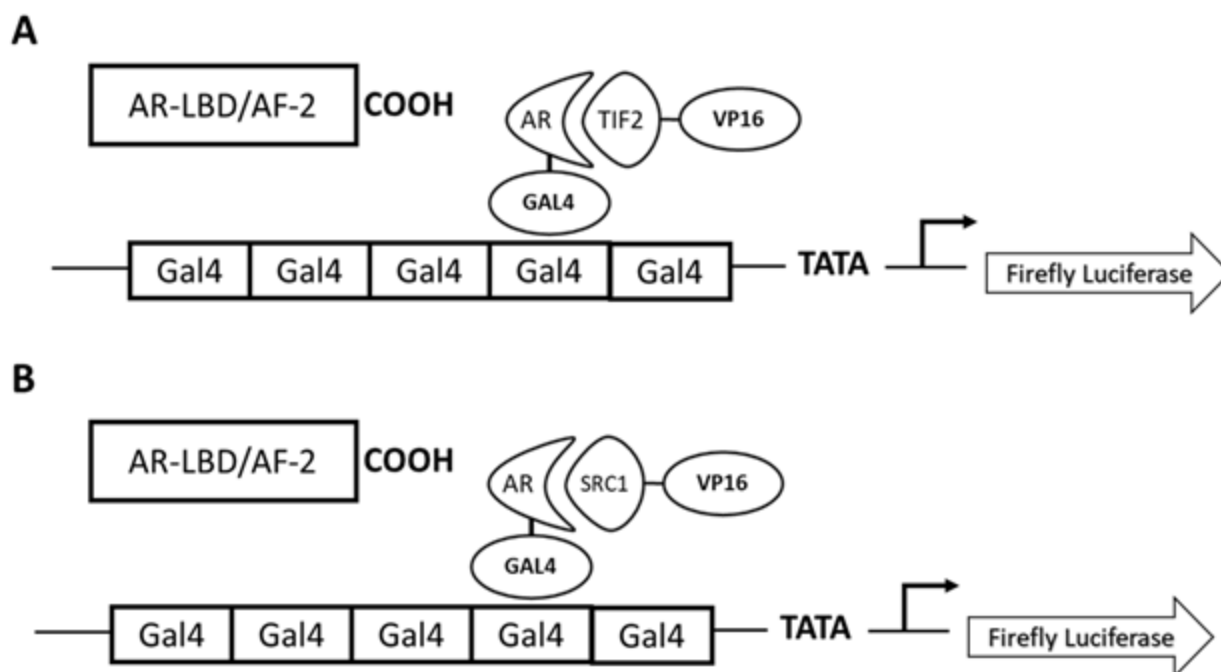


Figure 13. Mammalian 2-Hybrid assay principle

The mammalian 2-hybrid assay we developed involves the transfection of three main components including Gal4-AR-LBD, VP16-coactivator, and the 5xGal4-TATA-Luc reporter. Ligand binding to the nuclear receptor-Gal4 fusion protein directs it to bind to the DNA-binding response sequences in the 5xGal4-TATA-Luc reporter plasmid, while ligand-induced binding interactions between the nuclear receptor and the co-activator-VP16 fusion protein recruits the transcriptional machinery of the cell, leading to overall transcription of the luciferase gene. This reporter activity is an indirect measure of nuclear receptor::co-activator protein interactions in the cell. We have developed this assay in two different co-activator formats using the AR-LBD-Gal4 fusion protein; A) One involves the TIF2/SRC2 p160 coactivator cloned into the VP16 mammalian construct, and B) involves homologous SRC1 p160 coactivator cloned into VP16 vector.

Table 3. PCR primer sequence for amplification and cloning of full-length TIF2 into pVP16 vector

| Primer | PCR Primer Sequence |
|----------------------|---|
| TIF2_FwdPrimer_EcoRI | 5' - GCG GGA ATT CAT GGG AGA AAA TAC CTC TGA CCC C - 3' |
| TIF2pcDNA-BamHI-Rev | 5' - CCT GGA TCC TCG CAA TAT TTC CGT GTT GTG TCT C - 3' |

The pVP16-TIF2 construct was created via the traditional ligation-dependent method. The full-length TIF2 insert was amplified from pCR-BluntII-TOPO-NCoA2 (TIF2) containing the wild type cDNA of the human TIF2 coactivator. The primers for the PCR were designed with the addition of EcoRI and BamHI cloning sites at the 5' and 3' flanking regions, respectively (ThermoFisher Scientific). The TIF2 insert, and the VP16 vector were double digested with EcoRI and BamHI enzymes, and then insert and vector were ligated.

Table 4. Primers for sequence confirmation of pVP16-TIF2

| Primer | Sequencing Primers |
|------------------|---|
| TIF2_VP16_EcoR_F | 5' - GCA GGA ATT CAT GAG TGG GAT GGG AGA AAA TAC C - 3' |
| TIF2-706-F2 | 5' - GAT TCA GAA GAG GAG GGT CAT G - 3' |
| TIF2-1362-F3 | 5' - CAT AAA TGG CCC AAA GGA AC - 3' |
| TIF2-2049-F4 | 5' - GCC CTT AGC CAG CTC TTT G - 3' |
| TIF2-2645-F5 | 5' - CAC CTG TTG GAG CCC AGA AAA C - 3' |
| TIF2-3361-F6 | 5' - CTG GAG GAG ATT GAT AGA GC - 3' |
| TIF2-3954-F7 | 5' - GAT TCC CCA GGC AAA TGC AC - 3' |

After cloning TIF2 into the pVP16 vector, transforming ligation product into DH5 α cells, and plating DH5 α cells on ampicillin containing LB agar plates, colonies were selected and expanded. DNA from expanded colonies was isolated so that individual colonies could be analyzed via restriction analysis. Clones with bands at the correct molecular size were sent for sequencing to confirm the correct cloned construct, using the sequencing primers listed above.

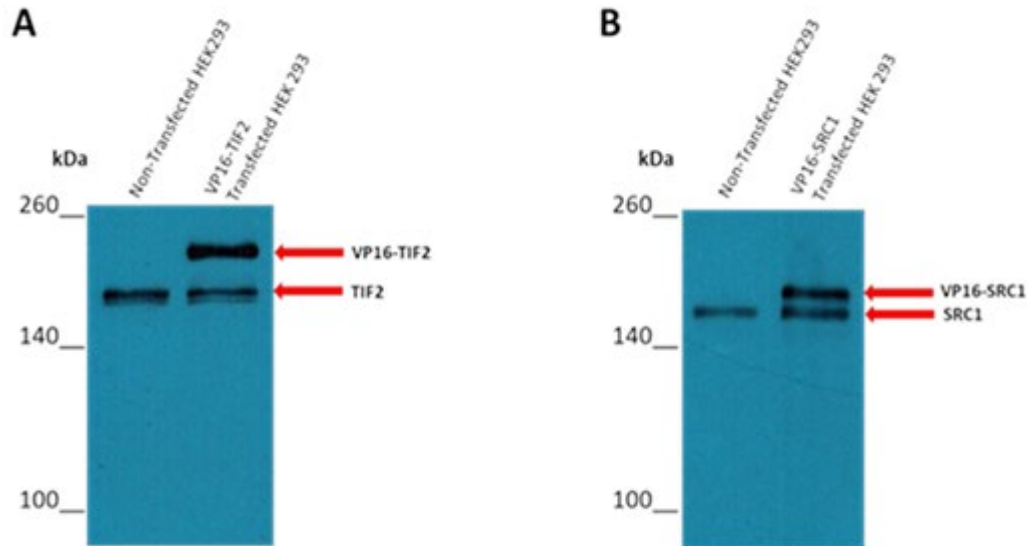


Figure 14. Western blot confirmation of pVP16-coactivator constructs

Coactivators, pVP16-TIF2 and pVP16-SRC1 were transfected into HEK 293 cells and allowed to express their respective fusion proteins for 48 hrs. Forty-eight hours post transfection, cells were lysed, and the BCA protein detection reagent was used to determine protein amount and concentration in transfected cell lysates. An SDS-PAGE gel was then run for protein separation, where 25 μ g of protein from each lysate was added to different lanes of the gel. Protein was transferred to nitrocellulose membranes, and the resulting western blots were then probed with either anti-TIF2 or anti-SRC1 antibodies. HEK 293 cells endogenously express TIF2 and SRC1 coactivators, which are evident in non-transfected HEK 293 lysates. A second band in pVP16-TIF2 and pVP16-SRC1 transfected HEK 293 cells is evident in transfected cell lysates, at a higher molecular weight due to the fusion with VP16.

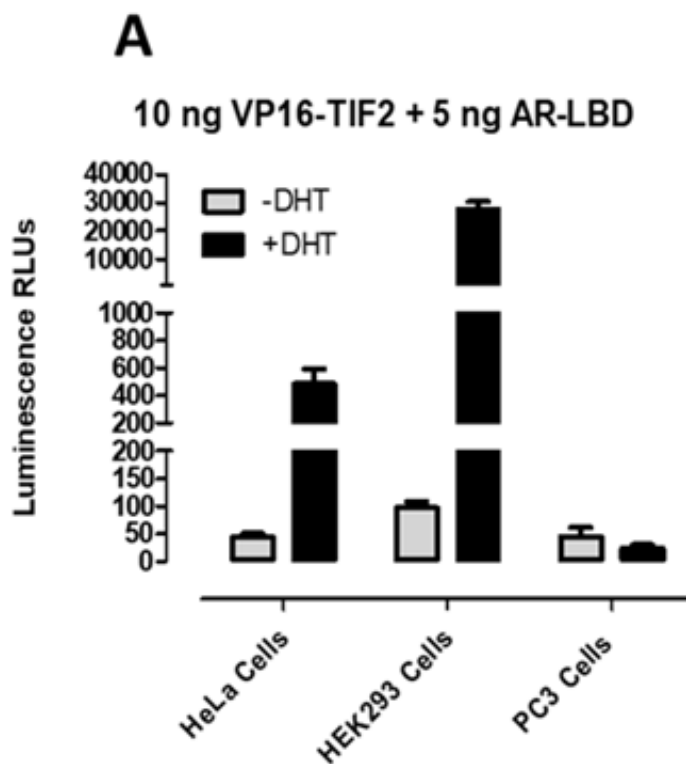


Figure 15. Determining which cell background enables the most robust mammalian 2-hybrid assay

The mammalian 2-hybrid assay was conducted in 3 different cell lines co-transfected with the pGal4-AR-LBD, pVP16-TIF2, and 5xGal4-TATA-Luc reporter, to see how the luciferase reporter luminescence signal behaved in each cell line. PC3 cells were chosen because they are an AR-null prostate cancer cell line, and both HeLa cells and HEK 293 cells were chosen because they have been historically used in mammalian 2-hybrid assays. Cell were transiently co-transfected with the three plasmids using the FuGene transfection reagent, and 5,000 cells were seeded into the wells of 384-well assay plates and cultured overnight at 37°C, 5% CO₂, and 95% humidity. After 24 h cells were exposed to 100 nM DHT and the assay plate was returned to the incubator for an additional 24 h before BrightGlo reagent was added to the plate and the RLUs were captured on a SpectraMax M5e microtiter plate reader. Luminescence RLU's were plotted in the presence or absence of DHT for the three cell lines. The data are presented as the mean \pm SD of triplicate wells per cell line \pm DHT treatment, and representative data from one of 2 independent experiments are shown.

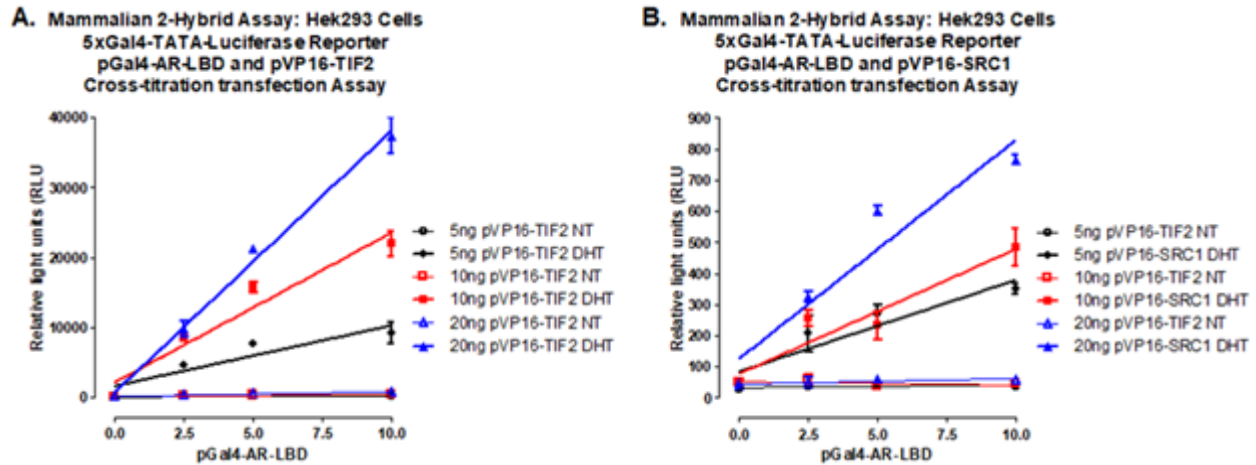


Figure 16. Mammalian 2-Hybrid assay development and optimization

To determine the appropriate amounts of pGal4-AR-LBD and pVP16-TIF2 or pVP16-SRC1 to use in the mammalian 2-hybrid assay, cross-titration co-transfection experiments were performed in HEK293 cells. Interacting partners, pGal4-AR-LBD with pVP16-TIF2 or pVP16-SRC1, plus the reporter construct 5xGal4-TATA-Luc, were transiently co-transfected into HEK293 cells using the FuGene6 transfection reagent, and 5,000 cells were seeded into the wells of 384-well assay plates and cultured overnight at 37°C, 5% CO₂, and 95% humidity. After 24 h cells were exposed to 100 nM DHT and the assay plate was returned to the incubator for an additional 24 h before BrightGlo reagent was added to the plate and the RLUs were captured on a SpectraMax M5e microtiter plate reader. Luminescence RLU's were plotted in the presence or absence of DHT for varying amounts of pGal4-AR-LBD with pVP16-TIF2 or pVP16-SRC1. The data are presented as the mean ± SD of triplicate wells per plasmid DNA combination.

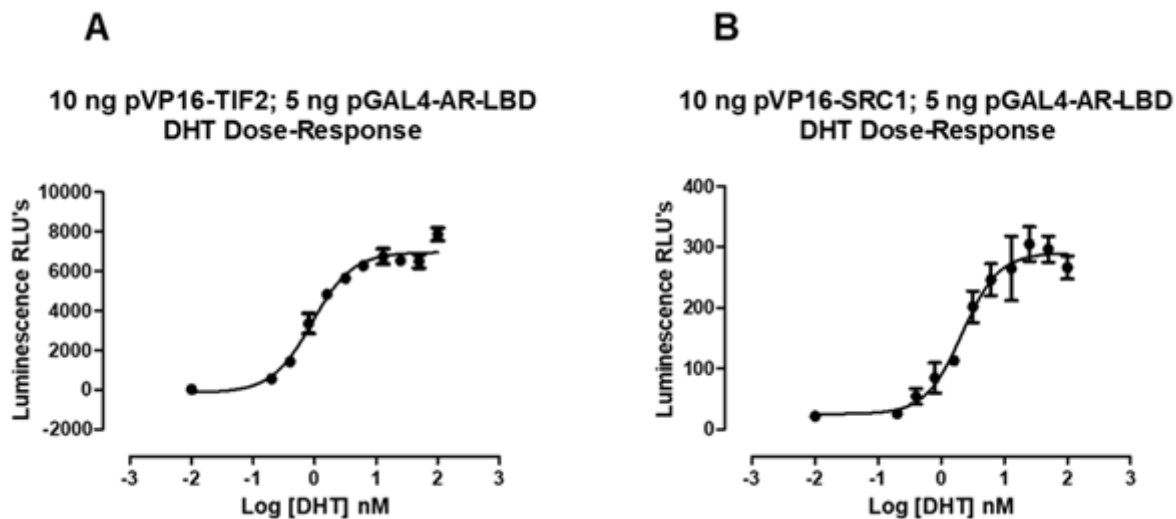


Figure 17. Concentration Responses of the mammalian 2-hybrid assays to measure DHT-induced AR-LBD interactions with the A) TIF2 or B) SRC1 Coactivators

DHT concentration response assays were conducted in HEK293 cells co-transfected with the pGal4-AR-LBD plasmid and either A) the pVP16-TIF2 or B) the pVP16-SRC1 coactivator constructs. HEK293 cells were transiently co-transfected with the appropriate plasmids using the FuGene transfection reagent, and 5,000 cells were seeded into the wells of 384-well assay plates and cultured overnight at 37°C, 5% CO₂, and 95% humidity. After 24 h cells were exposed to the indicated concentrations of DHT and the assay plate was returned to the incubator for an additional 24 h before BrightGlo reagent was added to the plate and the RLUs were captured on a SpectraMax M5e microtiter plate reader. The data are presented as the mean \pm SD of triplicate wells per DHT concentration, and representative data from one of 3 independent experiments are shown. DHT exhibited EC₅₀s of 1.45 \pm 1.29 nM and 1.12 \pm 0.845 nM for the TIF2 and SRC1 M2H formats, respectively.

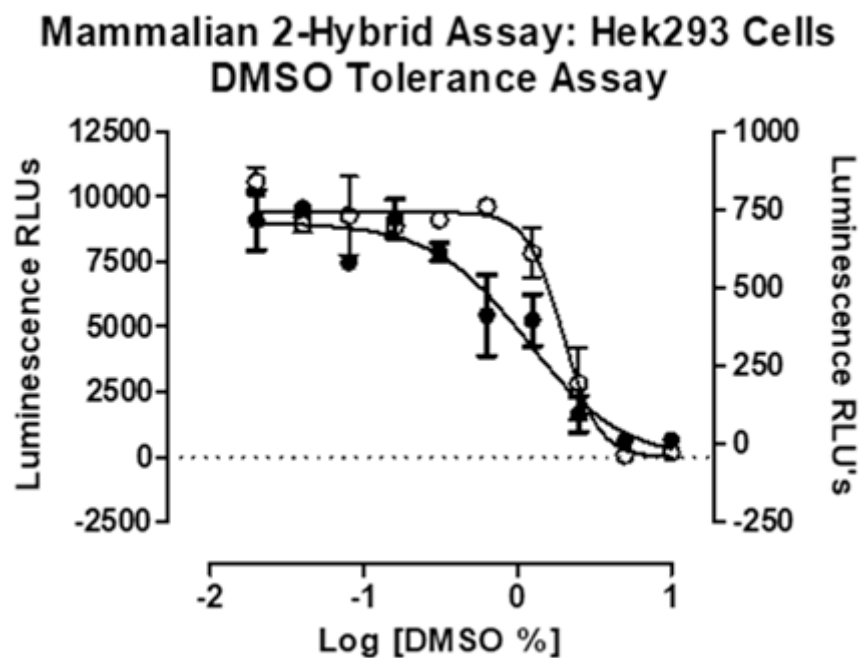


Figure 18. Mammalian 2-hybrid assay development and optimization: DMSO tolerance for HEK 293 cells transfected with pGal4-AR-LBD/pVP16-TIF2 and pGal4-AR-LBD/pVP16-SRC1

To determine the % DMSO that the M2H assay can tolerate, a DMSO concentration response was conducted in HEK293 cells. These cells were transiently co-transfected with the appropriate plasmids using the FuGene transfection reagent, and 5,000 cells were seeded into the wells of 384-well assay plates and cultured overnight at 37°C, 5% CO₂, and 95% humidity. After 24 h cells were exposed to the indicated concentrations of DMSO and the assay plate was returned to the incubator for an additional 24 h before BrightGlo reagent was added to the plate and the RLUs were captured on a SpectraMax M5e microtiter plate reader. The data are presented as the mean ± SD of duplicate wells per DMSO concentration. TIF2 (○) and SRC1 (●) M2H formats are plotted on the left and right Y axis respectively. DMSO exhibited IC₅₀s of 1.97% and 1.16% for the TIF2 and SRC1 M2H formats respectively.

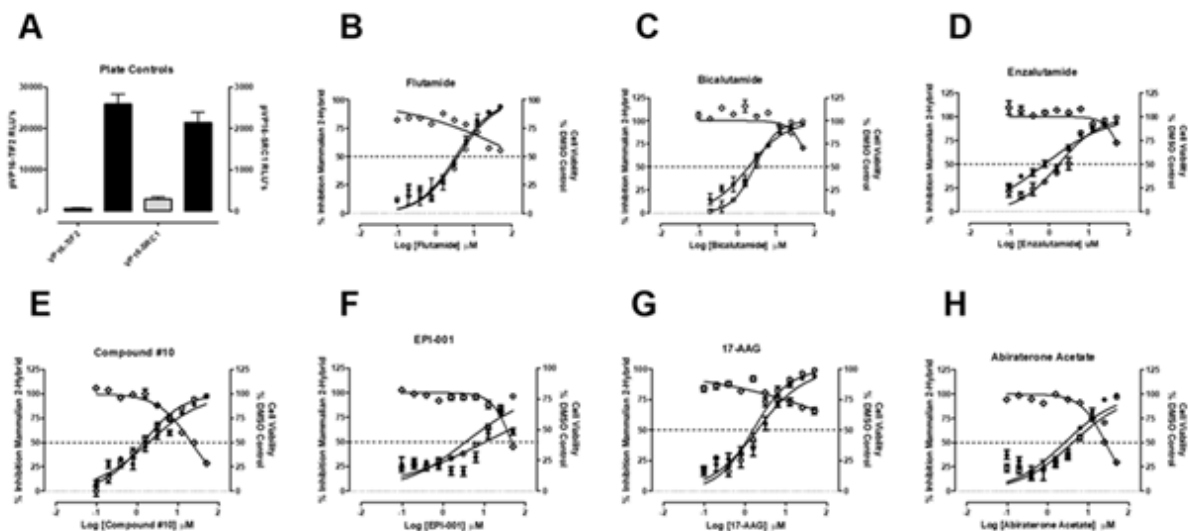


Figure 19. Inhibition of the mammalian 2-hybrid assays to measure DHT-induced AR-LBD interactions with TIF2 or SRC1 coactivators by test compounds

HEK293 cells were transfected with three M2H plasmid constructs, pGAL4-AR-LBD plus 5xGal4-TATA-Luc with either pVP16-TIF2 or pVP16-SRC1, and 5,000 cells were seeded into the wells of 384-well assay plates, and cultured overnight at 37°C, 5% CO₂, and 95% humidity. After 24 h cells were exposed to test compounds at the indicated concentrations for 3 h before overnight exposure to 25 nM DHT. The assay plate was returned to the incubator for an additional 24 h before BrightGlo reagent was added to the plate and the RLU's were captured on a SpectraMax M5e microtiter plate reader. The M2H RLU's data for compound treated wells were normalized to maximum (25 nM DHT + 0.5% DMSO, n=32) and minimum (0.5% DMSO, n=32) plate controls, and the % inhibition was plotted as the mean +/- SD (n = 3) values from triplicate wells for each compound concentration plotted on the left Y-axis. The corresponding cell viability data for compound treated wells were normalized to 0.5% DMSO control wells (n=64), and the % cell viability (\diamond) was plotted as the mean +/- SD (n = 3) values from triplicate wells for each compound concentration plotted on the right Y-axis. **A**) Representative plate control data for the TIF2 (\circ) and SRC1 (\bullet) M2H formats are plotted on the left and right Y axis respectively. The concentration dependent normalized % inhibition of the TIF2 and SRC1 M2H formats (left Y-axis) and cell viability data (right Y-axis) for **B**) Flutamide, **C**) Bicalutamide, **D**) Enzalutamide, **E**) Compound #10, **F**) EPI-001, **G**) 17-AAG, and **H**) Abiraterone acetate are presented. Representative experimental data from one of two independent experiments are shown.

Table 5. IC₅₀ results of test set run in mammalian 2-hybrid assay

| Assay | Mammalian 2-Hybrid | | | | | |
|---------------------|------------------------|------|------------------------|------|---------------------------|------|
| | Gal4-AR-LBD::VP16-TIF2 | | Gal4-AR-LBD::VP16-SRC1 | | HEK 293 Growth Inhibition | |
| | Mean IC50 (μM) | sdm | Mean IC50 (μM) | sdm | Mean IC50 (μM) | sdm |
| Flutamide | 3.01 | 0.75 | 2.53 | 0.66 | >50 | N/A |
| Bicalutamide | 2.01 | 0.99 | 1.49 | 0.69 | >50 | N/A |
| Enzalutamide | 2.36 | 1.44 | 1.37 | 0.91 | >50 | N/A |
| Compound #10 | 2.32 | 0.91 | 1.99 | 0.19 | 26.5 | 10.9 |
| EPI-001 | 9.15 | 2.47 | 8.15 | 1.27 | 36.6 | 9.3 |
| 17-AAG | 0.33 | 0.02 | 0.45 | 0.08 | >50 | N/A |
| Abiraterone Acetate | 4.47 | 1.96 | 2.43 | 0.64 | 30.5 | 7.72 |

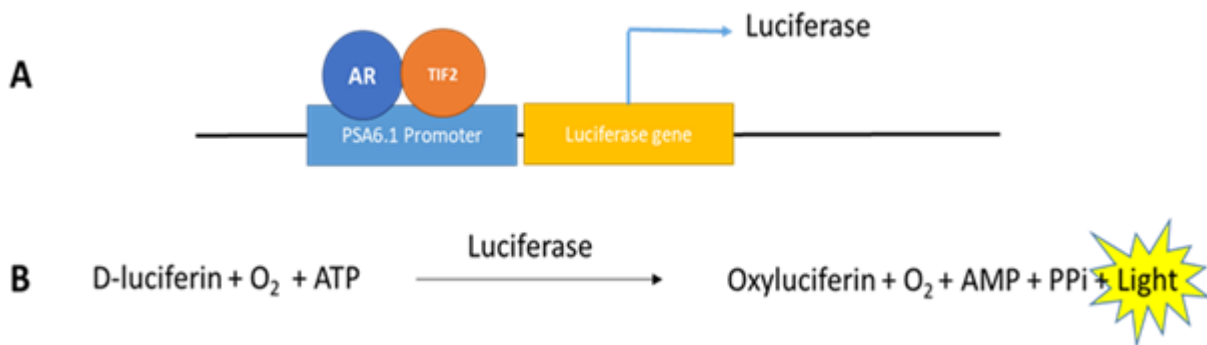


Figure 20. PSA6.1-luciferase reporter assay principle

The PSA reporter assay uses a promoter region from the prostate specific antigen gene, which is a target gene of AR, and a biomarker of PCa progression. The PSA promoter region is fused to a gene that codes for luciferase. If AR and TIF2 are bound to responsive elements on the promoter region of the PSA gene, this will lead to recruitment of the cell's transcriptional machinery, and ultimately, the transcription of luciferase enzyme, which will convert luciferin reagent into light output that can be quantified. If a compound run in this assay can disrupt the interaction between AR and TIF2, this should decrease reporter activity.

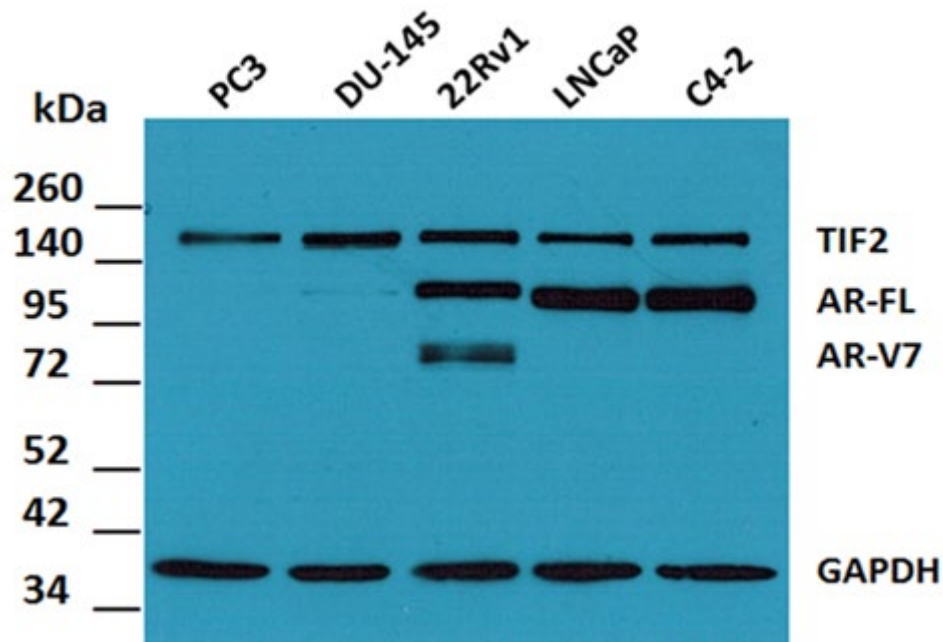


Figure 21. Endogenous expression of TIF2 and AR in 5 PCa cell lines

To determine which of the 5 PCa cell lines to use for developing the stably transfected GFP-AR-FL line, we characterized the endogenous expression levels of AR and coactivator TIF2, in 5 PCa cell lines we had in-house. 20 μ g of protein was added from each lysate, to each well of the SDS-PAGE gel. After the gel was run for protein separation, it was transferred to a nitrocellulose membrane. The membrane was then probed with α -TIF2 and α -AR rabbit polyclonal antibodies, as well as α -GAPDH antibody used as a loading control.

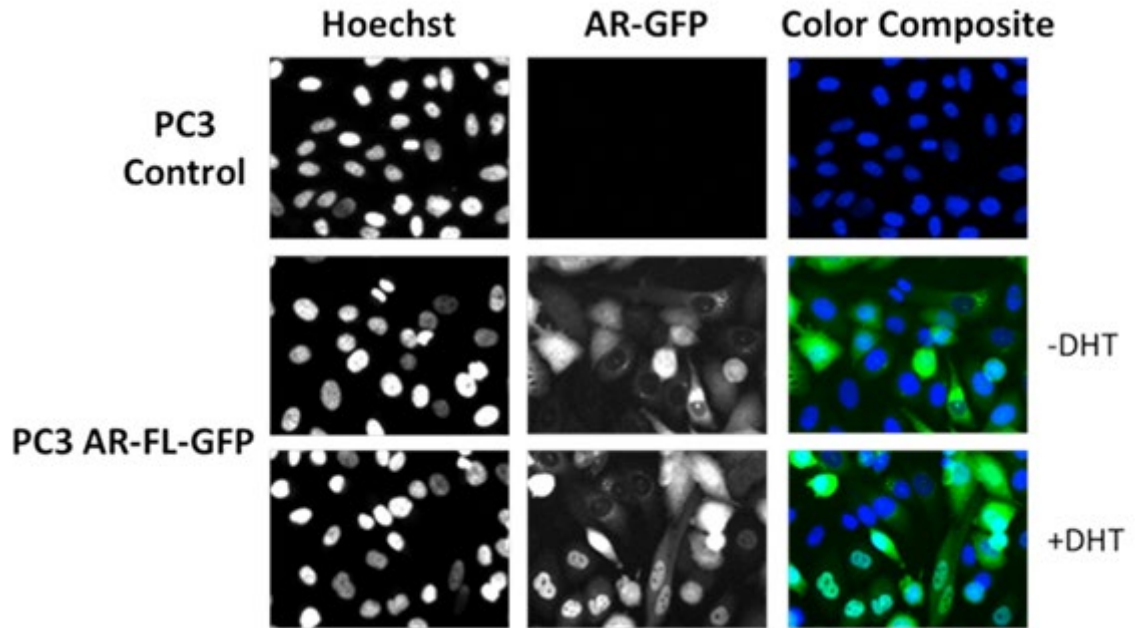


Figure 22. IXM images of PC3 cells stably transfected with pEGFP-C1-AR in the presence or absence of DHT

DHT response assays were conducted in PC3 cells stably transfected with pEGFP-C1-AR-FL plasmid construct. PC3 cells were seeded at a density of 3,000 cells/well into 384-well assay plates and cultured overnight at 37°C, 5% CO₂, and 95% humidity. After 24 h cells were exposed to the indicated concentrations of DHT for 24 before being fixed, and imaged on an IXU automated HCS platform (Molecular Devices LLC). These are representative images of PC3 cells stably transfected with the pEGFP-C1-AR plasmid construct. In untreated cells, AR-FL's distribution is predominantly in the cytoplasm. When these cells are treated with DHT, AR-FL is predominantly nuclear.

Low Expressing Population Inner/Outer Intensity Ratio

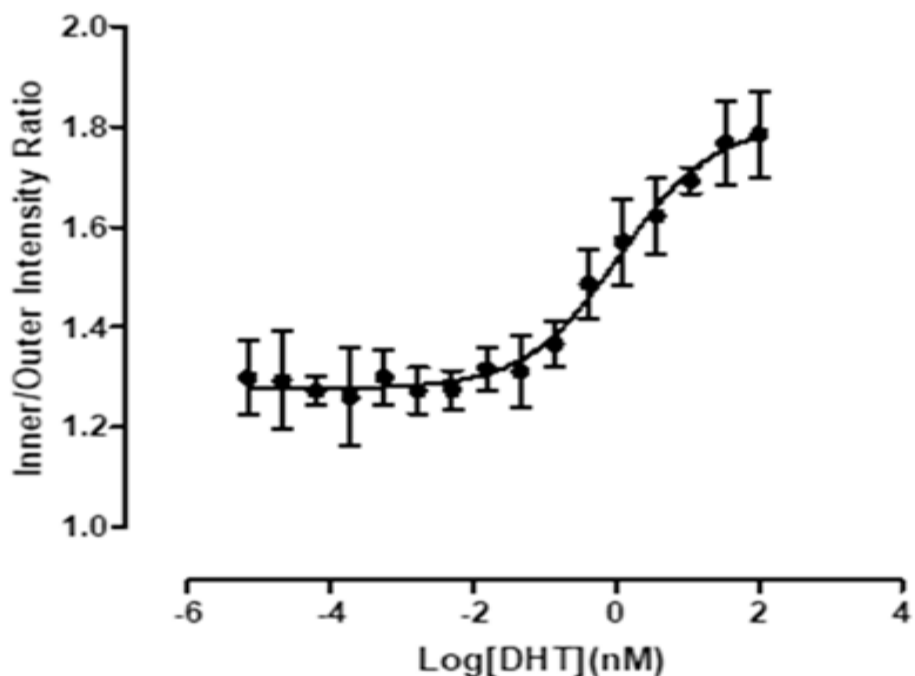


Figure 23. Nuclear Translocation of AR-FL-GFP in PC3 cells exposed to increasing concentrations of DHT

DHT concentration response assays were conducted in PC3 cells stably transfected with pEGFP-C1-AR-FL plasmid construct. PC3 cells were seeded at a density of 3,000 cells/well into 384-well assay plates and cultured overnight at 37°C, 5% CO₂, and 95% humidity. After 24 h cells were exposed to the indicated concentrations of DHT for 24 before being fixed and imaged on an IXU automated HCS platform (Molecular Devices LLC). Images were then analyzed with the TE image analysis module of the MetaXpress software (Molecular Devices LLC). The data are presented as the mean \pm SD of triplicate wells per DHT concentration, and representative data from one of 2 independent experiments are shown. DHT exhibited EC₅₀ of 1.23 \pm 0.131 nM.

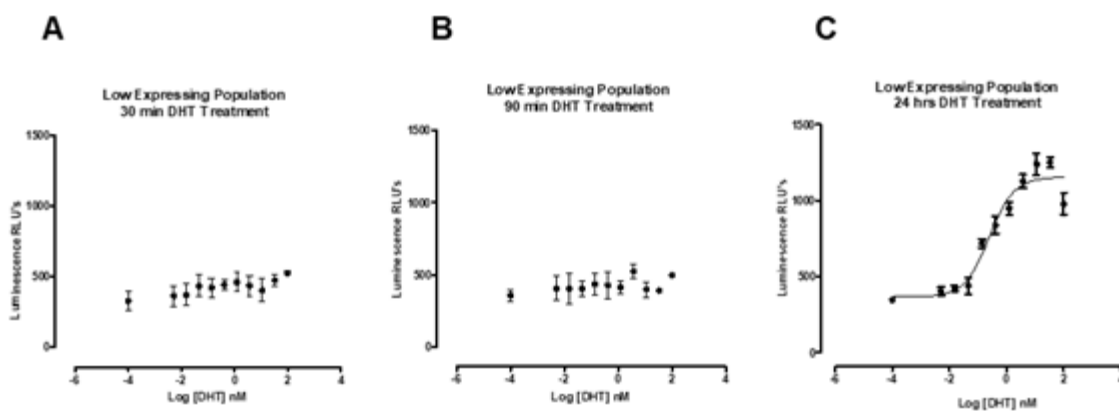


Figure 24. Concentration responses of the PSA6.1-Luc reporter assay to measure DHT-induced transcriptional activity of AR-FL-GFP in PC3 cells

DHT concentration response assays were conducted in PC3 cells stably transfected with pEGFP-C1-AR-FL plasmid and transiently transfected with the PSA6.1-LUC reporter construct. PC3 cells were transiently transfected with the appropriate plasmids using the FuGeneHD transfection reagent, and 3,000 cells were seeded into the wells of 384-well assay plates and cultured overnight at 37°C, 5% CO₂, and 95% humidity. After 24 h cells were exposed to the indicated concentrations of DHT and the assay plate was returned to the incubator for either 30 min, 90 min, or 24 h before BrightGlo reagent was added to the plate and the RLU's were captured on a SpectraMax M5e microtiter plate reader. The data are presented as the mean \pm SD of triplicate wells per DHT concentration, and representative data from one of 2 independent experiments are shown. DHT exhibited EC₅₀ of 0.280 \pm 0.033 nM at 24 hrs DHT exposure.

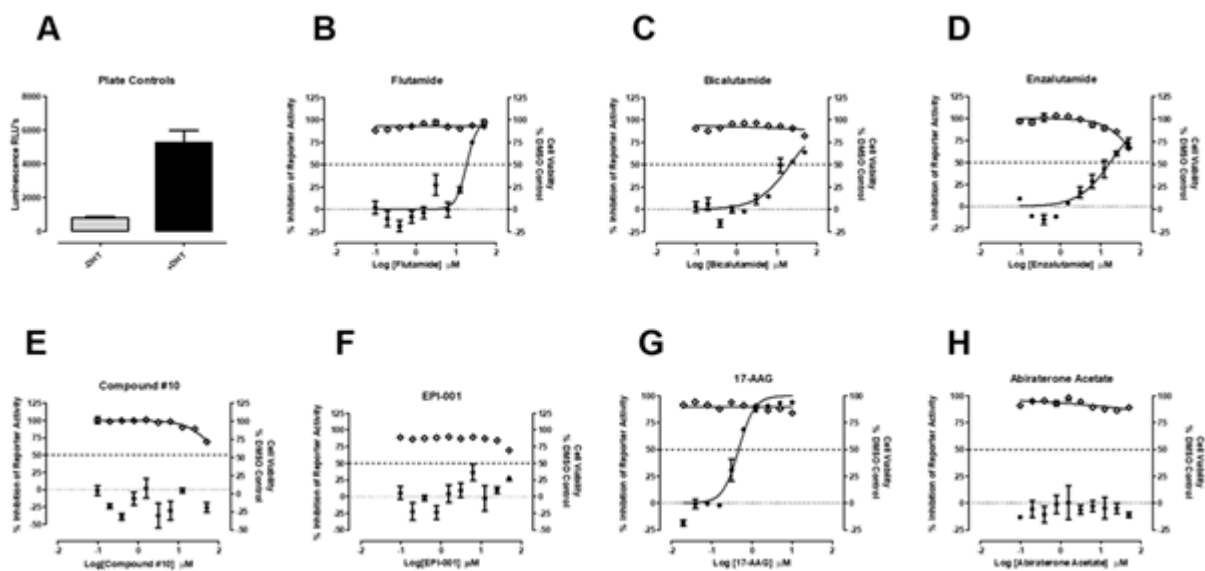


Figure 25. Test set performance in PSA6.1-Luc reporter assay

A DHT-induced PSA6.1-LUC reporter based assay was conducted with 7 test compounds. PC3-AR-FL-GFP cell lines were transiently bulk transfected with a 3:1 ratio of Fugene HD: PSA-6.1-LUC plasmid DNA (20 ng/well), then seeded into assay plates at a density of 3,000 cell per well, and finally incubated overnight at 5% CO₂, 95% humidity, and 37°C. PC3-AR-FL-GFP cells transfected with the PSA-6.1-LUC plasmid were exposed to the indicated concentrations of compounds for 3 h and were then treated with 25 nM DHT. The assay plate was returned to the incubator for an additional 24 h before BrightGlo reagent was added to the plate and the RLUs were captured on a SpectraMax M5e microtiter plate reader. The PSA6.1-LUC RLU's data for compound treated wells were normalized to maximum (25 nM DHT + 0.5% DMSO, n=32) and minimum (0.5% DMSO, n=32) plate controls, and the % inhibition was plotted as the mean +/- SD (n=3) values from triplicate wells for each compound concentration plotted on the left Y-axis. The corresponding cell viability data for compound treated wells were normalized to 25 nM DHT + 0.5% DMSO control wells (n=32), and the % cell viability (◇) was plotted as the mean +/- SD (n = 3) plotted on the right Y-axis. **A)** Representative plate control data for one run is plotted. The concentration dependent normalized % inhibition of the DHT-induced PSA6.1-LUC reporter activity for **B)** Flutamide, **C)** Bicalutamide, **D)** Enzalutamide, **E)** Compound #10, **F)** EPI-001, **G)** 17-AAG, and **H)** Abiraterone acetate are presented. Representative experimental data from one of two independent experiments are shown.

Table 6. IC₅₀ results of test set run in the PSA6.1-Luc reporter based assay

| Assay | PSA6.1-LUC Reporter | | Growth Inhibition | |
|---------------------|---------------------|------|---------------------|-----|
| | PC3-AR-FL-GFP Cells | | PC3-AR-FL-GFP Cells | |
| | Mean IC50 (μM) | sdm | Mean IC50 (μM) | sdm |
| Flutamide | 17.4 | 3.91 | >50 | N/A |
| Bicalutamide | 21.9 | 4.80 | >50 | N/A |
| Enzalutamide | 19.5 | 3.45 | >50 | N/A |
| Compound #10 | >50 | N/A | >50 | N/A |
| EPI-001 | >50 | N/A | >50 | N/A |
| 17-AAG | 1.72 | 0.48 | >50 | N/A |
| Abiraterone Acetate | >50 | N/A | >50 | N/A |

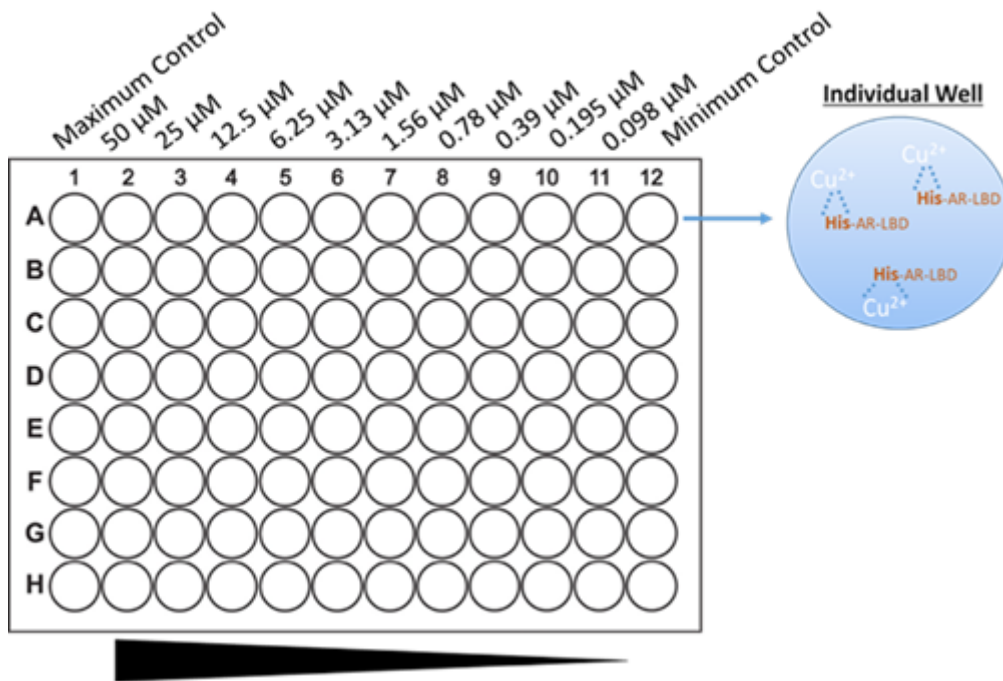


Figure 26. Radio ligand binding assay principle

The competitive radio ligand binding assay we developed employs histidine tagged AR-LBD, and radiolabel H^3 -DHT, a known ligand and agonist of our target. His₆-AR-LBD chelates to the Cu^{2+} coated plate surface, and then any unbound AR protein is washed away, after which 10 nM of the radiolabel and compound, is added to each well. After an hour incubation, any displaced radiolabel or compound is washed away. Columns 1 and 12 represent maximum and minimum controls, containing either the addition of 5% DMSO, or cold DHT, respectively. This assay specifically measures the displacement of H^3 -DHT from AR-LBD in the presence of increasing concentrations of each test compound, thereby identifying any compound acting as an AR-antagonist.

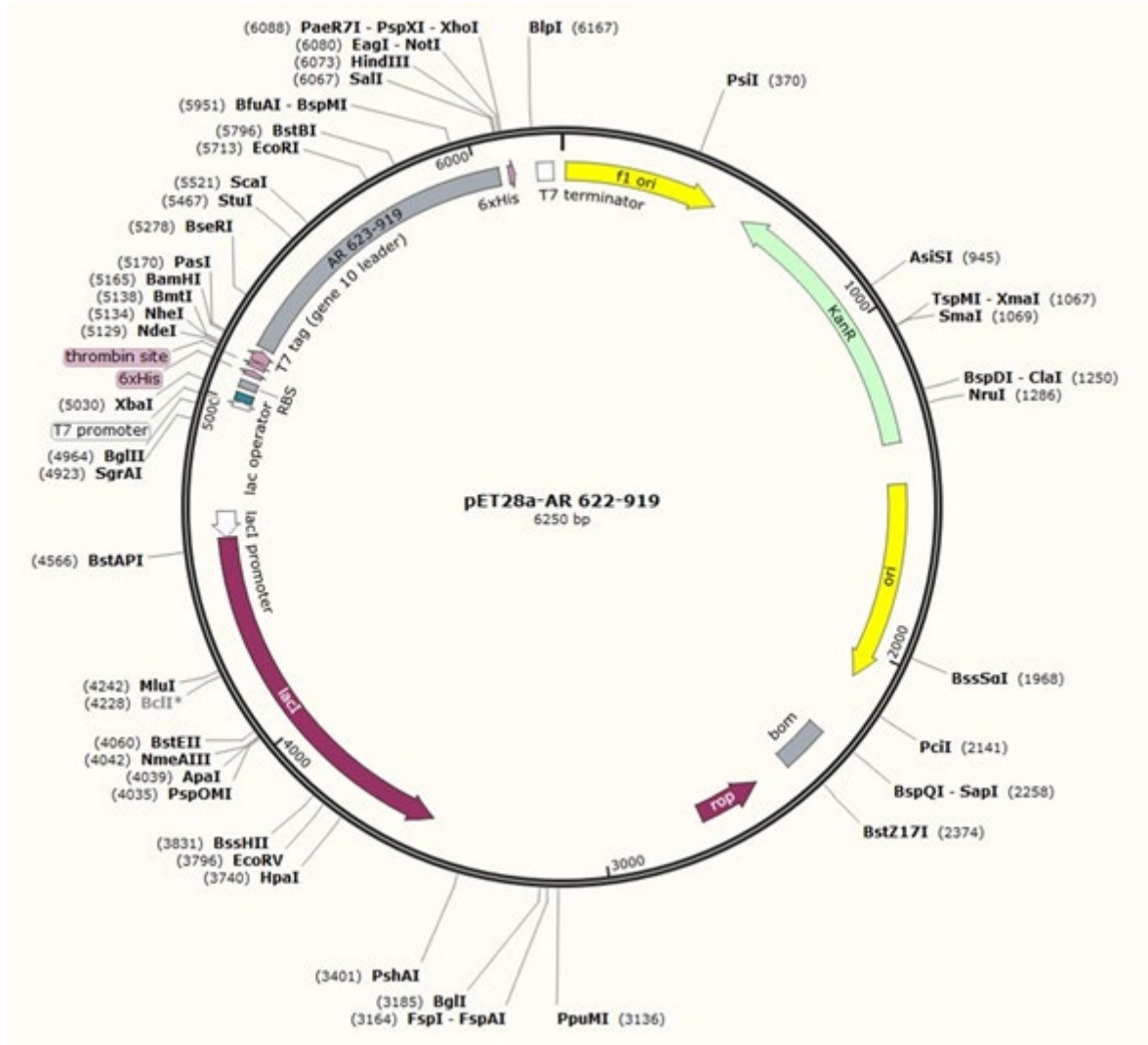


Figure 27. pET28a-His₆-AR-LBD construct

The pET28a-His₆-AR-LBD (622-919) construct was kindly provided by Dr. Fletterick and Dr. Ngyuen from the University of California, San Francisco. This construct was designed by cloning amino acids 622-919 of the androgen receptor, which encodes the ligand binding domain of the receptor, into a pET28 bacterial expression vector. The pET28 bacterial expression vector bears a 6x histidine tag, which allows for the fusion of this tag to the AR.

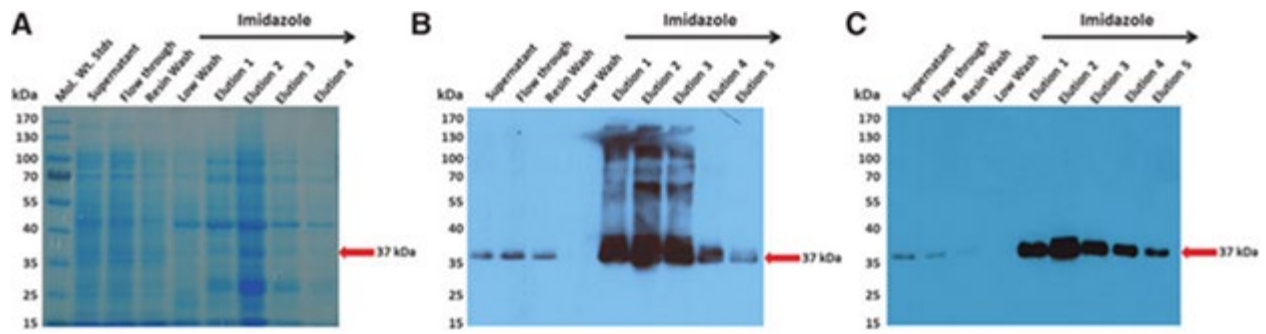


Figure 28. pET28a-His₆-AR-LBD

Fractions collected from the Ni²⁺ - based affinity column were eluted with 300 mM Imidazole and were separated on 12% SDS-PAGE gels. Coomassie blue stained bands with the correct AR-LBD protein molecular weight (37 kDa) were further confirmed on western blots probed with α -His and α -AR, antibodies.

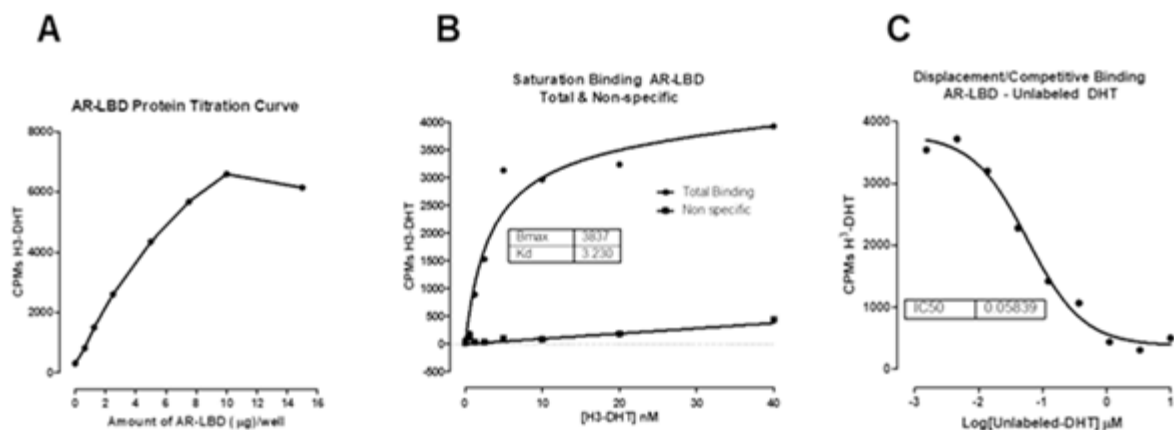


Figure 29. H³-DHT radio ligand binding assay development

To determine the appropriate amounts of His₆-AR-LBD to use in the radio ligand binding assay, we performed a protein titration by adding increasing amounts of His₆-AR-LBD to 96-well Cu²⁺-coated plates. Any unbound His₆-AR-LBD was aspirated from wells before blocking the plates with BSA before the addition of H³-DHT. The amount of H³-DHT used in the assay remained fixed at 10 nM. After 10 nM of H³-DHT was incubated for 1 hr, it was removed via aspiration. Next, scintillation buffer was added, and plates were sealed and read in a beta plate counter. CPM's were then plotted and representative experimental data from one of three independent experiments are shown. To determine the appropriate amounts of H³-DHT to use in the radio ligand binding assay, saturation binding experiments were performed. Increasing amounts of H³-DHT were bound to His₆-AR-LBD (5ug/well), and incubated for 1 hr before it was removed via aspiration. Once scintillation buffer was added, plates were sealed and read in a beta plate counter. CPM's were then plotted and representative experimental data from one of three independent experiments are shown. Finally, a displacement binding experiment was run by incubating 10 nM H³-DHT together with increasing concentration of cold-DHT to compete for binding at the His₆-AR-LBD. Again, scintillation buffer was added, plates were sealed and read in a beta plate counter. CPM's were then plotted and representative experimental data from one of three independent experiments are shown.

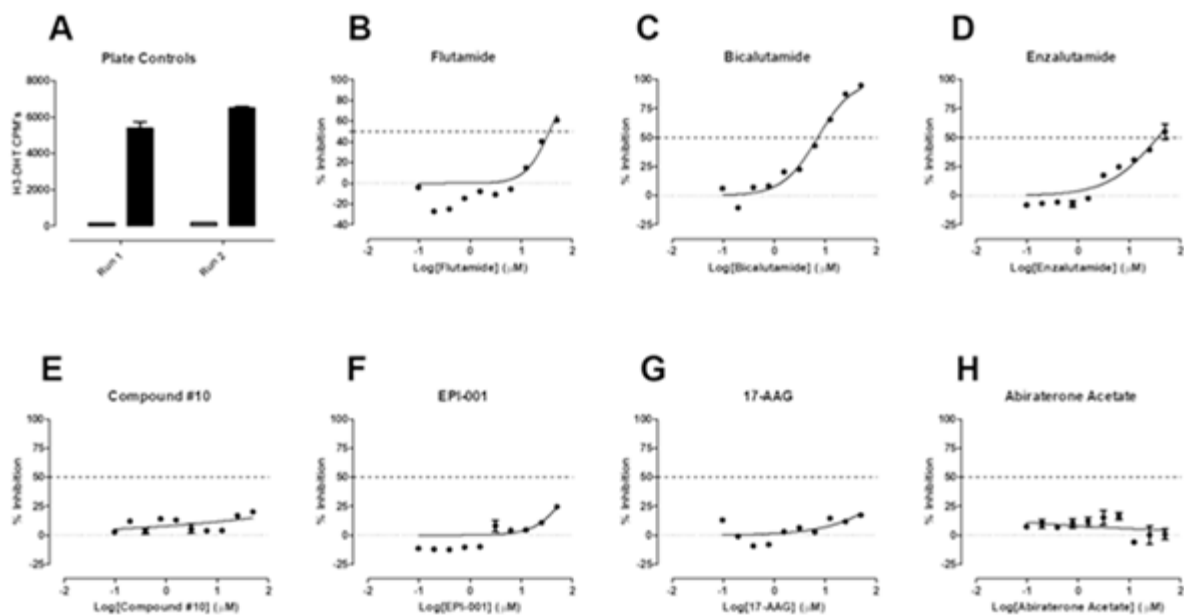


Figure 30. Test set performance in H^3 -DHT radio ligand binding assay

Competitive displacement binding of H^3 -DHT to His₆-AR-LBD run with the seven compounds in our test set. Five micrograms of His₆-AR-LBD protein was added to the wells of 96-well copper-coated plates and allowed to bind overnight at 4°C. Unbound protein was removed by aspiration; the plate was washed 3x with PBS-Tween 20 buffer and blocked for 1 h with 1 mg/mL BSA in PBS-Tween 20. After 3x washes with PBS-Tween 20 buffer, 10 nM H^3 -DHT was added to the wells of the plate in the presence or absence of the indicated concentrations of validation compounds and incubated at RT for 1 h. Unbound H^3 -DHT was removed by aspiration and washing, and micro-scintillation reagent was added to the wells, and the CPMs were captured on a TopCount NXT microtiter β -counter. β -emission RLU's data for compound treated wells were normalized to maximum (0.5% DMSO, n=8) and minimum (10 μ M cold DHT, n=8) plate controls, and the % inhibition was plotted as the mean \pm SD (n=3) values from duplicate wells for each compound concentration. **A)** Representative plate control data for Run 1 and Run 2 is plotted. The concentration dependent normalized % inhibition of the H^3 -DHT bound to His₆-AR-LBD for **B)** Flutamide, **C)** Bicalutamide, **D)** Enzalutamide, **E)** Compound #10, **F)** EPI-001, **G)** 17-AAG, and **H)** Abiraterone acetate are presented. Representative experimental data from one of two independent experiments are shown.

Table 7. IC₅₀ results of test set run in H³-DHT radio ligand binding assay

| Assay | H3-DHT RadioLigand Binding | |
|---------------------|----------------------------|------|
| | Mean IC50 (μM) | sdm |
| Flutamide | 48.6 | 19.5 |
| Bicalutamide | 5.53 | 3.27 |
| Enzalutamide | 50.2 | 14.4 |
| Compound #10 | >50 | N/A |
| EPI-001 | >50 | N/A |
| 17-AAG | >50 | N/A |
| Abiraterone Acetate | >50 | N/A |

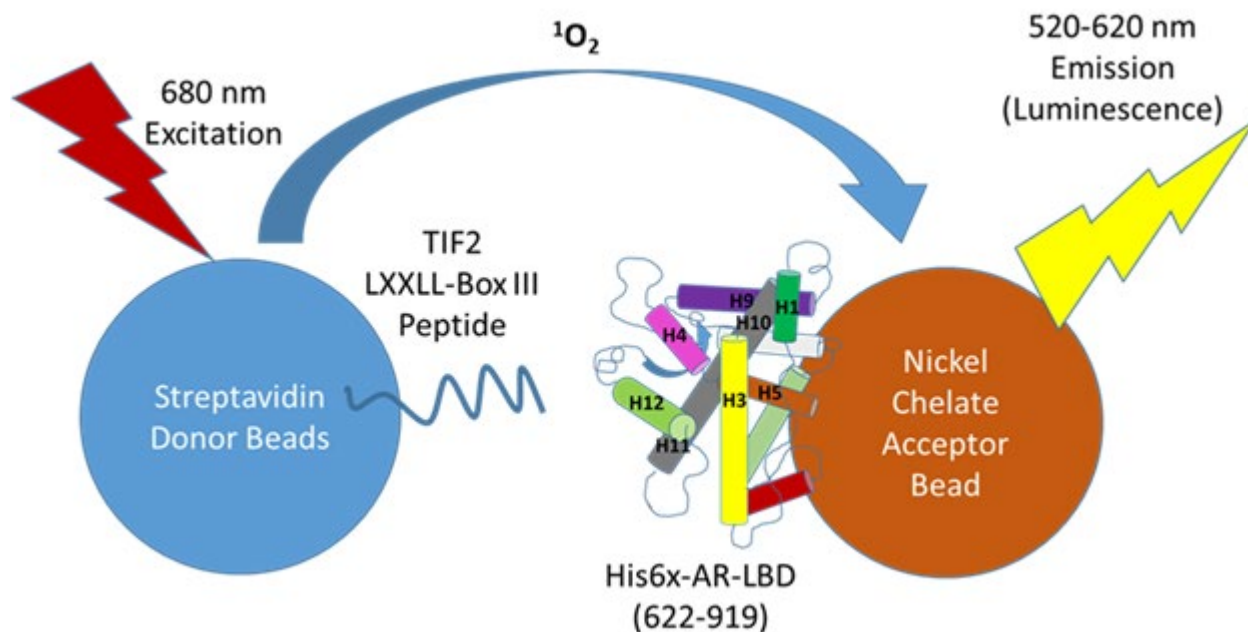


Figure 31. AR AF-2::LXXLL-TIF2 peptide binding ALPHAScreen assay principle

Schematic of ALPHAScreen assay. Histidine-tagged AR-LBD protein expressed and purified in *E. coli* cells is chelated to Ni^{2+} coated acceptor beads. TIF2-Box-III LXXLL motif peptides conjugated to biotin are immobilized to streptavidin donor beads. When AR-LBD and TIF2 interact, the beads are brought into close proximity. Subsequent excitation of the donor bead results in a chemical reaction releasing a singlet oxygen species. When a reagent contained in the acceptor bead is excited by the oxygen, it emits light at a wavelength between 520-620 nm. Any compound that acts to inhibit this protein-protein interaction will result in an attenuation of the signal.

Table 8. TIF2-box-III (738-756) peptide sequence used in ALPHAScreen assay

| Peptide | Sequence^a |
|---|---|
| Biotinylated-TIF2-box-III (738-756) | Biotin-HN-CKKKEN ALLRYLLDKDDTKD -CONH2 |
| Non-biotinylated TIF2-box-III (738-756) | H2N -CKKKEN ALLRYLLDKDDTKD -CONH2 |

^a Conserved LXXLL motifs required for p160 coactivator interaction with the AF2 surface of the AR-LBD are in bold.

Biotinylated and Non-biotinylated TIF2-box-III peptide were synthesized by the Peptide & Peptoid Synthesis Facility at the University of Pittsburgh's Health Sciences Core Research Facilities. TIF2-box-III amino acids 738-756 have been shown to be the most important for the interaction with the AR AF-2 surface. Biotinylated and Non-biotinylated TIF2-box-III are used in the development, and implementation of the ALPHAScreen assay.

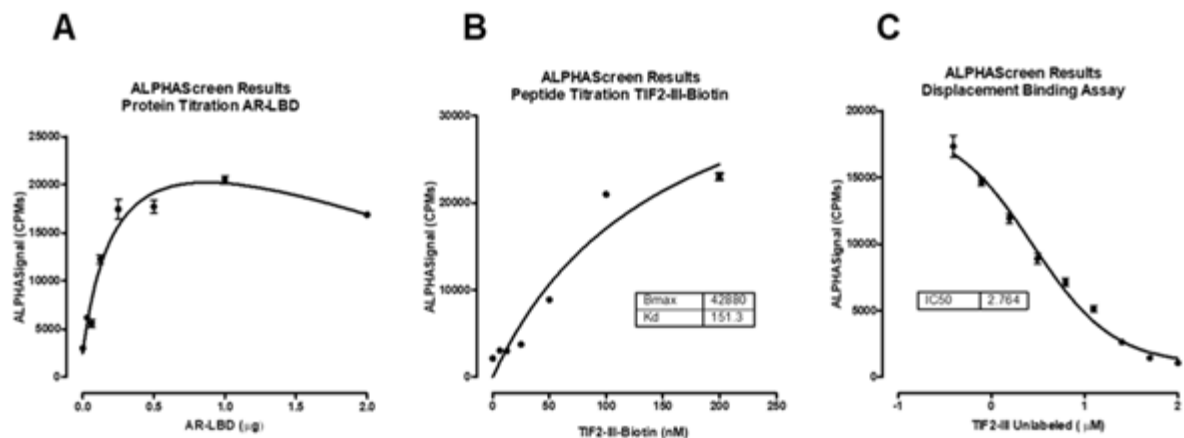


Figure 32. AR AF-2::LXXLL-TIF2 peptide binding ALPHAScreen assay development

A His₆-AR-LBD Protein Titration, biotinylated-TIF2-box-III titration, and displacement binding experiments were carried out in 384-well, white opaque plates. The protein titration was run using different amounts of His₆-AR-LBD 622-919, ranging from 0-2 µg/well, incubated with 10 µM DHT, and Ni²⁺ chelate acceptor beads for 30 min at room temperature in the dark. This mixture was combined with Biotinylated TIF2-box III that had been previously incubated with streptavidin donor beads, and was allowed to incubate together for 1 hr at RT in the dark, before being read on an envision plate reader to measure protein interactions. The biotinylated-TIF2-box-III titration was run using different amounts of biotinylated TIF2 peptide, ranging from 0-200 nM of peptide, incubated with streptavidin donor beads for 30 min at room temperature in the dark. This mixture was combined with His₆-AR-LBD (0.4 µg/well), 10 µM DHT, and Ni²⁺ chelate acceptor beads that had been previously incubated together, and was allowed interaction for 1 hr at RT in the dark. Finally, these were a read on an envision plate reader to measure protein interactions. Displacement binding assays were run with fixed amounts of biotinylated TIF2 peptide that were incubated with streptavidin donor beads for 30 min at room temperature in the dark. Different amounts of unlabeled TIF2 were added to biotinylated TIF2 peptide bound by streptavidin donor beads. Next, His₆-AR-LBD (0.4 µg/well), 10 uM DHT, and Ni²⁺ chelate acceptor beads that had been previously incubated together, was added to the previous mixture and allowed to mix for 1 hr at RT in the dark. Finally, these were a read on an envision plate reader to measure protein interactions.

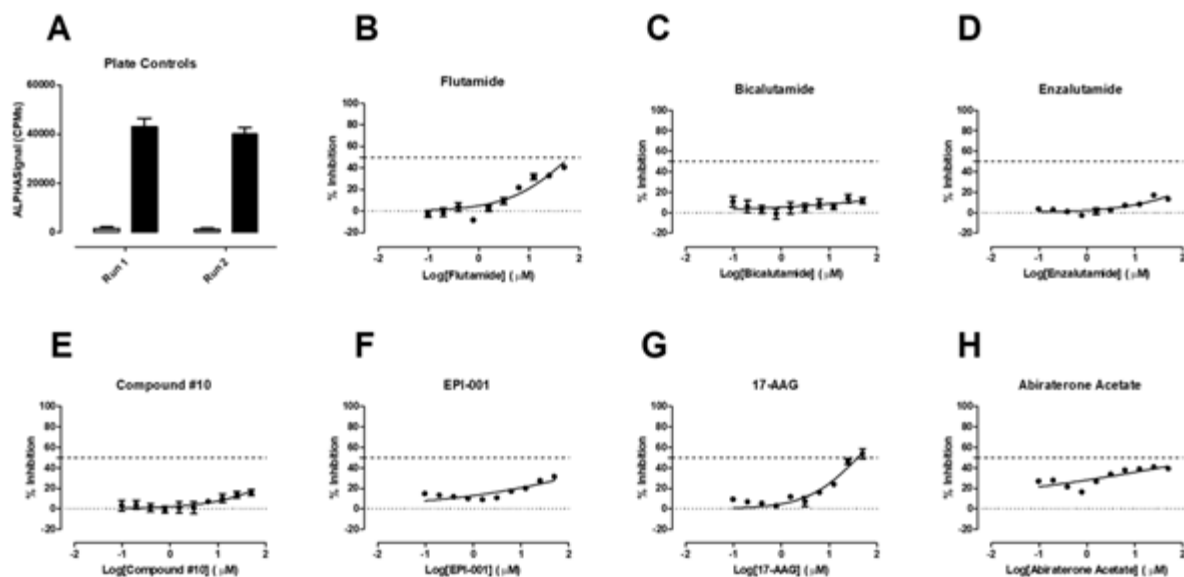


Figure 33. Test set performance in AR AF-2::LXXLL-TIF2 peptide binding ALPHAScreen assay

A competitive displacement binding of biotinylated-TIF2-box-III peptide to His6-AR-LBD was conducted with 7 test compounds to validate the ALPHAScreen assay. Biotinylated-TIF2 peptide was incubated with streptavidin donor beads for 30 min, in the dark, at RT, and then added to 384-well assay plates at a final concentration of 150 nM. Next, compound was added to the wells of the plate at the indicated concentrations, and incubated for 30 min, in the dark, at RT. Simultaneously, pET28a-His₆-AR-LBD (400ng/well) was incubated with DHT, and Ni²⁺ coated acceptor beads for 30 min. Finally, DHT bound pET28a-His₆-AR-LBD, chelated to acceptor beads were mixed with streptavidin bound TIF2-peptide in 384-well plates. After mixing the ALPHAScreen components, they were incubated for 1 hr at RT in the dark, and after, read on an envision plate reader. The ALPHASignal (CPMs) data for compound treated wells were normalized to maximum (0.5% DMSO, n=32) and minimum (0.5% DMSO and 75 μM unlabeled TIF2, n = 32) plate controls, and the % inhibition was plotted as the mean +/- SD (n=3) values from triplicate wells for each compound concentration. **A)** Representative plate control data for Run 1 and Run 2 are plotted. The concentration dependent normalized % inhibition of the AR-AF2::LXXLL-peptide binding for **B)** Flutamide, **C)** Bicalutamide, **D)** Enzalutamide, **E)** Compound #10, **F)** EPI-001, **G)** 17-AAG, and **H)** Abiraterone acetate are presented. Representative experimental data from one of two independent experiments are shown.

Table 9. IC₅₀ results of test set run in AR AF-2::LXXLL-TIF2 peptide binding ALPHAScreen assay

| Assay | ALPHAScreen | |
|---------------------|----------------------------|------|
| | Mean IC ₅₀ (μM) | sdm |
| Flutamide | >50 | N/A |
| Bicalutamide | >50 | N/A |
| Enzalutamide | >50 | N/A |
| Compound #10 | >50 | N/A |
| EPI-001 | >50 | N/A |
| 17-AAG | 29.8 | 9.78 |
| Abiraterone Acetate | >50 | N/A |

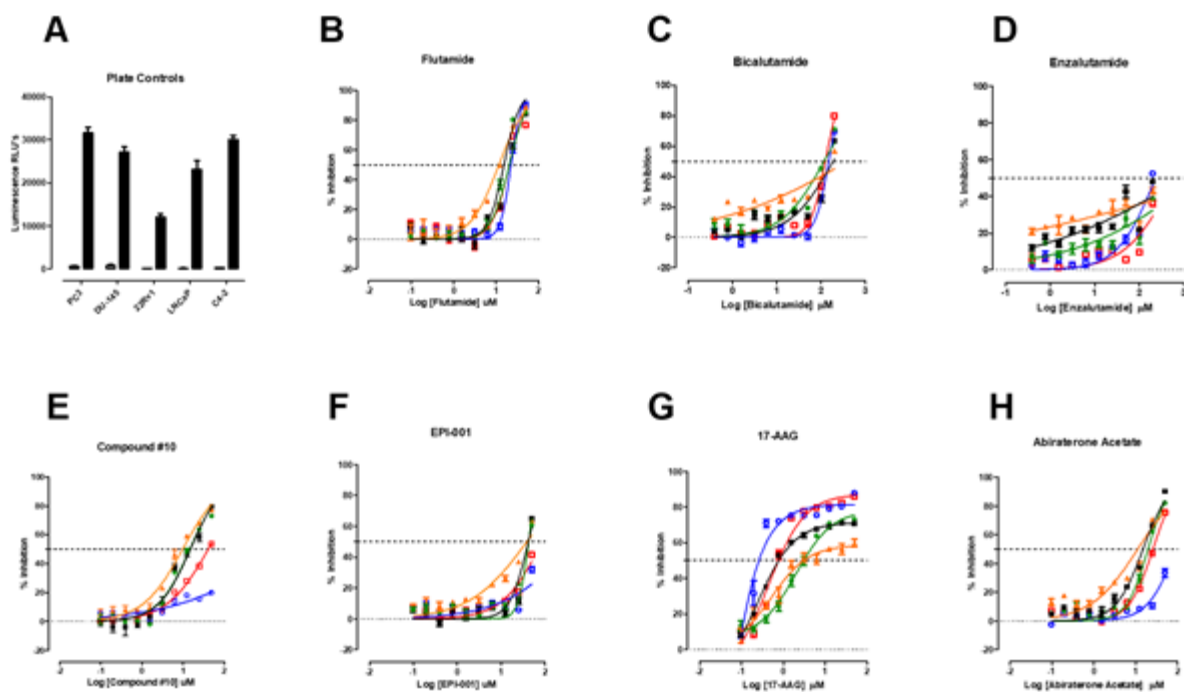


Figure 34. Test set performance in growth inhibition assays

Concentration-dependent inhibition of PCa cell line growth by 72 h exposure to test compounds. The five PCa cell lines were seeded into 384-well assay plates at 1,000 cells per well and incubated at 37°C in 5% CO₂ and 95% humidity for 24 h. After 24 h, the indicated concentrations of test compounds were transferred into the test wells of the 384-well assay plates that were then incubated at 37°C in 5% CO₂ and 95% humidity for an additional 72 h. The growth inhibition data for compound treated wells were normalized to maximum (0.5% DMSO, n=32) and minimum (200 μM Dox and 0.5% DMSO, n=32) plate controls, and the % inhibition was plotted as the mean \pm SD (n = 3) values from triplicate wells for each compound concentration plotted. **A)** Representative plate control data for each of the 5 cell lines: (\square) PC3, (\circ) DU-145, (\bullet) 22Rv1, (\blacktriangle) LNCaP, and (\blacksquare) C4-2 is plotted. The concentration dependent normalized % inhibition of each cell line for **B)** Flutamide, **C)** Bicalutamide, **D)** Enzalutamide, **E)** Compound #10, **F)** EPI-001, **G)** 17-AAG, and **H)** Abiraterone acetate are presented. Representative experimental data from one of two independent experiments are shown.

Table 10. IC₅₀ results of test set run in growth inhibition assays

| Assay | Growth Inhibition Assay | | | | | | | | | |
|---------------------|----------------------------|------|----------------------------|------|----------------------------|------|----------------------------|------|----------------------------|------|
| | PC3 | | DU-145 | | 22Rv1 | | LNCaP | | C4-2 | |
| | Mean IC ₅₀ (μM) | sdm |
| Flutamide | 19.9 | 0.67 | 21.0 | 1.69 | 19.2 | 1.38 | 13.7 | 1.94 | 14.9 | 0.57 |
| Bicalutamide | 124 | N/A | 148.6 | N/A | 117 | N/A | >200 | N/A | 188 | N/A |
| Enzalutamide | >50 | N/A |
| Compound #10 | 40.8 | 0.60 | >50 | N/A | 19.3 | 4.63 | 17.6 | 7.78 | 14.5 | 0.58 |
| EPI-001 | >50 | N/A | >50 | N/A | 41.2 | 1.30 | 33.0 | 5.97 | 38.6 | 3.25 |
| 17-AAG | 0.50 | 0.45 | 0.21 | 0.20 | 2.10 | 1.72 | 3.53 | 3.39 | 0.84 | 0.75 |
| Abiraterone Acetate | 22.6 | 3.37 | >50 | N/A | 19.3 | 0.53 | 12.5 | 1.28 | 15.3 | 0.27 |

4.0 Targeting the Transactivation potential of the AR amino-terminal domain

4.1 Introduction: Development of a Panel of Assays to Interrogate the Ability of Compounds to Block the Transactivation Potential of the AR-NTD

Resistance to androgen deprivation therapy is due to continued AR signaling in cells despite achieving serum testosterone levels of less than 50 ng/dL in PCa patients [166]. Continued AR signaling and AR transcriptional activity arises from the molecular mechanisms of resistance that occur in CRPC cells. AR dependent mechanisms of resistance contributing to CRPC include AR over-expression, continued intra-tumoral androgen synthesis, and promiscuous AR activation by non-androgenic ligands. These mechanisms compensate for lower cellular levels of DHT [48], [49], [50]. Other mechanisms that enable AR to signal in androgen depleted conditions include the emergence of AR splice variants, such as AR-V7 and ARv567es, which lack a ligand-binding domain (LBD), making them unresponsive to antiandrogens, [167], [168]. AR-V7's transcriptional activity which is both constitutively active and androgen independent, leads to the expression of target genes implicated in biosynthesis, such as the PCa biomarker PSA, and those associated with driving the cell cycle, such as UBE2C [67, 76, 166, 167, 169], both of which lead to disease progression. Since existing CRPC therapeutics are ineffective against splice variants like AR-V7, we developed PSA6.1-LUC and UBE2C-LUC promoter-based reporter assays to examine AR-V7's (AR-NTD) transcriptional activity in cells. Both the transcriptional activation reporter assays were developed using an AR-null PC3 cell background stably transfected with GFP-tagged AR-V7 and will allow us to determine if compounds can block AR-V7 mediated transcription.

Furthermore, it's been shown that coactivators, such as TIF2 and SRC1 can also bind to the AF-1 region, located in the receptor's amino terminal domain (NTD), which activates [79],[103, 170] AR splice variants like AR-V7, and are proposed to contribute to AR's continued transcriptional activity in the cell [50, 79, 85, 105, 106]. Studies have used GST-pull down assays, yeast two-hybrid assays, and mammalian 2-hybrid (M2H) assays to demonstrate that AR AF-1 interacts with both TIF2 and SRC1 [79-82, 171, 172]. Therefore, we set out to develop mammalian 2-hybrid assays using the 5xGal4-TATA-Luc reporter, Gal4-AR-NTD, and VP16-TIF2 or VP16-SRC1 transfected into HEK 293 cells. We had three amino-terminal constructs available to us of different amino acid lengths, and structures. pGal4-AR-V7 encodes the entirety of the AR-V7 splice isoform, pGal4-AR-NTD 1-558 encodes the entirety of the amino terminus of the AR, and pGal4-AR-NTD codes for the AR AF-1 transactivation surface. As expected, Gal4-AR-NTD mediated transcriptional activity in cells was independent of DHT.

Unexpectedly however, Gal4-AR-NTD induced transcription was not modulated by the co-expression of either the VP16-TIF2 or VP16-SRC1 coactivators, which contradicts previous reports [79-82, 171, 172]. In the AF-1 M2H format we developed, we substituted the AR-NTD for the AR-LBD in the Gal4 construct so that we could take advantage of the existing TIF2 and SRC1 VP16 constructs which worked in the AF-2 version of the M2H (Chapter 3). Differences between the AF-1 M2H format that we developed, and previously published assays might account for the observed lack of TIF2 or SRC1 coactivation (see below). Therefore, instead of using this assay to measure the ability of compounds to block the protein interactions between the AR-NTD AF-1 surface and TIF2 or SRC1 coactivators, we used it to interrogate their ability to block the constitutive transactivation of AR-NTD (1-503) (AF-1).

The two promoter-driven reporter assays, and the pGal4-AR-NTD transactivation assay enable us to determine whether hit compounds from the AR-TIF2 PPIB HCS can also block AR AF-1 mediated transcriptional activity, and might therefore block the CRPC enabling activities of AR splice variants. The development and optimization of these three assays are described in this chapter together with the results of seven test compounds that are known modulators of AR activation.

4.2 Assays Developed to Characterize AR-TIF2 PPIB Inhibitor/Disruptor Hits that Block the AR AF-1 Transactivation Domain

4.2.1 AR-NTD (1-503) Transactivation Assay

4.2.1.1 Assay Principle

We initially set out to develop M2H assays by transfecting 5xGal4-TATA-Luc reporter, Gal4-AR-NTD, and VP16-TIF2 or VP16-SRC1 in three different cell lines. We found that Gal4-AR-NTD mediated transcriptional activity was independent of both DHT or co-activation by either VP16-TIF2 or VP16-SRC1. During assay development and optimization, Gal4-AR-NTD (1-503) was transfected into 3 different cell lines, to determine which cell background exhibited the most robust signal for the M2H assays. The HEK 293 cell line was selected, and different concentrations of Gal4-AR-NTD constructs and VP16-coactivators were then cross-titrated to select the optimal amounts for the assays. Finally, three different AR-NTD constructs were compared to determine which of the three produced the most robust signal. After it was determined that VP16-coactivator expression did not enhance the transcriptional activity of any of the AR-NTD constructs, the assay

was instead developed to interrogate the ability of compounds to block the constitutive transactivation of AR-NTD(1-503) (AF-1) (Figure 35, on pg. 140).

4.2.1.2 Materials and Methods

Plasmid DNAs. The 5xGAL4-TATA-luciferase reporter plasmid was a gift from Dr. Richard Maurer from the Oregon Health and Science University [155], and constructs pGAL4-hAR-1-503, (AR-NTD amino acids 1-503 expressed as a fusion protein with Gal4-DBD) [156], pVP16-SRC1 (full-length SRC1 expressed as a fusion with VP16 activation domain)[157] and pVP16-Empty vector were kindly provided to us by Dr. Elizabeth Wilson, from UNC Chapel Hill. The generation of the pVP16-TIF2 construct was described in the chapter 3. An empty pGALO vector was kindly gifted to us by Dr. Gordon Tomaselli (Albert Einstein College of Medicine) and pGAL-hAR-1-558, and pGAL4-AR3 (AR-V7), were generated by ligating PCR amplified inserts into the pGALO mammalian 2-hybrid vector. Enzymes BamHI and XbaI were purchased from New England Biolabs (NEB), and all primers were synthesized and purchased from ThermoFisher Scientific.

Cloning of AR-NTD (1-558) into a mammalian 2-hybrid pGAL4 vector. The pGAL4 vector containing the AR-NTD 1-558 construct was created via the traditional ligation-dependent method. The AR-NTD 1-558 insert was PCR amplified from pEGFP-C1-AR full-length cDNA construct containing the wild type cDNA of the full-length androgen receptor. The primers for PCR were designed with the addition of BamHI and XbaI cloning sites at the 5' and 3' prime flanking regions, respectively (Table 11, on pg. 141). The AR-NTD 1-558 insert as well as the pGALO vector were double digested with BamHI and XbaI enzymes. After overnight ligation, using T4 DNA ligase (New England Biolabs) at 16°C the insert was cloned into the GAL4 vector. After ligation, a small amount of ligation mixture was transformed into DH5 α competent cells and

plated on ampicillin containing LB agar to select for bacteria containing the GAL4-AR-NTD 1-558 plasmid DNA. After overnight incubation at 37°C colonies were selected and expanded in ampicillin containing LB media, and clones were analyzed via restriction analysis to identify clones with bands at the correct molecular size.

Cloning of AR3 (AR-V7) into a mammalian 2-hybrid pGAL4 vector. The AR3 insert was amplified by polymerase chain reaction (PCR) from the pEGFP-C1-AR-V7 cDNA using Phusion High-Fidelity DNA Polymerase (NEB). The PCR primers were designed with the addition of BamHI and XbaI cloning sites at the 5' and 3' prime flanking regions, respectively (Table 12, on pg. 142). After PCR and the purification step, the insert, and pGALO vector were double digested with BamHI and XbaI. After overnight ligation, using T4 DNA ligase (New England Biolabs) at 16°C the insert was cloned into the pGAL4 vector. After ligation, a small amount of ligation mixture was transformed into DH5 α competent cells and plated on ampicillin containing LB agar to select for bacteria containing the pGAL4-AR3 plasmid DNA. After overnight incubation at 37°C colonies were selected and expanded in ampicillin containing LB media overnight and clones were analyzed via restriction analysis to identify clones with bands at the correct molecular size.

SDS-PAGE and Western Blot Confirmation of GAL4-AR-NTD Constructs. AR-NTD containing pGAL4 vectors were then confirmed through western blot analysis. pGAL4-AR-NTD (1-503), pGAL4-AR-NTD (1-558), and pGAL4-AR3 (AR-V7) were transfected into HEK 293 cells and allowed to express for 48 hrs. Forty-eight hours post transfection, cells were lysed, and the BCA reagent was used to determine protein concentrations of transfected cell lysates. An SDS-PAGE gel was then run to separate 25 μ g of transfected cell lysates per well and compared to non-transfected HEK 293 cells. Protein was then transferred to a nitrocellulose membrane and probed with an α -AR antibody (Cell Signaling; #D6FI1) specific for the amino terminal domain of the

receptor (Figure 36, on pg. 143). Immuno-positive bands of increasing size are seen in transfected HEK 293 cells, corresponding to GAL4-AR-NTD 1-503, GAL4-AR-NTD 1-558, and GAL4-AR3 (AR-V7), respectively. Bands at the correct molecular size are evident in transfected cell lysates (Figure 36).

AR N-terminal Domain (AR-NTD) Transactivation Assay. HEK 293 cells were co-transfected with 5 ng of pGal4-AR-NTD (1-503), and 20 ng of the 5xGal4-TATA-Luc reporter. Cells were transiently bulk co-transfected with these plasmids using the Fugene6 transfection reagent. Prior to the transfection of cells each of the pGAL4-hAR-1-503, and 5xGAL4-TATA-luciferase reporter, were individually incubated with Fugene6 at a 3:1 ratio for 25 min at room temperature (RT). Each Fugene6:plasmid DNA mixture was then added to HEK 293 cells that were suspended in DMEM (Cellgro10013CV) with 2 mM L-glutamine (Invitrogen) that was supplemented with 10% fetal bovine serum, and 5,000 cells in a volume of 40 μ L were seeded into the wells of 384-well assay plates and cultured overnight at 37°C, 5% CO₂, and 95% humidity. 24 h post cell seeding into assay plates, 5 μ L of the serially diluted test compounds was transferred to the wells using a Janus MDT automated liquid handling platform outfitted with a 384-well transfer head, and assay plates were returned to the incubator for an additional 24 h before BrightGlo® reagent was added to the plate and the relative luminescence units (RLUs) were captured on a SpectraMax M5e microtiter plate reader. Test compounds were run in the M2H assay in a 10-point 2-fold dilution series spanning a concentration range between 0.0977 to 50 μ M.

4.2.1.3 Assay Development and Optimization

Determining the optimal cell background for the AR-NTD Mammalian 2-Hybrid TIF2 and SRC1 Coactivator assays. We began by conducting the M2H assay in 3 different cell lines (Figure 37, on pg. 144). We selected PC3 cells because they provided an AR-null prostate cancer cell line

background, and we selected HeLa cells and HEK 293 cells because they have frequently been used in mammalian 2-hybrid assays [88, 92, 157-159]. In cells co-transfected with 5 ng of pGal4-AR-NTD (1-503), 10 ng of pVP16-TIF2 or pVP16-SRC1, and 20 ng of the 5xGal4-TATA-Luc reporter, both DHT treated and untreated cells exhibited a comparable luciferase response, which is consistent with AR-NTD's constitutive transcriptional activity [76, 80, 81, 169]. The reporter response in all three cell lines was equivalent in the presence or absence of DHT but the activity in HeLa and PC3 cells was ~ 400-fold and ~300-fold lower than in HEK 293 cells respectively. Based on our previous experience with other transient transfection assays, we attribute the much higher responses observed in HEK 293 cells to their much higher transfection efficiencies. We therefore selected the HEK 293 cell background to conduct further assay development experiments (Figure 37).

Determining the optimal amounts of DNA plasmid constructs to use in the M2H Assays.

The optimal amounts of GAL4-AR-NTD 1-503, VP16-Coactivator, and 5xGal4-TATA-Luc reporter construct to use in the HEK 293 M2H assay were determined to be 5 ng, 10 ng, and 20 ng, respectively, consistent with the amount of DNA previously determined to be optimal in HeLa cells (data not shown). To determine the optimal amounts of pGal4-AR-NTD (1-558), pGal4-AR3 (AR-V7), pVP16-TIF2, or pVP16-SRC1 plasmid DNA to use in the HEK 293 M2H assays cells we performed cross-titration transient transfection experiments with increasing amounts of the AR-NTD constructs and coactivator plasmid DNAs (Figures 37 & 38, on pgs. 144 & 145). We selected three different pGal4-AR-NTD plasmids to conduct experiments with: pGal4-AR-NTD (1-503), pGal4-AR-NTD (1-558), and pGal4-AR3 (AR-V7). The pGal4-AR-NTD (1-503) construct was chosen because it contains the entire AF-1 binding region and has been used

previously in reporter based assays [115, 173]. We selected the pGal4-AR-NTD (1-558) construct because it encodes the entire AR-NTD. The pGal4-AR3 construct encodes the entire the AR-V7 splice isoform (Figure 36). The amount of 5xGal4-TATA-Luc reporter construct in the assays was kept constant at 20 ng, which had been previously determined in transient transfection experiments conducted in our lab. The cross-titration experiments were performed in 384-well, white opaque plates. pGal4-AR-NTD was added to cells at increasing amounts (0, 5, 10 ng/well) of plasmid DNA, and cross-titrated with increasing amounts (0, 5, and 10 ng/well) of pVP16-TIF2 or pVP16-SRC1 plasmid DNA. Cells were either treated with DHT, or not treated (NT) for each transfection condition. In each of the M2H titration experiments, the luciferase response increased in a linear fashion independent of DHT treatment as the amount of pGal4-AR-NTD transfected into the HEK 293 cells was increased. However, there was no substantial increase in M2H luciferase reporter response as the amounts of the pVP16-coactivator constructs transfected into the HEK 293 cells were increased (Figures 38-39 on pgs. 145-146). Therefore, we selected 5 ng for pGal4-AR-NTD construct, and 10 ng each of the pVP16-Coactivator plasmid constructs to use for comparing the differences between reporter activity mediated by each pGal4-AR-NTD construct in the presence or absence of VP16-coactivators (Figure 40 on pg. 147).

Determining if each of the pGal4-AR-NTD plasmid constructs requires VP16-Coactivator to produce 5xGal4-TATA-Luc reporter based assay signal. In cells co-transfected with 20 ng of the 5xGal4-TATA-Luc reporter, 5 ng of either of the three pGal4-AR-NTD constructs, and either 0 ng or 10 ng of pVP16-TIF2 or pVP16-SRC1, both DHT treated and untreated cells exhibited comparable luciferase reporter responses, which is consistent to AR-NTD's constitutive activity. HEK 293 cells transfected with pGal4-AR-NTD (1-558) or pGal4-AR3 (AR-V7) produced a reporter response that was ~2-fold, and ~60-fold lower, respectively,

than HEK 293 cells transfected with pGal4-AR-NTD (1-503) (Figure 41 on pg. 148). We attribute the much lower responses observed in HEK 293 cells transfected with the pGal4-AR3 (AR-V7) due to the presence of an AR DNA-binding domain (AR-DBD) present in the AR-V7 construct. Since the pGal4 construct contains a DBD specific for the Gal4 binding sites on the reporter DNA, the presence of the AR-DBD sequence in the AR-V7 construct may lead to competitive DNA binding at ARE sites that are not in the reporter construct, thereby decreasing the 5xGal4-TATA-Luc reporter response. Although both pGal4-AR-NTD (1-503) and pGal4-AR-NTD (1-558) produced a robust signal, we selected pGal4-AR-NTD (1-503) for further assay development experiments.

Unexpectedly, we observed that none of the three AR-NTD constructs responded to SRC1 or TIF2 coactivation (Figure 41). This contradicts the published literature [79-82, 171, 172]. The differences that we have observed may be due to differences in the assay formats. For example, the other groups used CV-1 cells to conduct their assays, while we used the HEK 293 cell line. Furthermore, our assays were developed with the AR-NTD inserted into the Gal4-DBD construct and the coactivators inserted into the VP16 construct, whereas the other studies flipped the bait and prey protein constructs; TIF2 and SRC1 coactivators were inserted into Gal4-DBD vectors and AR-NTD inserted into the VP16 vector. Therefore, we could not use this assay to measure AR-NTD coactivator protein-protein interactions, but rather we used it to measure constitutive AR-NTD transactivation.

4.2.1.4 Test set performance in pGal4-AR-NTD based Transactivation assays

Testing Known AR Modulator Compounds in the Constitutive AR-NTD Transactivation

Assay. We first ran our test set of compounds in HEK 293 cells co-transfected with 20 ng 5xGal4-TATA-Luc, 5ng of pGal4-AR-NTD (1-503), and either 0 ng or 10 ng of VP16-SRC1 or VP16-

TIF2. The test set of compounds included FDA approved therapeutics and experimental drugs for the treatment of PCa.

In AR-NTD assays conducted without coactivators, flutamide, bicalutamide, and enzalutamide exhibited IC_{50} s of 4.83 +/- 0.14, 18.83 +/- 2.46, and 31.50 +/- 2.63 μ M, respectively. In assays conducted with the pVP16-TIF2 coactivator, anti-androgens flutamide, bicalutamide, and enzalutamide exhibited IC_{50} s of 4.65 +/- 0.74, 33.3 +/- 13.3, and 52.84 +/- 2.25 μ M, respectively (Figure 41B-D and Table 13, on pg. 150). In assays conducted with pVP16-SRC1, flutamide, bicalutamide, and enzalutamide exhibited IC_{50} s of 3.57 +/- 0.12, 29.4 +/- 14.0, and 39.88 μ M, respectively (Figure 42B-D, on pg. 149 and Table 13). It's important to note that the three AR antagonists behaved very similarly in all three assay formats, suggesting their AR-NTD transactivation assay compound responses were not altered in the presence of the TIF2 or SRC1 coactivators. We would anticipate that antiandrogens would not be as efficient at inhibiting AR-NTD transcription activity as they would be in assays that employ a ligand binding domain. As expected, two of the three antiandrogens exhibited less potent IC_{50} s in AR-NTD assays relative to those in assays using AR-LBDs; enzalutamide's AR-NTD IC_{50} was nearly ~22-fold higher than in the pGal4-AR-LBD TIF2 or SRC1 M2H assays, and bicalutamide's IC_{50} was nearly 15-fold higher. Surprisingly, flutamide performed similarly in the AR-NTD assay and in the pGal4-AR-LBD TIF2 or SRC1 M2H assays.

The CYP17A1 inhibitor abiraterone acetate produced IC_{50} s of 6.43 +/- 0.28 μ M, 14.7 +/- 3.02 μ M, and 12.5 +/- 2.75 μ M in the AR-NTD transactivation assays conducted alone or in the presence of the TIF2 or SRC1 coactivators, respectively (Figure 41H and Table 13).

The Hsp 90 inhibitor, 17-AAG, produced IC_{50} s of 3.54 +/- 0.54 μ M, 4.31 +/- 1.8 μ M, and 2.05 +/- 0.85 μ M in the AR-NTD transactivation assay conducted alone or in the presence of the

TIF2 or SRC1 coactivators, respectively (Figure 42G and Table 13). Since Hsp90 is involved with the maturation and folding processes of nearly 200 client proteins in mammalian cells, including AR-FL [174], it's plausible that inhibiting Hsp90 may also affect the maturation and folding of AR-NTD thereby inhibiting it's transactivation response. 17-AAG produced an AR-NTD IC₅₀ that was ~9-fold higher than in the pGal4-AR-LBD TIF2 or SRC1 M2H assays.

Compound #10 and EPI-001 both target the AR-NTD. Compound #10 produced IC₅₀s of 1.55 +/- 0.04 μ M, 4.64 +/- 0.39 μ M, and 3.56 +/- 0.03 in the AR-NTD transactivation assay conducted alone or in the presence of the TIF2 or SRC1 coactivators, respectively (Figure 42E,F and Table 13). EPI-001 produced IC₅₀s of 9.92 +/- 1.24 μ M, 19.5 +/- 2.82 μ M, and 15.3 +/- 3.27 μ M in the AR-NTD transactivation assay conducted alone or in the presence of the TIF2 or SRC1 coactivators, respectively (Figure. 42E, F and Table 13).

Compound #10, EPI-001, and Abiraterone acetate produced IC₅₀s in the associated viability counter assays run simultaneously with the AR-NTD transactivation assays, suggesting that compound-mediated cytotoxicity may be contributing significantly to the decreased reporter signals. Overall however, it was evident that all compounds behaved similarly in all three assay formats, AR-NTD alone or in the presence of TIF2 or SRC1 coactivators.

4.2.2 PSA6.1-Luc and UBE2C-Luc Reporter based assays developed in PC3-GFP-AR-V7

Cells

4.2.2.1 Assay Principle

The PSA6.1-Luc and UBE2C-Luc reporter-based assays measure the transcriptional activity of the AR-V7 splice-variant in PCa cells. As described previously, the PSA-6.1 LUC plasmid luciferase reporter activity is controlled by a fragment of the PSA promoter that contains three androgen

response elements (AREs), fused to a luciferase reporter gene. The UBE2C reporter is a luciferase construct driven by three repeats of an AR-V7-specific promoter element of the ubiquitin-conjugating enzyme E2C (UBE2C) gene (Figure 43, on pg. 151) [76]. AR-V7's binding to the promoter region of PSA or UBE2C leads to the transcription of the luciferase reporter gene, and in the presence of CellTiter Glo™, luciferase will convert the luciferin substrate into light output, a quantifiable measurement of this transcription. Any compound that has the ability to modulate AR-NTD (AF-1)'s transcriptional activity in the cell should inhibit reporter activity in these assays. During assay development and optimization, the DNA concentrations of PSA6.1-Luc reporter, and UBE2C-Luc reporter, as well as the ratios of FuGeneHD to DNA were titrated to select the optimal amounts to use in the assays. Next, we transiently transfected our reporter constructs, into 3 different cell lines: PC3's, PC3-AR-FL, and PC3-AR-V7, and compared reporter responses in the presence or absence of DHT, to determine their constitutive and DHT-induced reporter responses. Using the optimized conditions the PSA6.1-Luc and UBE2C-Luc reporter assays were used to characterize the hits from the 143K AR-TIF2 PPIB screen. The PSA6.1-Luc and UBE2C-Luc reporter assays allowed us to interrogate the ability of hit compounds to modulate AR-V7's transcriptional activity in PC3 cells. Any hit compound that could decrease reporter activity driven by the AR-splice variant AR-V7, would be prioritized for consideration as hits potentially suitable for lead optimization.

4.2.2.2 Materials and Methods

Reporter Constructs and Cell Lines. As described previously, the pPSA-6.1 LUC luciferase reporter plasmid was kindly provided by Dr. Zhou Wang in the Urology department of the University of Pittsburgh Cancer Institute. The pGL4.28-UBE2C 20bpX3 luciferase reporter plasmid was kindly provided by Dr. Yan Dong from Tulane University. We obtained the PC3 cell

line stably transfected with AR-splice variant, AR-V7, from Dr. Michael Mancini, Baylor College of Medicine. The PC3 cell line was purchased from the American Type Culture Collection.

PSA6.1-LUC Reporter Assay. Prior to the transfection of AR-V7-GFP containing PC3 cells, Fugene HD and PSA-6.1 LUC were combined at a 3:1 ($\mu\text{L}:\mu\text{g}$) ratio, respectively, in Opti-MEM and incubated for 25 min at room temperature (RT) before being added to cells that were suspended in RPMI 1640 media containing 1% L-glutamine, and 10% fetal bovine serum. Bulk transfected cells were then seeded into white opaque 384-well assay plates (#781080; Greiner Bio-one) at a seeding density of 3,000 cell per well in a volume of 40 μL and incubated at 5% CO_2 , 37C, and 95% humidity for 24 h. Each well received 20 ng of PSA-6.1 LUC plasmid DNA. After 24 h, 5 μL of serially diluted compounds was transferred to the wells using a Janus MDT automated liquid handling platform outfitted with a 384- well transfer head; then, 5 μL of SFM was transferred to each well; and the assay plates were returned to the incubator for an additional 24 h before 25 μL of BrightGlo luciferase reagent (Promega) was added to the wells and the relative light units (RLUs) were captured on a SpectraMax M5e plate reader (Molecular Devices LLC).

UBE2C-LUC Reporter Assay. Prior to the transfection of AR-V7-GFP containing PC3 cells, Fugene HD and UBE2C-LUC were combined at a 3:1 ($\mu\text{L}:\mu\text{g}$) ratio, respectively, in Opti-MEM and incubated for 25 min at room temperature (RT) before being added to cells that were suspended in RPMI 1640 media containing 1% L-glutamine, and 10% fetal bovine serum. Bulk transfected cells were then seeded into white opaque 384-well assay plates (#781080; Greiner Bio-one) at a seeding density of 3,000 cell per well in a volume of 40 μL and incubated at 5% CO_2 , 37C, and 95% humidity for 24 h. Each well received 10 ng of UBE2C LUC plasmid DNA. After 24 h, 5 μL of serially diluted compounds was transferred to the wells using a Janus MDT automated liquid handling platform outfitted with a 384- well transfer head; then, 5 μL of SFM was transferred to

each well; and the assay plates were returned to the incubator for an additional 24 h before 25 μ L of BrightGlo luciferase reagent (Promega) was added to the wells and the relative light units (RLUs) were captured on a SpectraMax M5e plate reader (Molecular Devices LLC).

4.2.2.3 Assay Development and Optimization

Optimizing Transfection Conditions: Determining the optimal amounts of DNA plasmid reporter construct and FuGeneHD:DNA ratio to use in the PSA6.1-LUC reporter assay.

We conducted our assays in PC3 cells stably transfected with PC3-AR-V7-GFP. Images taken of this cell line show that the GFP-tagged AR-V7 construct is constitutively nuclear in the presence or absence of DHT (Figure 44, on pg. 152). To determine the optimal amount of PSA6.1-Luc reporter plasmid DNA to use in the PSA6.1-Luc reporter assay conducted in PC3-AR-V7-GFP cells we performed titration experiments with increasing amounts of the PSA6.1-Luc plasmid DNAs. At the same time, we increased the ratio of FuGeneHD:DNA (Figure 45, on pg. 153). These experiments were performed in 384-well, white opaque plates. PSA6.1-Luc was added to cells at increasing amounts (0, 10, 15, 20 ng/well) of plasmid DNA, and transfected with increasing ratios of the FuGeneHD transfection reagent (2:1, 3:1, 4:1). These experiments were run in ligand-independent conditions, as AR-V7 does not require androgen stimulation for its transcriptional activation. The luciferase response increased in a linear fashion as the amount of pPSA6.1-Luc DNA transfected into PC3-AR-V7 cells was increased. However, there was only a slight difference in reporter response when the FugeneHD:DNA ratio was increased. The final amounts of plasmid DNAs selected for the optimized the PSA6.1-Luc assays conducted in PC3-AR-V7 cells were 20 ng for the pPSA6.1 construct, at a 3:1 FuGeneHD:DNA ratio. These are the same conditions that were used to conduct the PSA6.1-Luc reporter assay in PC3-AR-FL-GFP cells.

Optimizing Transfection Conditions: Determining the optimal amounts of DNA plasmid reporter construct and FuGeneHD:DNA ratio to use in the UBE2C-LUC reporter assay.

To determine the optimal amount of UBE2C-Luc reporter plasmid DNA to use in the UBE2C-Luc reporter assays conducted in PC3-AR-V7-GFP cells we performed titration experiments with increasing amounts of the UBE2C-Luc plasmid DNAs. At the same time, we increased the ratio of FuGeneHD:DNA (Figure 46, on pg. 154). These experiments were performed in 384-well, white opaque plates. UBE2C-Luc was added to cells at increasing amounts (0, 10, 20, 40 ng/well) of plasmid DNA, and transfected with increasing ratios of the FuGeneHD transfection reagent (2:1, 3:1, 4:1). These experiments were run in ligand-independent conditions, as AR-V7 does not require androgen stimulation for its transcriptional activity. The luciferase response increased in a linear fashion as the amount of UBE2C-Luc transfected into PC3-AR-V7 cells was increased. There was an increase in reporter response when the FugeneHD:DNA ratio was increased from 2:1 to 3:1, but the difference between 3:1 and 4:1 ratio was smaller. The final amounts of plasmid DNAs selected for the optimized the PSA6.1-Luc assays conducted in PC3-AR-V7 cells were 10 ng for the PSA6.1 construct, at a 3:1 FuGeneHD:DNA ratio.

Demonstrating Reporter Response in PSA6.1-Luc and UBE2C-Luc transfected cell lines: PC3, PC3-AR-FL-GFP, and PC3-AR-V7-GFP, in the presence or absence of DHT

To compare promoter-driven reporter responses in each cell line, in the presence or absence of DHT, PC3's, PC3-AR-FL-GFP, or PC3-AR-V7-GFP cells were transiently transfected with either PSA6.1-Luc or UBE2C-Luc reporter constructs before being seeded in 384-well, white, opaque plates and incubated at 5% CO₂, 37°C, and 95% humidity for 24 h. The next day either DHT (100nM) or SFM was added to each well and again incubated at 5% CO₂, 37°C, and 95% humidity for 24 h (Figure 47, on pg. 155). In PC3 cells transfected with either the PSA6.1-LUC or UBE2C-

LUC reporter plasmid, there was no reporter response, which was expected as these cells do not contain AR (Figure 47). When PC3-AR-FL-GFP cells were transfected with the PSA6.1-Luc reporter plasmid, reporter based response was only observed upon the addition of DHT to cells. When PC3-AR-FL-GFP cells were transfected with the UBE2C-LUC reporter plasmid, reporter based response was minimal, with response levels similar to those observed in PC3 cells (Figure 47). Finally, when the PSA6.1-LUC reporter plasmid was transfected into PC3-AR-V7-GFP cells, reporter activity was observed to the same degree both in the presence or absence of DHT (Figure 47). We attribute this to AR-V7's predominant nuclear subcellular localization in both untreated and treated cells (Figure 44). Similarly, when the UBE2C-LUC reporter plasmid was transfected into PC3-AR-V7-GFP cells, reporter activity was observed both in the presence or absence of DHT, indicating that AR-V7's transcriptional activity in the cell of the UBE2C-promoter is DHT-independent (Figure 47).

4.2.2.4 Test set performance in PSA6.1-Luc and UBE2C-Luc reporter assays

Testing the PSA6.1-LUC and UBE2C-LUC Reporter Assays with Known AR Modulator Compounds

In PC3-AR-V7-GFP cells transfected with PSA-6.1-LUC, anti-androgen flutamide, was able to inhibit reporter activity, exhibiting an IC_{50} value of $11.5 \pm 1.22 \mu\text{M}$, while bicalutamide, and enzalutamide failed to achieve an IC_{50} at $\leq 50 \mu\text{M}$ (Figure 48B-D, on pg. 156 and Table 14, on pg. 157). Since these compounds act by preventing DHT's binding to the AR-LBD, we predicted that none of these compounds would be able to prevent AR-V7's transcriptional activity in the cell. Unexpectedly, just as flutamide was able to inhibit reporter activity in the pGal4-AR-NTD transactivation assay, it was also able to inhibit AR-V7 driven PSA6.1-promoter based reporter activity. The Hsp 90 inhibitor 17-AAG produced an IC_{50} of $0.68 \pm 0.37 \mu\text{M}$ in the AR-V7-

PSA6.1-LUC reporter assay (Figure 48G and Table 14), likely due to its ability to prevent protein maturation and folding. Compound #10, and EPI-001 exhibited IC_{50} s of 50.3 +/- 11.3, and 25.3 +/- 4.05 μ M, respectively (Figure 48E, F and Table 14). This was expected as these compounds had been previously identified with the ability to target the AR-NTD [124, 147, 149, 175]. Abiraterone acetate also failed to achieve an IC_{50} at ≤ 50 μ M in the PSA-6.1-LUC reporter assay performed in PC3-AR-V7-GFP cells (Figure 48H and Table 14). This compound targets Cyp17a1's ability to synthesize androgen, and since the AR-NTD does not require DHT to be transcriptionally active, this compound does not affect AR-V7's ability to function in the cell. In PC3-AR-V7-GFP cells transfected with UBE2C-Luc, the anti-androgen flutamide, was able to inhibit reporter activity, exhibiting an IC_{50} value of 28.6 +/- 2.71 μ M, while bicalutamide, and enzalutamide failed to achieve an IC_{50} at ≤ 50 μ M (Figure 49B-D, on pg. 158 and Table 15, on pg. 159). As expected, both bicalutamide, and enzalutamide were unable to inhibit AR-V7 based transcriptional activity in these cells. Again, flutamide was able to inhibit AR-V7 based transcriptional activity in a concentration dependent manner. 17-AAG produced an IC_{50} of 0.75 +/- 0.50 μ M (Figure 49G and Table 15). Compound #10 and EPI-001 exhibited IC_{50} s of 58.6 +/- 0.79, and 49.2 +/- 0.76 μ M, respectively (Figure 49E, F and Table 15). However, they were only able to inhibit reporter activity at the highest concentration used in the assay. Abiraterone acetate did not inhibit UBE2C-LUC reporter activity in PC3-AR-V7-GFP cells at ≤ 50 μ M (Figure 49H and Table 15).

To control for the potential cytotoxicity of these compounds, growth inhibition assays were run for each compound, simultaneously, to determine whether any decrease in AR-V7 transcriptional activity was due to compound induced cell death. Under the conditions described above, none of the compounds from the test set exhibited any apparent cytotoxicity in the PC3 cell

line stably expressing pEGFP-AR-V7, indicating that any decrease in reporter signal was actually due to a compound's ability to block AR-V7 induced transcriptional activity (Figures 48 & 49 and Tables 14 & 15).

4.2.3 Conclusions

Given the emergence of splice variants that code for the AR-NTD, and whose expression has led to relapse in CRPC patients, we have developed three different characterizations that will allow us to identify compounds that can target AR-NTD's transcriptional activity in CRPC cells. We are looking for a compound that can disrupt pGal4-AR-NTD response in the transactivation assay, and is able to inhibit AR-V7's transcriptional activation in both promoter-driven reporter assays. A compound with a desirable biological profile is that which could disrupt transcription due to both the AR AF-1 and AR AF-2 transactivation domains. Flutamide and 17-AAG both inhibited all three assays in a concentration dependent manner. However, based on their known mechanisms of action, we believe that their activity may be non-specific to the AR-NTD. On the other hand, Compound #10 and EPI-001 both inhibited the pGal4-AR-NTD transactivation and AR-V7-PSA6.1-Luc reporter assays in a concentration dependent manner, and the AR-V7-UBE2C-Luc reporter assay at the highest concentrations tested. These two compounds are examples of those that might be prioritized, and possibly developed into therapeutics for CRPC.

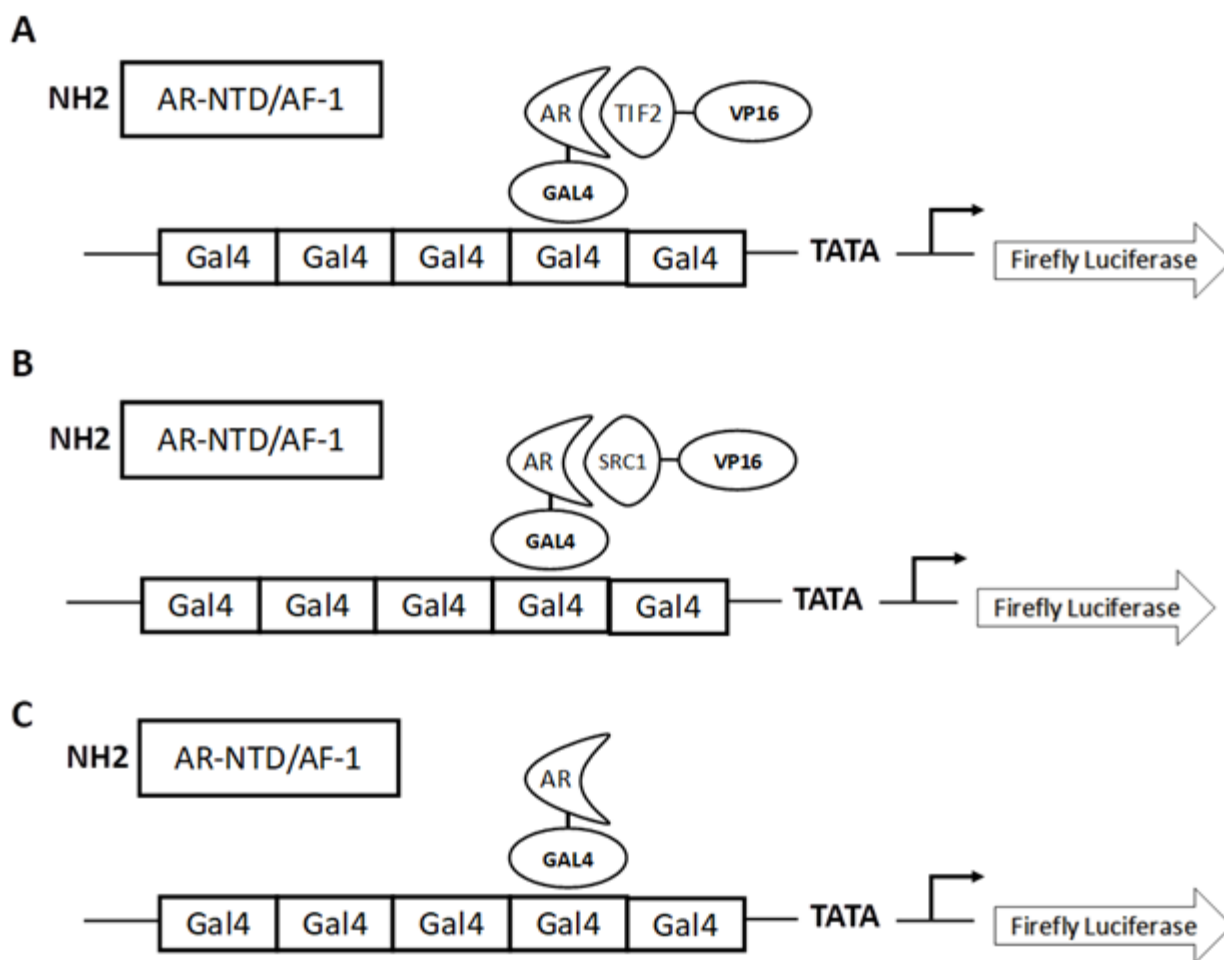


Figure 35. Mammalian 2-hybrid assay. pGal4-AR-NTD transactivation assay principle

The mammalian 2-hybrid assay we developed involves the transfection of three main components including Gal4-AR-NTD, VP16-coactivator, and the 5xGal4-TATA-Luc reporter. The nuclear receptor-Gal4 fusion protein binds to the DNA-binding response sequences in the 5xGal4-TATA-Luc reporter plasmid, while binding interactions between the nuclear receptor and the co-activator-VP16 fusion protein recruits the transcriptional machinery of the cell, leading to overall transcription of the luciferase gene. This reporter activity is an indirect measure of nuclear receptor::co-activator protein interactions in the cell. We have developed this assay in two different co-activator formats using the AR-NTD-Gal4 fusion protein; A) One involves the TIF2/SRC2 p160 coactivator cloned into the VP16 mammalian construct, B) the second involves homologous SRC1 p160 coactivator cloned into the VP16 vector. C) Involves neither coactivator for AR-AF-1 mediated 5xGal4-TATA-Luc reporter transcriptional activity.

Table 11. PCR primer sequence for amplification and cloning of AR-NTD (1-558) into pGal4 vector

| Primer | PCR Primer Sequence |
|--------------------|--|
| AR3 Fwd Primer | 5' - GTA GGA TCC ATG GAA GTG CAG TTA GGG CTG - 3' |
| Rev-AR-NTD (1-558) | 5' - CGT GTC TAG AGG TCT TCT GGG GTG GAA AGT AAT AG - 3' |

The constructs for the GAL4 vector containing the AR-NTD (1-558) was created via the traditional ligation-dependent method. The AR3 insert was amplified by polymerase chain reaction (PCR) from the pEGFP-C1-AR full-length cDNA. The primers for the PCR were designed with the addition of BamHI and XbaI cloning sites at the 5' and 3' prime flanking regions, respectively (ThermoFisher Scientific). The AR-NTD insert, and the pGALO vector were double digested with BamHI and XbaI enzymes, and then insert and vector were ligated.

Table 12. PCR primer sequence for amplification and cloning of AR-V7 (AR3) into pGal4 vector

| Primer | PCR Primer Sequence |
|----------------|--|
| AR3 Fwd Primer | 5' - GTA GGATCC ATG GAA GTG CAG TTA GGG CTG - 3' |
| AR3_XbaI_R | 5' - CAC GTC TAG AGG GTC TGG TCA TTT TGA GAT GCT - 3' |

The constructs for the GAL4 vector containing the AR-V7 (AR3) were created via the traditional ligation-dependent method. The AR3 insert was amplified by polymerase chain reaction (PCR) from the pEGFP-C1-AR full-length cDNA. The primers for the PCR were designed with the addition of BamHI and XbaI cloning sites at the 5' and 3' prime flanking regions, respectively (ThermoFisher Scientific). The AR-NTD insert, and the pGALO vector were double digested with BamHI and XbaI enzymes, and then insert and vector were ligated.

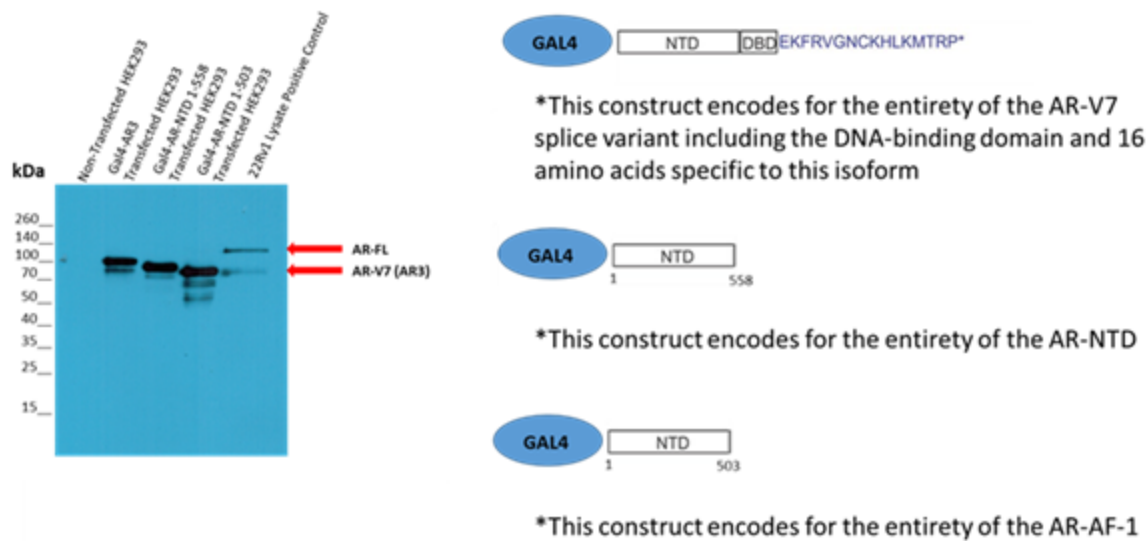


Figure 36. Western blot confirmation of pGal4-AR-NTD constructs

AR-NTD containing GAL4 vectors were transfected into HEK293 cells and allowed to express their respective fusion proteins for 48 hrs. Forty-eight hours post transfection, cells were lysed, and the BCA protein detection reagent was used to determine protein amount and concentration in transfected cell lysates. An SDS-PAGE gel was then run for protein separation, where 25 μ g of protein from each lysate was added to different lanes of the gel. Protein was transferred to nitrocellulose membranes, and the resulting western blots were then probed with an α -AR antibody (Cell Signaling; #D6F11), that recognizes a region in the amino terminal domain of the receptor. Immuno-positive bands of increasing size are seen in transfected HEK 293 cells, corresponding to GAL4-AR-NTD 1-503, GAL4-AR-NTD 1-558, and GAL4-AR3 (AR-V7), respectively. Bands at the correct molecular size are evident in transfected cell lysates (Figure 4).

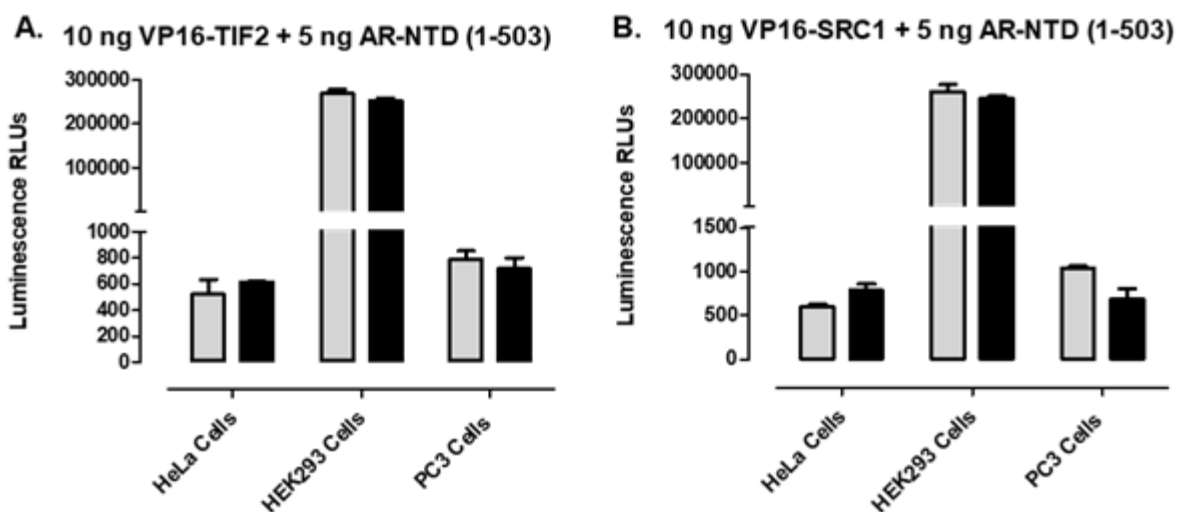


Figure 37. Determining which cell background enables the most robust mammalian 2-hybrid assays

The mammalian 2-hybrid assay was conducted in 3 different cell lines co-transfected with the pGal4-AR-NTD (1-503), pVP16-TIF2 or pVP16-SRC1 and the 5xGal4-TATA-Luc reporter, to see how the luciferase reporter luminescence signal behaved in each cell line. PC3 cells were chosen because they are an AR-null prostate cancer cell line, and both HeLa cells and HEK 293 cells were chosen because they have been historically used in mammalian 2-hybrid assays. Cells were transiently co-transfected with the three plasmids using the FuGene6 transfection reagent, and 5,000 cells were seeded into the wells of 384-well assay plates and cultured overnight at 37°C, 5% CO₂, and 95% humidity. After 24 h cells were exposed to 100 nM DHT and the assay plate was returned to the incubator for an additional 24 h before BrightGlo reagent was added to the plate and the RLUs were captured on a SpectraMax M5e microtiter plate reader. Luminescence RLU's were plotted in the presence or absence of DHT for the three cell lines. The data are presented as the mean ± SD of triplicate wells per cell line ± DHT treatment.

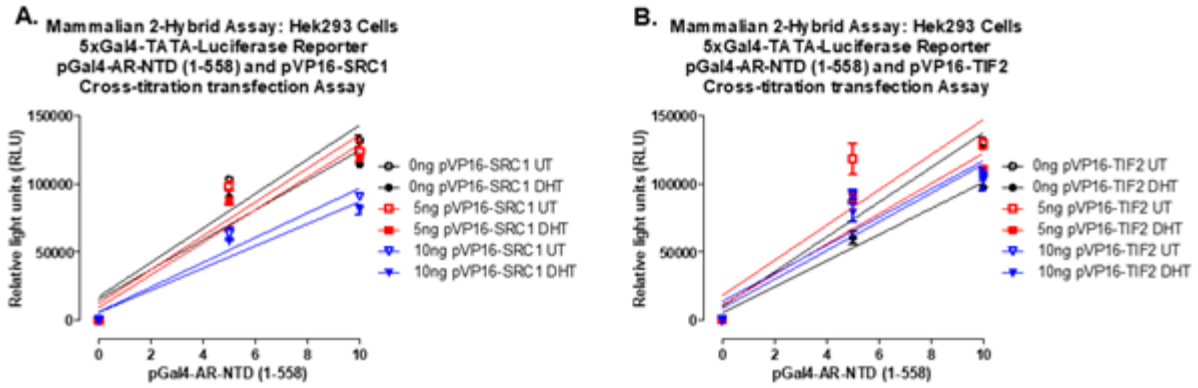


Figure 38. Mammalian 2-Hybrid assay development and optimization: cross-titration of pGal4-AR-NTD (1-558) with A) pVP16-TIF2 or B) pVP16-SRC1

To determine the appropriate amounts of pGal4-AR-NTD (1-558) and pVP16-TIF2 or pVP16-SRC1 to use in the mammalian 2-hybrid assay, cross-titration co-transfection experiments were performed in HEK293 cells. Interacting partners, pGAL4-AR-NTD (1-558) with pVP16-TIF2 or pVP16-SRC1, plus the reporter construct 5xGal4-TATA-Luc, were transiently co-transfected into HEK293 cells using the FuGene6 transfection reagent, and 5,000 cells were seeded into the wells of 384-well assay plates and cultured overnight at 37°C, 5% CO₂, and 95% humidity. After 24 h cells were exposed to 100 nM DHT and the assay plate was returned to the incubator for an additional 24 h before BrightGlo reagent was added to the plate and the RLU's were captured on a SpectraMax M5e microtiter plate reader. Luminescence RLU's were plotted in the presence or absence of DHT for varying amounts of pGAL4-AR-NTD (1-558) with pVP16-TIF2 or pVP16-SRC1. The data are presented as the mean ± SD of triplicate wells per plasmid DNA combination.

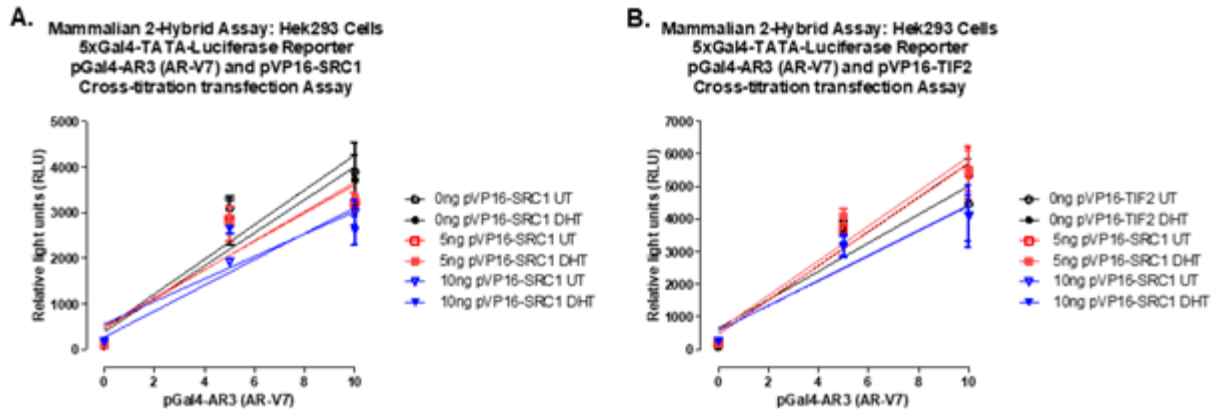


Figure 39. Mammalian 2-hybrid assay development and optimization: cross-titration of pGal4-AR3 (AR-V7) with A) pVP16-TIF2 or B) pVP16-SRC1

To determine the appropriate amounts of pGal4-AR3 (AR-V7) and pVP16-TIF2 or pVP16-SRC1 to use in the mammalian 2-hybrid assay, cross-titration co-transfection experiments were performed in HEK293 cells. Interacting partners, pGAL4-AR3 (AR-V7) with pVP16-TIF2 or pVP16-SRC1, plus the reporter construct 5xGal4-TATA-Luc, were transiently co-transfected into HEK293 cells using the FuGene6 transfection reagent, and 5,000 cells were seeded into the wells of 384-well assay plates and cultured overnight at 37°C, 5% CO₂, and 95% humidity. After 24 h cells were exposed to 100 nM DHT and the assay plate was returned to the incubator for an additional 24 h before BrightGlo reagent was added to the plate and the RLUs were captured on a SpectraMax M5e microtiter plate reader. Luminescence RLU's were plotted in the presence or absence of DHT for varying amounts of pGAL4-AR3 (AR-V7) with pVP16-TIF2 or pVP16-SRC1. The data are presented as the mean ± SD of triplicate wells per plasmid DNA combination.

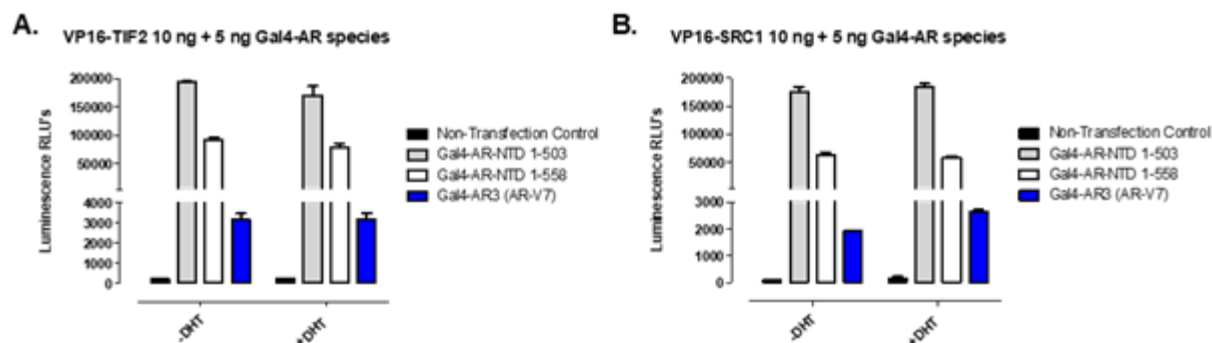


Figure 40. Determining which pGal4-AR-NTD plasmid construct enables the most robust mammalian 2-hybrid assays

The mammalian 2-hybrid assay was conducted in HEK 293 cell lines co-transfected with either of 3 different pGal4-AR-NTD constructs: pGal4-AR-NTD (1-503), pGal4-AR-NTD (1-558), or pGal4-AR3 (AR-V7), pVP16-TIF2 or pVP16-SRC1 and the 5xGal4-TATA-Luc reporter, to see how the different pGal4-AR-NTD constructs had an effect on luciferase reporter luminescence signal. We selected the pGal4-AR-NTD (1-503) construct because it encodes the entire AF-1 surface and had been used previously in reporter-based assays. We selected the pGal4-AR-NTD (1-558) construct because it encodes the entire AR-NTD, and we selected the pGal4-AR3 construct because it encodes the entire AR-V7 splice variant, making it the most biologically relevant construct for use in the M2H assay. Cells were transiently co-transfected with three plasmids using the FuGene6 transfection reagent, and 5,000 cells were seeded into the wells of 384-well assay plates and cultured overnight at 37°C, 5% CO₂, and 95% humidity. After 24 h cells were exposed to 100 nM DHT and the assay plate was returned to the incubator for an additional 24 h before BrightGlo reagent was added to the plate and the RLU's were captured on a SpectraMax M5e microtiter plate reader. Luminescence RLU's were plotted in the presence or absence of DHT for the three cell lines. The data are presented as the mean \pm SD of triplicate wells per cell line \pm DHT treatment. Representative experimental data from one of two independent experiments are shown.

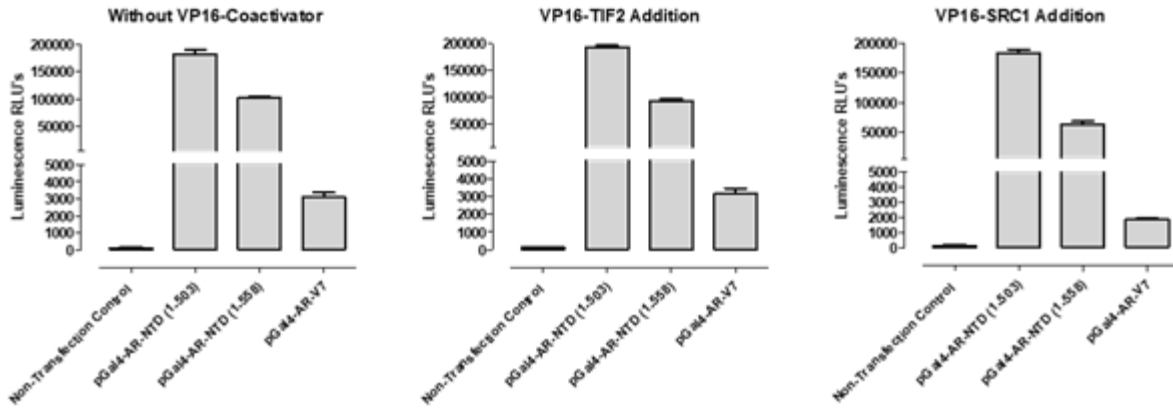


Figure 41. Determining if each of the pGal4-AR-NTD plasmid constructs requires pVP16-coactivator to produce 5xGal4-TATA-Luc reporter based assay signal

This experiment was conducted in HEK 293 cell lines co-transfected with either of 3 different pGal4-AR-NTD constructs: pGal4-AR-NTD (1-503), pGal4-AR-NTD (1-558), or pGal4-AR3 (AR-V7), either no coactivator, pVP16-TIF2 or pVP16-SRC1 and the 5xGal4-TATA-Luc reporter, to see if different pGal4-AR-NTD constructs had different coactivator requirements. Cells were transiently co-transfected with the indicated plasmids using the FuGene6 transfection reagent, and 5,000 cells were seeded into the wells of 384-well assay plates and cultured overnight at 37°C, 5% CO₂, and 95% humidity. After 48 h cells BrightGlo reagent was added to the plate and the RLU's were captured on a SpectraMax M5e microtiter plate reader. Luminescence RLU's were plotted in the absence of DHT for the three cell lines. The data are presented as the mean \pm SD of triplicate wells per cell line \pm DHT treatment. Representative experimental data from one of two independent experiments are shown.

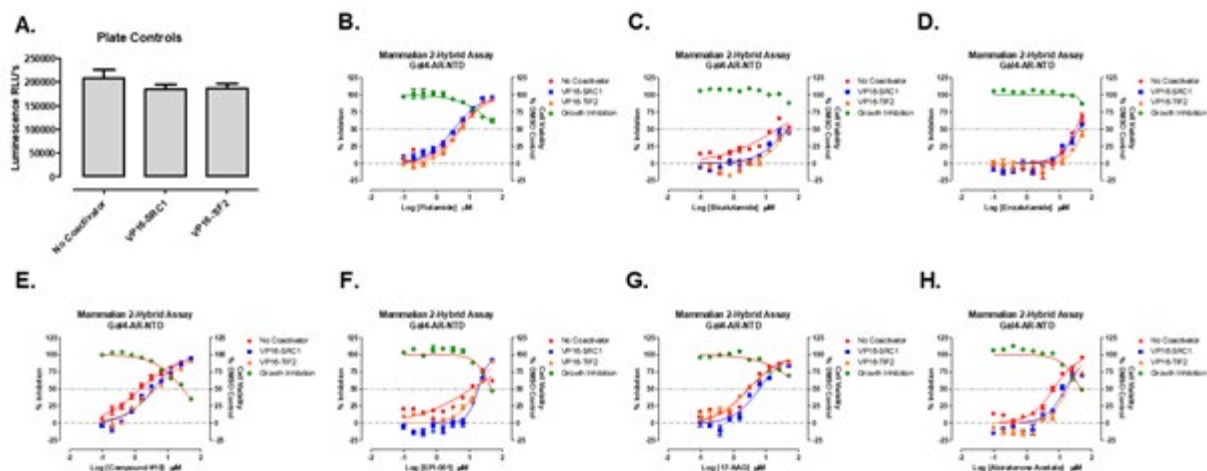


Figure 42. Test set performance in pGal4-AR-NTD based transactivation assays

HEK293 cells were transfected with three M2H plasmid constructs, pGAL4-AR-NTD (1-503) plus 5xGal4-TATA-Luc with either pVP16-TIF2 or pVP16-SRC1, and 5,000 cells were seeded into the wells of 384-well assay plates, and cultured overnight at 37°C, 5% CO₂, and 95% humidity. After 24 h cells were exposed to test compounds at the indicated concentrations and incubated overnight. The assay plate was returned to the incubator for an additional 24 h before BrightGlo reagent was added to the plate and the RLUs were captured on a SpectraMax M5e microtiter plate reader. The M2H RLU's data for compound treated wells were normalized to the 0.5% DMSO, n=32 plate controls, and the % inhibition was plotted as the mean +/- SD (n = 3) values from triplicate wells for each compound concentration plotted on the left Y-axis. The corresponding cell viability (◆) data for compound treated wells were normalized to 0.5% DMSO control wells (n=64), and the % cell viability was plotted as the mean +/- SD (n = 3) values from triplicate wells for each compound concentration plotted on the right Y-axis. **A)** Representative plate control data for No coactivator (●) the SRC1 (■) and TIF2 (▲) M2H formats are plotted on the left axis. The concentration dependent normalized % inhibition of No coactivator, TIF2 and SRC1 M2H formats (left Y-axis) and cell viability data (right Y-axis) for **B)** Flutamide, **C)** Bicalutamide, **D)** Enzalutamide, **E)** Compound #10, **F)** EPI-001, **G)** 17-AAG, and **H)** Abiraterone acetate are presented. Representative experimental data from one of two independent experiments are shown.

Table 13. IC₅₀ results of test set run in pGal4-AR-NTD based transactivation assays

| Assay | Mammalian 2-Hybrid | | | | | | Transactivation Assay | | | |
|---------------------|----------------------------|------|----------------------------|------|----------------------------|------|----------------------------|------|----------------------------|------|
| | Gal4-AR-NTD:VP16-TIF2 | | Gal4-AR-NTD:VP16-SRC1 | | HEK 293 Growth Inhibition | | Gal4-AR-NTD(1-503) | | HEK 293 Growth Inhibition | |
| | Mean IC ₅₀ (μM) | sdm |
| Flutamide | 4.65 | 0.74 | 3.47 | 0.12 | >50 | N/A | 4.83 | 0.14 | >50 | N/A |
| Bicalutamide | 33.3 | 13.3 | 29.4 | 14.0 | >50 | N/A | 18.8 | 2.46 | >50 | N/A |
| Enzalutamide | 52.8 | 2.25 | 39.9 | n=1 | >50 | N/A | 31.5 | 2.63 | >50 | N/A |
| Compound #10 | 4.64 | 0.39 | 3.56 | 0.03 | 26.8 | 9.5 | 1.55 | 0.04 | 26.5 | 10.9 |
| EPI-001 | 19.5 | 2.82 | 15.3 | 3.27 | 42.5 | 11.3 | 9.92 | 1.24 | 36.6 | 9.3 |
| 17-AAG | 4.31 | 1.80 | 2.05 | 0.85 | >50 | N/A | 3.54 | 0.54 | >50 | N/A |
| Abiraterone Acetate | 14.7 | 3.02 | 12.5 | 2.75 | 34.0 | 9.02 | 6.43 | 0.28 | 30.5 | 7.72 |

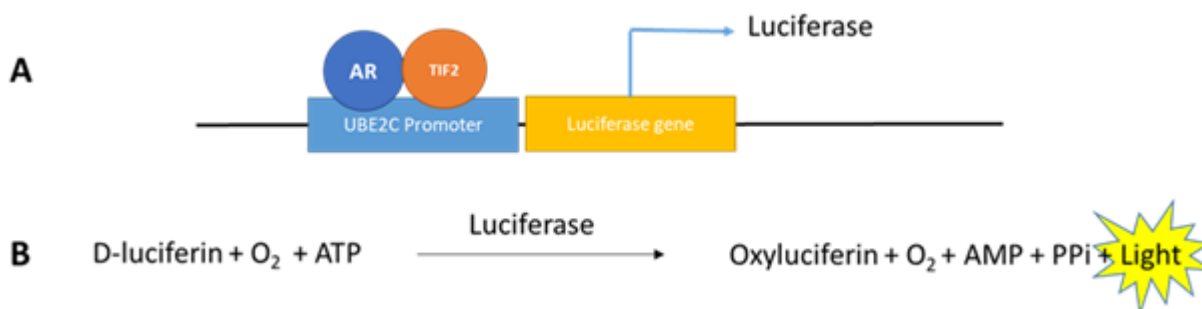


Figure 43. UBE2C-Luc reporter assay principle

The UBE2C reporter assay is a luciferase construct driven by three repeats of an AR-V7-specific promoter element of the ubiquitin-conjugating enzyme E2C (UBE2C) gene. The UBE2C promoter region is fused to a gene that codes for luciferase. If AR-V7 and one of its coactivators, such as TIF2 are bound to responsive elements on the promoter region of the UBE2C gene, this will lead to recruitment of the cell's transcriptional machinery, and ultimately, the transcription of luciferase enzyme, which will convert luciferin reagent into light output that can be quantified. If a compound run in this assay can disrupt the interaction between AR and TIF2, this should decrease reporter activity.

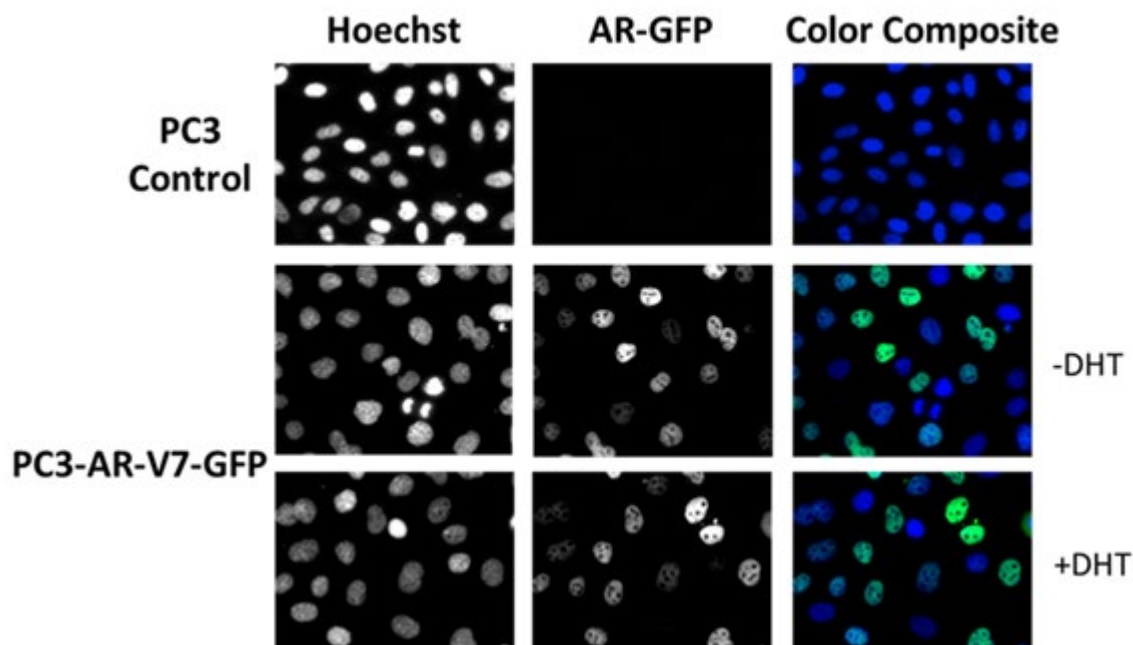


Figure 44. IXM images of PC3 cells stably transfected with pEGFP-C1-AR-V7 in the presence or absence of DHT

Subcellular localization assays were conducted in PC3 cells stably transfected with pEGFP-C1-AR-V7 plasmid construct in the presence or absence of DHT. PC3 cells were seeded at a density of 3,000 cells/well into 384-well assay plates and cultured overnight at 37°C, 5% CO₂, and 95% humidity. After 24 h cells were exposed +/- 100 nM DHT for 24 before being fixed, and imaged on an IXU automated HCS platform (Molecular Devices LLC). These are representative images of PC3 cells stably transfected with the pEGFP-C1-V7 plasmid construct. In both untreated and treated cells, AR-V7 is predominantly in the nuclear.

Optimizing Transfection Conditions PC3-AR-V7-GFP Cells

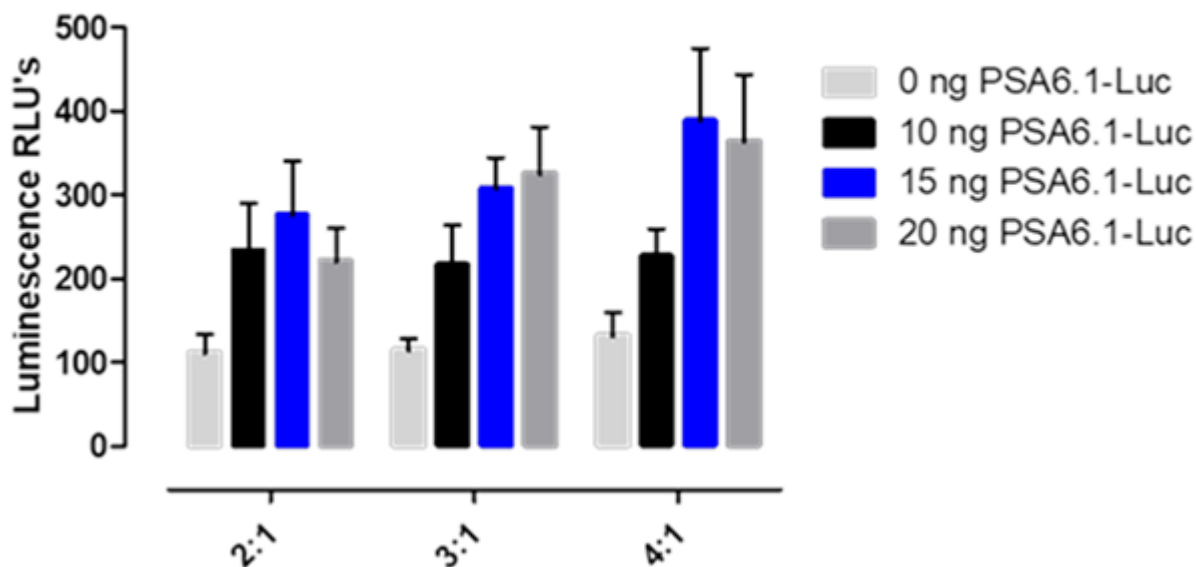


Figure 45. Optimizing transfection conditions: Determining the optimal amounts of DNA plasmid reporter construct and FuGENEHd:DNA ratio to use in the PSA6.1-Luc reporter assay

To determine the optimal amount of PSA6.1-Luc reporter plasmid DNA to use in the PSA6.1-Luc reporter assays we performed titration experiments by increasing amounts of the PSA6.1-Luc plasmid DNAs and the ratio of FuGene:DNA in PC3-AR-V7-GFP cells. After the reporter construct was transiently transfected into PC3-AR-V7-GFP cells, 3,000 cells were seeded into the wells of 384-well assay plates, and cultured overnight at 37°C, 5% CO₂, and 95% humidity. After 48 h BrightGlo reagent was added to the plate and the RLU's were captured on a SpectraMax M5e microtiter plate reader. Luminescence RLU's were plotted for the different conditions, and the data are presented as the mean \pm SD of triplicate wells per plasmid DNA combination.

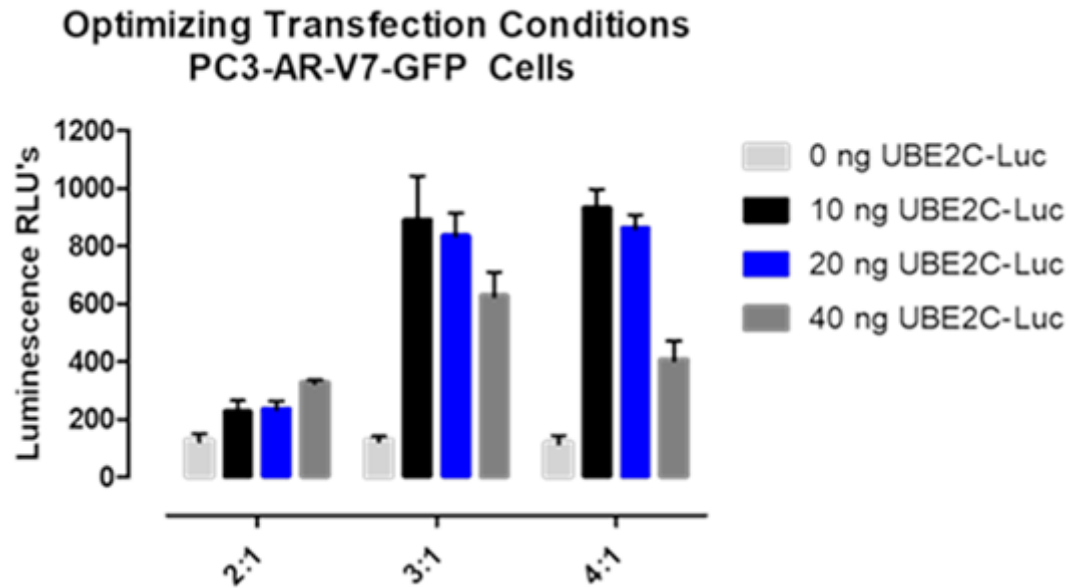


Figure 46. Optimizing transfection conditions: Determining the optimal amounts of DNA plasmid reporter construct and FuGENEHD:DNA ratio used in the UBE2C-Luc reporter assay

To determine the optimal amount of UBE2C-Luc reporter plasmid DNA to use in the UBE2C-Luc reporter assays we performed titration experiments by increasing amounts of the UBE2C-Luc plasmid DNAs and the ratio of FuGene:DNA in PC3-AR-V7-GFP cells. After the reporter construct was transiently transfected into PC3-AR-V7-GFP cells, 3,000 cells were seeded into the wells of 384-well assay plates, and cultured overnight at 37°C, 5% CO₂, and 95% humidity. After 48 h BrightGlo reagent was added to the plate and the RLU's were captured on a SpectraMax M5e microtiter plate reader. Luminescence RLU's were plotted for the different conditions, and the data are presented as the mean \pm SD of triplicate wells per plasmid DNA combination.

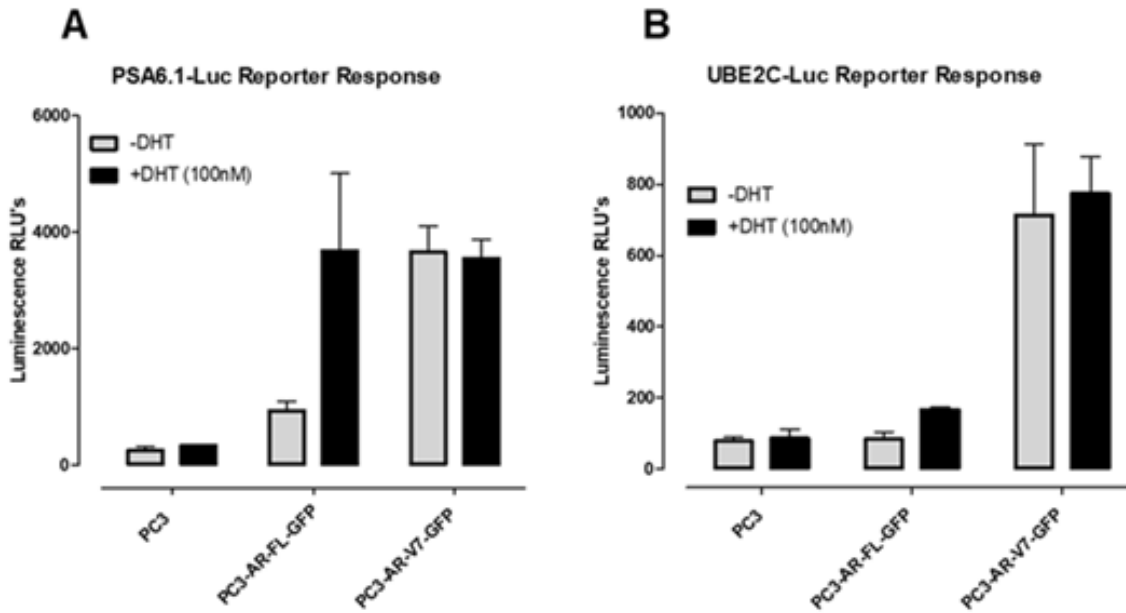


Figure 47. Demonstrating PSA6.1-Luc and UBE2C-Luc reporter response in different cell lines: PC3, PC3-AR-FL-GFP, and PC3-AR-V7-GFP

To compare the promoter-driven reporter response and its dependence on DHT in each cell line, PC3's, PC3-AR-FL-GFP, or PC3-AR-V7-GFP cells were transiently transfected with either pPSA6.1-Luc or pUBE2C-Luc reporter constructs before being seeded in 384-well, white, opaque plates (3,000 cells/well) and incubated at 5% CO₂, 37°C, and 95% humidity for 24 h. The next day either DHT (100nM) or SFM was added to each well and again incubated at 5% CO₂, 37°C, and 95% humidity for 24 h. The next day BrightGlo reagent was added to the plate and the RLU's were captured on a SpectraMax M5e microtiter plate reader. Luminescence RLU's were plotted for the different conditions, and the data are presented as the mean ± SD of six wells per condition.

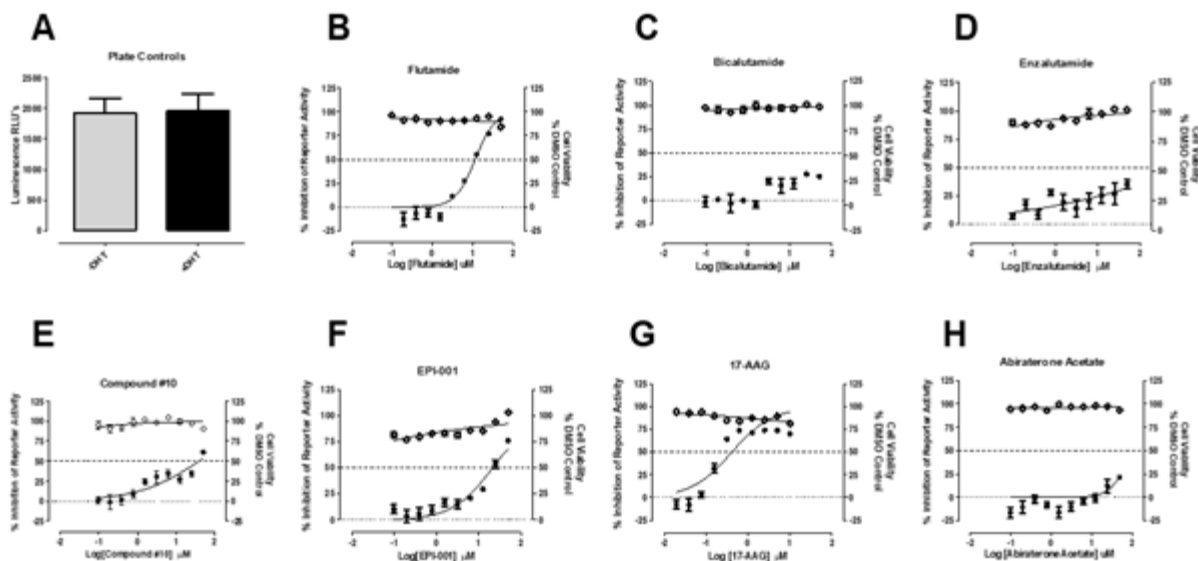


Figure 48. Test set performance in PSA6.1-Luc reporter assay

A PSA6.1-LUC reporter based assay was conducted with 7 test compounds to validate this assay. PC3-AR-V7-GFP cell lines were transiently bulk transfected with a 3:1 ratio of Fugene HD: PSA-6.1-LUC plasmid DNA (20 ng/well), then seeded into assay plates at a density of 3,000 cell per well, and finally incubated overnight at 5% CO₂, 95% humidity, and 37°C. PC3-AR-V7-GFP cells transfected with the PSA6.1-LUC plasmid were exposed to the indicated concentrations of compounds before the assay plate was returned to the incubator for an additional 24 h before BrightGlo reagent was added to the plate and the RLUs were captured on a SpectraMax M5e microtiter plate reader. The PSA6.1-LUC RLU's data for compound treated wells were normalized to plate controls (0.5% DMSO, n=32), and the % inhibition (●) was plotted on the left Y-axis as the mean +/- SD (n=3) values from triplicate wells for each compound concentration. The corresponding cell viability data for compound treated wells were normalized to 0.5% DMSO control wells (n=32), and the % cell viability (◇) was plotted on the right Y-axis as the mean +/- SD (n = 3). **A**) Representative plate control data for one run is plotted. The concentration dependent normalized % inhibition of the DHT-induced PSA6.1-LUC reporter activity for **B**) Flutamide, **C**) Bicalutamide, **D**) Enzalutamide, **E**) Compound #10, **F**) EPI-001, **G**) 17-AAG, and **H**) Abiraterone acetate are presented. Representative experimental data from one of two independent experiments are shown.

Table 14. IC₅₀ results of test set run in PSA6.1-Luc reporter based

| Assay | PSA6.1-LUC Reporter | | Growth Inhibition | |
|---------------------|---------------------|------|---------------------|-----|
| | PC3-AR-V7-GFP Cells | | PC3-AR-V7-GFP Cells | |
| | Mean IC50 (μM) | sdm | Mean IC50 (μM) | sdm |
| Flutamide | 11.5 | 1.22 | >50 | N/A |
| Bicalutamide | >50 | N/A | >50 | N/A |
| Enzalutamide | >50 | N/A | >50 | N/A |
| Compound #10 | 50.3 | 11.3 | >50 | N/A |
| EPI-001 | 25.3 | 4.05 | >50 | N/A |
| 17-AAG | 0.68 | 0.37 | >50 | N/A |
| Abiraterone Acetate | >50 | N/A | >50 | N/A |

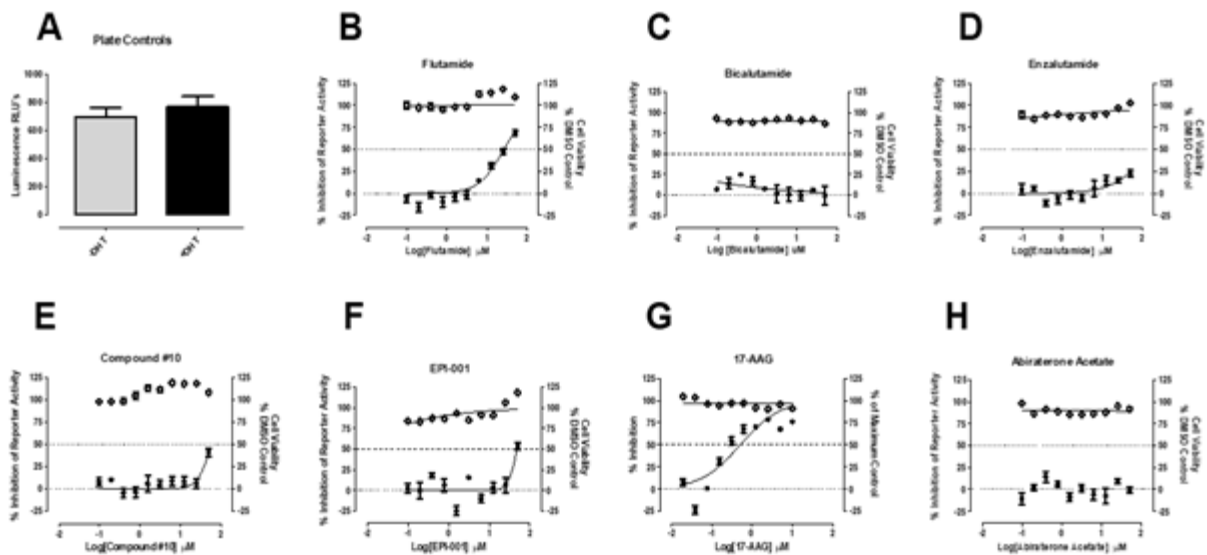


Figure 49. Test set performance in UBE2C-Luc reporter assay

A UBE2C-LUC reporter based assay was conducted with 7 test compounds to validate this assay. PC3-AR-V7-GFP cell lines were transiently bulk transfected with a 3:1 ratio of Fugene HD: PSA-6.1-LUC plasmid DNA (10 ng/well), then seeded into assay plates at a density of 3,000 cell per well, and finally incubated overnight at 5% CO₂, 95% humidity, and 37°C. PC3-AR-V7-GFP cells transfected with the UBE2C-LUC plasmid were exposed to the indicated concentrations of compounds before the assay plate was returned to the incubator for an additional 24 h before BrightGlo reagent was added to the plate and the RLUs were captured on a SpectraMax M5e microtiter plate reader. The UBE2C-LUC RLU's data for compound treated wells were normalized to plate controls (0.5% DMSO, n=32), and the % inhibition (●) was plotted on the left Y-axis as the mean +/- SD (n=3) values from triplicate wells for each compound concentration. The corresponding cell viability data for compound treated wells were normalized to 0.5% DMSO control wells (n=32), and the % cell viability (◇) was plotted on the right Y-axis as the mean +/- SD (n = 3). **A**) Representative plate control data for one run is plotted. The concentration dependent normalized % inhibition of the DHT-induced UBE2C-LUC reporter activity for **B**) Flutamide, **C**) Bicalutamide, **D**) Enzalutamide, **E**) Compound #10, **F**) EPI-001, **G**) 17-AAG, and **H**) Abiraterone acetate are presented. Representative experimental data from one of two independent experiments are shown.

Table 15. IC₅₀ results of test set run in UBE2C-Luc reporter based assay

| Assay | UBE2C-LUC Reporter | | Growth Inhibition | |
|---------------------|---------------------|------|---------------------|-----|
| | PC3-AR-V7-GFP Cells | | PC3-AR-V7-GFP Cells | |
| | Mean IC50 (μM) | sdm | Mean IC50 (μM) | sdm |
| Flutamide | 28.6 | 2.71 | >50 | N/A |
| Bicalutamide | >50 | N/A | >50 | N/A |
| Enzalutamide | >50 | N/A | >50 | N/A |
| Compound #10 | 58.6 | 0.79 | >50 | N/A |
| EPI-001 | 49.2 | 0.76 | >50 | N/A |
| 17-AAG | 0.75 | 0.50 | >50 | N/A |
| Abiraterone Acetate | >50 | N/A | >50 | N/A |

5.0 Compound Performance in Assays Developed to Prioritize Hits from the AR-TIF2

PPIB

5.1 Introduction

In this chapter I will describe how AR-TIF2 PPI inhibitor/disruptor hit compounds identified from the LOPAC set and three compound libraries run in the primary screen (detailed in chapter 2) were initially triaged, and then prioritized for testing in the AF-2 and AF-1 transactivation domain characterization assays developed and described in chapters 3 and 4. Compounds that produced calculable IC_{50} 's in the AR-TIF2 PPIB assay were initially tested in growth inhibition assays conducted in 5 different PCa cell lines, two AR null and three AR positive PCa cell lines, and a PSA6.1-Luc reporter assay conducted in C4-2 cells. The PCa growth inhibition assays were used to prioritize AR-TIF2 PPI inhibitor/disruptor hits that differentially inhibited the growth of AR positive cell lines, while the PSA6.1-Luc reporter assay was used to confirm that they inhibited AR-mediated transcriptional activation. Prioritized hits were then tested in a H^3 -DHT radioligandbinding assay using recombinantly expressed AR-LBD, and a TIF2 Box III LXXLL peptide ALPHAScreen AR-LBD binding assay.

Hit compounds that passed our testing paradigm with the desired biological activity profile were also subjected to a cheminformatics assessment of their physical and chemical properties. The initial hit triage resulted in a small set of 27 compounds that were confirmed in our secondary assays. Two hit compounds came from the 10K library, 7 from the 50K library, and 18 from the 83K library. These compounds were clustered manually, and both chem-informatically and bio-informatically assessed via the combined output of the FAFDrugs4 and SwissADME servers.

Compounds were assessed for PAINS, lead likeness, reactive functionality, induction of phospholipidosis, probability of good bioavailability via the Veber and Egan rules, and other parameters. Compounds that failed bio/chem informatics filters were removed from further consideration. The remaining compound clusters and singletons were queried in scifinder to ascertain if there is known literature around the general scaffold they belong to and if they have known biological activities that would be unwanted. Through this assessment several chemotypes were removed from further consideration. For example, several hits were chalcones, compounds known to have promiscuous activity that have been used as fluorescent probes [176-178]. Zeranol, a singleton hit, was deprioritized because it has potent estrogenic activity and is used as a growth promoter in cattle [179, 180]. Compounds with unknown biological activity and/or mention in patent and peer-reviewed literature were thought to be suitable candidates for further investigation. Hits that displayed favorable biological profiles in the secondary characterization assays and were not flagged in any of the cheminformatics filters were selected for further testing in our AF-2 and AF-1 transactivation domain characterization assays.

5.2 Initial Hit Triage

5.2.1 LOPAC Set

The 17 confirmed actives from the LOPAC set were run in 3 different counter-screens. The first was the p53-hDM2 PPIB assay that utilizes the same assay format and biosensor design but different protein interacting partners as the AR-TIF2 PPIB assay and therefore served as an assay interference and PPI selectivity counter-screen. None of the 15 AR-TIF2 PPI LOPAC hits were

active in the p53-hDM2 PPIB assay, indicating that they are unlikely to interfere with either the biosensor assay format or to be non-selective PPI inhibitors [118]. In an HCS assay designed to identify compounds that altered the sub-cellular distribution and/or expression of AR-GFP, the AR-TIF2 PPI LOPAC hits either enhanced the nuclear localization of AR-GFP or were inactive. The AR-GFP data suggest that some of the AR-TIF2 PPI LOPAC hits may be partial AR agonists, and, therefore, would not be expected to inhibit or disrupt AR-TIF2 PPIs. To evaluate the nuclear receptor (NR) selectivity of the AR-TIF2 PPI LOPAC hits, we tested their activity in a dexamethasone (Dex)-induced glucocorticoid receptor (GR) nuclear translocation assay. Although none of the steroid NR AR-TIF2 LOPAC hits inhibited Dex-induced GR nuclear translocation, the five non-steroid hits inhibited GR trafficking in a concentration-dependent manner [118].

We would expect that AR-TIF2 PPI inhibitor/disruptor hits would be able to inhibit AR transcriptional activity, and to test this notion we examined their ability to inhibit the DHT-induced luciferase reporter activity of the PSA-6.1-LUC plasmid transiently transfected into the C4-2 and 22Rv1 CRPC cell lines. Pre-exposure to the 15 AR-TIF2 PPI LOPAC hits inhibited DHT-induced PSA-6.1-LUC luciferase reporter activity in C4-2 and 22Rv1 cell lines in a concentration-dependent manner (Table 16, on pg. 176) [118].

We would also anticipate that AR-TIF2 PPI inhibitors/disruptors would be more effective at inhibiting the growth of PCa cell lines that express AR relative to those that do not express AR. To test this hypothesis, we developed and implemented CellTiter-Glo™ (CTG) growth inhibition assays in five PCa cell lines: LnCaP, C4-2, and 22Rv1 cells express AR, while PC3 and DU-145 are AR null. Four of the 10 steroid NR ligand AR-TIF2 PPI LOPAC hits failed to inhibit the growth of any of the PCa cell lines at $\leq 50 \mu\text{M}$ (estrone, cortexelone, 17- α -H-PG, and nilutamide) and of the 6 others, only 2-methoxyestradiol (2-MOED) inhibited the growth of all five PCa cell

lines. None of the steroid NR ligand AR-TIF2 PPI LOPAC hits differentially inhibited the growth of AR-positive PCa cell lines relative to AR-null PCa cell lines. Although the non-steroid AR-TIF2 PPI LOPAC hits were more potent and inhibited the growth of all five PCa cell lines in a concentration-dependent manner, they were equally effective at inhibiting the growth of AR-positive and AR-negative PCa cell lines (Table 16). Therefore, none of the AR-TIF2 PPI LOPAC hits exhibited evidence of differential/selective growth inhibitory activity for AR positive over AR negative CaP cell lines that might be expected [118].

Finally, since one potential mechanism of blocking the formation of DHT-induced AR-TIF2 PPIs would be to prevent DHT binding to the AR-LBD, we developed a secondary assay to identify AR antagonists among the AR-TIF2 PPI hits. The ten steroid LOPAC hits exhibited AR-antagonist activity in our H³-DHT radioligandbinding assay (Table 16), and this is likely the basis of their activity in the AR-TIF2 PPIB assay. Since several of the steroid LOPAC hits have activities against other steroid nuclear receptors, including the estrogen, progesterone, mineralocorticoid, and glucocorticoid receptors, they lack selectivity. The five non-nuclear receptor ligand LOPAC hits, 4-P-3-FOCN, TPCK, ZPCK, Bay 11-7085, and parthenolide were inactive in the H³-DHT radioligandbinding assay with IC₅₀s >50 μM (Table 16). However, based on the cytoplasmic AR-RFP distribution phenotypes of the non-steroid hits and their inhibition of Dex-induced GR-GFP nuclear translocation, it is possible that these compounds interfere with a common component of NR activation and trafficking. Among the possibilities are the following: the Hsp 90 and Hsp 70 chaperones maintain both NRs in high-affinity structural conformations in the cytoplasm ready for ligand binding; ligand-bound AR and GR are both cargos of dynein mediated retrograde trafficking on microtubules to the nucleus; and the importin-α/β adaptor system mediates entry through the

nuclear pore complex of both NRs. Since none of the LOPAC hits exhibit the biological profile of a selective AR-TIF2 inhibitor/disruptor, they were deprioritized and not pursued further.

5.2.2 10K Library

Of the fourteen compounds from the 10K library that were confirmed active in both formats of the AR-TIF2 PPIB HCS assay, none of them exhibited activity in the 3 counter screens, indicating that they did not interfere with the biosensor assay format, and were not either nonselective PPI inhibitors or promiscuously active against GR, another member of the steroid nuclear receptor family. In AR-TIF2 PPIB concentration response assays, 5 of the confirmed actives produced calculable IC_{50} s for inhibition of DHT-induced AR-TIF2 PPI formation and two produced calculable IC_{50} s for disruption of pre-existing AR-TIF2 complexes (Table 16). All 5 hit compounds inhibited DHT-induced PSA6.1-Luc reporter-based activity in 22Rv1 and C4-2 cells in a concentration dependent manner, indicating that they blocked AR-mediated transcriptional activation. However, only 2 of the hits selectively inhibited the growth of AR-positive PCa cell lines over AR-null cell lines (Table 16). However, neither of the 2 hits exhibited activity in either the H^3 -DHT radioligand or TIF2 Box III LXXLL peptide ALPHAScreen binding assays (Table 16). Furthermore, our cheminformatics analysis of the two hit structures raised a couple of concerns; PPS-00052526 was predicted to exhibit low overall bioavailability, and PPS-000059998 was predicted to exhibit low solubility. Based on these data and analysis neither of the two 10K hits were prioritized for further hit characterization.

5.2.3 50K Library

When AR-TIF2 PPIB confirmed actives from the 50K library were run in the 3 counter screens, only one was active in the AR-GFP nuclear localization assay, perhaps indicating that this compound may be reducing the AR-RFP biosensor expression levels or restricting its sub-cellular localization to the cytoplasm. We performed a medicinal chemistry structural classification and clustering of the 124 confirmed actives in the AR-TIF2 PPIB HCS assay to identify and eliminate potential liabilities, reactive and/or promiscuous assay interference compounds, and compounds that were not considered chemically tractable. The 124 compounds were sub-divided into 24 structurally related clusters and 19 singletons, but not all the compounds were ordered from clusters with multiple representatives. 74 compounds were chosen for repurchase but only 70 were available. The purchased confirmed actives were tested in the AR-TIF2 PPIB assay in 10-point 2-fold serial dilution series in triplicate starting at a maximum concentration of 50 μM . Fifty-six compounds inhibited DHT-induced AR-TIF2 PPI formation with $\text{IC}_{50\text{s}} < 50 \mu\text{M}$, and 52 compounds disrupted pre-existing DHT-induced AR-TIF2 PPI complexes with $\text{IC}_{50\text{s}} < 50 \mu\text{M}$ (Table 16). Twenty-four of the most potent AR-TIF2 PPIB hits that exhibited some degree of selectivity for AR-positive cell lines in the five PCa growth inhibition assays were then tested in the C4-2-PSA6.1-Luciferase reporter assay. Eighteen of the AR-TIF2 PPIB hits were shown to inhibit DHT-induced reporter activity in a concentration dependent manner, indicating that they also blocked AR-mediated transcriptional activation. The 18 hits were then run in the H^3 -DHT radioligand and TIF2 Box III LXXLL peptide binding assays. Eight compounds produced $\text{IC}_{50\text{s}} < 50 \mu\text{M}$ in the H^3 -DHT radioligand binding assay, and 7 produced $\text{IC}_{50\text{s}} < 50 \mu\text{M}$ in the TIF2 Box III LXXLL peptide binding assay or displayed concentration dependent inhibition responses with an extrapolated $\text{IC}_{50} < 100 \mu\text{M}$ (Table 16).

A medicinal chemistry analysis of the physical chemical properties of the 7 prioritized hit compounds predicted that 5026223 would have low aqueous solubility and was flagged by a Pan Assay Interference and Nuisance (PAINS) filter. 87237916 was also predicted to have low aqueous solubility, was flagged by both PAINS and Lilly filters, and did not share many of the characteristics of published PPI inhibitors. The remaining 5 hits were then used to perform a structural similarity based query of the ChemBridge 410K core library database, using a tanimoto score of above 0.7 as a threshold for compound similarity selection.

5.2.4 83K Library

Thirty-six of the confirmed AR-TIF2 PPI inhibitor/disruptor actives from the 83K library were also active in two of the three counter-screens. Twenty-eight of the compounds reduced AR-GFP nuclear localization by >50%, suggesting that they might be indirectly inhibiting the AR-TIF2 PPIB assay by reducing the AR-RFP biosensor expression levels or restricting its sub-cellular localization to the cytoplasm. Eight confirmed actives in the AR-TIF2 PPIB assay also inhibited GR nuclear translocation by >50%, and therefore either lack AR specificity/selectivity or they inhibit a shared component of the AR and GR signaling pathways. We therefore deprioritized these 36 confirmed AR-TIF2 PPIB actives. Two hundred four confirmed actives were then run in concentration response assays in the AR-TIF2 PPIB assay, the C4-2-PSA6.1-Luc reporter assay, and the 5 PCa growth inhibition assays. One hundred seventeen hit compounds exhibited calculable IC₅₀'s in one or both of the AR-TIF2 PPIB formats (Table 16). Twenty one compounds were also able to inhibit DHT-induced PSA6.1-Luc reporter activity in a concentration manner, with IC₅₀'s <40 μM (Table 16), and 20 compounds were either able to inhibit the growth all 5 PCa cell lines or were able to target AR-positive cell lines in a selective manner run in the PCa GI₅₀

assays. Only 18 of the 117 AR-TIF2 PPIB hits were also able to block AR-mediated transcriptional activation and the growth of PCa cell lines. Four of the 18 hit compounds also inhibited H³-DHT radioligand binding in a concentration dependent manner, but couldn't achieve >50% inhibition at ≤40 μM. Similarly, 3 of the 18 hit compounds also inhibited TIF2 Box III LXXLL peptide binding in a concentration dependent manner but failed to register an IC₅₀ at ≤40 μM. Our structural classification, clustering and cheminformatics analysis of the 18 hit compounds from the 83K library grouped the hits into 3 major clusters and 8 singletons. The three clusters include: 1) Phenyl-acryloyl-2-methoxybenzyl-thio-acetic acids, 2) Oxprop-en-yl benzoic acids, and 3) Nitrophenyl-acrylaldehydes. Cluster two contains alpha beta unsaturated ring structures which are highly reactive species, while cluster 3 contains highly reactive aldehyde species. Compounds assigned as singletons also contained problematic functional groups. Since all of the hits from the 83K library were flagged as problematic/reactive compounds, we deprioritized them from further characterization.

5.3 Prioritized Hit Characterization

After the initial triage of the AR-TIF2 inhibitor/disruptor hits described in section I of this chapter only 5 compounds from the 50K library met our bioassay profile and chemical tractability criteria. Based on the chemical structures of the 5 hits, 20 structurally similar analogs were selected via a similarity search query of the ChemBridge 410K core library database. These 25 compounds were profiled in the AR-TIF2 PPIB, C4-2-PSA6.1-Luc reporter, and 5 PCa cell lines growth inhibition assays. Six of the purchased analogs were inactive in both formats of the AR-TIF2 PPIB assays. Four of the 6 inactive analogs were also inactive in the PSA6.1-Luc reporter assay and 3 of the

compounds were unable to inhibit the growth of any of the 5 PCa cell lines. 4 of the inactive compounds were analogs of the cluster 1 compound 55803561, the 1B series containing thiadiazol-5-piperidine-carboxamides. The remaining 19 compounds that were active in one or both AR-TIF2 PPIB formats were also active in the PSA6.1-Luc reporter assay, although one exhibited substantial cytotoxicity in both the biosensor and reporter assays. The 19 compounds were also able to inhibit the growth of at least 2/5 PCa cell lines (Tables 17 & 19, on pgs. 178 & 180). We then tested the 18 most potent hit compounds in the TIF2 and SRC1 mammalian 2-hybrid assays, the H³-DHT radioligand binding assay, and the TIF2 Box III LXXLL peptide binding assay. All 18 compounds produced IC₅₀'s in the TIF2 and SRC1 M2H assays confirming that they block DHT-induced AR-LBD interactions with both coactivators. However, 7 of the compounds displayed measurable cytotoxicity in the M2H assays (Table 18, on pg. 179). Ten of the 18 compounds were active in the LXXLL binding assay, and 3 of these were also active in the H³-DHT binding assay.

Based on these data ten compounds were selected for testing in the panel of AF-1 and AF-2 transactivation domain assays described in chapters 2 and 3 (Figure 50, on pg. 177). From cluster 1, we selected the two hits 98648798 and 55803564 together with one analog 26996278. From cluster 2, we selected the two hits 14977726 and 36998335 together with three analogs 21302587, 24843178 and 60134988. From cluster 3, we selected two analogs 63718298 and 72508471. In addition to the H³-DHT and LXXLL peptide binding assays the ten compounds were also tested in the PSA6.1-Luc reporter assay conducted in PC3-AR-FL-GFP cells to evaluate AF-2 transactivation domain interactions. To evaluate AF-1 transactivation domain interactions the ten compounds were profiled in the pGal4-AR-NTD assay, and in two reporter assays, the PSA6.1-Luc and the UBE2C-Luc reporter assays both performed in PC3 cells stably transfected with

pEGFP-C1-AR-V7. The following section details how these ten AR-TIF2 PPI hits performed in each characterization assay.

5.3.1 Implementation of Assays Developed for Characterizing hits from the AR-TIF2 PPIB

5.3.1.1 PSA6.1-Luc Reporter Assay in PC3-AR-FL-GFP Cells

It was our expectation that compounds which inhibit or disrupt AR-TIF2 PPI's should also inhibit or disrupt AR transcriptional activity. Seven of 10 prioritized AR-TIF2 PPI inhibitor/disruptor hits inhibited the DHT-induced PSA6.1-Luc reporter activity in PC3-AR-FL-GFP cells in a concentration dependent manner and produced calculable IC₅₀s <50 μM (Figure 51B-G, on pg. 181 and Table 20, on pg. 184). Compounds 26996278 and 63718298 also exhibited substantial levels of cytotoxicity which potentially contributed to and complicated the interpretation of the reporter data (Figure 51C, J and Table. 20). For both compounds the reporter IC₅₀s were lower than the corresponding GI₅₀ for cell loss, indicating that the inhibition of transcription occurred at lower compound concentrations before the apparent cytotoxicity became a contributing factor. Two other hits, 24843178 and 72508471, showed evidence of concentration dependent inhibition of reporter activity but failed to achieve 50% inhibition even at 100 μM (Figure 51I, K and Table 20). Compound 21302587 was inactive in the AR-FL driven PSA6.1-Luc reporter assay at ≤100 μM (Figure 51H and Table 20). In sum therefore, 9 of the 10 prioritized AR-TIF2 PPI inhibitor/disruptor hits showed evidence of inhibiting DHT-induced AR-FL-mediated activation of transcription.

5.3.1.2 AR-LBD H³-DHT Radioligand Binding Assay

The radioligand binding assay specifically measures the competitive displacement of H³-DHT from AR-LBD in the presence of increasing concentrations of each compound, and it was used to determine if any of the AR-TIF2 PPI hits inhibited the PPIB assay because they were AR-antagonists. Only 3 of the hit analogs inhibited H³-DHT binding to the AR-LBD in the radioligand binding assay in a concentration dependent manner that produced calculable IC₅₀s (Figure 52, on pg. 182). 98648798, 36998335, and 63718298 exhibited IC₅₀'s of 43.7 ± 0.03, 62.9 ± 12.9, and 56.2 ± 8.65 μM, respectively (Figure 52C, F, K and Table 20). The IC₅₀s for inhibiting DHT-induced AR-TIF2 PPI formation were many folds lower than for inhibiting ligand binding. The AR-TIF2 PPI IC₅₀s for 98648798, 36998335, and 63718298 were 7.7-fold, 29.5-fold and 13.7-fold lower than their corresponding ligand binding IC₅₀s respectively. Six more AR-TIF2 PPI inhibitor/disruptor hits showed evidence of concentration dependent inhibition of H³-DHT binding to the AR-LBD but failed to achieve 50% inhibition even at 100 μM; 55803564, 26996278, 14977726, 21302587, 24843178 and 60134988. The corresponding IC₅₀s for inhibiting DHT-induced AR-TIF2 PPI formation for the 6 hits were in the 1.1 to 14.5 μM range, and in the 5.8 to 51.8 μM range for disrupting pre-existing AR-TIF2 PPIs. Only 72508471 exhibited no inhibition of H³-DHT binding to the AR-LBD at ≤100 μM. Although 9 of the 10 prioritized AR-TIF2 PPI inhibitor/disruptor hits inhibited H³-DHT binding to the AR-LBD to some extent, the IC₅₀s for inhibiting/disrupting AR-TIF2 PPIs were many folds lower than for disrupting ligand binding. It seems unlikely that the apparent weak AR antagonism of the hits is a major contributor to their ability to inhibit and/or disrupt AR-TIF2 PPIs. Another possibility is that 9 hits bind to allosteric sites on the AR-LBD to induce a conformation shift which negatively impacts ligand binding.

5.3.1.3 TIF2 Box III LXXLL peptide binding ALPHAScreen Assay

The ALPHAScreen AR-LBD::LXXLL-peptide binding assay is a biochemical assay that measures the interaction of the AR AF-2 domain formed by the AR-LBD and a peptide containing the LXXLL motif located in box III of the TIF2 coactivator's nuclear interaction domain (NID). Eight of the 10 prioritized AR-TIF2 PPI inhibitor/disruptor hits inhibited AR-LBD::LXXLL-peptide binding to produce calculable IC₅₀s. Five of the hit compounds produced IC₅₀s <50 μM: 98648798, 36998335, 60134988, 14977726, and 63718298 (Figure 52C, F-H, K and Table 20). Three more of the hits produced IC₅₀s in the 50 to 100 μM range; 26996278, 55803564 and 24843178 (Figure 52D, E, J and Table 20). Compound 21302587 showed evidence of concentration dependent inhibition of AR-LBD::LXXLL-peptide binding but failed to achieve 50% inhibition even at 100 μM (Figure 52I and Table 20). 72508471 was inactive in the AR-LBD::LXXLL-peptide binding assay (Figure 52L and Table 20).

5.3.1.4 Growth Inhibition Assays

We anticipated that any compounds that were able to disrupt the interactions between AR and TIF2 might selectively inhibit the growth of AR-positive PCa cell lines. For example, hit compound 55803564 produced GI₅₀s against all 3 AR-positive cell lines but not in the two AR-null cell lines (Table 19 on pg. 180). In contrast, 26996278 and 63718298 were equipotent against all 5 PCa cell lines and therefore did not demonstrate any selectivity for AR expressing cell lines. The remaining 7 hits exhibited differential selectivity for growth inhibition in 2/3 AR-positive PCa cell lines relative to AR-null cell lines.

5.3.1.5 Transactivation Assay using pGal4-AR-NTD

To determine if the prioritized AR-TIF2 PPI inhibitor/disruptor hit compounds could inhibit AR-NTD constitutive transcription, we used a 5xGal4 based luciferase reporter assay. Nine out of the ten hits produced calculable IC₅₀'s <100 uM (Figure 53B-I, K, on pg. 185 and Table 21, on pg. 188). Compound 63718298 produced a strange biphasic concentration response curve in the pGal4-AR-NTD-luciferase reporter assay. Nine of the 10 hits also displayed concentration dependent cytotoxicity in HEK 293 cells, and 7 produced calculable IC₅₀'s <100 uM (Figure 53B-I, K and Table 21). In general, pGal4-AR-NTD-luciferase reporter IC₅₀s were lower than the corresponding GI₅₀s for cell loss, indicating that the inhibition of transcription occurred at lower compound concentrations before the apparent cytotoxicity became a contributing factor. Compounds that inhibit the constitutive activation of the pGal4-AR-NTD-luciferase reporter assay may be able to prevent the transcriptional activity mediated by the AR AF-1 domain of splice variants such as AR-V7 which are upregulated during the relapse of CRPC patients receiving ADT therapy.

5.3.1.6 PSA6.1-Luc & UBE2C-Luc Reporter Based Assay Development in PC3-AR-V7-GFP Cells

To determine if the prioritized AR-TIF2 PPI inhibitor/disruptor hit compounds were able to inhibit the transcriptional activity of the AR-V7 splice variant, we ran them in two reporter assays which involved the transient transfection of the PSA6.1-Luc and UBE2C-Luc reporter constructs into PC3-AR-V7-GFP cells. Since the PSA6.1-Luc reporter can be activated by AR-FL and AR splice variants such as AR-V7, we incorporated the UBE2C-Luc reporter because it can only be activated by AR splice variants. Nine of 10 ten compounds inhibited the AR-V7 driven PSA-6.1-Luc reporter activity in a concentration dependent manner, producing IC₅₀s <100 μM (Figure 54B-J,

on pg. 186 and Table 21). Only 26996278 also displayed cytotoxicity in growth inhibition assays run simultaneously with the reporter assays (Figure 54C and Table 21). The reporter IC₅₀ for 26996278 was much lower than the corresponding GI₅₀ for cell loss, indicating that the inhibition of transcription occurred at lower compound concentrations before the apparent cytotoxicity became a contributing factor. Compound 72508471 was completely unable to inhibit AR-V7's activation of the PSA6.1-Luc reporter (Figure 54K and Table 21).

In PC3-AR-V7-GFP cells transiently transfected with the UBE2C-LUC reporter, 7 of 10 prioritized AR-TIF2 PPI inhibitor/disruptor hits inhibited AR-V7 induced reporter activity in a concentration dependent manner, producing IC₅₀s <100 μM (Figure 55B-H, on pg. 187 and Table 21). Again, only 26996278 also displayed cytotoxicity in growth inhibition assays run simultaneously with the reporter assays (Figure 55C and Table 21). The UBE2C-Luc reporter IC₅₀ for 26996278 was much lower than the corresponding GI₅₀ for cell loss, indicating that the inhibition of transcription occurred at lower compound concentrations before the apparent cytotoxicity became a contributing factor. 63718298 and 72508471 showed evidence of concentration dependent inhibition of UBE2C-Luc reporter activity but failed to achieve 50% inhibition even at 100 μM (Figure 55J, K and Table 21). Only 24843178 was unable to inhibit AR-V7 driven UBE2C-LUC reporter activity (Figure 55I and Table 21).

5.3.2 Conclusion: Which Compounds are Prioritized and Why?

Cluster 1 hits – 98648798, 26996278, and 55803564. All three cluster 1 analogs produced calculable IC₅₀s or demonstrated concentration dependent inhibition in our panel of AF-2 and AF-1 domain transactivation assays. While 26996278 was equipotent at inhibiting the growth of all 5 PCa cell lines, 55803564 only produced GI₅₀s against the 3 AR-positive cell lines. 98648798 also

exhibited differential selectivity for growth inhibition in 2/3 AR-positive PCa cell lines relative to AR-null cell lines. The cluster 1 series of AR-TIF2 PPI inhibitor/disruptor hit compounds exhibit the desired biological activity profile with acceptable physiochemical properties and have the potential to block both AF-1 and AF-2 domain mediated transactivation. This class of AR-TIF2 PPI inhibitor/disruptor hits remains on the priority list for consideration as starting points for a medicinal chemistry hit to lead optimization effort.

Cluster 2 hits – 14977726, 21302587, 24843178, 36998335 and 60134988. Three of the 5 analogs produced calculable IC₅₀s or showed concentration dependent inhibition in all 3 of the AF-2 domain transactivation assays. In contrast, 21302587 and 24843178 only exhibited minimal or no activity in the AF-2 domain transactivation assays. Four of the 5 analogs produced calculable IC₅₀s in all 3 of the AF-1 domain transactivation assays, 24843178 was active in only 1 of the 3 AF-1 assays. All five analogs exhibited differential selectivity for growth inhibition in either 3/3 or 2/3 AR-positive PCa cell lines relative to AR-null cell lines. The less potent analogs of cluster 2 might be considered evidence of an emerging structure activity relationship (SAR) but additional analogs would have to be purchased/synthesized and tested to confirm this. The cluster 2 series of AR-TIF2 PPI inhibitor/disruptor hit compounds exhibit the desired biological activity profile with acceptable physiochemical properties and have the potential to block both AF-1 and AF-2 domain mediated transactivation. This class of AR-TIF2 PPI inhibitor/disruptor hits remains on the priority list for consideration as starting points for a medicinal chemistry hit to lead optimization effort.

Cluster 3 hits – 63718298 and 72508471. Compound 72508471 was not very active in any of the three AF-2 transactivation domain assays and was also not very active in two of the three AF-1 transactivation domain assays. The apparent lack of activity in the AF-2 domain assays was

surprising since it had produced calculable IC₅₀'s in the DHT-induced AR-TIF2 PPI formation assay, the TIF2 and SRC1 M2H assays, the C4-2-PAS6.1 reporter assay and exhibited evidence of differential selectivity toward AR-positive cell lines in the PCa growth inhibition assays. 72508471 also exhibited strange biphasic concentration response curves in three of the assays; the AR-FL PSA6.1 reporter assay, the constitutively active pGal4-AR-NTD-luciferase reporter assay, and the AR-V7 driven PSA6.1-Luc reporter assay. Compound 63718298, the other member of cluster 3, was equipotent against all 5 PCa cell lines and therefore did not demonstrate any selectivity for AR expressing cell lines. Compound 63718298 also exhibited strange biphasic concentration response curves in two of the assays; the AR-FL PSA6.1 reporter assay and the constitutively active pGal4-AR-NTD-luciferase reporter assay. Based on these data we decided to deprioritize both cluster 3 compounds, 63718298 and 72508471.

Table 16. Selection process used to prioritize hits from the AR-TIF2 HCS campaign

| Selection Process used to Prioritize Hits from the AR-TIF2 HCS Campaign | LOPAC | 10K | 50K | 83K | Total |
|---|-------|-----|-----|-----|-------|
| Confirmed in Triplicate in AR-TIF2 PPIB | | | | | |
| Not cytotoxic or autofluorescent assay interference compounds | 17 | 14 | 124 | 204 | 359 |
| Not active in the counter screens; p53-hDM2 PPIB, GR-GFP NTA & AR-GFP NLA | | | | | |
| Exhibited Calculable IC50 in AR-TIF2 PPIB to inhibit DHT-induced AR-TIF2 PPI | 15 | 5 | 56 | 117 | 193 |
| Exhibited Calculable IC50's in AR-TIF2 PPIB to disrupt pre-existing DHT-induced AR-TIF2 PPI | 15 | 2 | 52 | 117 | 186 |
| Compounds that generate IC50's in the PSA6.1-LUC Assay | 15 | 5 | 18 | 21 | 59 |
| Compounds that generate IC50's in the Growth Inhibition Assay | 11 | 2 | 24 | 20 | 57 |
| Compounds that generate IC50's in the Radio Ligand Binding Assay | 10 | 0 | 8 | 5 | 23 |
| Compounds that generate IC50's in the ALPHAScreen Assay | NT | 0 | 7 | 3 | 10 |

Compounds that were confirmed in triplicate in the AR-TIF2 PPIB, were not cytotoxic or fluorescent, and were inactive in all three counter screens were run in the AR-TIF2 PPIB in a concentration dependent manner. Those that confirmed in concentration response were then run in a PSA6.1-Luc reporter assay developed in C4-2 cells, and in growth inhibition assays run in 5 different PCa cell lines. Compounds that could inhibit AR's transcriptional activity, and growth of PCa cell lines were run in an ALPHAScreen assay and radio ligand binding assay. Those that displayed favorable and potent biological activity in these assays were further prioritized with bioinformatics filters, and run in a set of characterization assays.

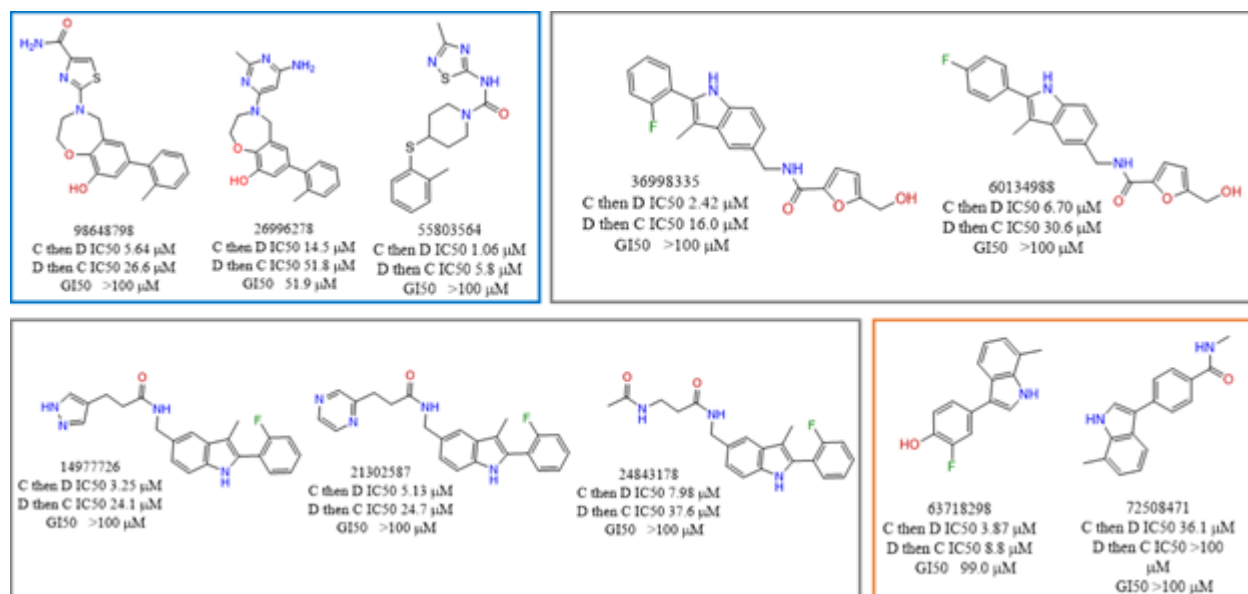


Figure 50. AR-TIF2 PPI inhibitor/disruptor hit analogs selected for testing in characterization assays

Presented here are the chemical structures of hit compounds identified from the 50K Chembridge library plus their hit analogs which were prioritized based on their activities in the AR-TIF2 PPIB, PSA6.1 reporter assay in C4-2 cells, growth inhibition assays, and mammalian 2-hybrid assays. We characterized these compounds in a radio ligand binding assay, ALPHAScreen assay, PSA6.1-Luc reporter assay developed in PC3's stably transfected with AR-FL, pGal4-AR-NTD transactivation assay, and PSA6.1-Luc and UBE2C-Luc reporter assays developed in PC3's stably transfected with AR-V7. These compounds were grouped based on their structure into three different chemical clusters. Those within the blue border represent compounds from cluster 1. Those within the gray border represent compounds from cluster 2, and those identified with an orange border are from cluster 3.

Table 17. IC₅₀ results of selected AR-TIF2 PPI inhibitor/disruptor hit analogs tested in initial hit triage assays

| Assay | AR-TIF2 PPIB Assay IC ₅₀ μ M | | | | | | C4-2 PSA6.1-Luciferase Reporter | | | |
|----------|---|------|----------|------|-----------|------|---------------------------------|------|-----------------------|------|
| | D then C | | C then D | | Cell Loss | | Mean IC ₅₀ | sdm | Mean GI ₅₀ | sdm |
| | Mean | sdm | Mean | sdm | Mean | sdm | | | | |
| 98648798 | 26.6 | 2.71 | 5.64 | 2.81 | >100 | | 17.7 | 11.8 | >100 | |
| 26996278 | 51.8 | 21.4 | 14.5 | 8.52 | 51.9 | 10.9 | 11.0 | 5.05 | 51.1 | 6.21 |
| 74301431 | 63.1 | n=1 | 30.5 | 17.4 | >100 | | 29.7 | 19.5 | >100 | |
| 71147047 | >100 | | 26.2 | n=1 | >100 | | 37.0 | 31.9 | >100 | |
| 61741848 | >100 | | >100 | | >100 | | 32.5 | 25.4 | >100 | |
| 55803564 | 5.83 | 0.90 | 1.06 | 0.96 | >100 | | 2.3 | 1.61 | >100 | |
| 26522479 | >100 | | >100 | | >100 | | >100 | | >100 | |
| 36589964 | >100 | | >100 | | >100 | | >100 | | >100 | |
| 53406864 | >100 | | >100 | | >100 | | >100 | | >100 | |
| 69691085 | >100 | | >100 | | >100 | | >100 | | >100 | |
| 36998335 | 26.2 | 8.90 | 5.11 | 5.01 | >100 | | 7.0 | 8.10 | >100 | |
| 60134988 | 29.1 | 17.8 | 3.20 | 0.14 | >100 | | 9.0 | 4.13 | 69.2 | 20.0 |
| 14977726 | 26.7 | 11.4 | 4.24 | 1.77 | >100 | | 7.7 | 5.3 | >100 | |
| 21302587 | 41.3 | 12.5 | 7.16 | 2.57 | >100 | | 58.5 | 58.7 | >100 | |
| 24843178 | 10.8 | 6.10 | 4.06 | 1.30 | 96.2 | 8.5 | 7.88 | 10.0 | >100 | |
| 36023172 | >100 | | 19.3 | 10.7 | >100 | | 30.1 | 29.8 | >100 | |
| 59706383 | >100 | | 71.8 | 29.8 | >100 | | 42.0 | 14.7 | >100 | |
| 62182397 | >100 | | 37.5 | 9.63 | >100 | | 41.9 | 0.80 | >100 | |
| 99269016 | >100 | | 52.7 | 27.7 | >100 | | 44.3 | 14.1 | >100 | |
| 63718298 | >100 | | 36.1 | 32.8 | >100 | | 39.6 | 15.8 | >100 | |
| 72508471 | >100 | | 36.1 | 32.8 | >100 | | 39.6 | 15.8 | >100 | |
| 71233599 | 28.1 | 9.68 | 8.99 | 8.56 | >100 | | | >100 | | |
| 44744397 | 78.2 | 16.5 | 61.5 | 41.9 | 22.2 | | 6.0 | 2.19 | 40.4 | 4.56 |
| 31153802 | >100 | | >100 | | >100 | | 26.4 | 2.66 | >100 | |
| 62209680 | 37.8 | 11.9 | 4.25 | 4.6 | >100 | | 29.3 | 29.9 | >100 | |

Table 18. IC₅₀ results of selected AR-TIF2 PPI inhibitor/disruptor hit analogs tested in mammalian 2-hybrid assays

| Assay | Mammalian 2-Hybrid Assays IC ₅₀ μM | | | | |
|----------|---|------|-------------|------|---------------------|
| | M2H AR-TIF2 | | M2H AR-SRC1 | | HEK-293 |
| | Mean | SDM | Mean | sdm | GI ₅₀ μM |
| 98648798 | 5.77 | 0.89 | 3.57 | 0.86 | 58.6 |
| 26996278 | 3.88 | 0.79 | 2.99 | 0.41 | 18.3 |
| 74301431 | 7.46 | 1.26 | 5.19 | 0.21 | >100 |
| 71147047 | 42.3 | 26.8 | 20.7 | 7.04 | >100 |
| 61741848 | NDA | | NDA | | NDA |
| 55803564 | 0.08 | 0.05 | 0.46 | 0.31 | >100 |
| 26522479 | NDA | | NDA | | NDA |
| 36589964 | NDA | | NDA | | NDA |
| 53406864 | NDA | | NDA | | NDA |
| 69691085 | NDA | | NDA | | NDA |
| 36998335 | 3.32 | 1.32 | 2.99 | 1.15 | 25.6 |
| 60134988 | 6.38 | 1.83 | 4.79 | 1.19 | 30.6 |
| 14977726 | 5.44 | 0.62 | 3.93 | 0.98 | >100 |
| 21302587 | 18.0 | 0.82 | 11.7 | 0.73 | >100 |
| 24843178 | 18.2 | 7.85 | 9.75 | 6.20 | 20.7 |
| 36023172 | 4.40 | 0.47 | 3.38 | 0.02 | >100 |
| 59706383 | 14.7 | 1.34 | 9.91 | 1.56 | >100 |
| 62182397 | 21.6 | 0.56 | 14.8 | 0.13 | >100 |
| 99269016 | 9.41 | 1.94 | 6.92 | 0.71 | 50.8 |
| 63718298 | 18.2 | 7.85 | 9.75 | 6.20 | 20.7 |
| 72508471 | 18.2 | 1.58 | 10.6 | 3.02 | >100 |
| 71233599 | 37.8 | n=1 | 28.5 | 34.2 | >100 |
| 44744397 | NDA | | NDA | | |
| 31153802 | NDA | | NDA | | |
| 62209680 | 5.92 | 3.67 | 7.06 | 2.88 | >100 |

Table 19. IC₅₀ results of selected AR-TIF2 PPI inhibitor/disruptor hit analogs screened in PCa cell line growth inhibition assays

| Assay | Growth Inhibition Assay | | | | | | | | | |
|----------|----------------------------|------|----------------------------|------|----------------------------|------|----------------------------|------|----------------------------|------|
| | PC3 | | DU-145 | | 22Rv1 | | LNCaP | | C4-2 | |
| | Mean IC ₅₀ (μM) | sdm |
| 98648798 | 56 | 4.84 | >100 | N/A | 41 | 1.06 | 28.9 | 5.14 | 32 | 0.85 |
| 26996278 | 12.1 | 0.56 | 11.0 | 0.99 | 11.8 | 0.08 | 13.0 | 0.64 | 12.9 | 1.15 |
| 74301431 | >100 | N/A | >100 | N/A | 75.2 | 24.4 | 43.4 | 11.1 | 45.5 | 5.08 |
| 71147047 | >100 | N/A |
| 61741848 | 20.7 | 0.95 | 12.2 | 0.23 | 22.9 | 1.15 | 5.01 | 0.07 | 5.12 | 0.39 |
| 55803564 | >100 | N/A | >100 | N/A | 17.6 | 0.63 | 19.2 | 3.52 | 14.1 | 4.73 |
| 26522479 | 94.2 | 25.7 | 93.1 | 12.2 | 30.5 | 4.69 | 64.0 | 21.0 | 46.8 | 12.1 |
| 36589964 | >100 | N/A |
| 53406864 | >100 | N/A |
| 69691085 | >100 | N/A |
| 36998335 | 23.7 | 0.51 | 24.3 | 2.60 | 17.4 | 2.43 | 14.0 | 0.59 | 16.8 | 0.15 |
| 60134988 | 32.6 | 3.05 | 18.0 | 1.61 | 15.0 | 1.34 | 7.4 | 0.86 | 7.9 | 0.89 |
| 14977726 | 18.4 | 2.58 | 6.82 | 0.75 | 20.5 | 6.54 | 1.92 | 0.32 | 1.92 | 0.30 |
| 21302587 | >100 | N/A | >100 | N/A | >100 | N/A | 67.2 | 7.08 | 69.8 | 6.65 |
| 24843178 | 26.4 | 4.97 | 40.3 | 2.22 | 45.0 | 1.48 | 30.9 | 1.72 | 37.2 | 3.88 |
| 36023172 | >100 | N/A | >100 | N/A | >100 | N/A | 39.2 | 6.17 | 33.5 | 6.08 |
| 59706383 | >100 | N/A | >100 | N/A | >100 | N/A | 73.3 | 5.80 | 79.6 | 5.03 |
| 62182397 | >100 | N/A | >100 | N/A | >100 | N/A | 55.6 | 4.75 | 66.8 | 15.5 |
| 99269016 | 24.2 | 2.79 | 44.4 | 4.80 | 42.8 | 11.5 | 13.7 | 2.77 | 11.9 | 1.68 |
| 63718298 | 26.4 | 6.09 | 40.3 | 2.7 | 45.0 | 1.82 | 30.9 | 2.10 | 37.2 | 4.76 |
| 72508471 | >100 | N/A | 55.3 | 7.5 | 26.5 | 5.70 | 13.0 | 1.44 | 12.6 | 3.00 |
| 71233599 | >100 | N/A |
| 44744397 | 23.6 | 6.4 | 22.3 | 2.03 | 13.5 | 0.85 | 15.4 | 0.77 | 17.4 | 1.53 |
| 31153802 | >100 | N/A | >100 | N/A | 53.7 | 0.74 | 48.0 | 1.89 | 53.7 | 4.51 |
| 62209680 | >100 | N/A |

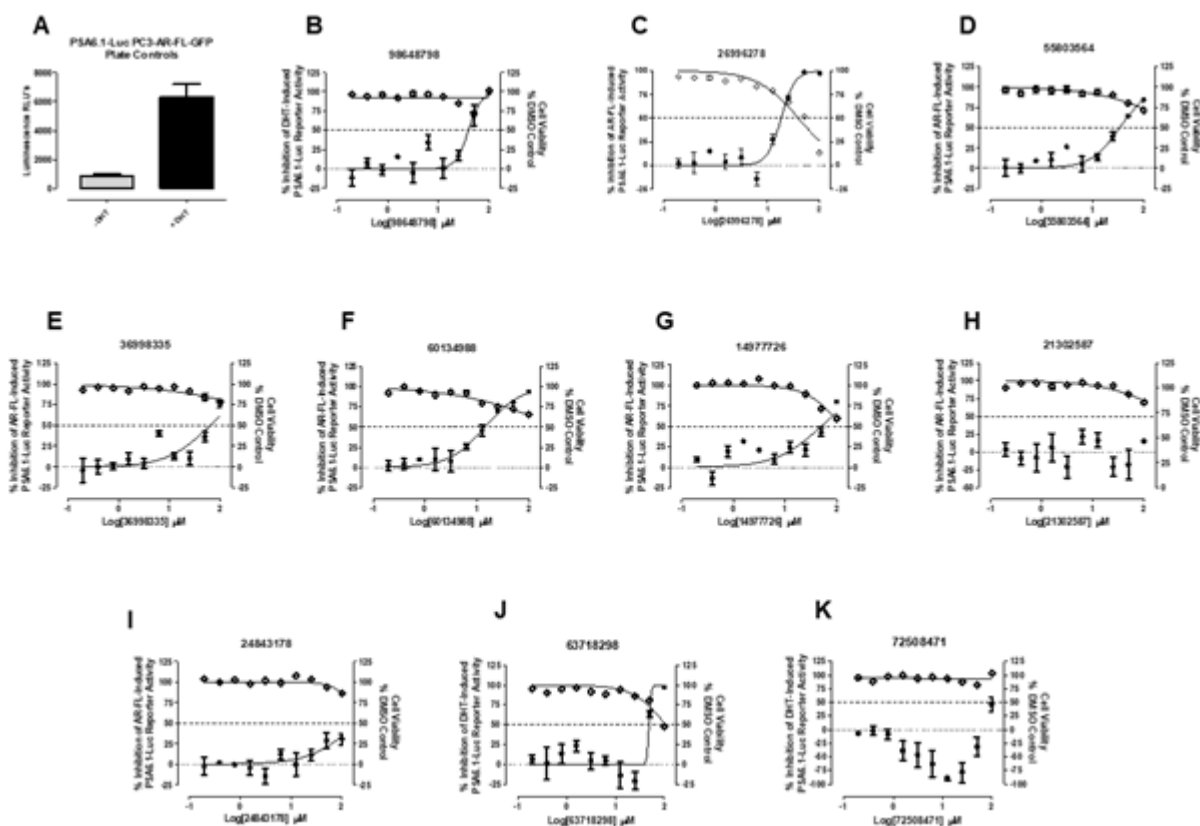


Figure 51. Performance of prioritized AR-TIF2 PPI inhibitor/disruptor hits in the AR-FL directed PSA6.1 reporter assay performed in PC3-AR-FL-GFP cells

A DHT-induced PSA6.1-LUC reporter-based assay was conducted with 10 hit analog compounds. PC3-AR-FL-GFP cell lines were transiently bulk transfected with a 3:1 ratio of Fugene HD: PSA-6.1-LUC plasmid DNA (20 ng/well), then seeded into assay plates at a density of 3,000 cell per well, and finally incubated overnight at 5% CO₂, 95% humidity, and 37°C. PC3-AR-FL-GFP cells transfected with the PSA-6.1-LUC plasmid were exposed to the indicated concentrations of compounds for 3 h and were then treated with 25 nM DHT. The assay plate was returned to the incubator for an additional 24 h before BrightGlo reagent was added to the plate and the RLUs were captured on a SpectraMax M5e microtiter plate reader. The PSA6.1-LUC RLU's data for compound treated wells were normalized to maximum (25 nM DHT + 0.5% DMSO, n=32) and minimum (0.5% DMSO, n=32) plate controls, and the % inhibition (●) was plotted on the left Y-axis as the mean +/- SD (n=3) values from triplicate wells for each compound concentration. The corresponding cell viability data for compound treated wells were normalized to 0.5% DMSO control wells (n=32), and the % cell viability (◇) was plotted on the right Y-axis as the mean +/- SD (n = 3). **A**) Representative plate control data for one run is plotted. The concentration dependent normalized % inhibition of the DHT-induced PSA6.1-LUC reporter activity for **B**) 98648798, **C**) 26996278, **D**) 55803564, **E**) 36998335, **F**) 60134988, **G**) 14977726, **H**) 21302587, **I**) 24843178, **J**) 63718298, and **K**) 72508471 are presented. Representative experimental data from one of two independent experiments are shown.

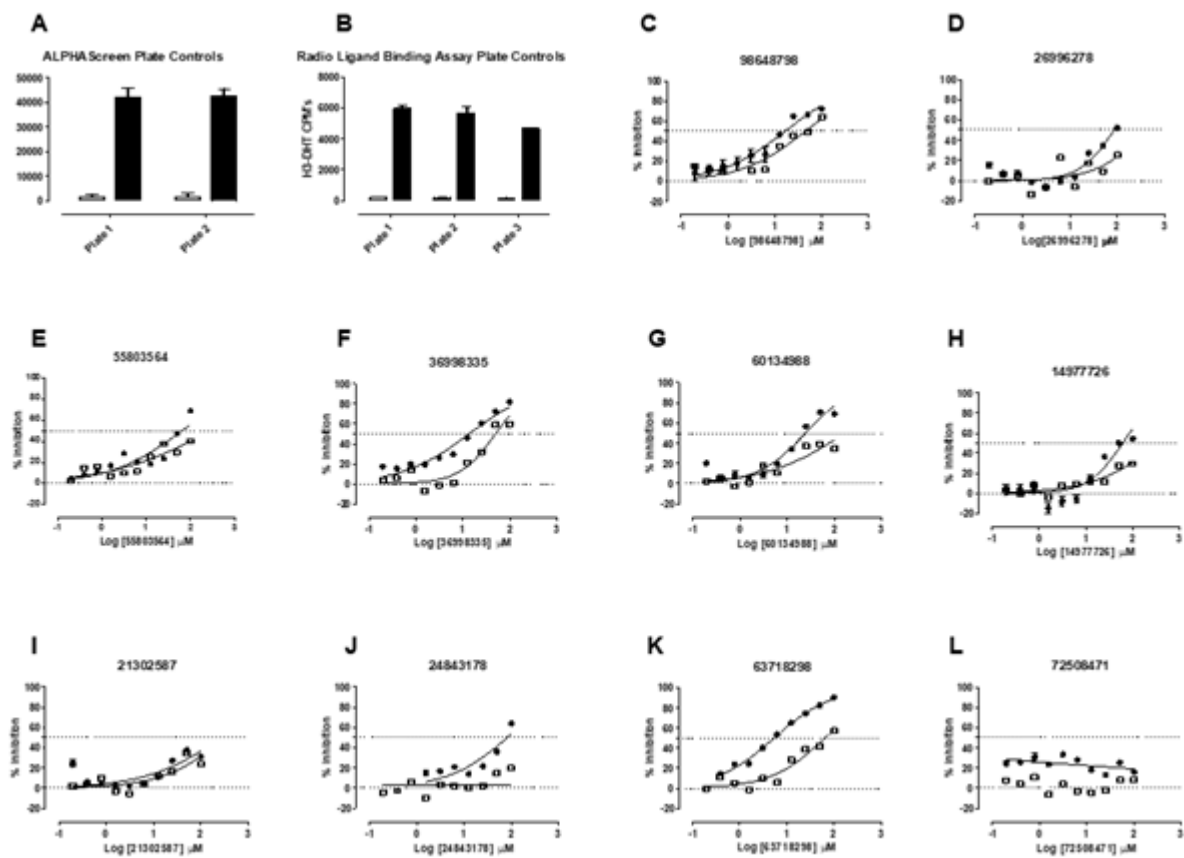


Figure 52. Performance of prioritized AR-TIF2 PPI inhibitor/disruptor hits in the H³-DHT radio ligand and TIF2 Box III LXXLL peptide ALPHAScreen binding assays

H³-DHT Radioligand Binding Assay. Competitive displacement binding of H³-DHT to His₆-AR-LBD run with the ten analog hits. Five micrograms of His₆-AR-LBD protein was added to the wells of 96-well copper-coated plates and allowed to bind overnight at 4°C. Unbound protein was removed by aspiration; the plate was washed 3x with PBS-Tween 20 buffer and blocked for 1 h with 1 mg/mL BSA in PBS-Tween 20. After 3x washes with PBS-Tween 20 buffer, 10 nM H³-DHT was added to the wells of the plate in the presence or absence of the indicated concentrations of compounds and incubated at RT for 1 h. Unbound H³-DHT was removed by aspiration and washing, and micro-scintillation reagent was added to the wells, and the CPMs were captured on a TopCount NXT microtiter β-counter. β-emission RLU's data for compound treated wells were normalized to maximum (0.5% DMSO, n=8) and minimum (10 μM cold DHT, n=8) plate controls, and the % inhibition was plotted as the mean +/- SD (n=3) values from duplicate wells for each compound concentration. **A)** Representative plate control data for one run is plotted. The concentration dependent normalized % inhibition (□) of the H³-DHT bound to His₆-AR-LBD for **B)** 98648798, **C)** 26996278, **D)** 55803564, **E)** 36998335, **F)** 60134988, **G)** 14977726, **H)** 21302587, **I)** 24843178, **J)** 63718298, and **K)** 72508471 are presented. Representative experimental data from one of two independent experiments are shown.

TIF2 Box III LXXLL peptide ALPHAScreen assay. A competitive displacement binding of biotinylated-TIF2-box-III peptide to His₆-AR-LBD was conducted with ten analog hits. Biotinylated-TIF2 peptide was incubated with streptavidin donor beads for 30 min, in the dark, at RT, and then added to 384-

well assay plates at a final concentration of 150 nM. Next, compound was added to the wells of the plate at the indicated concentrations, and incubated for 30 min, in the dark, at RT. Simultaneously, pET28a-His₆-AR-LBD (400ng/well) was incubated with DHT, and Ni²⁺ coated acceptor beads for 30 min. Finally, DHT bound pET28a-His₆-AR-LBD, chelated to acceptor beads were mixed with streptavidin bound TIF2-peptide in 384-well plates. After mixing the ALPHAScreen components, they were incubated for 1 hr at RT in the dark, and after, read on an envision plate reader. The ALPHASignal (CPMs) data for compound treated wells were normalized to maximum (0.5% DMSO, n=32) and minimum (0.5% DMSO and 75 μM unlabeled TIF2, n = 32) plate controls, and the % inhibition (●) was plotted as the mean +/- SD (n=3) values from triplicate wells for each compound concentration. **A)** Representative plate control data for one run is plotted. The concentration dependent normalized % inhibition of the AR-AF2::LXXLL-peptide binding for **B)** 98648798, **C)** 26996278, **D)** 55803564, **E)** 36998335, **F)** 60134988, **G)** 14977726, **H)** 21302587, **I)** 24843178, **J)** 63718298, and **K)** 72508471 are presented. Representative experimental data from one of two independent experiments are shown.

Table 20. IC₅₀ results of prioritized AR-TIF2 PPI inhibitor/disruptor hit analogs in AF-2 transactivation domain hit characterization assays that employ the AR-LBD

| Assay | PSA6.1-LUC Reporter | | Growth Inhibition | | H3-DHT RadioLigand Binding | | ALPHAScreen | |
|----------|----------------------------|------|----------------------------|------|----------------------------|------|----------------------------|------|
| | PC3-AR-FL-GFP Cells | | PC3-AR-FL-GFP Cells | | | | | |
| | Mean IC ₅₀ (μM) | sdm |
| 98648798 | 43.5 | 4.25 | >100 | N/A | 43.7 | 0.0 | 17.8 | 6.50 |
| 26996278 | 18.7 | 0.38 | 31.4 | 7.57 | >100 | N/A | 83.3 | 2.53 |
| 55803564 | 28.2 | 6.29 | >100 | N/A | >100 | N/A | 68.6 | 4.40 |
| 36998335 | 47.5 | 15.7 | >100 | N/A | 62.9 | 12.9 | 22.8 | 14.3 |
| 60134988 | 9.85 | 4.39 | >100 | N/A | >100 | N/A | 19.6 | 4.88 |
| 14977726 | 45.7 | 4.20 | >100 | N/A | >100 | N/A | 44.2 | 16.4 |
| 21302587 | >100 | N/A | >100 | N/A | >100 | N/A | >100 | N/A |
| 24843178 | >100 | N/A | >100 | N/A | >100 | N/A | 91.6 | 8.63 |
| 63718298 | Ambiguous | N/A | >100 | N/A | 56.2 | 8.65 | 4.23 | 0.58 |
| 72508471 | >100 | N/A | >100 | N/A | >100 | N/A | >100 | N/A |

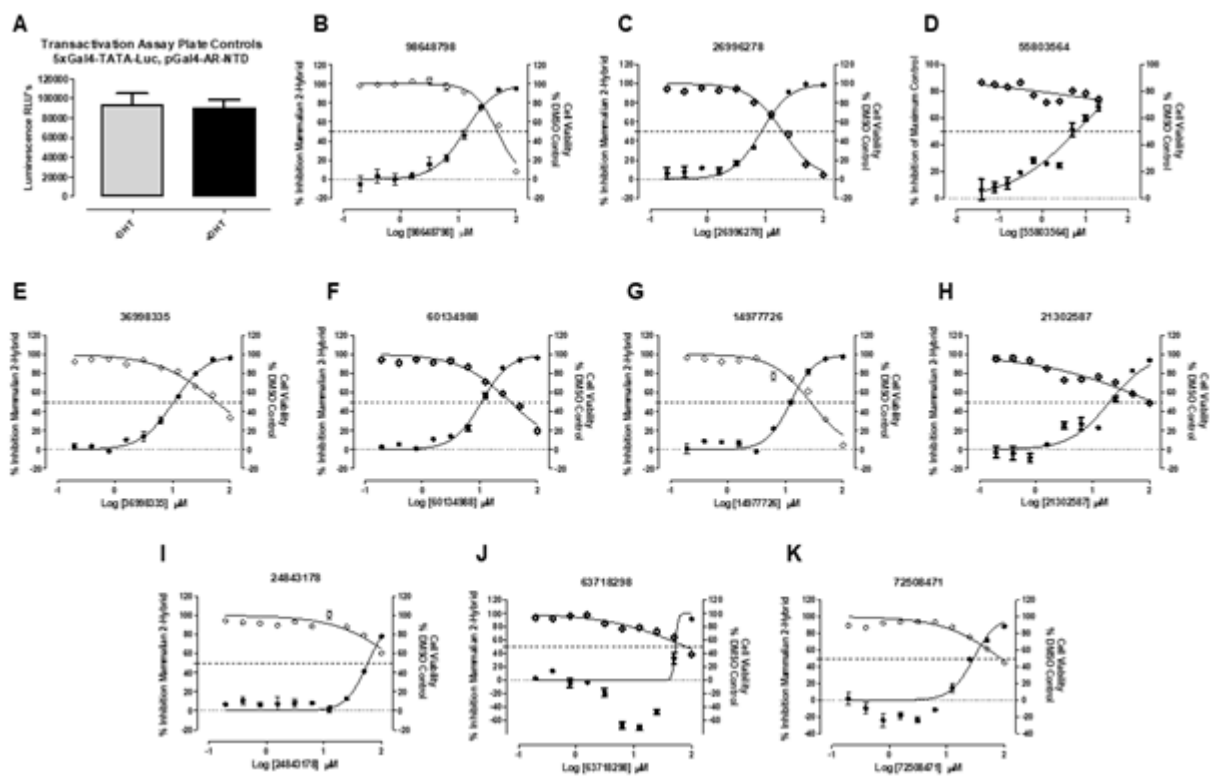


Figure 53. Performance of prioritized AR-TIF2 PPI inhibitor/disruptor hit analogs in the pGal4-AR-NTD transactivation assay

HEK293 cells were transfected with pGAL4-AR-NTD (1-503) and 5xGal4-TATA-Luc, and 5,000 cells were seeded into the wells of 384-well assay plates, and cultured overnight at 37°C, 5% CO₂, and 95% humidity. After 24 h cells were exposed to hit analog compounds at the indicated concentrations and incubated overnight. The assay plate was returned to the incubator for an additional 24 h before BrightGlo reagent was added to the plate and the RLUs were captured on a SpectraMax M5e microtiter plate reader. The M2H RLU's data for compound treated wells were normalized to the 0.5% DMSO, n=32 plate controls, and the % inhibition (●) was plotted on the left Y-axis as the mean +/- SD (n = 3) values from triplicate wells for each compound concentration plotted on the left Y-axis. The corresponding cell viability data for compound treated wells were normalized to 0.5% DMSO control wells (n=64), and the % cell viability (◇) was plotted on the right Y-axis as the mean +/- SD (n = 3) values from triplicate wells for each compound concentration plotted on the right Y-axis. **A)** Representative plate control data for the pGal4-AR-NTD transactivation assay are plotted in the presence or absence of DHT. The concentration dependent normalized % inhibition of pGal4-AR-NTD transcription (left-axis) and cell viability data (right Y-axis) for **B)** 98648798, **C)** 26996278, **D)** 55803564, **E)** 36998335, **F)** 60134988, **G)** 14977726, **H)** 21302587, **I)** 24843178, **J)** 63718298, and **K)** 72508471 are presented. Representative experimental data from one of two independent experiments are shown.

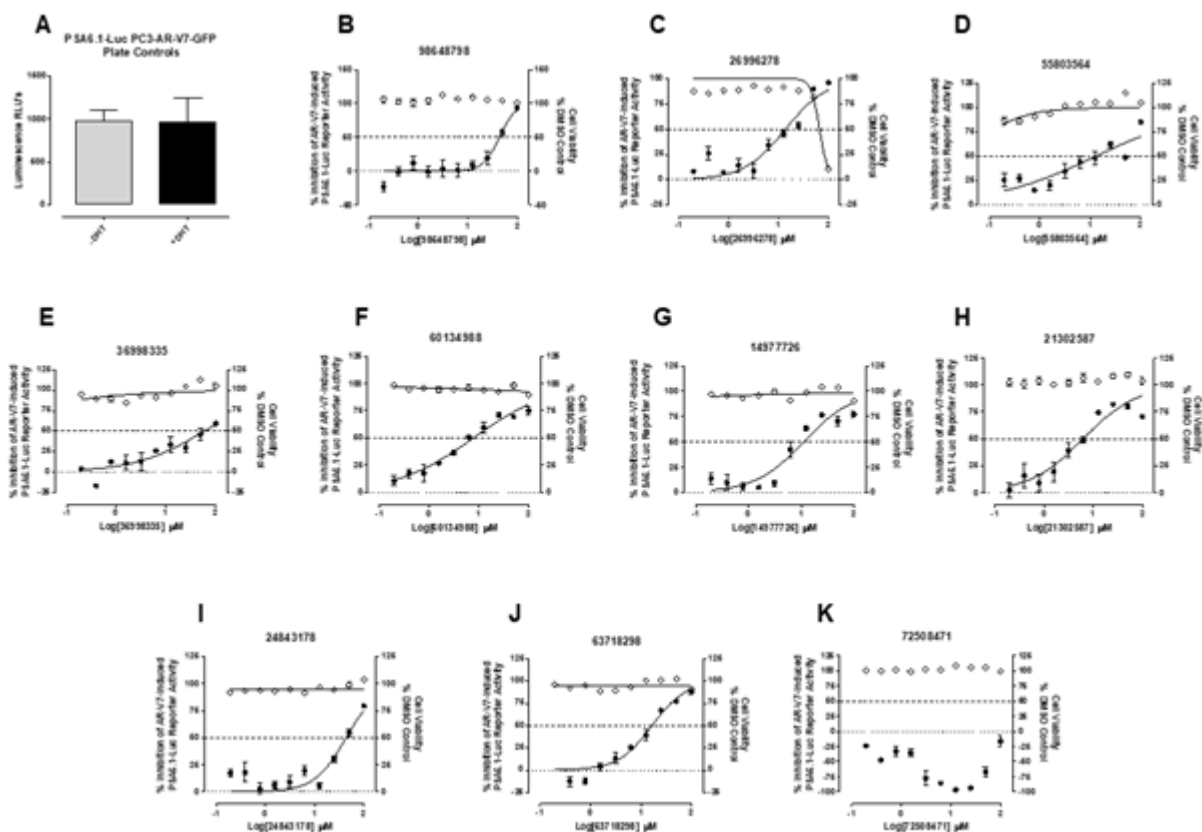


Figure 54. Inhibition of the PSA6.1-Luc reporter assay to measure AR-V7's transcriptional activity in the presence of AR-TIF2 PPI inhibitor/disruptor hit compound analogs

A PSA6.1-LUC reporter-based assay was conducted with 10 hit analog compounds. PC3-AR-V7-GFP cell lines were transiently bulk transfected with a 3:1 ratio of Fugene HD: PSA-6.1-LUC plasmid DNA (20 ng/well), then seeded into assay plates at a density of 3,000 cell per well, and finally incubated overnight at 5% CO₂, 95% humidity, and 37°C. PC3-AR-V7-GFP cells transfected with the PSA6.1-LUC plasmid were exposed to the indicated concentrations of compounds before the assay plate was returned to the incubator for an additional 24 h before BrightGlo reagent was added to the plate and the RLU's were captured on a SpectraMax M5e microtiter plate reader. The PSA6.1-LUC RLU's data for compound treated wells were normalized to plate controls (0.5% DMSO, n=32), and the % inhibition (●) was plotted on the left Y-axis as the mean +/- SD (n=3) values from triplicate wells for each compound concentration. The corresponding cell viability data for compound treated wells were normalized to 0.5% DMSO control wells (n=64), and the % cell viability (◇) was plotted on the right Y-axis as the mean +/- SD (n = 3) values from triplicate wells for each compound concentration plotted on the right Y-axis. **A)** Representative plate control data for one run is plotted. The concentration dependent normalized % inhibition of the DHT-induced PSA6.1-LUC reporter activity for **B)** 98648798, **C)** 26996278, **D)** 55803564, **E)** 36998335, **F)** 60134988, **G)** 14977726, **H)** 21302587, **I)** 24843178, **J)** 63718298, and **K)** 72508471 are presented. Representative experimental data from one of two independent experiments are shown.

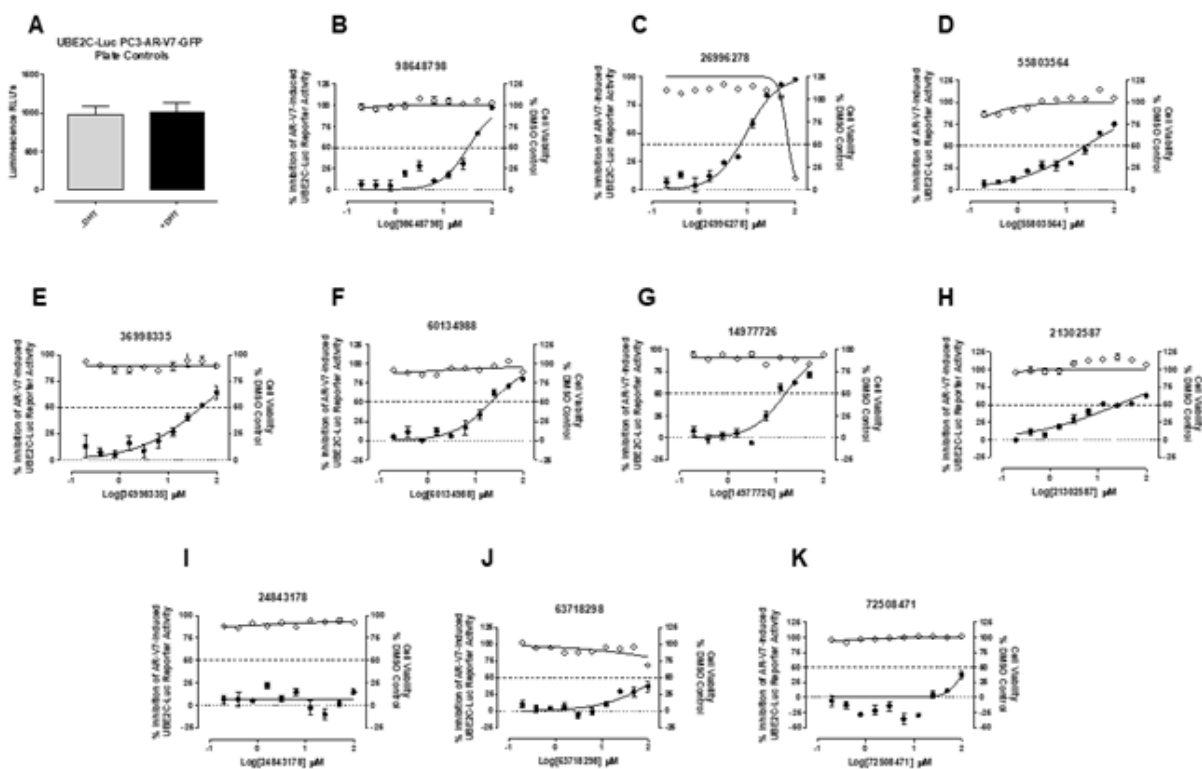


Figure 55. Inhibition of the UBE2C-Luc reporter assay to measure AR-V7's transcriptional activity in the presence of AR-TIF2 PPI inhibitor/disruptor hit compound analogs

A UBE2C-LUC reporter-based assay was conducted with 10 hit analog compounds to validate this assay. PC3-AR-V7-GFP cell lines were transiently bulk transfected with a 3:1 ratio of Fugene HD: PSA-6.1-LUC plasmid DNA (10 ng/well), then seeded into assay plates at a density of 3,000 cell per well, and finally incubated overnight at 5% CO₂, 95% humidity, and 37°C. PC3-AR-V7-GFP cells transfected with the UBE2C-LUC plasmid were exposed to the indicated concentrations of compounds before the assay plate was returned to the incubator for an additional 24 h before BrightGlo reagent was added to the plate and the RLU's were captured on a SpectraMax M5e microtiter plate reader. The UBE2C-LUC RLU's data for compound treated wells were normalized to plate controls (0.5% DMSO, n=32), and the % inhibition (●) was plotted on the left Y-axis as the mean +/- SD (n=3) values from triplicate wells for each compound concentration. The corresponding cell viability data for compound treated wells were normalized to 0.5% DMSO control wells (n=64), and the % cell viability (◇) was plotted on the right Y-axis as the mean +/- SD (n = 3) values from triplicate wells for each compound concentration plotted on the right Y-axis. **A**) Representative plate control data for one run is plotted. The concentration dependent normalized % inhibition of the DHT-induced UBE2C-LUC reporter activity for **B**) 98648798, **C**) 26996278, **D**) 55803564, **E**) 36998335, **F**) 60134988, **G**) 14977726, **H**) 21302587, **I**) 24843178, **J**) 63718298, and **K**) 72508471 are presented. Representative experimental data from one of two independent experiments are shown.

Table 21. IC₅₀ results of prioritized AR-TIF2 PPI inhibitor/disruptor hit analogs in AF-1 transactivation domain hit characterization assays developed with the AR-NTD

| Assay | pGal-AR-NTD Transactivation Assay | | Growth Inhibition Assay | | PSA6.1-LUC Reporter | | UBE2C-LUC Reporter | | Growth Inhibition | |
|----------|-----------------------------------|------|----------------------------|------|----------------------------|------|----------------------------|------|----------------------------|------|
| | | | HBK 293 Cells | | PC3-AR-V7-GFP Cells | | PC3-AR-V7-GFP Cells | | PC3-AR-V7-GFP Cells | |
| | Mean IC ₅₀ (μM) | sdm | Mean IC ₅₀ (μM) | sdm | Mean IC ₅₀ (μM) | sdm | Mean IC ₅₀ (μM) | sdm | Mean IC ₅₀ (μM) | sdm |
| 98648798 | 13.6 | 0.82 | 50.4 | 5.84 | 33.6 | 10.1 | 34.7 | 2.76 | >100 | N/A |
| 26996278 | 8.14 | 0.28 | 18.8 | 0.62 | 12.2 | 1.57 | 8.27 | 0.96 | 61.3 | 5.23 |
| 55803564 | 2.23 | 1.97 | >100 | N/A | 7.88 | 4.86 | 14.5 | 10.2 | >100 | N/A |
| 36998335 | 8.37 | 0.68 | 54.3 | 13.9 | 44.2 | 14.5 | 46.0 | 1.39 | >100 | N/A |
| 60134988 | 9.79 | 0.92 | 34.4 | 7.54 | 10.1 | 2.33 | 18.5 | 3.19 | >100 | N/A |
| 14977726 | 12.4 | 0.04 | 33.3 | 6.39 | 10.7 | 0.57 | 21.0 | 5.20 | >100 | N/A |
| 21302587 | 18.1 | 1.73 | >100 | N/A | 8.17 | 2.00 | 17.7 | 8.14 | >100 | N/A |
| 24843178 | 52.4 | 5.50 | >100 | N/A | 51.7 | 8.14 | >100 | N/A | >100 | N/A |
| 63718298 | Ambiguous | N/A | 38.0 | 17.3 | 20.6 | 4.2 | >100 | N/A | >100 | N/A |
| 72508471 | 29.1 | 0.04 | 80.9 | 5.53 | >100 | >100 | >100 | N/A | >100 | N/A |

6.0 Perspectives, Limitations and Future Directions

6.1 Perspectives

Protein-Protein Interaction Inhibitors. Modulation of the activities of transcription factors (TFs) is viewed as a highly desirable therapeutic strategy because TFs are involved in the regulation of gene expression which controls major cellular functions involved in development, growth, and proliferation [181, 182]. TFs function in cells by binding to specific DNA sequences and orchestrating a complex and diverse set of protein-protein interactions that lead to the changes in gene expression which contribute to many disease states, including cancer. Although modulating the activities of TFs could have therapeutic potential for many diseases, the small molecule tools that are available to researchers remains limited and it is generally accepted that disrupting the protein-DNA and protein-protein interactions (PPIs) of TFs is challenging from both the drug discovery and development perspectives [181-183]. For example, the contact surfaces involved in PPIs are often large, flat, and seem to lack the pockets that ligands and small drug-like molecules typically bind to [184, 185]. Furthermore, rational drug design for targeting PPIs can be challenging especially when there is not an existing small molecule inhibitor to use as a starting point. It has also been reported that high-throughput screening does not routinely identify compounds that disrupt PPIs. Despite these observations, recent successes have indicated that disrupting PPIs with small molecules is achievable [183-186]. Advances in structure based drug design and the development of novel high-throughput screening assay formats have recently produced an uptick in small molecule PPI inhibitor discoveries. Nevertheless, the perception persists that PPI interfaces are flat, occur over very large surfaces, and present challenging targets

for drug-like molecules. Mutational studies have demonstrated that much smaller regions of amino acids at the PPI interface contribute most of the free binding energy. These regions are considered ‘hotspots’ and they typically make up less than half of the PPI surface and provide a means for therapeutic intervention by small molecules or peptide mimetics [183-185]. For example, PPIs between the hMD2 E3 ligase and the tumor suppressor p53 regulate the degradation and expression levels of p53. hDM2 binds to a 15-residue alpha-helical region of p53 and the structure of the complex shows an interface that is largely hydrophobic. A mutational analysis of the 15-residues identified 3 dominant amino acids in the center of the interface, including Phe19, Trp23, and Leu 26, that acted as a hot spot for compound binding. A combined HTS and medicinal chemistry optimization effort conducted by Roche identified a series of tetra-substituted imidazoles termed Nutlins. Specifically, Nutlin-3 disrupted hDM2-p53 complexes with high potency (IC₅₀ of 90 nM) and demonstrated potent p53-stabilizing activity *in vitro* and inhibition of tumor xenograft growth *in vivo* [183]. Another example of a PPI that has been able to be modulate with a small molecule is the interaction between anti-apoptotic protein, Bcl-2, and pro-apoptotic protein BAD or BAK. BCL proteins are involved in apoptosis, and pro-apoptotic proteins (BAD or BAK) function is inhibited through their binding to anti-apoptotic protein (Bcl). This interaction is important as it’s been shown that there’s an upregulation of anti-apoptotic proteins seen in certain cancers which allows cells to escape cell death when targeted by certain chemotherapies. Therefore, inhibiting this interaction is a way to prevent cancer cells from avoiding death. Compound ABT-199 represents a small molecule modification of ABT-737 which was identified by methods of NMR-fragment discovery, and medicinal chemistry lead optimization efforts to mitigate adverse events seen with ABT-737. Currently, ABT-199 is in phase 1 clinical trials for the treatment of chronic lymphocytic leukemia [183].

One way to modulate the cellular functions of TF's is to disrupt their interactions with transcriptional coactivators. Coactivators amplify AR transcription complex assembly and context-specific gene expression, and coactivator recruitment profiles influence the tissue-specific spatiotemporal gene expression responses to ligands [104, 187]. Increased coactivator levels produce a more rapid transcriptional response and reduce ligand concentration requirements [187]. Our lab is interested in finding novel therapeutics for the treatment of more advanced forms of prostate cancer (PCa) that inhibit or disrupt the PPI's between the androgen receptor (AR) and one of its coactivators transcriptional intermediary factor 2 (TIF2). One way in which PCa patients are seen to relapse after treatment with standard of care therapeutics is due to the overexpression of a number of coactivators [49, 94, 96, 97]. Cumulative evidence suggests that elevated TIF2 expression might be especially relevant to CRPC as TIF2 stabilizes AR-ligand binding, enhances receptor stability, and promotes both the recruitment of chromatin remodeling coactivators and assembly of the transcriptional machinery on the promoters of AR target genes [98]. Furthermore, the over-expression of TIF2 enhanced AR responses to androgens, compensating for reduced androgen levels [49, 96, 111]. Therefore, an inhibitor or disruptor of this disease relevant PPI could represent a strategy for preventing PCa progression.

AR-TIF2 Protein-Protein Interaction Assay and HCS Campaign. We have developed and implemented a novel HCS assay to identify inhibitor and/or disruptors of the PPIs between the androgen receptor and one of its coactivators TIF2. The assay is a positional biosensor that utilizes recombinant adenoviruses to express the AF-2 containing AR-LBD as a chimeric fusion protein with RFP, and the box III LXXLL motifs from the nuclear receptor interacting domain of TIF2 as a chimeric fusion protein with GFP [118, 119, 127, 188]. The AR-RFP “prey” protein interaction partner shuttles between the cytoplasm and nucleus in a ligand dependent manner while the TIF2-

GFP “bait” protein interaction partner is targeted to and anchored in the nucleoli within the cell nucleus [118, 119, 127, 188]. In unstimulated U-2 OS or PC3 cells co-infected with the AR-RFP and TIF2-GFP adenoviruses, AR-RFP expression is localized predominantly to the cytoplasm and TIF2-GFP expression is localized only to nucleoli within nuclei [118, 188]. After exposure to an AR agonist such as DHT, the AR-RFP biosensor traffics into the nucleus and then the PPIs between AR and TIF2 causes the AR-RFP to colocalize with the TIF2-GFP biosensor in nucleoli [118, 188]. Exposure to DHT dramatically alters the AR-RFP sub-cellular distribution phenotype observed in the Texas Red channel images from predominantly cytoplasmic to almost exclusively nucleolar. [118, 119, 127, 188] We used the AR-TIFs PPIB assay to screen 143,000 compounds that inhibited or disrupted AR-TIF2 PPIs [127]. After removing compounds that were false positives due to either cytotoxicity or auto-fluorescence in the FITC and Texas red channels, we implemented three counter screens to further refine and triage the active compound list. Our lab previously implemented the same HCS biosensor PPIB assay design and format to measure the PPIs between p53 and hDM2 and screened 220,000 compounds to find p53-hDM2 PPI inhibitors [122, 123]. The p53-hDM2 PPIB assay served as an AR-TIF2 counter screen to identify and eliminate compounds that interfere with the assay format or that behave as either non-selective or non-specific PPIs inhibitors [118]. The dexamethasone-induced GR-GFP translocation assay provided a counter screen to identify and eliminate compounds that were not selective for AR over GR, or that inhibited nuclear receptor trafficking from the cytoplasm into the nucleus [118, 189]. The AR-GFP nuclear localization assay provided a counter screen to identify and eliminate compounds that reduced AR expression levels and/or altered AR’s sub-cellular localization [118, 190]. After eliminating cytotoxic and auto-fluorescent compounds and those that exhibited activity in the counter screens, a total of 178 (0.12%) hit compounds exhibited concentration dependent

inhibition and/or disruption of AR-TIF2 PPIs and produced calculable IC_{50} 's in the AR-TIF2 PPIB assay [127]. The hit compounds were then tested in a PSA6.1-Luc reporter assay conducted in C4-2 or 22Rv1 cells to confirm that they inhibited AR-mediated transcriptional activation, and in growth inhibition assays conducted in 5 different PCa cell lines, two AR null and three AR positive PCa cell lines. The growth inhibition assays were used to confirm that the hits killed PCa cells and to prioritize those that differentially inhibited the growth of AR positive cell lines. These hit characterization assays allowed us to triage the 178 AR-TIF2 PPI hits down to 38 prioritized compounds for medicinal chemistry evaluation and additional bioassay profiling; 2 from the 10K library, 18 from the 50K library, and 18 from the 83K library.

Medicinal Chemistry Evaluation. The 38 prioritized hits from the AR-TIF2 PPIB HCS campaign were also evaluated from a cheminformatics and medicinal chemistry perspective. Compounds were manually clustered based on their structural similarities, which involved the identification of a maximum common substructure (MCS). These compounds were then assessed using cheminformatics and bioinformatics servers (as described in chapter 5). Compounds that failed these informatics filters were removed from further consideration. The remaining compound clusters and singletons were queried in scifinder to ascertain if there was existing literature around the general scaffold and if any known biological activities would be undesirable. Through this assessment several chemotypes that considered as problematic were removed from further consideration. Compounds of unknown biological activity and/or mention in patent and peer-reviewed literature were thought to be suitable candidates for further consideration. For example, all of the hits from the NCI 83K library were flagged as problematic/reactive compounds and were deprioritized. From the 143,000 compound AR-TIF2 PPIB HCS campaign and subsequent hit

characterization testing paradigm (see below), 5 hit compounds from the 50K library met our bioassay profile and chemical tractability criteria and were selected for further investigation.

AR-TIF2 PPI Inhibitor/Disruptor Hit Characterization and Prioritization. During the development optimization and validation of the AR-TIF2 PPIB assay and characterization of hits identified in a pilot screen of the LOPAC set, we established that known AR antagonists inhibited/disrupted DHT-induced AR-TIF2 PPIs in a concentration dependent manner; including the anti-androgen PCa drugs flutamide, bicalutamide, enzalutamide, nilutamide and cyproterone acetate [118, 119, 188]. To determine if any of the 38 prioritized hits might also be antagonizing DHT binding to the AR receptor at its orthosteric ligand binding pocket, we developed and implemented an AR-LBD H³-DHT radioligand binding assay [118]. Initially, we used the AR-LBD H³-DHT radioligand binding assay to characterize the hits identified in the LOPAC HCS and were able to show that in addition to nilutamide and cyproterone acetate, the eight other nuclear receptor hits also behaved as AR antagonists and competitively displaced H³-DHT binding to AR-LBD even though they were classified as ligands of other nuclear receptors; progesterone, glucocorticoid, estrogen, mineralocorticoid, and farnesoid X (FXR) nuclear receptors [118]. The LOPAC nuclear receptor ligand hits lacked selectivity for AR and likely exhibited activity in the AR-TIF2 PPIB assay because they antagonized DHT binding to the AR-LBD containing AR-RFP biosensor. The six non-nuclear receptor ligand hits from the LOPAC set did not displace H³-DHT binding to AR-LBD but inhibited the GR-GFP translocation counter screen indicating that they were also not selective for AR, and likely inhibited some shared component of nuclear receptor trafficking from the cytoplasm into the nucleus [118]. Based on these data we deprioritized the AR-TIF2 PPI inhibitor/disruptor hits from the LOPAC set.

Originally, the strategy of our testing paradigm was to deprioritize any compound which behaved as an AR antagonist in the H³-DHT binding assay, because CRPC patients inevitably develop resistance to the anti-androgens used in ADT and relapse [111, 191]. However, the AR AF2 domain also serves as the binding site for steroid receptor coactivator (SRC)/p160 coactivator LXXLL motifs, and we therefore developed an assay to measure the binding of a peptide containing the LXXLL motif located in box III of TIF2's nuclear interaction domain (NID) to the AR-LBD. When we tested the 38 prioritized AR-TIF2 PPIB hit compounds in both the AR-LBD H³-DHT and LXXLL-peptide binding assays (Figure 56, on pg. 204), we found that many of the compounds exhibited concentration dependent responses in both assays, even though some may not have achieved $\geq 50\%$ inhibition and failed to produce calculable IC₅₀s. A subset of the compounds that were active in both the AR-TIF2 PPIB and AR-LBD::LXXLL-peptide binding assays were also active in the H³-DHT binding assay, albeit with less potent IC₅₀'s. The apparent rightward shift in potencies between the H³-DHT binding assay and both the AR-TIF2 PPIB and AR-LBD::LXXLL-peptide binding assays may indicate that such compounds don't directly antagonize binding to the orthosteric ligand binding pocket of AR, but rather may instead bind to a distinct allosteric site that negatively impacts both AR-TIF2 PPIs and ligand binding. Small molecules that bind to allosteric sites on AR to change the structures of the AF-2 and AF-1 domains on AR could inhibit the coactivator recruitment and transcriptional activity of AR-FL and/or AR-V7 and might also have a negative impact on ligand binding. Negative allosteric modulators have been successfully used in lieu of orthosteric antagonists to achieve the same biological response, and thus may represent an alternative to the stereotypical PPI surface disruptors that tend to be non-drug like and/or chemically intractable [192]. Therefore, we modified our selection criteria to include some compounds that exhibited evidence of concentration dependent inhibition of H³-

DHT binding to the AR-LBD. Hit compounds would be prioritized if they were active in the AR-TIF2 PPIB and AR-LBD::LXXLL-peptide binding assays and displayed no evidence of antagonism in the H³-DHT binding assay. However, AR-TIF2 PPI hits that were active in the AR-TIF2 PPIB and both the H³-DHT and LXXLL-peptide binding assays would also be prioritized, especially those that were substantially less potent in the H³-DHT binding assay and might therefore be negative allosteric modulators. However, hits with compounds that demonstrated activity in both the AR-TIF2 PPIB and H³-DHT binding assays, but were inactive in the AR-LBD::LXXLL-peptide binding assay would still be deprioritized as likely AR antagonists. Twenty-three of the 38 prioritized AR-TIF2 inhibitor/disruptor hits from the AR-TIF2 PPIB HCS campaign failed to exhibit activity in both the H³-DHT and LXXLL-peptide AR-LBD binding assays, and because this was a less desirable biological profile these compounds were not progressed (Figure 57A, on pg. 205). Additionally, 6 more of the hits showed concentration dependent activity in both the AR-TIF2 PPIB and H³-DHT binding assays (Figure 57B), but because they were inactive in the LXXLL-peptide AR-LBD binding assay they were deprioritized as likely AR antagonists. Three of the AR-TIF2 PPI hits were active in the AR-TIF2 PPIB and LXXLL-peptide AR-LBD binding assays but were not antagonists in the H³-DHT binding assay (Figure 57C), and 6 more exhibited concentration dependent activity in all three assays (Figure 57D). Nine of the 38 prioritized hits from the AR-TIF2 PPIB HCS campaign therefore exhibited desirable biological profiles and were also considered suitable starting points for a medicinal chemistry hit to lead optimization effort.

AR-TIF2 PPI Inhibitor/Disruptor Hit Selection for Lead Optimization – AF-2 and AF-1 Profiling. The chemical structures of the 5 prioritized AR-TIF2 PPI inhibitor/disruptor hits from the 50K library were used to perform a similarity search query of the ChemBridge 410K core

library database, and 20 structurally related analogs from 3 chemical clusters were selected for purchase (Figures 58-60, on pgs. 206-208). After the 25 compounds were profiled in the AR-TIF2 PPIB, C4-2-PSA6.1-Luc reporter, and 5 PCa cell lines growth inhibition assays, 18 of the most potent compounds, the 5 parent hits and 13 analogs, were then profiled in the H³-DHT and TIF2 Box III LXXLL peptide binding assays. 5 of the 13 analogs were active in the AR-TIF2 PPIB assay only, 2 were active in both the AR-TIF2 PPIB and LXXLL peptide binding assays, and 6 were active in all three assays (Figure 61, on pg. 209). We selected 10 compounds, 4 of the parent hits and 6 analogs from three clusters for further testing in our suite of AF-2 and AF-1 bioassays. From cluster 1, we selected the two parent compounds 98648798 and 5580364 along with the 26996278 analog that were active in the AR-TIF2 PPIB and both the H³-DHT and LXXLL-peptide binding assays. From cluster 2, we selected the parent compounds 1497726 and 36998335 and three analogs 21302587, 60134988 and 24843178 that were active in all three assays. From cluster 3 we chose analogs 63718298 and 72508471. Compound 63718298 was active in all 3 assays while 72508471 was only active in the AR-TIF2 PPIB assay.

Mammalian 2-hybrid (M2H) assays are the gold standard assays to measure nuclear receptor coactivator recruitment [139, 140, 142], and they provided an orthogonal assay format to measure AR-TIF2 PPIs and to evaluate selectivity versus SRC1. All ten of the selected AR-TIF2 hit compounds produced IC₅₀'s in both the TIF2 and SRC1 M2H assays confirming that they block DHT-induced AR-LBD interactions with both coactivators (Figure 62, on pg. 210). However, none of the hits exhibited selectivity for TIF2 versus SRC1. The PC3-AR-FL-PSA6.1-Luc reporter assay provided an independent confirmation that the AR-TIF2 PPI inhibitor/disruptor hits inhibited AR mediated transcription. Nine of the 10 prioritized AR-TIF2 PPI inhibitor/disruptor hits showed evidence of inhibiting DHT-induced AR-FL-mediated transcriptional activation

(Figure 62). Compound 21302587 from cluster 2 was inactive in the AR-FL driven PSA6.1-Luc reporter assay at $\leq 100 \mu\text{M}$.

It's been demonstrated that AR-V7 splice variants which contain only the AF-1 domain of AR also require coactivators to recruit the general transcriptional machinery and activate gene transcription [79, 81, 105]. AR-NTD mediated assays will allow us to identify AR-TIF2 PPI inhibitor/disruptor hits that also block AF-1 mediated AR transcriptional activity and might therefore be effective against AR splice variants. However, during the development of mammalian 2-hybrid assays using the pGal4-AR-NTD with the VP16-TIF2 and VP16-SRC1 coactivator constructs, we observed that transcriptional activation was independent of either coactivator. As expected, because of the lack of a ligand binding domain pGal4-AR-NTD's transcriptional activity was also independent of DHT. AR-NTD's transcriptional activity was constitutively activated in HEK-293 cells, and all 10 of the AR-TIF2 hits inhibited AF-1 mediated transcriptional activity (Figure 63, on pg. 211). The expression of splice variants such as AR-V7 are upregulated in CRPC patients that relapse after receiving ADT therapy [71, 78]. We tested the 10 AR-TIF2 hits in two reporter assays performed in PC3 cells stably expressing AR-V7-GFP. Since the PSA6.1-Luc reporter can be activated by AR-FL and AR splice variants such as AR-V7, we also included the UBE2C-Luc reporter because it can only be activated by AR splice variants. Nine of the 10 AR-TIF2 hits inhibited AR-V7 mediated reporter activity, but only 8 inhibited both reporters (Figure 63). Only 8 of the AR-TIF2 hits inhibited all three AF-1 mediated transcriptional activity assays.

The cluster 1 hits (98648798, 26996278 and 55803564) produced calculable IC_{50} s or demonstrated concentration dependent inhibition in both our panels of AF-2 and AF-1 domain transactivation assays. While 26996278 was equipotent at inhibiting the growth of all 5 PCa cell lines, 55803564 only produced GI_{50} s against the 3 AR-positive cell lines, and 98648798 showed selectivity for

inhibiting the growth of 2/3 AR-positive PCa cell lines relative to AR-null cell lines. Figure 64 (on pg. 212) shows the bioassay activity profile of 55803564, a representative AR-TIF2 PPI hit from Cluster 1. Three of the cluster 2 hits (14977726, 36998335 and 60134988) produced calculable IC_{50} s or showed concentration dependent inhibition in the AF-2 domain transactivation assays. However, 21302587 and 24843178 only exhibited minimal or no activity in the AF-2 assays. Four of the 5 cluster 2 hits also produced calculable IC_{50} s in the AF-1 domain transactivation assays, while 24843178 was active in only 2 of these assays. All five cluster 2 hits showed differential selectivity for PCa growth inhibition in either 3/3 or 2/3 AR-positive cell lines relative to AR-null cell lines. Although there is preliminary evidence of an emerging structure activity relationship (SAR) for the cluster 2 hits, additional analogs would have to be purchased or synthesized to establish this. Figure 65 (on pg. 213) shows the bioassay activity profile of 36998335, a representative AR-TIF2 PPI hit from Cluster 2. Both the cluster 1 and 2 hit compound series exhibit the desired biological activity profiles with acceptable physiochemical properties and are under consideration as potential starting points for a medicinal chemistry hit to lead optimization effort. The cluster 3 hit 72508471 was not very active in the AF-2 and 2/3 AF-1 transactivation domain assays. This profile was surprising since it had produced calculable IC_{50} 's in the DHT-induced AR-TIF2 PPI formation assay, the TIF2 and SRC1 M2H assays, the C4-2-PAS6.1 reporter assay and showed some degree of differential selectivity toward AR-positive cell lines in PCa growth inhibition assays. 72508471 also exhibited strange biphasic concentration response curves in three of the assays. Compound 63718298, the other member of cluster 3, did not demonstrate any evidence of selectivity for AR expressing PCa cell lines and exhibited strange biphasic concentration response curves in some assays. Based on these data we deprioritized the cluster 3 compounds.

Conclusions. The development and implementation of a suite of counter screens and hit characterization assays has enabled us to effectively triage the hits from the AR-TIF2 PPIB HCS campaign and identify two hit series that are now being considered as potential starting points for a future medicinal chemistry hit to lead optimization effort. The goal of these future studies will be to develop more potent and effective inhibitors of AR-TIF2 PPIs and subsequently these leads might be developed into new therapies for CRPC.

6.2 Limitations

The design of the constructs used to express the biosensors used in the AR-TIF2 PPIB HCS assay did not utilize full length AR or TIF2. The AR-RFP biosensor encodes AR-LBD residues 662-919 and therefore is biased towards the C-terminal part of AR and the AF-2 transactivation domain. In addition to the N-terminal domain, the DNA binding domain and hinge regions of AR are missing for the AR-RFP biosensor. Similarly, the TIF2 residues 725-840 in the other biosensor only encodes a single box III LXXLL motif from the nuclear receptor interacting domain (NID) of TIF2, while the full-length protein encodes 3 LXXLL motifs and several other domains. Although the AR-TIF2 PPIB assay design was pragmatic and enabled us to screen 143K compounds, we will need to confirm that our hits will also inhibit or disrupt full-length AR-TIF2 PPIs. This will likely involve the development of full-length AR and TIF2 co-immunoprecipitation (co-IP) assays and potentially chromatin immunoprecipitation (ChIP) assays performed with AR and TIF2 specific antibodies in PCa cell backgrounds. AR and TIF2 co-IP assays using recombinantly expressed and purified AR and TIF2 is another possibility

In addition, the AR-TIF2 PPIB assay requires exposure to agonists such as DHT to induce AR-TIF2 PPI formation which involves the trafficking of the AR-RFP from the cytoplasm into the nucleus and colocalization with the TIF2-GFP biosensor anchored in the nucleolus. The AR-TIF2 PPIB assay was therefore sensitive to inhibition by AR antagonists, compounds that disrupted the chaperone mediated maturation and folding of the biosensors, and molecules that blocked trafficking through the cytoplasm into the nuclear and nucleolar compartments or potentially that altered the sub-cellular targeting and localization of the biosensors. This required us to develop and implement the panel of counter screens and cell based and biochemical hit characterization assays described in this dissertation to identify and triage out non-PPI inhibitor/disruptor hits.

Although our suite of cell based and biochemical assays have effectively enabled us to select two hit series as potential starting points for a future medicinal chemistry hit to lead optimization effort, none of the assays we have implemented provide information on three critical questions; (1) do any of the hits bind directly to either of the AR or TIF2 protein interacting partners or both, (2) where on AR or TIF2 do the hits bind, and (3) how does the binding of the hits to either AR or TIF2 inhibit or disrupt AR-TIF2 PPIs? These will be critical questions to answer before embarking upon a medicinal chemistry hit-to-lead optimization effort and will likely involve the development of biophysical assays; surface plasmon resonance (SPR), isothermal calorimetry (ITC) and NMR assay for AR and TIF2.

6.3 Future Directions

We plan to develop full-length AR and TIF2 co-immunoprecipitation (co-IP) assays and potentially chromatin immunoprecipitation (ChIP) assays performed with AR and TIF2 specific antibodies in

PCa cell backgrounds. We will test compounds from the two prioritized hit series to confirm that they inhibit or disrupt full-length AR-TIF2 PPIs. In addition to the AR-LBD, we have expressed and partially purified recombinant AR and TIF2 in bacteria. We could use recombinantly expressed and purified AR and TIF2 in co-IP assays to confirm that compounds from the two prioritized hit series inhibit or disrupt full-length AR-TIF2 PPIs.

Several biophysical techniques and assays can be used to confirm that small molecules bind to proteins. We could use recombinantly expressed and purified AR and TIF2 for these assays. Techniques such as surface plasmon resonance (SPR), isothermal calorimetry (ITC) and Nuclear Magnetic Resonance (NMR) will allow us to determine whether our hit compounds bind to AR, TIF2 or both, and to determine binding thermodynamics. SPR can be used to determine if our compound hits are binding to AR or to TIF2, and to measure real-time on and off binding kinetics to further prioritize hits based on their binding affinities. SPR involves the immobilization of a protein on a sensor chip, while compound is present in solution that flows over the surface to which the protein is bound. Interactions between the compound and target protein are determined by measuring changes in the refractive index at the sensor surface of bound protein induced by small molecule association and dissociation [193, 194]. Isothermal calorimetry (ITC) can be used to determine the thermodynamic binding properties of hit compounds. ITC is a gold standard for determining the affinity of biomolecular interactions. ITC directly measures heat that is generated upon protein::compound interaction. Heat is generated by the sequential addition of compound to the cell, which is measured over a given period. A binding isotherm is generated from this data, from which enthalpy and binding affinity can be derived, and free energy and entropy can be calculated. Once K_D , enthalpy, and entropy values are determined, compound affinities, and enthalpic and entropic parameters for each protein can be compared [194]. Finally, NMR

spectroscopy will be used to detect whether interactions occur between our hits and AR or TIF2, and where this interaction takes place on the protein. Protein resonances represent one type of information that can be observed in an NMR-spectra which can detect physical interactions between proteins and compounds. Double isotope-labelling and additional experimentation, usually from triple-resonance approaches, can allow for the direct assessment of protein resonances, and ultimately unveils where on the protein an interaction may occur and also how this interaction is made [195]. Results from these assays will allow us to prioritize AR-TIF2 hit compounds that will move forward into lead optimization. Collectively, these assays will allow us to rank hit compounds based on their molecular target, binding affinities, and preliminary SAR. Based on the information that we learn from the biophysical studies and level of resolution on where the compounds bind to AR or TIF2 and the availability of crystal structures, we could use rational drug design, and computer aided platforms to predict how and where to modify compounds to exhibit tighter binding affinities. Ideally the two chemically tractable hit series we have identified will be pursued in a medicinal chemistry hit-to-lead optimization effort, and 1-2 of the most promising AR-TIF2 PPI disruptor leads would be tested in established castration resistant prostate cancer mouse xenograft models to demonstrate efficacy.

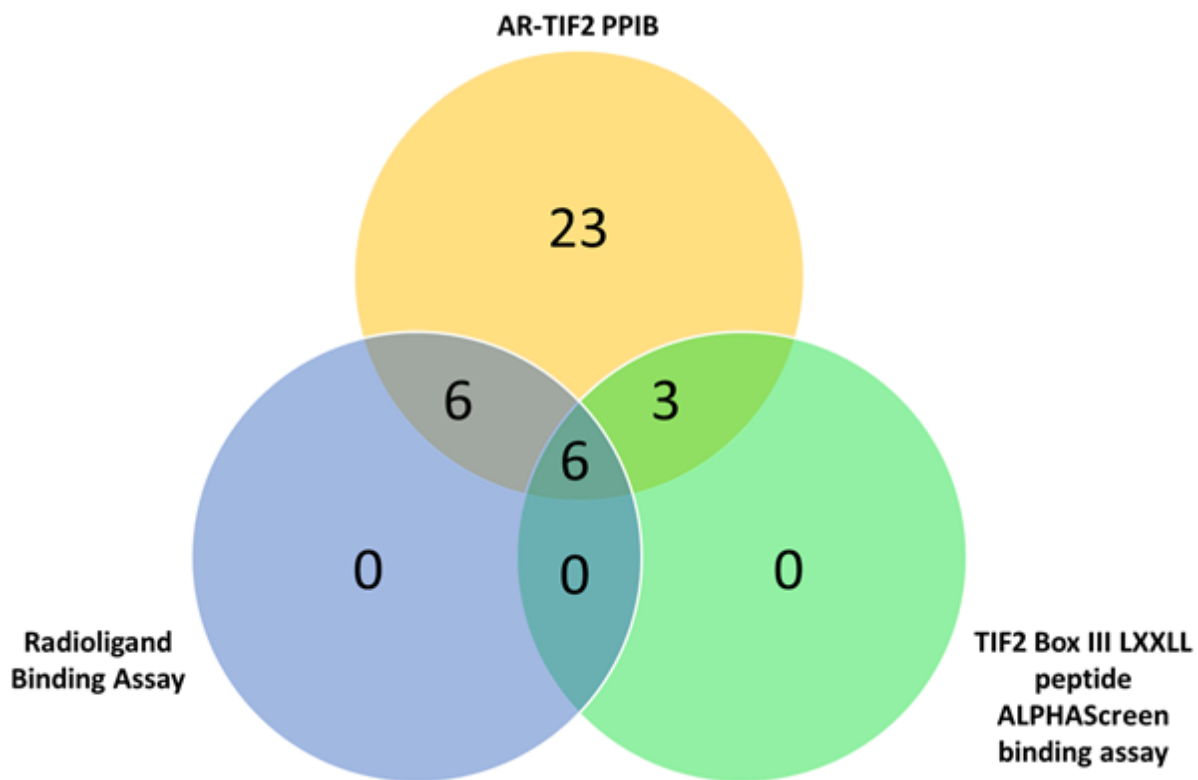


Figure 56. AR-TIF2 PPI inhibitor/disruptor hit characterization and prioritization bioactivity profiles

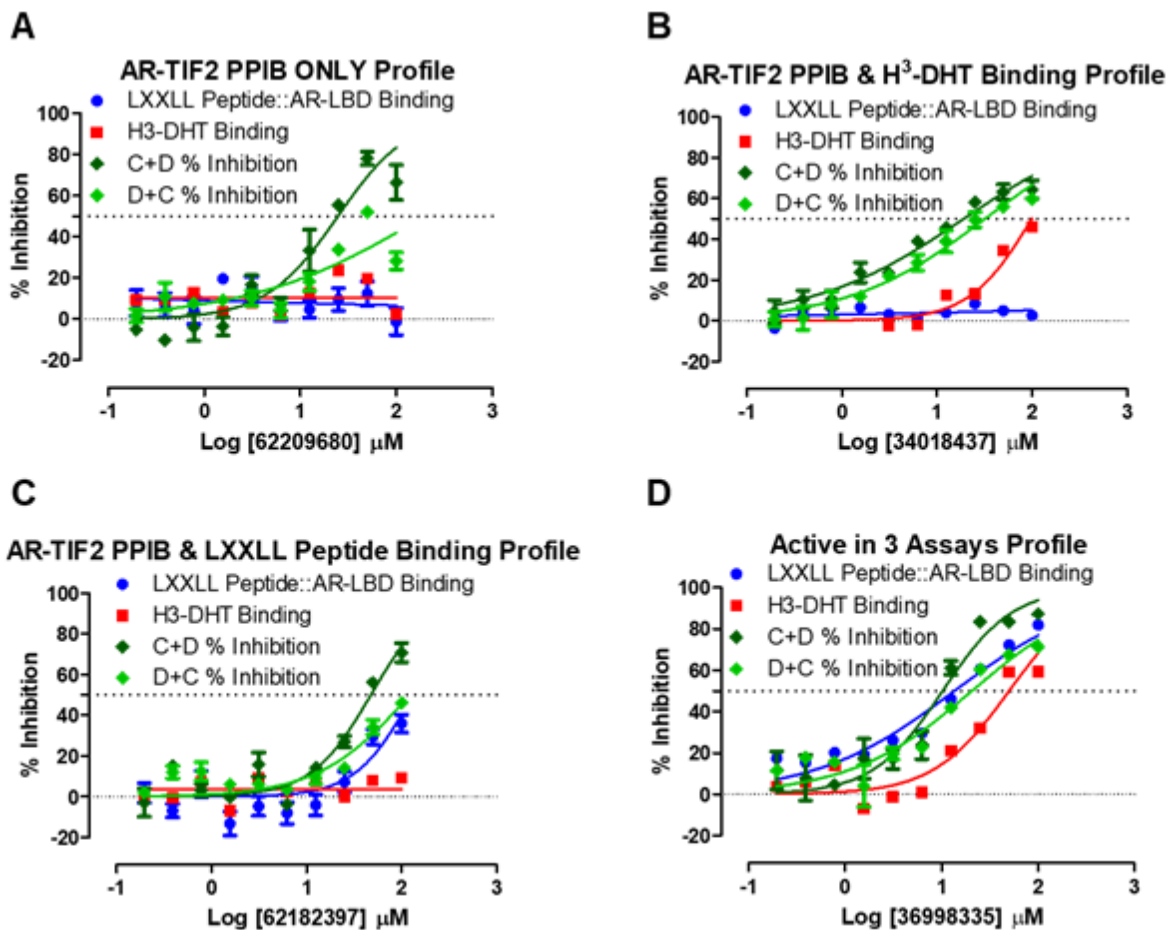


Figure 57. AR-TIF2 PPI inhibitor/disruptor hit compound profiles

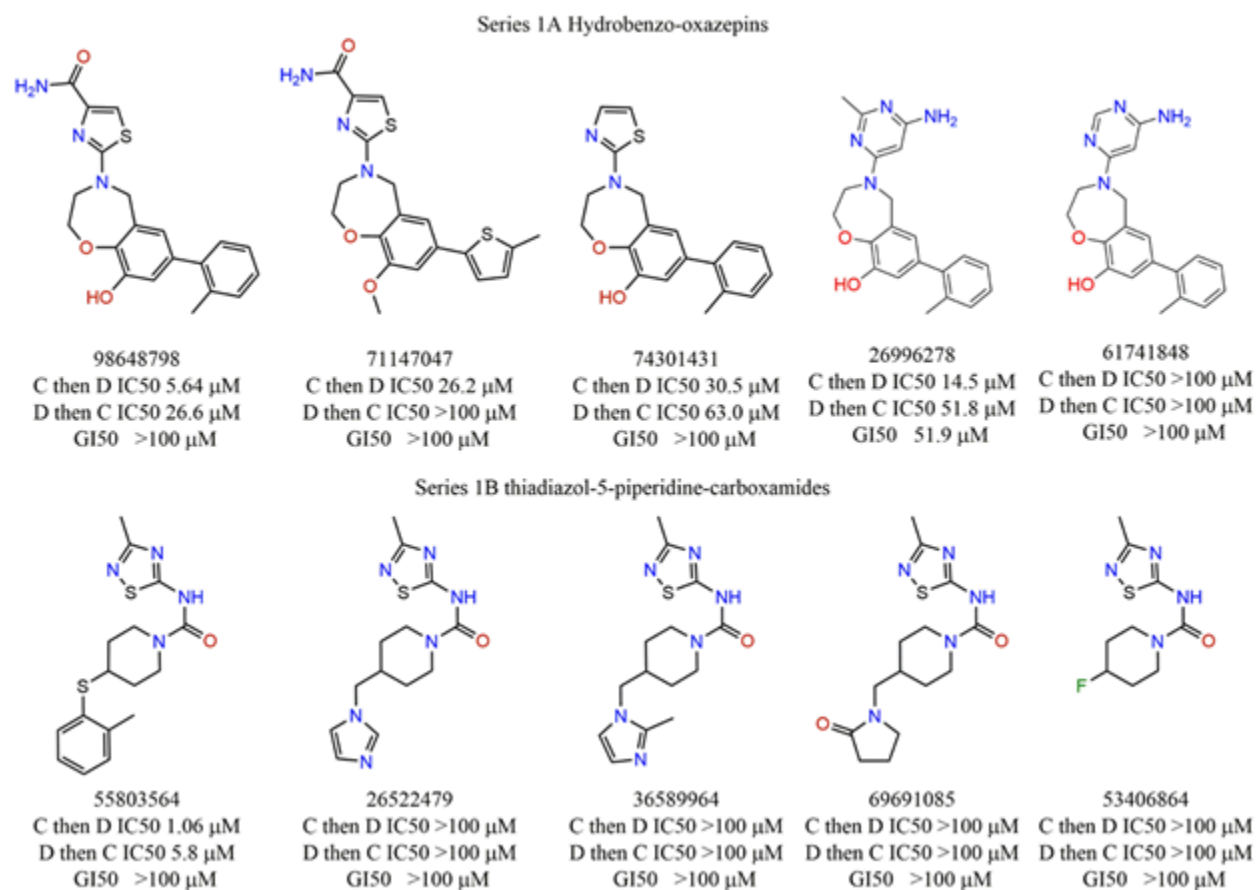


Figure 58. 9864798 & 55803564 analogs

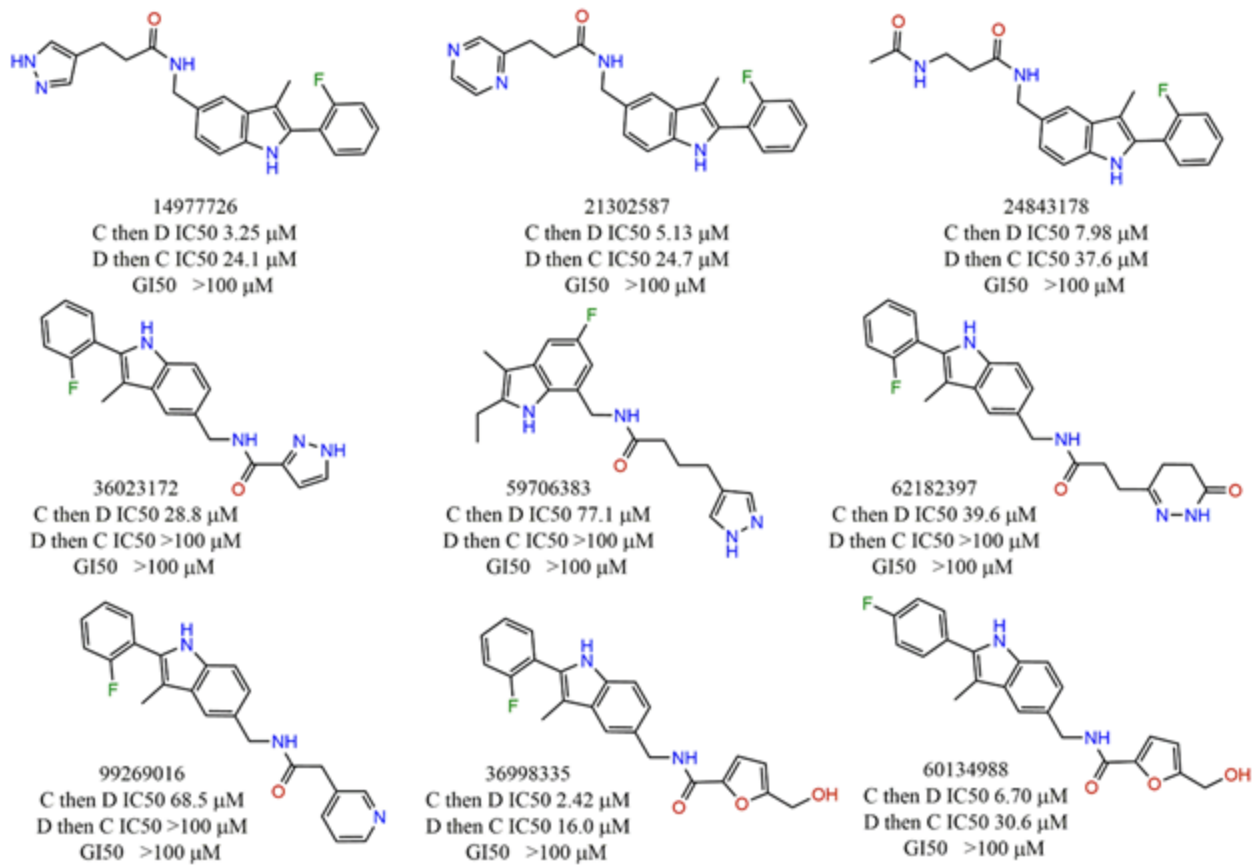


Figure 59. 1497726 & 36998335 analogs

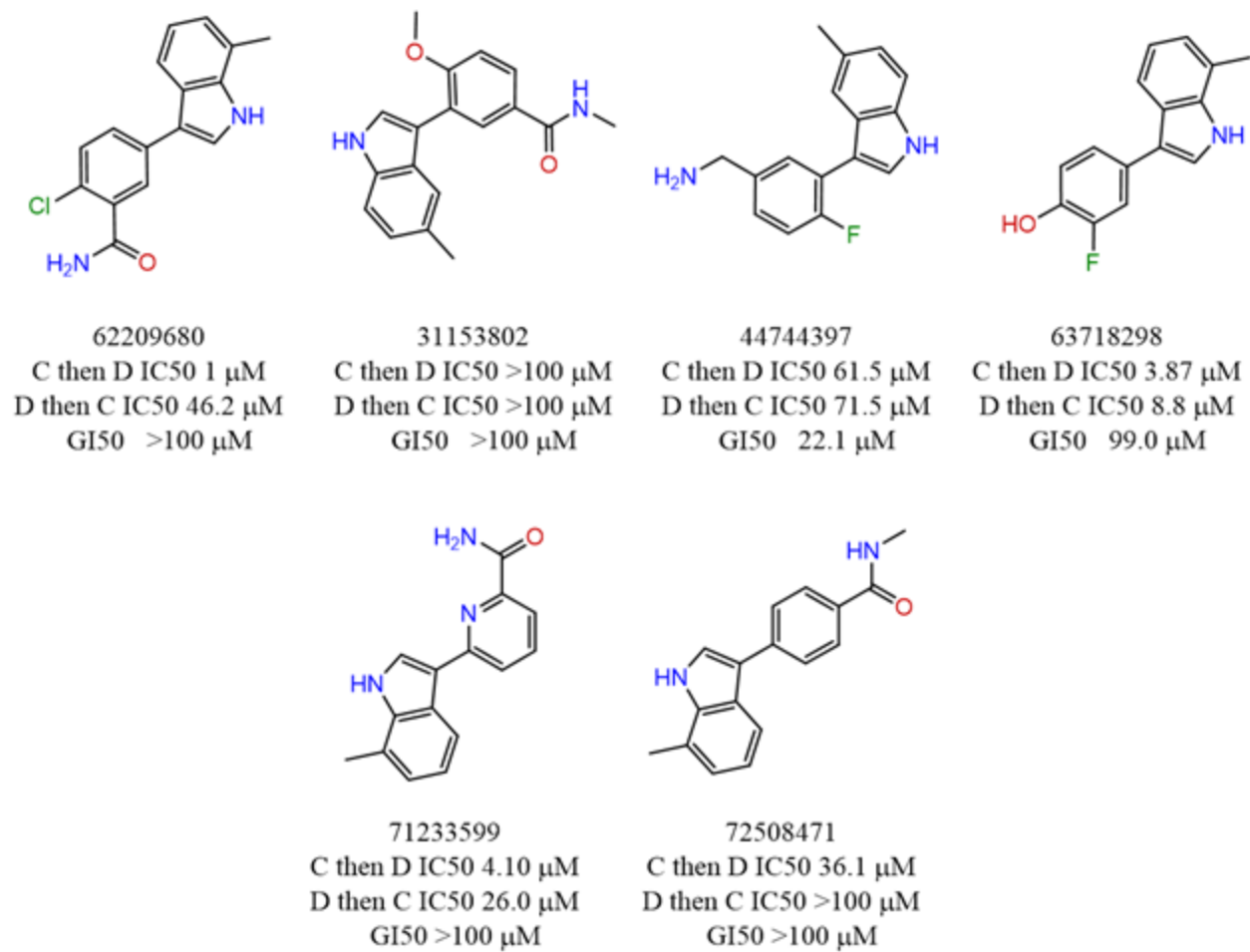


Figure 60. 62209680 analogs



Figure 61. AR-TIF2 PPI parent hits & structurally related analog hit characterization profiles

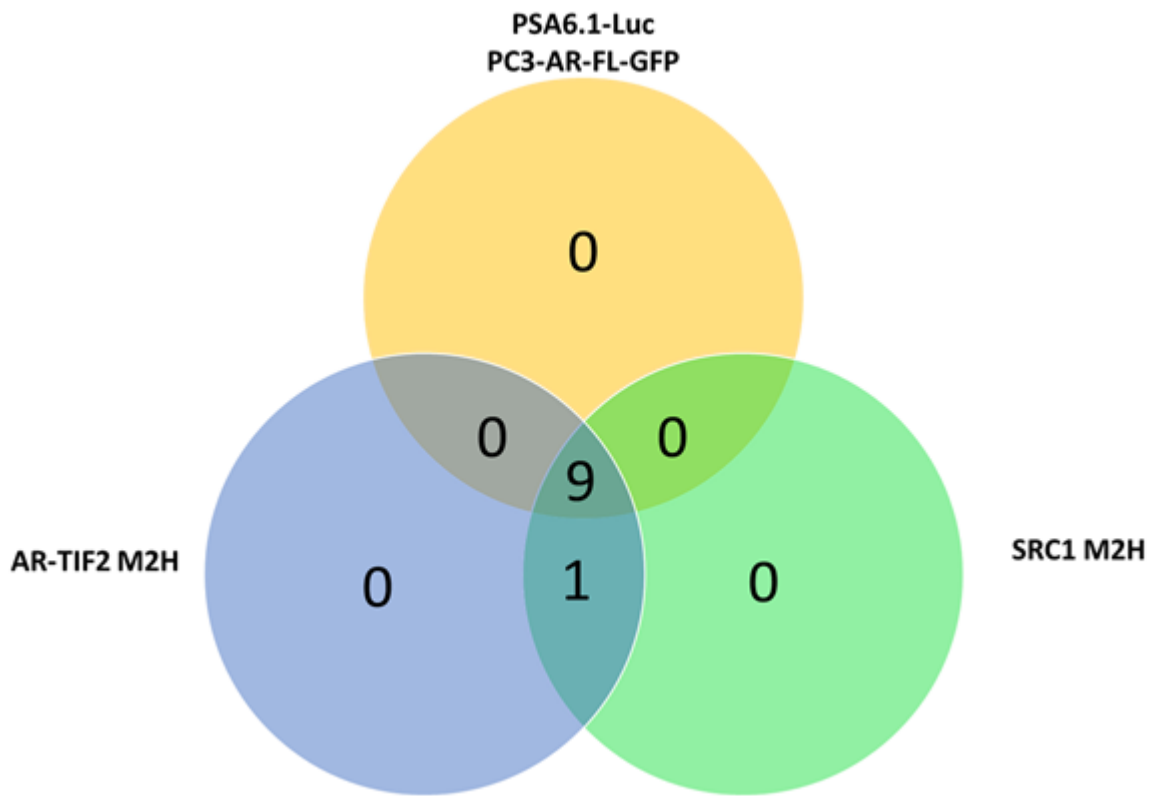


Figure 62. AR AF-2 transactivation domain assay profiles

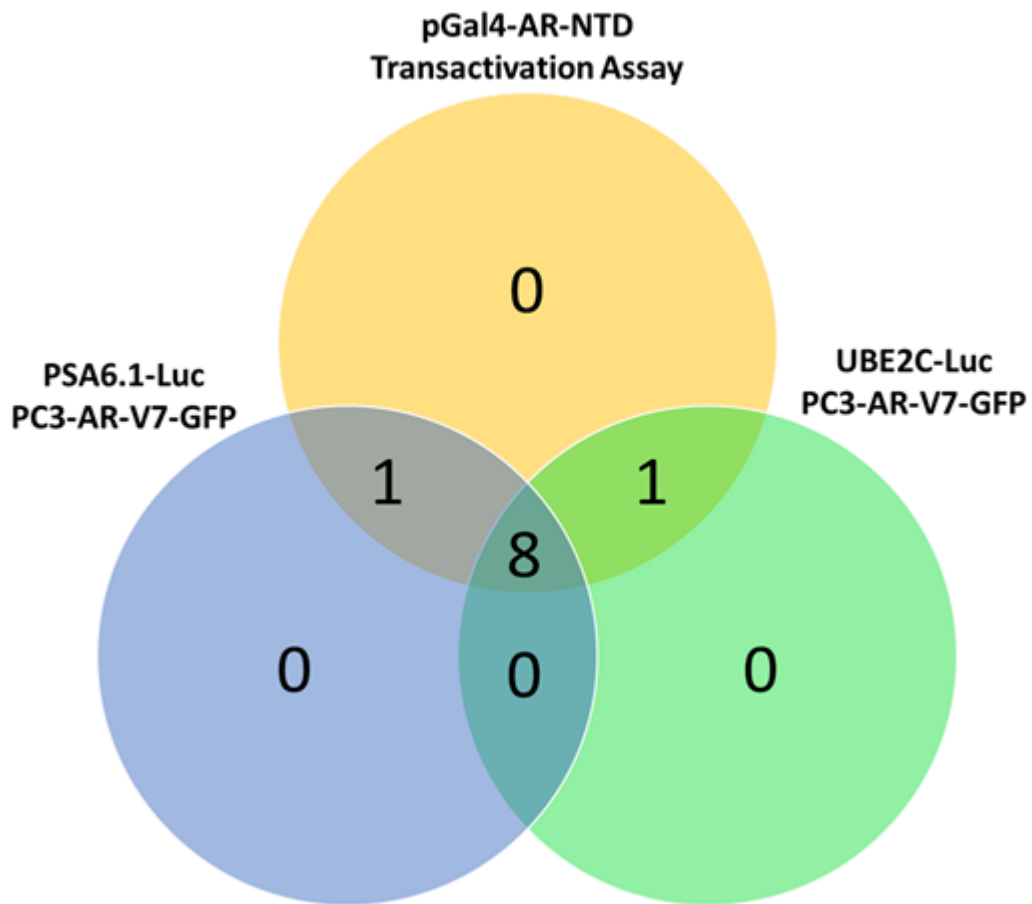


Figure 63. AR AF-1 transactivation domain assay profiles

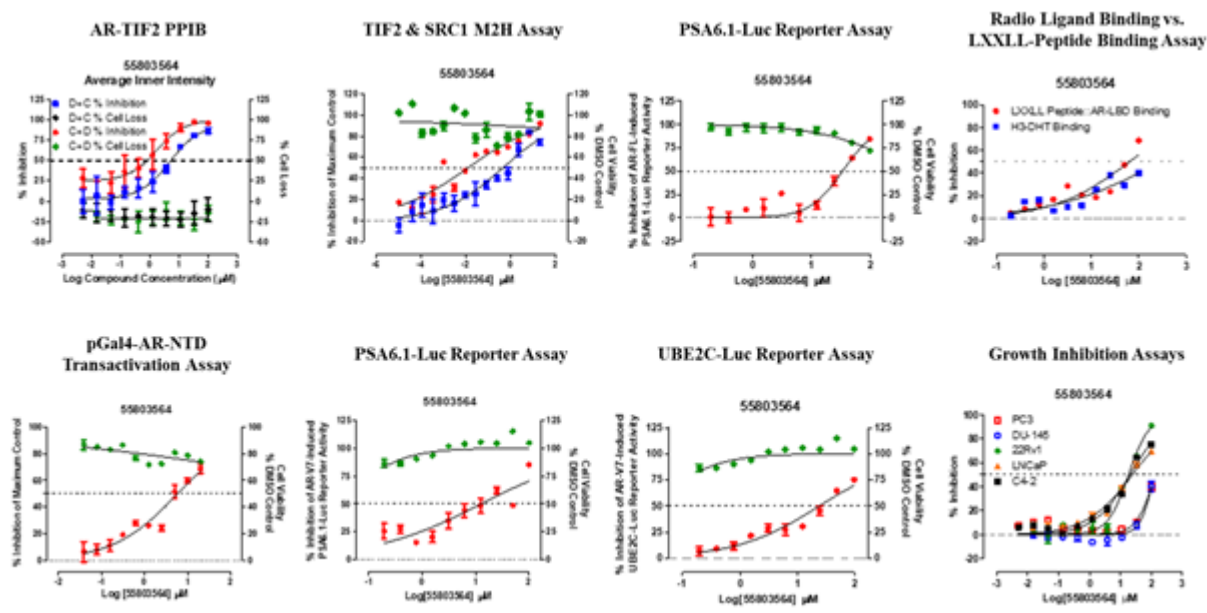


Figure 64. Bioassay activity profile of a representative AR-TIF2 PPI hit from cluster 1

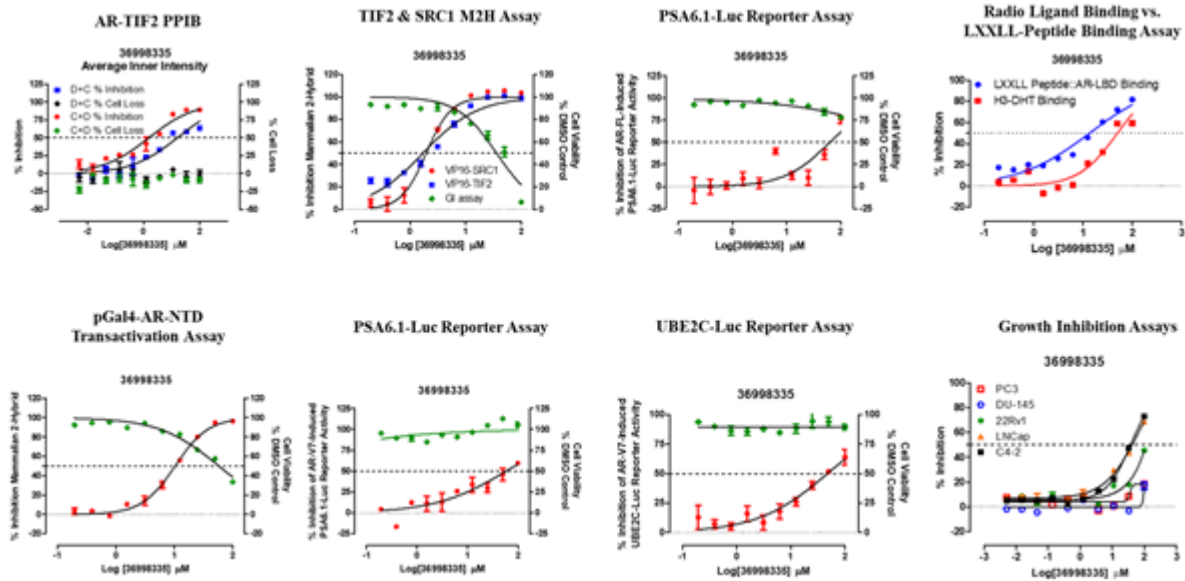


Figure 65. Bioassay activity profile of a representative AR-TIF2 PPI hit from cluster 2

Bibliography

1. Siegel, R., D. Naishadham, and A. Jemal, *Cancer statistics, 2013*. CA Cancer J Clin, 2013. **63**(1): p. 11-30.
2. Scher, H.I., et al., *Prevalence of Prostate Cancer Clinical States and Mortality in the United States: Estimates Using a Dynamic Progression Model*. PLoS One, 2015. **10**(10): p. e0139440.
3. Brawley, O.W., *Trends in prostate cancer in the United States*. J Natl Cancer Inst Monogr, 2012. **2012**(45): p. 152-6.
4. Cetin, K., et al., *Recent time trends in the epidemiology of stage IV prostate cancer in the United States: analysis of data from the Surveillance, Epidemiology, and End Results Program*. Urology, 2010. **75**(6): p. 1396-404.
5. Kirby, M., C. Hirst, and E.D. Crawford, *Characterising the castration-resistant prostate cancer population: a systematic review*. Int J Clin Pract, 2011. **65**(11): p. 1180-92.
6. Milonas, D., et al., *Long-Term Oncological Outcomes for Young Men Undergoing Radical Prostatectomy for Localized Prostate Cancer*. Biomed Res Int, 2017. **2017**: p. 9858923.
7. Haas, G.P., et al., *The worldwide epidemiology of prostate cancer: perspectives from autopsy studies*. Can J Urol, 2008. **15**(1): p. 3866-71.
8. Fabiani, R., et al., *A Western Dietary Pattern Increases Prostate Cancer Risk: A Systematic Review and Meta-Analysis*. Nutrients, 2016. **8**(10).
9. Taitt, H.E., *Global Trends and Prostate Cancer: A Review of Incidence, Detection, and Mortality as Influenced by Race, Ethnicity, and Geographic Location*. Am J Mens Health, 2018. **12**(6): p. 1807-1823.
10. Calle, E.E., et al., *Overweight, obesity, and mortality from cancer in a prospectively studied cohort of U.S. adults*. N Engl J Med, 2003. **348**(17): p. 1625-38.
11. Ben-Shlomo, Y., et al., *Differences in the epidemiology and presentation of prostate cancer in Black and White men in England: lessons learnt from the process study*. BJU Int, 2009. **103**(6): p. 723-4.
12. Verhage, B.A. and L.A. Kiemeny, *Genetic susceptibility to prostate cancer: a review*. Fam Cancer, 2003. **2**(1): p. 57-67.
13. Lynch, H.T., et al., *Screening for familial and hereditary prostate cancer*. Int J Cancer, 2016. **138**(11): p. 2579-91.
14. Eastham, J., *Prostate cancer screening*. Investig Clin Urol, 2017. **58**(4): p. 217-219.
15. Stephan, C., et al., *PSA and other tissue kallikreins for prostate cancer detection*. Eur J Cancer, 2007. **43**(13): p. 1918-26.
16. Shariat, S.F., P.T. Scardino, and H. Lilja, *Screening for prostate cancer: an update*. Can J Urol, 2008. **15**(6): p. 4363-74.
17. DeAntoni, E.P., *Age-specific reference ranges for PSA in the detection of prostate cancer*. Oncology (Williston Park), 1997. **11**(4): p. 475-82, 485; discussion 485-6, 489.
18. Alford, A.V., et al., *The Use of Biomarkers in Prostate Cancer Screening and Treatment*. Rev Urol, 2017. **19**(4): p. 221-234.

19. Force, U.S.P.S.T., et al., *Screening for Prostate Cancer: US Preventive Services Task Force Recommendation Statement*. JAMA, 2018. **319**(18): p. 1901-1913.
20. Liu, A.Y. and L.D. True, *Characterization of prostate cell types by CD cell surface molecules*. Am J Pathol, 2002. **160**(1): p. 37-43.
21. Lee, S.H. and M.M. Shen, *Cell types of origin for prostate cancer*. Curr Opin Cell Biol, 2015. **37**: p. 35-41.
22. Long, R.J., et al., *Prostate cancer: a clinical and basic science review*. J Androl, 1997. **18**(1): p. 15-20.
23. Kweldam, C.F., et al., *Disease-specific death and metastasis do not occur in patients with Gleason score ≤ 6 at radical prostatectomy*. BJU Int, 2015. **116**(2): p. 230-5.
24. Srigley, J.R., et al., *Updated protocol for the examination of specimens from patients with carcinomas of the prostate gland*. Arch Pathol Lab Med, 2006. **130**(7): p. 936-46.
25. Cheng, L., et al., *Staging of prostate cancer*. Histopathology, 2012. **60**(1): p. 87-117.
26. Bhatia-Gaur, R., et al., *Roles for Nkx3.1 in prostate development and cancer*. Genes Dev, 1999. **13**(8): p. 966-77.
27. Gopalan, A., et al., *TMPRSS2-ERG rearrangement in dominant anterior prostatic tumours: incidence and correlation with ERG immunohistochemistry*. Histopathology, 2013. **63**(2): p. 279-86.
28. Lopergolo, A. and N. Zaffaroni, *Biomolecular markers of outcome prediction in prostate cancer*. Cancer, 2009. **115**(13 Suppl): p. 3058-67.
29. Martin, P., et al., *Prostate epithelial Pten/TP53 loss leads to transformation of multipotential progenitors and epithelial to mesenchymal transition*. Am J Pathol, 2011. **179**(1): p. 422-35.
30. Saad, F. and S.J. Hotte, *Guidelines for the management of castrate-resistant prostate cancer*. Can Urol Assoc J, 2010. **4**(6): p. 380-4.
31. Cook, T. and W.P. Sheridan, *Development of GnRH antagonists for prostate cancer: new approaches to treatment*. Oncologist, 2000. **5**(2): p. 162-8.
32. Labrie, F., et al., *Gonadotropin-releasing hormone agonists in the treatment of prostate cancer*. Endocr Rev, 2005. **26**(3): p. 361-79.
33. Datta, D., et al., *Human Prostate Cancer Hallmarks Map*. Sci Rep, 2016. **6**: p. 30691.
34. Bekelman, J.E., R.B. Rumble, and S.J. Freedland, *Clinically Localized Prostate Cancer: ASCO Clinical Practice Guideline Endorsement of an AUA/ASTRO/SUO Guideline Summary*. J Oncol Pract, 2018. **14**(10): p. 618-624.
35. Connolly, R.M., M.A. Carducci, and E.S. Antonarakis, *Use of androgen deprivation therapy in prostate cancer: indications and prevalence*. Asian J Androl, 2012. **14**(2): p. 177-86.
36. Mohler, J.L., et al., *Prostate Cancer, Version 2.2019, NCCN Clinical Practice Guidelines in Oncology*. J Natl Compr Canc Netw, 2019. **17**(5): p. 479-505.
37. Thompson, I.M., *Flare Associated with LHRH-Agonist Therapy*. Rev Urol, 2001. **3 Suppl 3**: p. S10-4.
38. Ryan, C.J., et al., *Abiraterone acetate plus prednisone versus placebo plus prednisone in chemotherapy-naive men with metastatic castration-resistant prostate cancer (COU-AA-302): final overall survival analysis of a randomised, double-blind, placebo-controlled phase 3 study*. Lancet Oncol, 2015. **16**(2): p. 152-60.
39. Sartor, O., et al., *Novel therapeutic strategies for metastatic prostate cancer in the post-docetaxel setting*. Oncologist, 2011. **16**(11): p. 1487-97.

40. Scher, H.I., et al., *Antitumour activity of MDV3100 in castration-resistant prostate cancer: a phase 1-2 study*. Lancet, 2010. **375**(9724): p. 1437-46.
41. Lowrance, W.T., et al., *Castration-Resistant Prostate Cancer: AUA Guideline Amendment 2018*. J Urol, 2018.
42. Kumar, R.J., A. Barqawi, and E.D. Crawford, *Adverse events associated with hormonal therapy for prostate cancer*. Rev Urol, 2005. **7 Suppl 5**: p. S37-43.
43. Crawford, E.D., et al., *A controlled trial of leuprolide with and without flutamide in prostatic carcinoma*. N Engl J Med, 1989. **321**(7): p. 419-24.
44. Rathkopf, D.E., et al., *Radiographic Progression-Free Survival as a Clinically Meaningful End Point in Metastatic Castration-Resistant Prostate Cancer: The PREVAIL Randomized Clinical Trial*. JAMA Oncol, 2018. **4**(5): p. 694-701.
45. Caffo, O., et al., *Abiraterone acetate and its use in the treatment of metastatic prostate cancer: a review*. Future Oncol, 2018. **14**(5): p. 431-442.
46. Agoulnik, I.U. and N.L. Weigel, *Androgen receptor action in hormone-dependent and recurrent prostate cancer*. J Cell Biochem, 2006. **99**(2): p. 362-72.
47. Suzuki, H. and H. Ito, *Role of androgen receptor in prostate cancer*. Asian J Androl, 1999. **1**(3): p. 81-5.
48. Waltering, K.K., A. Urbanucci, and T. Visakorpi, *Androgen receptor (AR) aberrations in castration-resistant prostate cancer*. Mol Cell Endocrinol, 2012. **360**(1-2): p. 38-43.
49. Gregory, C.W., et al., *Androgen receptor stabilization in recurrent prostate cancer is associated with hypersensitivity to low androgen*. Cancer Res, 2001. **61**(7): p. 2892-8.
50. Chen, Y., C.L. Sawyers, and H.I. Scher, *Targeting the androgen receptor pathway in prostate cancer*. Curr Opin Pharmacol, 2008. **8**(4): p. 440-8.
51. Chandrasekar, T., et al., *Mechanisms of resistance in castration-resistant prostate cancer (CRPC)*. Transl Androl Urol, 2015. **4**(3): p. 365-80.
52. Quigley, D.A., et al., *Genomic Hallmarks and Structural Variation in Metastatic Prostate Cancer*. Cell, 2018. **175**(3): p. 889.
53. Koivisto, P., et al., *Androgen receptor gene amplification: a possible molecular mechanism for androgen deprivation therapy failure in prostate cancer*. Cancer Res, 1997. **57**(2): p. 314-9.
54. Newmark, J.R., et al., *Androgen receptor gene mutations in human prostate cancer*. Proc Natl Acad Sci U S A, 1992. **89**(14): p. 6319-23.
55. Dehm, S.M. and D.J. Tindall, *Androgen receptor structural and functional elements: role and regulation in prostate cancer*. Mol Endocrinol, 2007. **21**(12): p. 2855-63.
56. Fujimoto, N., et al., *Prostate cancer cells increase androgen sensitivity by increase in nuclear androgen receptor and androgen receptor coactivators; a possible mechanism of hormone-resistance of prostate cancer cells*. Cancer Invest, 2007. **25**(1): p. 32-7.
57. Gao, X., B.W. Loggie, and Z. Nawaz, *The roles of sex steroid receptor coregulators in cancer*. Mol Cancer, 2002. **1**: p. 7.
58. Lonard, D.M. and B.W. O'Malley, *Molecular Pathways: Targeting Steroid Receptor Coactivators in Cancer*. Clin Cancer Res, 2016. **22**(22): p. 5403-5407.
59. Xu, J., R.C. Wu, and B.W. O'Malley, *Normal and cancer-related functions of the p160 steroid receptor co-activator (SRC) family*. Nat Rev Cancer, 2009. **9**(9): p. 615-30.
60. Feldman, B.J. and D. Feldman, *The development of androgen-independent prostate cancer*. Nat Rev Cancer, 2001. **1**(1): p. 34-45.

61. Liu, Y., et al., *Targeted overexpression of vav3 oncogene in prostatic epithelium induces nonbacterial prostatitis and prostate cancer*. *Cancer Res*, 2008. **68**(15): p. 6396-406.
62. Li, X., et al., *Epithelial Hic-5/ARA55 expression contributes to prostate tumorigenesis and castrate responsiveness*. *Oncogene*, 2011. **30**(2): p. 167-77.
63. Yang, Z., et al., *Transgelin functions as a suppressor via inhibition of ARA54-enhanced androgen receptor transactivation and prostate cancer cell growth*. *Mol Endocrinol*, 2007. **21**(2): p. 343-58.
64. Alland, L., et al., *Role for N-CoR and histone deacetylase in Sin3-mediated transcriptional repression*. *Nature*, 1997. **387**(6628): p. 49-55.
65. Dehm, S.M. and D.J. Tindall, *Alternatively spliced androgen receptor variants*. *Endocr Relat Cancer*, 2011. **18**(5): p. R183-96.
66. Liu, L.L., et al., *Mechanisms of the androgen receptor splicing in prostate cancer cells*. *Oncogene*, 2014. **33**(24): p. 3140-50.
67. Hu, R., et al., *Ligand-independent androgen receptor variants derived from splicing of cryptic exons signify hormone-refractory prostate cancer*. *Cancer Res*, 2009. **69**(1): p. 16-22.
68. Dehm, S.M., et al., *Splicing of a novel androgen receptor exon generates a constitutively active androgen receptor that mediates prostate cancer therapy resistance*. *Cancer Res*, 2008. **68**(13): p. 5469-77.
69. Lu, C. and J. Luo, *Decoding the androgen receptor splice variants*. *Transl Androl Urol*, 2013. **2**(3): p. 178-186.
70. Chan, S.C., Y. Li, and S.M. Dehm, *Androgen receptor splice variants activate androgen receptor target genes and support aberrant prostate cancer cell growth independent of canonical androgen receptor nuclear localization signal*. *J Biol Chem*, 2012. **287**(23): p. 19736-49.
71. Antonarakis, E.S., et al., *Androgen Receptor Splice Variant 7 and Efficacy of Taxane Chemotherapy in Patients With Metastatic Castration-Resistant Prostate Cancer*. *JAMA Oncol*, 2015. **1**(5): p. 582-91.
72. Scher, H.I., et al., *Association of AR-V7 on Circulating Tumor Cells as a Treatment-Specific Biomarker With Outcomes and Survival in Castration-Resistant Prostate Cancer*. *JAMA Oncol*, 2016. **2**(11): p. 1441-1449.
73. Onstenk, W., et al., *Efficacy of Cabazitaxel in Castration-resistant Prostate Cancer Is Independent of the Presence of AR-V7 in Circulating Tumor Cells*. *Eur Urol*, 2015. **68**(6): p. 939-45.
74. Antonarakis, E.S., et al., *AR-V7 and resistance to enzalutamide and abiraterone in prostate cancer*. *N Engl J Med*, 2014. **371**(11): p. 1028-38.
75. Hu, R., et al., *Distinct transcriptional programs mediated by the ligand-dependent full-length androgen receptor and its splice variants in castration-resistant prostate cancer*. *Cancer Res*, 2012. **72**(14): p. 3457-62.
76. Xu, D., et al., *Androgen Receptor Splice Variants Dimerize to Transactivate Target Genes*. *Cancer Res*, 2015. **75**(17): p. 3663-71.
77. Lecker, S.H., A.L. Goldberg, and W.E. Mitch, *Protein degradation by the ubiquitin-proteasome pathway in normal and disease states*. *J Am Soc Nephrol*, 2006. **17**(7): p. 1807-19.

78. Guo, Z., et al., *A novel androgen receptor splice variant is up-regulated during prostate cancer progression and promotes androgen depletion-resistant growth*. *Cancer Res*, 2009. **69**(6): p. 2305-13.
79. Bevan, C.L., et al., *The AF1 and AF2 domains of the androgen receptor interact with distinct regions of SRC1*. *Mol Cell Biol*, 1999. **19**(12): p. 8383-92.
80. Christiaens, V., et al., *Characterization of the two coactivator-interacting surfaces of the androgen receptor and their relative role in transcriptional control*. *J Biol Chem*, 2002. **277**(51): p. 49230-7.
81. Callewaert, L., N. Van Tilborgh, and F. Claessens, *Interplay between two hormone-independent activation domains in the androgen receptor*. *Cancer Res*, 2006. **66**(1): p. 543-53.
82. Ueda, T., et al., *Ligand-independent activation of the androgen receptor by interleukin-6 and the role of steroid receptor coactivator-1 in prostate cancer cells*. *J Biol Chem*, 2002. **277**(41): p. 38087-94.
83. Tan, M.H., et al., *Androgen receptor: structure, role in prostate cancer and drug discovery*. *Acta Pharmacol Sin*, 2015. **36**(1): p. 3-23.
84. Roy, A.K., et al., *Androgen receptor: structural domains and functional dynamics after ligand-receptor interaction*. *Ann N Y Acad Sci*, 2001. **949**: p. 44-57.
85. Lavery, D.N. and I.J. McEwan, *Structure and function of steroid receptor AF1 transactivation domains: induction of active conformations*. *Biochem J*, 2005. **391**(Pt 3): p. 449-64.
86. Davey, R.A. and M. Grossmann, *Androgen Receptor Structure, Function and Biology: From Bench to Bedside*. *Clin Biochem Rev*, 2016. **37**(1): p. 3-15.
87. van Royen, M.E., et al., *Stepwise androgen receptor dimerization*. *J Cell Sci*, 2012. **125**(Pt 8): p. 1970-9.
88. Wilson, E.M., *Analysis of interdomain interactions of the androgen receptor*. *Methods Mol Biol*, 2011. **776**: p. 113-29.
89. Kim, J. and G.A. Coetzee, *Prostate specific antigen gene regulation by androgen receptor*. *J Cell Biochem*, 2004. **93**(2): p. 233-41.
90. Moras, D. and H. Gronemeyer, *The nuclear receptor ligand-binding domain: structure and function*. *Curr Opin Cell Biol*, 1998. **10**(3): p. 384-91.
91. Dubbink, H.J., et al., *Distinct recognition modes of FXXLF and LXXLL motifs by the androgen receptor*. *Mol Endocrinol*, 2004. **18**(9): p. 2132-50.
92. He, B., et al., *The FXXLF motif mediates androgen receptor-specific interactions with coregulators*. *J Biol Chem*, 2002. **277**(12): p. 10226-35.
93. Dubbink, H.J., et al., *Androgen receptor ligand-binding domain interaction and nuclear receptor specificity of FXXLF and LXXLL motifs as determined by L/F swapping*. *Mol Endocrinol*, 2006. **20**(8): p. 1742-55.
94. Culig, Z. and F.R. Santer, *Androgen receptor co-activators in the regulation of cellular events in prostate cancer*. *World J Urol*, 2012. **30**(3): p. 297-302.
95. Culig, Z. and F.R. Santer, *Molecular aspects of androgenic signaling and possible targets for therapeutic intervention in prostate cancer*. *Steroids*, 2013. **78**(9): p. 851-9.
96. Agoulnik, I.U., et al., *Androgens modulate expression of transcription intermediary factor 2, an androgen receptor coactivator whose expression level correlates with early biochemical recurrence in prostate cancer*. *Cancer Res*, 2006. **66**(21): p. 10594-602.

97. Linja, M.J., et al., *Expression of androgen receptor coregulators in prostate cancer*. Clin Cancer Res, 2004. **10**(3): p. 1032-40.
98. Shi, X.B., et al., *Prolonged androgen receptor loading onto chromatin and the efficient recruitment of p160 coactivators contribute to androgen-independent growth of prostate cancer cells*. Prostate, 2008. **68**(16): p. 1816-26.
99. Hu, Y.C., et al., *Functional domain and motif analyses of androgen receptor coregulator ARA70 and its differential expression in prostate cancer*. J Biol Chem, 2004. **279**(32): p. 33438-46.
100. Shiota, M., et al., *Tip60 promotes prostate cancer cell proliferation by translocation of androgen receptor into the nucleus*. Prostate, 2010. **70**(5): p. 540-54.
101. Heemers, H.V., J.D. Debes, and D.J. Tindall, *The role of the transcriptional coactivator p300 in prostate cancer progression*. Adv Exp Med Biol, 2008. **617**: p. 535-40.
102. McGrath, M.J., et al., *Regulation of the transcriptional coactivator FHL2 licenses activation of the androgen receptor in castrate-resistant prostate cancer*. Cancer Res, 2013. **73**(16): p. 5066-79.
103. Chmelar, R., et al., *Androgen receptor coregulators and their involvement in the development and progression of prostate cancer*. Int J Cancer, 2007. **120**(4): p. 719-33.
104. McKenna, N.J. and B.W. O'Malley, *Minireview: nuclear receptor coactivators--an update*. Endocrinology, 2002. **143**(7): p. 2461-5.
105. Nakka, M., I.U. Agoulnik, and N.L. Weigel, *Targeted disruption of the p160 coactivator interface of androgen receptor (AR) selectively inhibits AR activity in both androgen-dependent and castration-resistant AR-expressing prostate cancer cells*. Int J Biochem Cell Biol, 2013. **45**(4): p. 763-72.
106. Agoulnik, I.U., et al., *Role of SRC-1 in the promotion of prostate cancer cell growth and tumor progression*. Cancer Res, 2005. **65**(17): p. 7959-67.
107. Bolton, E.C., et al., *Cell- and gene-specific regulation of primary target genes by the androgen receptor*. Genes Dev, 2007. **21**(16): p. 2005-17.
108. Nelson, P.S., et al., *The program of androgen-responsive genes in neoplastic prostate epithelium*. Proc Natl Acad Sci U S A, 2002. **99**(18): p. 11890-5.
109. Sharma, N.L., et al., *The androgen receptor induces a distinct transcriptional program in castration-resistant prostate cancer in man*. Cancer Cell, 2013. **23**(1): p. 35-47.
110. Henshall, S.M., et al., *Altered expression of androgen receptor in the malignant epithelium and adjacent stroma is associated with early relapse in prostate cancer*. Cancer Res, 2001. **61**(2): p. 423-7.
111. Karantanos, T., P.G. Corn, and T.C. Thompson, *Prostate cancer progression after androgen deprivation therapy: mechanisms of castrate resistance and novel therapeutic approaches*. Oncogene, 2013. **32**(49): p. 5501-11.
112. Gregory, C.W., et al., *A mechanism for androgen receptor-mediated prostate cancer recurrence after androgen deprivation therapy*. Cancer Res, 2001. **61**(11): p. 4315-9.
113. Dehm, S.M. and D.J. Tindall, *Molecular regulation of androgen action in prostate cancer*. J Cell Biochem, 2006. **99**(2): p. 333-44.
114. Ahmed, A., S. Ali, and F.H. Sarkar, *Advances in androgen receptor targeted therapy for prostate cancer*. J Cell Physiol, 2014. **229**(3): p. 271-6.
115. Schulman, I.G. and R.A. Heyman, *The flip side: Identifying small molecule regulators of nuclear receptors*. Chem Biol, 2004. **11**(5): p. 639-46.

116. Berrevoets, C.A., et al., *Functional interactions of the AF-2 activation domain core region of the human androgen receptor with the amino-terminal domain and with the transcriptional coactivator TIF2 (transcriptional intermediary factor2)*. Mol Endocrinol, 1998. **12**(8): p. 1172-83.
117. Feng, S., et al., *Interleukin-6 increases prostate cancer cells resistance to bicalutamide via TIF2*. Mol Cancer Ther, 2009. **8**(3): p. 665-71.
118. Fancher, A.T., et al., *Reconfiguring the AR-TIF2 Protein-Protein Interaction HCS Assay in Prostate Cancer Cells and Characterizing the Hits from a LOPAC Screen*. Assay Drug Dev Technol, 2016. **14**(8): p. 453-477.
119. Hua, Y., et al., *High Content Positional Biosensor Assay to Screen for Compounds that Prevent or Disrupt Androgen Receptor and Transcription Intermediary Factor 2 Protein-Protein Interactions*. Methods Mol Biol, 2018. **1683**: p. 211-227.
120. Daghestani, H.N., et al., *Characterization of inhibitors of glucocorticoid receptor nuclear translocation: a model of cytoplasmic dynein-mediated cargo transport*. Assay Drug Dev Technol, 2012. **10**(1): p. 46-60.
121. Dudgeon, D.D., et al., *Characterization and optimization of a novel protein-protein interaction biosensor high-content screening assay to identify disruptors of the interactions between p53 and hDM2*. Assay Drug Dev Technol, 2010. **8**(4): p. 437-58.
122. Dudgeon, D.D., et al., *Implementation of a 220,000-compound HCS campaign to identify disruptors of the interaction between p53 and hDM2 and characterization of the confirmed hits*. J Biomol Screen, 2010. **15**(7): p. 766-82.
123. Hua, Y., C.J. Strock, and P.A. Johnston, *High content screening biosensor assay to identify disruptors of p53-hDM2 protein-protein interactions*. Methods Mol Biol, 2015. **1278**: p. 555-65.
124. Johnston, P.A., et al., *Development and Implementation of a High-Throughput High-Content Screening Assay to Identify Inhibitors of Androgen Receptor Nuclear Localization in Castration-Resistant Prostate Cancer Cells*. Assay Drug Dev Technol, 2016. **14**(4): p. 226-39.
125. Johnston, P.A., et al., *Development and validation of a high-content screening assay to identify inhibitors of cytoplasmic dynein-mediated transport of glucocorticoid receptor to the nucleus*. Assay Drug Dev Technol, 2012. **10**(5): p. 432-56.
126. Htun, H., et al., *Visualization of glucocorticoid receptor translocation and intranuclear organization in living cells with a green fluorescent protein chimera*. Proc Natl Acad Sci U S A, 1996. **93**(10): p. 4845-50.
127. Fancher, A.T., et al., *High-Content Screening Campaign to Identify Compounds That Inhibit or Disrupt Androgen Receptor-Transcriptional Intermediary Factor 2 Protein-Protein Interactions for the Treatment of Prostate Cancer*. Assay Drug Dev Technol, 2018. **16**(6): p. 297-319.
128. Narayanan, R., et al., *Selective androgen receptor modulators in preclinical and clinical development*. Nucl Recept Signal, 2008. **6**: p. e010.
129. Gao, W. and J.T. Dalton, *Expanding the therapeutic use of androgens via selective androgen receptor modulators (SARMs)*. Drug Discov Today, 2007. **12**(5-6): p. 241-8.
130. Huang, P., V. Chandra, and F. Rastinejad, *Structural overview of the nuclear receptor superfamily: insights into physiology and therapeutics*. Annu Rev Physiol, 2010. **72**: p. 247-72.

131. Hua, Y., et al., *High-content positional biosensor screening assay for compounds to prevent or disrupt androgen receptor and transcriptional intermediary factor 2 protein-protein interactions*. *Assay Drug Dev Technol*, 2014. **12**(7): p. 395-418.
132. Wells, J.A. and C.L. McClendon, *Reaching for high-hanging fruit in drug discovery at protein-protein interfaces*. *Nature*, 2007. **450**(7172): p. 1001-9.
133. Lundholt, B.K., et al., *A simple cell-based HTS assay system to screen for inhibitors of p53-Hdm2 protein-protein interactions*. *Assay Drug Dev Technol*, 2006. **4**(6): p. 679-88.
134. Culig, Z., et al., *Androgen receptor--an update of mechanisms of action in prostate cancer*. *Urol Res*, 2000. **28**(4): p. 211-9.
135. Culig, Z., et al., *Androgen receptors in prostate cancer*. *J Urol*, 2003. **170**(4 Pt 1): p. 1363-9.
136. Burd, C.J., L.M. Morey, and K.E. Knudsen, *Androgen receptor corepressors and prostate cancer*. *Endocr Relat Cancer*, 2006. **13**(4): p. 979-94.
137. Grossmann, M.E., H. Huang, and D.J. Tindall, *Androgen receptor signaling in androgen-refractory prostate cancer*. *J Natl Cancer Inst*, 2001. **93**(22): p. 1687-97.
138. Darimont, B.D., et al., *Structure and specificity of nuclear receptor-coactivator interactions*. *Genes Dev*, 1998. **12**(21): p. 3343-56.
139. Lievens, S., I. Lemmens, and J. Tavernier, *Mammalian two-hybrids come of age*. *Trends Biochem Sci*, 2009. **34**(11): p. 579-88.
140. Mendonca, D.B., G. Mendonca, and L.F. Cooper, *Mammalian two-hybrid assays for studies of interaction of p300 with transcription factors*. *Methods Mol Biol*, 2013. **977**: p. 323-38.
141. Stynen, B., et al., *Diversity in genetic in vivo methods for protein-protein interaction studies: from the yeast two-hybrid system to the mammalian split-luciferase system*. *Microbiol Mol Biol Rev*, 2012. **76**(2): p. 331-82.
142. Ravasi, T., et al., *An atlas of combinatorial transcriptional regulation in mouse and man*. *Cell*, 2010. **140**(5): p. 744-52.
143. Goldspiel, B.R. and D.R. Kohler, *Flutamide: an antiandrogen for advanced prostate cancer*. *DICP*, 1990. **24**(6): p. 616-23.
144. Goa, K.L. and C.M. Spencer, *Bicalutamide in advanced prostate cancer. A review*. *Drugs Aging*, 1998. **12**(5): p. 401-22.
145. Beer, T.M. and B. Tombal, *Enzalutamide in metastatic prostate cancer before chemotherapy*. *N Engl J Med*, 2014. **371**(18): p. 1755-6.
146. Rehman, Y. and J.E. Rosenberg, *Abiraterone acetate: oral androgen biosynthesis inhibitor for treatment of castration-resistant prostate cancer*. *Drug Des Devel Ther*, 2012. **6**: p. 13-8.
147. De Mol, E., et al., *EPI-001, A Compound Active against Castration-Resistant Prostate Cancer, Targets Transactivation Unit 5 of the Androgen Receptor*. *ACS Chem Biol*, 2016. **11**(9): p. 2499-505.
148. Yang, Y.C., et al., *Targeting Androgen Receptor Activation Function-1 with EPI to Overcome Resistance Mechanisms in Castration-Resistant Prostate Cancer*. *Clin Cancer Res*, 2016. **22**(17): p. 4466-77.
149. Masoodi, K.Z., et al., *Inhibition of Androgen Receptor Function and Level in Castration-Resistant Prostate Cancer Cells by 2-[(isoxazol-4-ylmethyl)thio]-1-(4-phenylpiperazin-1-yl)ethanone*. *Endocrinology*, 2017. **158**(10): p. 3152-3161.

150. Solit, D.B., H.I. Scher, and N. Rosen, *Hsp90 as a therapeutic target in prostate cancer*. Semin Oncol, 2003. **30**(5): p. 709-16.
151. Fields, S. and O. Song, *A novel genetic system to detect protein-protein interactions*. Nature, 1989. **340**(6230): p. 245-6.
152. Drees, B.L., *Progress and variations in two-hybrid and three-hybrid technologies*. Curr Opin Chem Biol, 1999. **3**(1): p. 64-70.
153. Edwards, D.P., *The role of coactivators and corepressors in the biology and mechanism of action of steroid hormone receptors*. J Mammary Gland Biol Neoplasia, 2000. **5**(3): p. 307-24.
154. Torchia, J., C. Glass, and M.G. Rosenfeld, *Co-activators and co-repressors in the integration of transcriptional responses*. Curr Opin Cell Biol, 1998. **10**(3): p. 373-83.
155. Gonzalez, G.A. and M.R. Montminy, *Cyclic AMP stimulates somatostatin gene transcription by phosphorylation of CREB at serine 133*. Cell, 1989. **59**(4): p. 675-80.
156. Askew, E.B., et al., *Modulation of androgen receptor activation function 2 by testosterone and dihydrotestosterone*. J Biol Chem, 2007. **282**(35): p. 25801-16.
157. He, B., et al., *Activation function 2 in the human androgen receptor ligand binding domain mediates interdomain communication with the NH(2)-terminal domain*. J Biol Chem, 1999. **274**(52): p. 37219-25.
158. Fiebitz, A. and D. Vanhecke, *High-throughput mammalian two-hybrid screening for protein-protein interactions using transfected cell arrays (CAPPIA)*. Methods Mol Biol, 2011. **723**: p. 165-83.
159. He, B., et al., *An androgen receptor NH2-terminal conserved motif interacts with the COOH terminus of the Hsp70-interacting protein (CHIP)*. J Biol Chem, 2004. **279**(29): p. 30643-53.
160. Feau, C., et al., *A high-throughput ligand competition binding assay for the androgen receptor and other nuclear receptors*. J Biomol Screen, 2009. **14**(1): p. 43-8.
161. Zhou, X.E., et al., *Identification of SRC3/AIB1 as a preferred coactivator for hormone-activated androgen receptor*. J Biol Chem, 2010. **285**(12): p. 9161-71.
162. Estebanez-Perpina, E., et al., *The molecular mechanisms of coactivator utilization in ligand-dependent transactivation by the androgen receptor*. J Biol Chem, 2005. **280**(9): p. 8060-8.
163. Eglen, R.M., et al., *The use of AlphaScreen technology in HTS: current status*. Curr Chem Genomics, 2008. **1**: p. 2-10.
164. Pereira de Jesus-Tran, K., et al., *Comparison of crystal structures of human androgen receptor ligand-binding domain complexed with various agonists reveals molecular determinants responsible for binding affinity*. Protein Sci, 2006. **15**(5): p. 987-99.
165. Russell, P.J. and E.A. Kingsley, *Human prostate cancer cell lines*. Methods Mol Med, 2003. **81**: p. 21-39.
166. He, Y., et al., *Androgen receptor splice variants bind to constitutively open chromatin and promote abiraterone-resistant growth of prostate cancer*. Nucleic Acids Res, 2018. **46**(4): p. 1895-1911.
167. Krause, W.C., et al., *Androgen receptor and its splice variant, AR-V7, differentially regulate FOXA1 sensitive genes in LNCaP prostate cancer cells*. Int J Biochem Cell Biol, 2014. **54**: p. 49-59.
168. Wadosky, K.M. and S. Koochekpour, *Androgen receptor splice variants and prostate cancer: From bench to bedside*. Oncotarget, 2017. **8**(11): p. 18550-18576.

169. Wang, Q., et al., *Androgen receptor regulates a distinct transcription program in androgen-independent prostate cancer*. Cell, 2009. **138**(2): p. 245-56.
170. Eder, I.E., et al., *Molecular biology of the androgen receptor: from molecular understanding to the clinic*. Eur Urol, 2001. **40**(3): p. 241-51.
171. Irvine, R.A., et al., *Inhibition of p160-mediated coactivation with increasing androgen receptor polyglutamine length*. Hum Mol Genet, 2000. **9**(2): p. 267-74.
172. Ma, H., et al., *Multiple signal input and output domains of the 160-kilodalton nuclear receptor coactivator proteins*. Mol Cell Biol, 1999. **19**(9): p. 6164-73.
173. Langley, E., Z.X. Zhou, and E.M. Wilson, *Evidence for an anti-parallel orientation of the ligand-activated human androgen receptor dimer*. J Biol Chem, 1995. **270**(50): p. 29983-90.
174. Makhnevych, T. and W.A. Houry, *The role of Hsp90 in protein complex assembly*. Biochim Biophys Acta, 2012. **1823**(3): p. 674-82.
175. Brand, L.J., et al., *EPI-001 is a selective peroxisome proliferator-activated receptor-gamma modulator with inhibitory effects on androgen receptor expression and activity in prostate cancer*. Oncotarget, 2015. **6**(6): p. 3811-24.
176. Zhuang, C., et al., *Chalcone: A Privileged Structure in Medicinal Chemistry*. Chem Rev, 2017. **117**(12): p. 7762-7810.
177. Zhou, B., et al., *Characterization of the Fluorescence Properties of 4-Dialkylaminochalcones and Investigation of the Cytotoxic Mechanism of Chalcones*. Arch Pharm (Weinheim), 2016. **349**(7): p. 539-52.
178. Zhou, B. and C. Xing, *Diverse Molecular Targets for Chalcones with Varied Bioactivities*. Med Chem (Los Angeles), 2015. **5**(8): p. 388-404.
179. Zhong, S., et al., *Zeranol induces cell proliferation and protein disulfide isomerase expression in mammary gland of ACI rat*. Anticancer Res, 2011. **31**(5): p. 1659-65.
180. Aw, T.C., et al., *Occupational exposure to zeranol, an animal growth promoter*. Br J Ind Med, 1989. **46**(5): p. 341-6.
181. Frank, D.A., *Targeting transcription factors for cancer therapy*. IDrugs, 2009. **12**(1): p. 29-33.
182. Redell, M.S. and D.J. Tweardy, *Targeting transcription factors in cancer: Challenges and evolving strategies*. Drug Discov Today Technol, 2006. **3**(3): p. 261-7.
183. Arkin, M.R., Y. Tang, and J.A. Wells, *Small-molecule inhibitors of protein-protein interactions: progressing toward the reality*. Chem Biol, 2014. **21**(9): p. 1102-14.
184. Tsomaia, N., *Peptide therapeutics: targeting the undruggable space*. Eur J Med Chem, 2015. **94**: p. 459-70.
185. Thangudu, R.R., et al., *Modulating protein-protein interactions with small molecules: the importance of binding hotspots*. J Mol Biol, 2012. **415**(2): p. 443-53.
186. Arkin, M.R. and J.A. Wells, *Small-molecule inhibitors of protein-protein interactions: progressing towards the dream*. Nat Rev Drug Discov, 2004. **3**(4): p. 301-17.
187. McKenna, N.J. and B.W. O'Malley, *Combinatorial control of gene expression by nuclear receptors and coregulators*. Cell, 2002. **108**(4): p. 465-74.
188. Hua, Y., Shun, TY, Strock, CJ, Johnston, PA., *High-content positional biosensor screening assay for compounds to prevent or disrupt androgen receptor and transcriptional intermediary factor 2 protein-protein interactions*. Assay Drug Dev Technol., 2014. **12**: p. 395-418.

189. Johnston, P.A., Shinde, SN, Hua, Y, Shun, TY, Lazo, JS, Day, BW., *Development and validation of a high-content screening assay to identify inhibitors of cytoplasmic Dynein-mediated transport of glucocorticoid receptor to the nucleus*. Assay Drug Dev Technol., 2012. **10**(5): p. 432-456.
190. Johnston, P., Nguyen, MM, Dar, JA, Ai, J, Wang, Y, Masoodi, KZ, Shun, T, Shinde, S, Camarco, DP, Hua, Y, Huryn, DM, Wilson, GM, Lazo, JS, Nelson, JB, Wipf, P, Wang, Z., *Development and Implementation of a High-Throughput High-Content Screening Assay to Identify Inhibitors of Androgen Receptor Nuclear Localization in Castration-Resistant Prostate Cancer Cells*. Assay Drug Dev Technol. , 2016. **14**: p. 226-239.
191. Nakazawa, M., C. Paller, and N. Kyprianou, *Mechanisms of Therapeutic Resistance in Prostate Cancer*. Curr Oncol Rep, 2017. **19**(2): p. 13.
192. Conn, P.J., A. Christopoulos, and C.W. Lindsley, *Allosteric modulators of GPCRs: a novel approach for the treatment of CNS disorders*. Nat Rev Drug Discov, 2009. **8**(1): p. 41-54.
193. Patching, S.G., *Surface plasmon resonance spectroscopy for characterisation of membrane protein-ligand interactions and its potential for drug discovery*. Biochim Biophys Acta, 2014. **1838**(1 Pt A): p. 43-55.
194. Pfaff, S.J., et al., *Biophysical methods for identifying fragment-based inhibitors of protein-protein interactions*. Methods Mol Biol, 2015. **1278**: p. 587-613.
195. Dias, D.M. and A. Ciulli, *NMR approaches in structure-based lead discovery: recent developments and new frontiers for targeting multi-protein complexes*. Prog Biophys Mol Biol, 2014. **116**(2-3): p. 101-12.